



UNIVERSITATEA POLITEHNICA din BUCUREŞTI

Facultatea de Chimie Aplicată și Știința Materialelor

Departamentul de Inginerie Chimică și Biochimică

ȘCOALA DOCTORALĂ CHIMIE APLICATĂ ȘI ȘTIINȚA MATERIALELOR

Nr. Decizie Senat.....din.....

TEZĂ DE DOCTORAT

Modelarea și simularea proceselor de tratare în regim dinamic a deșeurilor radioactive lichide cu activitate joasă și medie

Dynamic modelling and simulation of low and intermediate level radioactive liquid waste treatment processes

Autor: **Ing. Laura Ruxandra VOICHIȚĂ (ZICMAN)**
Conducător de doctorat: **Prof. Dr. Ing. Tănase DOBRE**

COMISIA DE DOCTORAT

Președinte	Prof. dr. ing. Dănuț-Ionel VĂIREANU	de la	Universitatea Politehnica din București
Conducător de doctorat	Prof. dr. ing. Tănase DOBRE	de la	Universitatea Politehnica din București
Referent	Conf. dr. ing. Oana Cristina PÂRVULESCU	de la	Universitatea Politehnica din București
Referent	CS 1 dr.ing. Mitică DRĂGUȘIN	de la	IFIN Horia Hulubei din București
Referent	Prof.dr.ing. Alexandru OZUNU	de la	Universitatea Babeș-Bolyai Cluj-Napoca

București
-2018-

Abstract

This PhD thesis addresses a topical issue, namely the treatment of low and intermediate level aqueous radioactive waste using a combination of treatment methods in a modular installation. A key step in the treatment process is the characterization from radionuclidic and physicochemical points of view because aqueous waste represents a multi-component system that contains both radionuclides and non-radioactive impurities, present in dissolved and/or suspended solids forms. The purification of this type of waste should be done by combining several treatment methods, each addressed to a particular type of contaminant.

The objectives of the thesis refer to the purification of low and intermediate level aqueous radioactive waste by combining four treatment methods: (1) deep filtration through sand, washed and dried, with particle size of 0.5 - 0.8 mm; (2) ultrafiltration through an artificial polysulfonamide membrane with a 50 nm pore size; (3) reverse osmosis using an artificial membrane of polyamide composite with pore sizes down to 1 nm; (4) adsorption of ^{137}Cs radioisotopes on nickel ferrocyanide precipitated on silica gel with a particle size of 0.5 - 0.8 mm, showing selectivity and specificity for Cs ions.

The theoretical and experimental studies on treatment methods were performed with real and/or simulated waste, in laboratory and *in situ*. Research performed aimed at: (i) identification of mathematical models that satisfactorily describe the purification process by that specific method; (ii) experiments to identify the parameters of the selected models based on the response of process influencing factors; (iii) verification of models.

These mathematical models serve to solve operational problems, reduce the number of experiments in the radiation field and, implicitly, lower costs.

Această teză de doctorat abordează o temă de actualitate și anume tratarea deșeurilor radioactive apoase de joasă și medie activitate utilizând o combinație de metode de tratare într-o instalație modulară. Caracterizarea din punct de vedere radionuclidic și fizico-chimic a deșeului apose care constituie un sistem multicomponent cu compozitie mixtă de radionuclizi și impuriuți non-radioactive, prezente sub formă dizolvată și/sau de solide suspendate, reprezentă un pas-cheie în procesul de tratare. Purificarea unui astfel de deșeu trebuie realizată prin combinarea mai multor metode de tratare, fiecare adresată unui anumit tip de contaminant.

Obiectivele tezei se referă la purificarea deșeurilor radioactive apoase de joasă și medie activitate prin combinarea a patru metode de tratare: (1) filtrare în adâncime prin nisip sortat, spălat și uscat, cu dimensiunea particulelor de 0,5 – 0,8 mm; (2) ultrafiltrare printr-o membrană artificială din polisulfonamidă cu dimensiunea porilor de 50 nm; (3) osmoză inversă utilizând o membrană artificială din poliamidă compozită cu dimensiuni ale porilor care coboară până la 1 nm; (4) adsorbția radioizotopilor ^{137}Cs pe ferocianură de nichel, precipitată pe silica gel, cu dimensiunea particulelor 0,5 – 0,8 mm, care prezintă selectivitate și specificitate pentru ionii de Cs.

*Studiile teoretice și experimentale efectuate asupra metodelor de tratare au fost efectuate cu deșeuri reale și/sau simulate, în laborator și *in situ*. Ele au avut drept scop: (i) identificarea unor modele matematice care să descrie în mod satisfăcător procesul de purificare prin metoda respectivă; (ii) experimente pentru identificarea parametrilor modelelor selectate, pe baza răspunsului la factorii de influență ai procesului; (iii) verificarea modelelor.*

Aceste modele matematice servesc la rezolvarea problemelor operaționale, reduc numărul de experimente în câmp de radiații și, implicit, scad costurile.

Short description of thesis content

Radioactive waste represents the radioactive material in gaseous, liquid or solid form for which no further use can be anticipated. It contains, or is contaminated with, radionuclides at concentrations or activities greater than the levels established by the regulatory rules. The management of radioactive wastes (collection, handling, treatment, conditioning, storage, transport and disposal) must be developed in such way that human health and the environment remain protected with no imposed burden on next generations.

For a better fixing of the role and importance of processing of waste waters with intermediate and low radioactivity the first chapter presents some considerations on sources and classification of nuclear/radioactive wastes, on physical and chemical methods used in processing of nuclear/radioactive waters, especially of radioactive polluted waters, respectively, on basic characterization of liquid radioactive waste.

In modern practice, the aqueous radioactive waste (ARW) processing can be carried out in modular low or medium capacity installations. A mobile and modular design is more flexible and adequate for the relatively small volumes of waste having a variety of characteristics. A modular ARW processing installation contains a set of autonomous treatment modules (three to six) that can be combined in a technological arrangement, depending on requirements.

The second chapter contains considerations on some unit operations and on some technical procedures, which are present in the modular installation for ARW treatment from IFIN-HH Bucharest. The modular installations for low and intermediate level liquid radioactive waste treatment at IFIN-HH, Magurele, Romania contains an ultrafiltration device, which can be used in designing a technology for a given radioactive waste water.

The basic of ultrafiltration, experimental measurements for testing and characterization of the operation procedure with the ultrafiltration device having a given ARW and respectively the clogging modelling and the device modelling define the content of the third chapter.

The fixed bed sorption process is one of the most used sorption procedure for species (target species in industrial applications, pollutants, etc.) separation from gases or liquid media. The fluidised bed and the moving bed procedures are also frequently employed in this type of separations because they confer the capacity to work in continuous steady state regime. Fixed bed sorption procedure works in an unsteady state regime, normally with two steps corresponding to adsorption and desorption. The first part of the fourth chapter contains literature data on sorbents, fluid-sorbent equilibrium and dynamics for fixed bed separation. The second part presents the

obtained experimental data and modelling for the case of ^{137}Cs species separation using nickel ferrocyanide fixed on silicagel sorbent.

Reverse osmosis (RO) as an efficient technology for removing the cesium, strontium, technetium and uranium species from ARW, in order to respect the regulatory limits, was successfully researched and applied in more concrete cases. For a large variety of separation membrane matrices, literature data show that the rejection rates were acceptable at low concentrations of contaminants. However, rejections of ^{137}Cs and ^{90}Sr species at higher concentrations may not be adequate even when using sophisticated membranes. After a short introduction in the theory of reverse osmosis the fifth chapter is oriented on quantitative characterization of RO system from the ARW treatment installation presented in the second chapter of this work.

The sixth chapter presents the filtration separation process that is widely used as an engineering practice for a long time. The filtration process is composed of two steps: the initial one, and the transient one. In the initial stage, particle deposition takes place onto a clean filter, the particles are directly deposited onto filter grains. Deep-bed filtration (DBF) is a method widely used for separation of inorganic and organic particles from suspensions with low levels of suspended solids. The deep bed filtration clarifies suspensions with small solid content by flowing through a granular bed formed by poured particles. By flowing inside the granular bed, interaction forces could appear between one particle from the suspension and one particle from the granular bed.

In the modelling of a process, the focus is upon developing equations that describe the process behavior.

Two categories of models explain the deep bed filters behavior. Fundamental (or microscopic) models consider the importance of actual transport and attachment mechanisms. Phenomenological (or macroscopic) models attempt to explain the physical progression of the filtration cycle, by ripening, effective filtration, and breakthrough, though this is performed with empirical parameters acquired from experimentaly studies rather than fundamental mechanisms. In ARW processing, the knowledge that exists on water purification can be applied. However, there are some additional problems referring to the specialized requirements of radioactive waste management. ARW treatment by deep-bed sand filtration (DBSF) could lead to an effluent with an acceptable level of residual radioactivity for discharge or further processing by other separation methods (*e.g.*, ion exchange, fixed-bed adsorption, ultrafiltration, reverse osmosis) as well as a low amount of secondary radioactive waste.

Two experimental studies of DBSF were conducted under various operating conditions using silica sand as a filtering medium. Diluted clay suspensions were processed in the first study, whereas ARW was treated in the second one.

A semiempirical deterministic model and a stochastic one were used to describe the deposition of clay particles on the sand grains. Adjustable model parameters were fitted based on experimental data and correlated by multiple linear relationships with the process factors. These correlations were used to predict the pressure loss dynamics and the bed radioactivity dynamics due to the deposition of radioactive solid particles.

In the final chapter are presented the general conclusions and future perspectives.

The results obtained and presented can form a tool that allows the investigation of the ARW treatment in a modular installation without performing – or at least reducing – the number of practical experiments that could involve time, extra-costs and, very important, works in radioactive environments. The mathematical models can be very helpful in order to develop a library of mathematical models able to reproduce the behavior of ARW treatments. In addition, this knowledge may be very useful in the upgrading of the existing treatment plants or in the design of the plants to be constructed in the future.

Acknowledgments

Firstly, I would like to express my gratitude and special appreciation to my advisor **Prof. Dr. Eng. Tănase DOBRE** for the constant support of my Ph.D thesis and connected research. Without his guidance and continuous feedback this work would not have been achievable.

My sincere thanks also go to the rest of my thesis committee, **Dr. Eng. IDT II Elena NEACŞU**, **Prof. Dr. Eng. Marta STROESCU and Conf. Dr. Eng. Oana-Cristina PÂRVULESCU** who provided me with guidance and helped me all the time. I would like to thank you for encouraging my research and for allowing me to grow.

Besides my advisors, very special thanks also go to my colleagues from IFIN-HH who helped and supported me during the laboratory and *in-situ* works and analysis: **Dr. Felicia Drăgolici**, **Eng. Bogdan Obreja**, **Dr. Laurențiu Done**, **Dr. Liviu Tugulan**, **Eng Cătălin Ciobanu**, **CS Mihaela Nicu**, **CS Laura Ionașcu**, **IDTI Gheorghe Dogaru**.

I would like to express my special appreciation and thanks to **Prof. Dr. Eng. Dănuț Văireanu**, **Prof. Dr. Eng. Alexandru Ozunu, and Dr. Eng. CS I Mitică Drăgușin**, for their insightful comments and encouragement.

Last but not the least, my deepest gratitude goes to my family for their patience and help throughout the 5 years of encouragement and continuous support in every way possible.

List of tables

Table 1.1. Radioactive waste classification [5].....	2
Table 1.2. Sources of ARW [5].....	4
Table 1.3. Features and limitations of different ARW treatment options [5]	4
Table 1.4. Physical characteristics of an ARW batch	18
Table 1.5. Radioactive characteristics of an ARW batch.....	18
Table 1.6. Chemical characteristics of an ARW batch	19
Table 2.1. Recommended procedure for radioactive wastes treatment upon state and source	23
Table 3.1. Short description of flux limiters type	38
Table 3.2. Main characteristics of the ERU-100-1016 membrane element	49
Table 3.3. Experimental measurement results for untreated ARW at different feed flow rates	51
Table 3.4. Experimental measurement results for pretreated ARW at different feed flow rates ...	51
Table 3.5. Experimental matrix of 2^3 factorial experiment.....	53
Table 3.6. Characteristics of feed, permeate and concentrate	54
Table 3.7. Computation of α and β with data from table 3.6 using Matchad soft.....	60
Table 3.8. Physical characteristics of processed ARW	61
Table 4.1. Estimation of elements participation at PNF-SG composition (normalized values without C and N elements).....	91
Table 4.2. Estimation of elements participation at PNF-SG composition (natural values without C and N elements).....	91
Table 4.3. The calculated parameters of the pseudo first-order and pseudo second-order kinetic models for Cs^+ ions sorbed onto PNF – SG at 298 K, pH = 3, $r = 0.02$ g/mL	97
Table 4.4. Computed thermodynamic parameters of Cs^+ adsorption on PNF – SG sorbent ($r = 0.02$ g/mL, pH = 3, $\tau = 2$ h).....	98
Table 4.5. Adsorption isotherm parameters for Cs^+ on PNF – SG sorbent.....	100
Table 4.6. Thomas model parameters for Cs uptake of PNF-SG for different experimental conditions	104
Table 4.7. Yoon Nelson model parameters for Cs uptake of PNF-SG for different experimental conditions	105
Table 5.1. SWC1-4040 membrane characteristics	134
Table 5.2. Radioactivity concentration of RO module feed.....	136
Table 5.3. Physico-chemical parameters of ARW feed in RO module.....	136
Table 6.1.Effect of process factors (D , H , c_{p0} , w , and t) on characteristic parameters of FC deterministic model (λ_0 , α) and TS stochastic model (β , γ).....	174
Table 6.2. Physical parameters of feed and treated ARW	175
Table 6.3. Characteristic parameters of multicomponent sorption model for ARW processing by DBSF	178

List of figures

Figure 1.1. Waste classification scheme: EW – exempt waste, VLLW – very low level waste, VSLW – very short lived waste, LLW – low level waste, ILW – intermediate level waste, HLW – high level waste	3
Figure 1.2. Gamma spectrometric installation Canberra 1, Detector 1 (a) and Canberra 1, Detector 2 (b)	12
Figure 1.3. TriCarb 2910 TR Analyzer	13
Figure 1.4. MPC-2000-DP model ORTEC – Protean	15
Figure 1.5. UV-Vis Spectrophotometer, model Pharo 300	16
Figure 1.6. Ion-chromatography system model Dionex ICS-5000	16
Figure 1.7. Inductively coupled plasma optical emission spectrometer model Spectroblue	17
Figure 2.1. Filtration, ultrafiltration, reverse osmosis modules (a) and adsorption module (b)....	26
Figure 2.2. Technological flow sheet of aqueous radioactive effluent treatment plant (STERAJMA).....	27
Figure 2.3. Hydraulic line diagram of Filtration Module (F1-F3 – poured filters, V1-V13 – ball-valves, VA1-VA3 - valves for air, VT1-VT3 – ball-valves for sampling, D1-D3 - ball-valves for hydraulic unloading, M1-M5 – manometers.....	28
Figure 2.4. Filtration Module	28
Figure 2.5. Hydraulic line diagram of Ultrafiltration Module (UF – ultrafiltration apparatus, E1-E2 – tanks of processed waste and flushing solution accordingly, P2 – drowned pump, V14-V24 – ball-valves, VT4 – ball-valve for sampling, M6 – manometer, Q1 – flowmeter, T1 – thermometer, TN – electric heating unit.	29
Figure 2.6. Ultrafiltration Module	29
Figure 2.7. Hydraulic line diagram of Reverse Osmosis Module (RO1 and RO2 – reverse osmosis apparatus, MF - bag filter, E3-E4 – tanks of processed waste and flushing solution accordingly, P4 – rotary pump, P5 - three-plung pump, IR1 – needle valve, V25-V37 – ball-valves, VT5 – ball-valve for sampling, K1 - air through off valve, M7-M8 – manometers, Q2 – flowmeter, FL1, FL2 - rotameters, T2 – thermometer, TN – electric heating unit).....	30
Figure 2.8. Reverse Osmosis Module	30
Figure 2.9. Schematic view of a RO spirally wound membrane.....	31
Figure 2.10. Hydraulic line diagram of Sorption Module (FC - filter-container) with synthetic inorganic sorbent	33
Figure 2.11. Sorption Module	33
Figure 3.1. Comparison of flux decline caused by asymptotic concentration polarisation and fouling: a) plot of flux vs. pressure cases, b) pure fouling (clogging), c) plot of flux vs. time in a practical case (CP –pure polarization by concentration).....	38
Figure 3.2. Hydraulic resistances for permeate flow in ultrafiltration processes	39
Figure 3.3. Graphical representation of a two-level design with 2 (left) and 3 factors (right)	48
Figure 3.4. Ultrafiltration membrane element type ERU-100-1016	49
Figure 3.5. Schematic view of a spirally wound membrane section [45].	49

Figure 3.6. Technological scheme for experiment with ultrafiltration.....	50
Figure 3.7. Permeate volumetric flux and TSS vs. operating pressure for different feed flow rates of untreated ($TSS_F = 60 \text{ mg/L}$) and pretreated ($TSS_F = 15 \text{ mg/L}$) ARW (untreated: $\blacklozenge G_V = 7 \text{ m}^3/\text{h}$, $\blacksquare G_V = 10 \text{ m}^3/\text{h}$; pretreated: $\square G_V = 7 \text{ m}^3/\text{h}$, $G_V = 10 \text{ m}^3/\text{h}$)	52
Figure 3.8. Variation of TSS_F with TSS_C at 0.25 MPa pressure and 10 m^3/h feed flow rate	54
Figure 3.9. Variation of j_P and TSS_P with TSS_F at 0.25 MPa pressure and 10 m^3/h feed flow rate	54
Figure 3.10. Elementary process states of the membrane clogging made of surface pores coverage	56
Figure 3.11. Flowsheet for ultrafiltration device for processing of ARW resulted from deep bed filtration.....	59
Figure 4.1. Adsorption isotherms	71
Figure 4.2. Breakthrough curve for the sorption process in fixed beds (C_0 concentration of the inlet solution, C_b concentration of the breakthrough, t_b breakpoint time, t_s saturation time).....	75
Figure 4.3. Mass transfer in adsorption process	82
Figure 4.4. SEM images of PNF-SG sorbent. (a) Scale of 100 μm . (b) Scale of 10 μm	89
Figure 4.5. SEM images of PNF-SG sorbent. (a), (b), (c) Scale of 1 μm	90
Figure 4.6. SEM images of PNF-SG sorbent. (a), (b) Scale of 1 μm	90
Figure 4.7. The XRD analysis of PNF-SG sorbent.	91
Figure 4.8. Local spectrum in an area and intensity of identified species (major species: SiO_2 type 1	92
Figure 4.9. Erlenmeyer flasks containing PNF-SG and 1000 mg/L Cs^+ solution on shaker mixer	93
Figure 4.10. Effect of solid/liquid ratio on Cs^+ activity in liquid phase ($\text{pH} = 3$, $t = 25^\circ\text{C}$)	94
Figure 4.11. Effect of contact time on Cs content in sorbent ($r = 0.02 \text{ g/mL}$, $t = 25^\circ\text{C}$)	94
Figure 4.12. Effect of initial pH on Cs^+ activity in liquid phase ($r = 0.02 \text{ g/mL}$, $t = 25^\circ\text{C}$).....	95
Figure 4.13. Effect of temperature on PNF - SG Cesium sorbent ($\tau = 2 \text{ h}$, $r = 0.02 \text{ g/mL}$, $\text{pH} = 3$)	95
Figure 4.14. Pseudo first-order kinetic plots for the sorption of Cs^+ onto PNF – SG at 298 K, $\text{pH} = 3$, $r = 0.02 \text{ g/mL}$	96
Figure 4.15. Pseudo second-order kinetic plots of Cs^+ sorption onto PNF – SG at 298 K, $\text{pH} = 3$, $r = 0.02 \text{ g/mL}$	96
Figure 4.16. Linear least square plots for obtaining E_{ad} for Cesium species.....	97
Figure 4.17. Van't Hoff plot of Cs^+ adsorption on PNF – SG sorbent	98
Figure 4.18. Sorption isotherm of Cs^+ on PNF – SG sorbent at 298 K and $\text{pH} = 3$	99
Figure 4.19. Langmuir plots of data from fig. 4.18.....	99
Figure 4.20. Characteristic Freundlich plots of data from fig. 4.18	100
Figure 4.21. DF versus pH and solid/liquid ratio ($\tau = 2 \text{ h}$, 298 K, $C_0 = 1000 \text{ mg/L}$).....	101
Figure 4.22. DF versus temperature ($\tau = 2 \text{ h}$, $r = 0.02 \text{ g/mL}$, $\text{pH} 3$ and initial $C_0 = 1000 \text{ mg/L}$).....	101
Figure 4.23. DF versus initial Cs^+ concentration ($\tau = 2 \text{ h}$, $r = 0.02 \text{ g/mL}$, $\text{pH} 3$ and 298 K)	101

Figure 4.24. Breakthrough curves for sorption of Cs species on PNF – SG sorbent : a) the effect of influent concentrations ($Q = 3 \text{ mL/min}$; $H = 20 \text{ mm}$); b) the effect of bed heights ($C_0 = 150 \text{ mg/L}$; $Q = 3 \text{ mL/min}$); c) the effect of flow rates of feed ($C_0 = 150 \text{ mg/L}$; $H = 20 \text{ mm}$)	102
Figure 4.25. Comparison of experimental and model breakthrough curves for.....	106

Figure 5.1. Schematic of normal osmosis (a) and reverse osmosis (c) phenomena.....	114
Figure 5.2. Flow diagram for NF/RO unit.....	119
Figure 5.3. Schematic of a Membrane Pore	129
Figure 5.4. Hydranautics SWC1-4040 RO membrane element (a), system elements and membrane warping (b) and geometric dimensions (c) [85].	135
Figure 5.5. Electron micrographs of the polyamide (PA) layer:	135
Figure 5.6. Technological scheme for treating the ARW.....	136
Figure 5.7. Permeate flux versus time and feed pressure at the begining of RO process	137
Figure 5.8. Effect of feed waste pressure on permeate conductivity/salt rejection.....	138
Figure 5.9. Effect of feed waste pressure on Co concentration in permeate/Co rejection	138
Figure 5.10. Permeate flux versus time and pH of feed ARW ($p= 2.5 \text{ MPa}$, $t= 25^\circ\text{C}$).....	139
Figure 5.11. Effect of feed waste pH on permeate conductivity/salt rejection	139
Figure 5.12. Effect of feed waste pH on Co concentration in permeate/Co rejection.....	139
Figure 5.13. Effect of feed waste temperature on permeate flux	140
Figure 5.14. Effect of feed waste temperature on permeate conductivity/salt rejection	140
Figure 5.15. Effect of feed waste temperature on Co concentration in permeate/Co rejection ..	141

Figure 6.1. Effect of deposition on filter performance (a) performance enhanced with time, (b) performance declined with time, (c) mixed behavior.	154
Figure 6.2. The scheme for the retained solid balance in the deep bed filtration.....	156
Figure 6.3. Particle retention by a filter grain [36]: (1) filter grain, (2) particle from suspension, (3) particle input in the boundary layer, (4) non-deposition trajectory of particle, (5) deposition trajectory of particle, (6) boundary layer around the filter grain, (7) flow direction of suspension (r and θ are radial coordinates of particle trajectory, θ_i is the input angle of particle, D is the diameter of filter grain, x is the distance between particle and filter grain).	162
Figure 6.4. Pilot-scale set-up: a) column and filtrate collector bottle, b) valve and manometer at column top, c) column bottom with manometer, d) gravels for supporting the sand bed, e) sand particles before loading into column.....	170
Figure 6.5. Clay micro suspensions 1 g/L (a) and 2 g/L (b).....	170
Figure 6.6. Metallic columns for ARW treatment by DBSF.....	171
Figure 6.7. Effect of sand grain diameter (D) on c_p/c_{p0} dynamics	172
Figure 6.8. Effect of bed depth (H) on c_p/c_{p0} dynamics	172
Figure 6.9. Effect of suspended solid concentration in the influent (c_{p0}) on c_p/c_{p0} dynamics.....	173
Figure 6.10. Effect of suspension superficial velocity (w) on c_p/c_{p0} dynamics.....	173
Figure 6.11. Effect of operating temperature (t) on c_p/c_{p0} dynamics	173
Figure 6.12. Dynamics of pressure loss for DBSF with a constant flow rate ($D = 0.8 \text{ mm}$, $H = 0.4 \text{ m}$, $c_{p0} = 2 \text{ kg}_p/\text{m}^3$, $t = 25^\circ\text{C}$, $f = 0.7 \text{ m}_p^3/\text{m}^3$, $\varepsilon_b = 0.377 \text{ m}^3/\text{m}_b^3$, $\rho_p = 1400 \text{ kg}_p/\text{m}_p^3$).....	175

- Figure 6.13.** Predicted space and time variations of bed radioactivity determined by the deposition of radioactive suspended particles ($d_p > 50$ nm) from ARW on the sand grains ($D = 0.5$ mm, $H = 0.3$ m, $c_{p0} = 0.223 \text{ kg}_p/\text{m}^3$, $w = 0.003 \text{ m/s}$, and $t = 25^\circ\text{C}$) 176
- Figure 6.14.** Experimental (points) and predicted (line) dynamics of dimensionless concentration of radionuclides ((1) ^{60}Co , (2) ^{137}Cs , (3) ^{241}Am , (4) ^3H) in the collecting tank ($c_{\text{Co},0} = 1.49 \text{ kBq}/\text{m}^3$, $c_{\text{Cs},0} = 18.50 \text{ kBq}/\text{m}^3$, $c_{\text{Am},0} = 0.25 \text{ kBq}/\text{m}^3$, $c_{\text{H},0} = 32000 \text{ kBq}/\text{m}^3$, $D = 0.5$ mm, $H = 0.3$ m, $c_{p0} = 0.223 \text{ kg}_p/\text{m}^3$, $w = 0.003 \text{ m/s}$, and $t = 25^\circ\text{C}$) 177
- Figure 6.15.** Predicted space and time variations of activity concentration of j radionuclide in the filtering bed for radionuclide sorption from liquid phase ((1) ^{60}Co , (2) ^{137}Cs , (3) ^{241}Am , (4) ^3H) 179

Table of Contents

Abstract	i
Short description of thesis content	ii
Acknowledgments	v
List of tables	vi
List of figures	vii
CHAPTER 1. IDENTIFICATION AS SOURCES, PROPERTIES AND TREATMENT SIGNIFICANCE OF MAIN LIQUID RADIOACTIVE WASTE	1
1.1. Sources of Radioactive Waste	1
1.2. Operations used in processing of aqueous radioactive waste; Treatment significance	3
1.3. Liquid radioactive waste characterization	7
1.4. Characterization and analysis methods used in DMDR IFIN-HH	11
CHAPTER 2. AQUEOUS RADIOACTIVE WASTE (ARW) TREATMENT BY COMBINED METHODS IN MODULAR INSTALLATIONS	21
2.1. General considerations	21
2.2. Modular installation for low and intermediate level aqueous radioactive waste treatment at IFIN-HH, Magurele, Romania	25
CHAPTER 3. CHARACTERIZATION AND MODELLING THE ULTRAFILTRATION PROCESS IN LIQUID RADIOACTIVE WASTE TREATMENT	36
3.1. Ultrafiltration – general description. Specific membranes.....	36
3.2. Modelling UF processes	38
3.3. Experimental investigation of UF in ARW treatment.....	48
3.3.1. Module description	48
3.3.2. Working procedure	50
3.3.3. Experimental results and discussion.....	51
3.3.4. Use of j_p , TSS_F and TSS_C in modelling of ultrafiltration system with membrane clogging.....	55
3.3.5. Conclusions	63
CHAPTER 4. CHARACTERIZATION AND MODELLING OF FIXED BED SORPTION PROCESS IN LIQUID RADIOACTIVE WASTE TREATMENT	67
4.1. Sorbents and their specificity	67
4.1.1. Organic ion exchange resins.....	68
4.1.2. Inorganic ion exchange adsorption materials	69
4.1.3. Short considerations on solute ion exchange equilibrium	69
4.2. Modelling of sorption process	70
4.2.1. Batch systems	70
4.2.2. Dynamic systems.....	74

4.3. Treatment of Aqueous Radioactive Wastes containing Cs by sorption method	84
4.4. Experimental investigation of Ni ferrocyanides deposited onto silicagel beds in ARW treatment	87
4.4.1. Working procedure and equipment	88
4.4.2. Results and discussion.....	88
4.4.3. Conclusions	107
CHAPTER 5. THE USE OF THE REVERSE OSMOSIS METHOD IN THE COMBINED TREATMENT OF AQUEOUS RADIOACTIVE WASTE (ARW)	114
5.1. Short RO characterization	114
5.2. Modelling RO process.....	116
5.3. Experimental investigation of Reverse Osmosis process in ARW treatment	133
5.3.1. Materials and method	134
5.3.2. Results and discussion.....	137
5.4. Conclusions	141
CHAPTER 6. CHARACTERIZATION AND MODELLING THE DEEP BED FILTRATION PROCESS IN LIQUID RADIOACTIVE WASTE TREATMENT	149
6.1. Deep bed filtration – general description	149
6.2. Deep bed filtration modelling.....	151
6.2.1. Phenomenological (semi-empirical) modelling of bed filtration	152
6.2.2. Stochastic modelling of bed filtration	158
6.3. Experimental investigation of deep bed filtration in ARW treatment.....	166
6.3.1. Models for deep bed filtration of ARW	167
6.3.2. Experimental set-up.....	169
6.3.3. Results and discussion.....	171
6.4. Conclusions	179
CHAPTER 7. CONCLUSIONS AND DIRECTIONS FOR FUTURE RESEARCH	185
AUTHOR RESEARCH CONTRIBUTIONS	190

CHAPTER 1. IDENTIFICATION AS SOURCES, PROPERTIES AND TREATMENT SIGNIFICANCE OF MAIN LIQUID RADIOACTIVE WASTE

Radioactive waste represents the radioactive material in gaseous, liquid or solid form for which no further use can be anticipated. It contains, or is contaminated with, radionuclides at concentrations or activities greater than the levels established by the regulatory rules. The management of radioactive wastes (collection, handling, treatment, conditioning, storage, transport and disposal) must be developed in such way that human health and the environment remain protected with no imposed burden on next generations. Related to radioactive wastes management, the International Atomic Energy Agency (IAEA) has provided a set of fundamental safety principles for waste disposal that have been accepted on international scale. These principles have later been sustained by safety standards and safety guides [1, 2], generally accepted by all IAEA members, ie all countries that process radioactive materials. For a better fixing of the role and importance of processing of waste waters with intermediate and low radioactivity this chapter presents some considerations on sources and classification of nuclear/radioactive wastes, on physical and chemical methods used in processing of nuclear/radioactive waters, especially of radioactive polluted waters, respectively, on basic characterization of liquid radioactive waste.

1.1. Sources of Radioactive Waste

Radioactive waste is generally made up of a combination of discarded materials or components originating from the production and/or use of radioactive material. Radioactive waste is an inevitable by-product of the radioactive material and nuclear technology application but also of military activities. Nonetheless, it is also produced in hospitals from radioactive material used in diagnosing and treating sick people and sterilizing medical products, in universities and research institutions that perform research studies, and in domains as biology, chemistry, engineering and also in industry from gammagraphy (a nondestructive inspection technique of some material systems).

The generated radioactive waste may present itself in different forms (solid, liquid or gaseous). Different types of radioactive waste and contamination can be generated in various activities. The level of activity of radioactive waste is variable from very high, corresponding to spent fuel and residues from fuel reprocessing, to very low corresponding to radioisotope applications in

laboratories, hospitals, etc. Moreover, the range of half-lives of the radionuclides comprised in the radioactive waste is equally broad [3].

The most important aspect regarding radioactive waste (and also radioactive sources) is the potential hazard to health. That is why it is essential to be managed in a safe way in order to protect people and the environment. From the point of view of health and environmental hazard a good waste management starts before waste generation and contains the analysis of all activities producing radioactive waste with the purpose of prevention or minimisation of waste generation at its source.

If the primary waste generation is minimised then the amount of waste requiring disposal is considerably diminished.

Classification of radioactive waste is extremely useful for the development of one realistic management process starting from generation through collection, segregation, treatment, conditioning, storage, transportation to final disposal. The ontology criteria in radioactive waste classifications derive mostly from different standpoints, i.e., safety, the physical/chemical characteristics of the waste, process engineering demands or regulatory issues [4, 5]. The selection of different waste management options is based upon the radioactivity level of the waste because of corresponding shielding requirements. The current accepted classification system on international scale takes into consideration the radioactivity level and half life of species from the waste. According to this system the radioactive wastes are categorized in: exempt (EW), low- and intermediate-level wastes (LILW), which may be subdivided into short-lived (LILW-SL) and long-lived (LILW-LL) wastes, and high-level wastes (HLW). Table 1.1 lists the basic characteristics of these waste classes [5].

Table 1.1. Radioactive waste classification [5]

Waste classes	Typical characteristics
EW	Radioactivity levels at or below radioactivity acceptance levels, which are based on an annual dose to an exposed member of the public of less than 0.01 mSv*
LILW	Radioactivity levels above acceptance level and thermal power which can be generated by waste (energy source rate) below about 2 kW/m ³
LILW-SL	Restricted long lived radionuclide concentrations (limitation of long lived alpha emitting radionuclides to 4,000 Bq**/g in individual waste packages and to an overall average of 400 Bq/g per waste package)
LILW-LL	Long lived radionuclide concentrations exceeding limitations for short lived waste
HLW	Thermal power above 2 kW/m ³ and long lived radionuclide concentrations exceeding limitations for short lived waste

* mSv (milisievert): 1mSv represents a dose of radiation energy of 0.001 J dissipated in a kilogram of receiving body (SI unit m²/s²),

**Bq (Becquerel): One becquerel is defined as the activity of a quantity of radioactive material in which one nucleus decays per second (SI unit: s⁻¹)

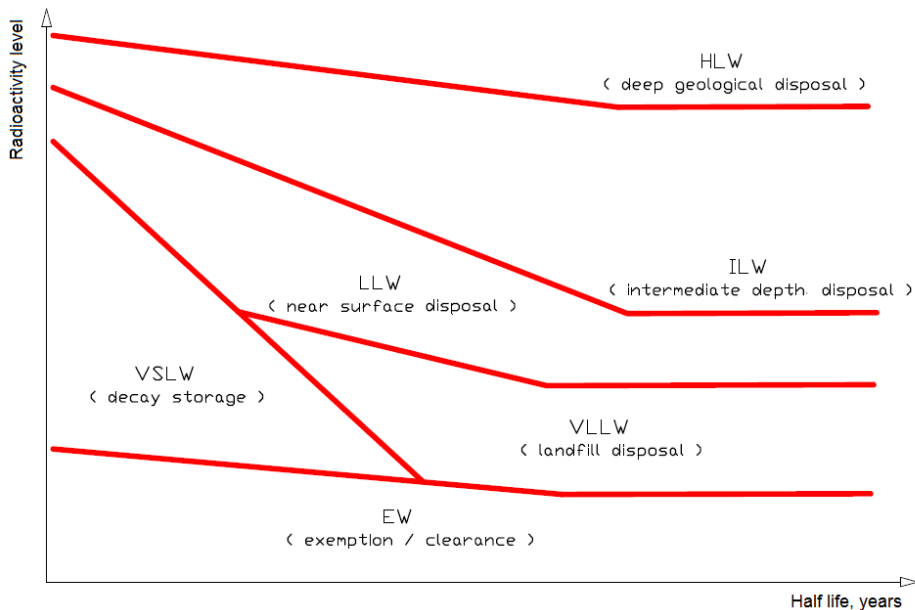


Figure 1.1. Waste classification scheme: EW – exempt waste, VLLW – very low level waste, VSLW – very short lived waste, LLW – low level waste, ILW – intermediate level waste, HLW – high level waste

In addition to Table 1.1 the figure 1.1 contributes to a better understanding of the radioactive waste classification.

Aqueous radioactive waste (ARW) is created throughout the duration of the operations regarding nuclear reactor and also during radioisotopes application in industrial and institutional domain. The most volume of ARW is generated from nuclear power plants. During their operation, some equipment and installations are contaminated and need to be decontaminated. As a result of decontamination process, ARW is produced. The chemical compositions and radioactivity levels of the generated waste are directly related to the operation that generated them. Practice has shown that it is preferable the treatment at the place of production of any type of ARW. Mixing of ARW from different sources and then treating them is less common. In Table 1.2 can be found the ARW sources and characteristics [5]. Aqueous wastes containing short lived beta/gamma activity are kept in storage. After decay to exclusion limit, if these wastes meet the regulatory requirements on chemical and biological hazards, they can be safely discharged into the environment.

1.2. Operations used in processing of aqueous radioactive waste; Treatment significance

Aqueous radioactive waste (ARW) is a complex system of the liquid micro-suspension type having the radioactive species solubilized in the liquid phase or fixed (by sorption or

chemically generated) on the solid micro-particles. In some cases, the ARW can be considered as a homogenous solution containing ionized species. For separation of radioactive species from ARW can be used different procedures, starting with classical hydrodynamics procedures and finishing with membrane and chemical procedures.

Aqueous wastes that have higher radioactivity content and/or long lived radionuclides may be treated using ion exchange/sorption, chemical precipitation, and/or evaporation, reverse osmosis, filtration and solvent extraction [6]. The main characteristics and limitations of some from the mentioned treatment processes are mentioned in Table 1.3.

Table 1.2. Sources of ARW [5]

Source	Typical radioisotopes	Characteristics
Nuclear research centers	Might include relatively long lived, mixed with short lived	- Generally uniform batches with nearly neutral pH from regeneration of ion exchange resins
Radioisotopes Lab. production	Wide variety depending upon production and purity of targets	- Small volumes of high specific activity and high chemical concentrations - Larger volumes of low specific activity
Radiolabelling and radiopharmaceuticals	¹⁴ C, ³ H, ³² P, ³⁵ S, ¹²⁵ I	- Small volume of predictable chemical composition
Medical diagnosis and treatment	^{99m} Tc, ¹³¹ I, ⁸⁵ Sr	- Large volumes of urine from patients - Small volumes from preparation and treatment
Scientific research	Variable, with short and long lived radioisotopes	- Extremely variable
Industrial and pilot plants	Depends upon application	- Volumes could be large and chemical composition undefined
Laundry and decontamination	Wide variety likely	- Large volumes with low specific activity but containing complexing agents

Table 1.3. Features and limitations of different ARW treatment options [5]

Treatment methods	Features	Limitations
- Chemical precipitation, coagulation, flocculation, separation	- Suitable for large volumes and high salt content of ARW - Easy industrial operations - Not expensive	- Generally lower DF* than other processes ($10 < DF < 10^2$) - Efficiency depends on solid-liquid separation step (final process step)
Ion exchange with polymeric resins	- DF good at low salt content in ARW (10^2) - Good mechanical strength - Regenerable resin	- Limited stability of resins at radiation, thermal and chemical stress - Resins cost is important - Complex immobilization of ions by resins
Ion exchange with inorganic materials	- Chemical, thermal and radiation stability better than organic ion exchangers - Relatively easy immobilization - Large choice of products ensuring	- Affected by high salt content - Blockage problems of ion exchange - Possible high cost - Difficult regeneration and recycling

	high selectivity DF > 10 to 10^4	
Evaporation	- Well established technology - High volume can be processed - Suitable for a large number of radionuclides - DF > 10^4 to 10^6	- Process limitations (scaling, foaming, corrosion, volatility of certain radionuclides) - Very high operation costs - High capital costs
Reverse osmosis	- Removes dissolved salts - Economical process Established for large scale operations - $10^2 < \text{DF} < 10^3$	- High pressure system, limited by osmotic pressure - Non-backwashable - Subject to fouling
Ultrafiltration	- Separation of dissolved salts from particulate and colloidal materials - Good chemical and radiation stability for inorganic membranes - Work at moderate pressure	- Fouling-need for chemical cleaning and backflushing - Organic membranes subject to radiation damage - Clogging of membranes in some cases
Microfiltration	- Low pressure operation (100 – 150 kPa) - High recovery (99%) of microsolid - Can be used as an excellent ARW pretreatment stage - Low fouling when air backwash is used for regeneration	- Backwash frequency can be high, depending on solid content of waste stream (ARW) - In some cases requires special filtration surface
Electrochemical	- Electroosmosis or electrolysis are the basic processes - Low energy consumption - Enhances the effectiveness of electrode reactions	- Sensitive to impurities in waste stream - Ionic strength of waste stream can effect the separation performance - Fouling is a problem in concentrated media (over 10 g/L total solids)
Solvent extraction	- Selectivity enables removal, - Can recover for recycling of actinides	- Organic material (solvent) appears in aqueous raffinate - Generates aqueous and organic secondary waste

*DF – decontamination factor that is the ratio of pollutant concentration for initial and processed solution

The main goal of radioactive waste treatment is to increase the safety and to improve technical and economical parameters of further radioactive waste management phases by:

- Radioactive waste volume reduction;
- Removal or concentration reduction of radionuclides from the waste;
- Changing radioactive waste characteristics;
- Changing radioactive waste composition.

Treatment is an essential step in the management of radioactive waste, it has as purpose the volume minimization of generated wastes in order to increase the safety and/or cost reduction of

further management stages. The selection of the waste treatment process is related to its radiological and physicochemical properties and also to the volume that has to be processed.

After the treatment stage, the wastes are separated in two parts, the first contains a small volume of concentrate containing the most part of radionuclides that remains in the management process and the second contains the bigger volume with no or low radioactivity that can be discharged to the environment if it meets the regulatory requirements.

On global scale, awareness regarding the treatment of radioactive is becoming more and more significant due to the recognition of how important it is to protect human health and the environment from the side effects of radiation connected to these wastes. The treatment of liquid radioactive wastes consists generally in conventional methods after the chemical and biological characteristics are taken into consideration.

In liquid radioactive waste processing, as a rule, two major problems are to be solved:

- (1) decontamination from radionuclides and harmful chemical substances to levels prescribed by regulations and
- (2) reduction of the volume of secondary radioactive waste to a maximum possible extent.

Regarding the significance of the ARW treatment must be considered the fact that the treatment itself is a technological process, usually quite complex, which produces a radioactive concentrate associated with the treated waste and applied method. The radioactive concentrate requires advanced processing and disposal. The knowledge that is available for classical water purification processes can be applied to radioactive waters. However, in the attempt to use these water treatment processes for the specific needs of radioactive waste management some supplementary problems may occur. The selected treatment process can be based on conventional chemical treatment principles, but the individual sources and the characteristics listed below of each waste stream must be considered.

Recently, worldwide, some tendencies have come up that influence the choice and application of radioactive waste management strategy and technology. These tendencies include: issuing new legislation and regulations, new strategies for waste minimization, strengthening the quality assurance procedures, increasing the use of safety and risk assessment physical protection and safeguards measures in the design and operation of waste management facilities, and new technological options [7].

1.3. Liquid radioactive waste characterization

The extremely important precondition for the efficient and economic management of all types of radioactive wastes is a comprehensive knowledge of their amount and composition. The properties of wastes arise from their origins. Reliable and effective methods for measuring radiological, physical, chemical, radiochemical and other characteristics are available to characterize wastes generated by various technological operations.

Sometimes, there is the opportunity to influence the waste generating process design so that wastes generated will require little or no treatment. If that is not possible and treatment is required, proper control of physical, chemical and radiochemical parameters of radioactive waste has a great importance in the evaluation and implementation of appropriate treatment technologies.

Generally and particularly, in the case of radioactive waste, the characterization signifies establishing the radiological, chemical and physical properties of the waste in order to determine the need for treatment, handling, processing, storage or disposal of radioactive materials.

Waste acceptance criteria (WAC) represent the conditions imposed by the regulator for a waste generator and/or operator of a waste (handling, transportation, storage, processing and/or disposal service). The WAC generally state such information as the required physical form of the waste, maximum levels of radioactivity, packaging requirements, etc. as well as what wastes are excluded from their service.

The main components in any waste management strategy are: adequate control of chemical and radiochemical parameters of radioactive waste during the entire waste management life cycle, and testing of the quality of final waste forms and waste packages. Any inaccuracy in control procedures during the management process can have as result important unwanted consequences as non-compliant waste packages that cannot be long term stored or disposed according to regulations and waste acceptance criteria.

Various characterization actions can be completed during different stages of the radioactive waste life cycle: during generation, processing (treatment, conditioning) and storage/disposal and these depend on:

- waste type or waste form;
- the disposal concept;
- the regulatory regime;
- the available process knowledge;
- the required characteristics to be measured [8].

For a proper waste characterization is required the collection of data regarding its properties and also the processing parameters and quality assurance. Based on the experiences from various waste generators, waste processing organizations, and waste characterization laboratories it can be said that the main elements include, but are not limited to, the radioactivity, physico-chemical, mechanical, thermal and biological properties.

It is essential to identify the most important criteria for waste characterization as soon as possible during the life cycle of waste management. The main benefits of waste characterization can be observed when the waste generator takes into consideration the investments and operating costs of the process at this early stage.

Generally, radiological waste characterization involves detecting the presence of individual radionuclides and quantifying them in the waste. This characterization can be performed by different techniques, depending on the waste form, radionuclides involved and level of accuracy required.

In order to characterize the waste from a chemical point of view one must determine the chemical components and the properties of the waste by performing a chemical analysis of a waste sample. For physical characterization, one must inspect the waste in order to determine its physical form, strength, resistance, etc.

Process knowledge, non-destructive examination and non-destructive assay (NDE and NDA) and destructive analysis (DA) are considered the main techniques employed for waste characterization purposes.

Radiological and chemical waste characterization can be indirectly determined from process knowledge. For example, for a researcher who only uses specific radionuclides for his experimental conditions, or for a manufacturer who uses specific chemicals, can be determined from the "knowledge of the process" which radionuclide(s) and/or chemicals may be found in the waste.

NDA techniques are based on the detection of a photon flux and/or neutron flux from waste or waste package surfaces. The accuracy of the results depends on the complexity of the waste being measured and the sophistication of the systems. These systems can range from low resolution gamma spectrometry to segmented gamma scanning (SGS) with transmission correction (TC), transmission/emission computed tomography (T/ECT) and from passive neutron counting to active/pассивneutron interrogation combined with SGS.

Characterization of waste by destructive methods (DA) leads to an accurate and complete determination of the radionuclide inventory. The reliability of these determinations regarding the

waste flux to be characterized depends on the sample representativeness and homogeneity of the waste stream. The concentration of difficult to measure (DTM) nuclides (alpha, pure beta and X ray and low energy gamma emitters) is usually determined by destructive assay.

Counting systems for isolated alpha emitting nuclides are solid scintillation counters ($\text{ZnS}(\text{Ag})$) or proportional counters. In the case of a mixture of alpha emitting nuclides, alpha-beta discrimination liquid scintillation counters (LSC) can be used, which give alpha spectra with low resolution. More accurate measurement can be achieved with alpha spectrometry with semiconductor detectors (approx. 12 keV of resolution), which allows the determination but does not avoid the chemical separation process.

Pure beta emitting nuclides can be determined by proportional counters but the most effective method is LSC, which can determine beta emitters with $\beta_{\max} \leq 2000$ keV with previous separation processes.

X ray and low gamma emitting nuclides can be determined by low energy gamma spectrometry with complex mixtures germanium detectors. The low concentration of these emitters, when compared with the high-energy macro-component gamma nuclides (e.g. ^{137}Cs), may require chemical separations prior to measurements. If no interference is found in a complex mixture of X ray and low energy gamma emitters, direct measurement could be carried out.

High energy gamma emitting nuclides can be determined by direct measurement in an appropriate geometry by solid scintillation gamma spectrometry (low resolution). High resolution gamma spectrometry with semiconductor detectors may be applied when a complex mixture of gamma emitters is treated before separation or if the waste has a simple composition of gamma emitters by direct measurement of the dissolved sample.

In our case, liquid radioactive waste, is categorized as aqueous and organic liquid wastes. The composition of ARW can cover a very wide range with respect to both radioactivity and the presence of hazardous chemical species. The characterization of ARW in order to allow the selection of liquid waste treatment strategy has to be focused on knowing the following characteristics:

Specific radioactivity of ARW. Many ARW will contain specific groups of nuclides. It must be known the γ emitting radionuclides presence and the radioactivity concentration for each radionuclide and also, the presence of alpha-emitting and beta/gamma-emitting nuclides. Some streams will contain all three categories.

Chemical composition of ARW. Specific activity and radiological safety are reasons that these wastes are regulated, but the chemical and in some cases the biological characteristics, can create

problems and have to be considered for a proper management of the waste. Incomplete informations regarding the chemical nature of the ARW may result in inadequate decontamination and could even damage the waste processing facilities.

pH value. The pH value is important in collection, storage and treatment strategies. The control of feedwater pH can sometimes be advantageously employed in the treatment of waste containing metal ion complexes, in order to form an undissociated acid or base. Adjustment of the pH can be used to modify the state of ionic species present in the waste stream. This may influence the choice of separation materials and the operating conditions used in the treatment process.

Zeta potential. The Zeta potential is important for heterogenous ARW containing dispersed particles. Because it measures the potential difference between the dispersion medium and the stationary layer of fluid attached to the dispersed particle, the Zeta potential is important in chemical treatment that involves coagulation and flocculation dosages.

Electrical conductivity. The electrical conductivity of an aqueous liquid gives a measure of its total dissolved salt/salts content and will indicate if electrochemical treatment can be considered. Also, it is important in reverse osmosis treatment methods.

Turbidity. Turbidity indicates the presence and gives a measure of concentration of colloidal particles in ARW. It is a suitable measuring method for some kind of separation process, as microfiltration, ultrafiltration or deep bed filtration.

Chemical oxygen demand (COD). The chemical oxygen demand of a liquid (solution, polluted water, ARW, etc) is a measure of the amount of oxygen that can be consumed by oxidation reactions due to their organic content. Sometimes it is an important characteristic in chemical treatment methods. If organic liquids are present in ARW there, depending of these concentration, is a possibility of emulsion formation which would adversely affect the performance of flocculation and filtration techniques. [9].

Harmful chemical substances. Some ARW can contain hazardous materials and such radioactive waste is called mixed waste. Hazardous wastes are defined as wastes that are toxic, corrosive, flammable, or reactive and can contain: a) halogenated solvents (carbon tetrachloride, TCE, chloroform), b) aromatics, c) toxic organics (EDTA, PCBs, TBP, etc.), d) other toxic (heavy metals (Hg, Cr, Cd), Be, cyanides, etc.), e) nitrates, f) corrosive chemicals, g) oils, flammables, h) reactive chemicals as explosives, pyrophorics, strong oxidizers, k) biohazardous agents. The proper characterization of mixed waste is very important in selecting of waste treatment technology (methods and facilities).

Form of the impurities. The concentration of chemicals dissolved in the ARW and the amount of suspended matter have a considerable influence in establishing if a pretreatment step is necessary before the main treatment can be applied and on the performance of decontamination processes. For example, filtration may be necessary to remove suspended solids before applying ion exchange or membrane separation processes.

1.4. Characterization and analysis methods used in DMDR IFIN-HH

The experimental part of this thesis was developed at Horia Hulubei National Institute for Physics and Nuclear Engineering (IFIN-HH). In its development, has been used ARW from different sources. In cases where it was not necessary to work with ARW (measurements to identify the parameters of some investigated processes), synthetic solutions were used. Measurements were performed with high accuracy using working procedures and measuring/control equipment available at IFIN, which will be reviewed in the following.

Gamma spectrometry. Gamma ray spectrometry is an analytical technique that permits the detection and quantitative determination of gamma emitting isotopes in different matrices. This type of analysis allows the identification of several gamma emitting radionuclides in one measurement and easy sample preparation. The result of the measurement is a spectrum of lines, the amplitude being proportional to the activity of the radionuclide and its position on the horizontal axis indicates its energy.

Most radioactive sources produce gamma rays of various energies and intensities. When these are gathered and analyzed with a gamma-ray spectroscopy system, a gamma-ray energy spectrum can be obtained. A thorough analysis of this spectrum is generally used to determine the type and amount of gamma emitters existent in the source.

A typical gamma spectrometry system consists of a Germanium (Ge) detector, liquid nitrogen or mechanical cooling system, preamplifier, detector bias supply, linear amplifier, analog-to-digital converter (ADC), multichannel storage of the spectrum, and data readout devices. The detector is often housed within a shield to reduce the background caused by sources other than the sample. The shield is constructed of a dense material (such as lead) that will absorb a large portion of background gamma rays. The sample is positioned within the shield at some distance from the detector. The distance will depend on a number of parameters, such as expected count rate and geometry of the sample container [10].

Equipment and working conditions. The equipment currently used in IFIN-HH DMDR-Lab for this type of analysis is **Gamma spectrometric installation Canberra 1 (Detector 1)** (fig. 1.2a)

having a HPGe coaxial GC3019 type detector. The following data show the device characteristics: measuring interval 50 – 10 000 keV; detector diameter 76 mm, Ge crystal diameter 60.5 mm; Ge crystal length 50.5 mm; resolution 0.863 keV at 122 keV (Co-57) and 1.76 keV at 1332 keV (Co-60); peak/compton ratio 58.2: 1; relative efficacy 31.2%; lead shield type 7500SL; DSA 1000 type Multichannel Analyzer; data acquisition and spectra processing software GENIE 2000. The efficacy calibration of the detector was performed by LMR - IFIN-HH [11] with specific calibration sources for each analysis geometry. The calibration sources were manufactured by LMR - IFIN-HH [12, 13]. The device **Gamma spectrometric installation Canberra 1 (Detector 1)** (fig. 1.2a) is based on REGe namely Germanium Reverse-Electrode (REGe) detector type GR4020 with thin carbonate window, manufactured by CANBERRA. The device permits/contains the following characteristics: measuring interval 5 – 10 000 keV; detector diameter 76 mm, Ge crystal diameter 61 mm; Ge crystal length 65 mm; resolution 0.895 keV at 122 keV (Co-57) and 1.96 keV at 1332 keV (Co-60); peak/compton ratio: 58.9 : 1; relative efficacy 47.5%; lead shield, type 747 CANBERRA; DSA 1000 type Multichannel Analyzer; data acquisition software, using the Monte Carlo simulation to calculate the efficiency and gamma spectra analysis is GENIE 2000 and LabSOCS.

Measuring parameters were:

- Marinelli geometry;
- sample volume – 900 mL;
- spectra recording time - 60 000 s;
- detector distance – 0 cm.



(a)



(b)

Figure 1.2. Gamma spectrometric installation Canberra 1, Detector 1 (a) and Canberra 1, Detector 2 (b)

Tritium determination by liquid scintillator method. Tritium can be found in different occupational environments. Its half-life is 12.35 years. Because tritium has a very low beta radiation energy, liquid scintillation counting is the best method to determine its activity concentration in a given sample. Liquid scintillation counting is based on conversion of the kinetic energy of beta particles into light photons. In the sample vial, the scintillation cocktail converts the radiation emitted from the radionuclide into light pulses. The liquid scintillation analyser detects the light photons when they enter in the photomultiplier tubes. Samples often contain materials that interfere with the radiation detection process. These materials are known as quenching agents. Two types of quenching can occur. First, a chemical quenching agent interferes with the production of photons in the scintillator. Second, a colour-quenching agent hinders the detection of the photons. Both types of quenching will decrease the counting efficiency. In general, for quantitative measurements, corrections must be made for quenching. However, when counting tritium in the form of HTO, the sample can be distilled. The tritiated water follows the H₂O and the purified sample does not require quench correction.

Equipment and working conditions. The Tri-Carb 2910TR is a computer-controlled benchtop versatile and sensitive liquid scintillation analyzer, for detecting small amounts of alpha, beta and gamma radioactivity. The Tri-Carb liquid scintillation counter relies on the interaction between a beta-emitting radionuclide and a scintilator, a component of the scintillation cocktail. The scintillator converts ionizing radiation from the radionuclide into photons of light (scintillation). The intensity of the light produced during scintillation is proportional to the initial energy of the beta particle.



Figure 1.3. TriCarb 2910 TR Analyzer

For tritium concentration measurement in ARW samples is used the TriCarb analyzer, type 2910 TR and the liquid scintillator Ultima Gold type, manufactured by PerkinElmer.

Figure 1.3 shows a general image of this analyzer. It has the following components: Varisette™ automatic sample changer; measuring chamber, located under the automatic sample changer level; two photomultipliers mounted at 180° and coupled to a reflective optical chamber; coincidence time set at 18 ns; the sample to be measured and the photomultipliers are surrounded by a minimum of 2 inches of lead; external standard: Ba-133 (695.6 KBq/15 ian. 2011); multichannel analyzer with 1/10 keV resolution, with luminescence and colour; correction possibility; adjustable temperature by cooling device; PC for analyzer control, spectra acquisition and data processing; QuantaSmart software. The sample-LCS mixture is performed in glass vials, 20 ml volume, low K content and plastic lids with optical reflector. The equipment is calibrated at LMR - IFIN-HH.

Gross α, β determination. Gross alpha/beta activity measurement is applied widely as a screening technique in the field of radioecology, environmental monitoring and industrial applications. Generally, gross alpha and beta activities are analyzed as the first step to determine whether analyses for specific radionuclides with sophisticated procedures are needed. Gross alpha is more of a concern than gross beta as it refers to the radioactivity of Th, U, Ra as well as Rn and descendants. For anthropogenic radioactivity, gross alpha may pertain to screening for transuranics in wastes, while gross beta to screening for fission products. Samples are slowly evaporated (avoiding boiling) on a heating plate (70°C) to 30–50 ml volume. Afterwards are transferred quantitatively to a porcelain crucible and evaporated to dryness. The samples are allowed to cool down in a desiccator before determining the weight. Because the sample is evaporated and later heat-treated, the method does not allow determination of the volatile radionuclides (e.g. ^3H , ^{210}Po , ^{137}Cs), which escape from the sample and the residue during heat treatment. Therefore, even the gross alpha and beta activity concentration might be underestimated, ^3H is measured by liquid scintillation method and ^{137}Cs by gamma spectrometry.

Equipment and working conditions. The equipment used is the MPC-2000-DP model, manufactured by ORTEC – Protean (fig. 1.4). It allows the measurement and monitoring of gross α and β radioactive concentrations, in different media and for different materials by means of a low background alpha and beta activity measurements, with multiple detectors. The equipment can be used for: i) gross α and β radioactive concentrations for solids and liquids, ii) gross α and β radioactive concentrations monitoring for environmental factors, ores, radioactive waste,

nuclear industry materials and iii) gross α and β radionuclide content characterization in different samples.



Figure 1.4. MPC-2000-DP model ORTEC – Protean

Physical characterization methods. The most important physical properties of a waste stream which could influence its treatment are the pH, conductivity (as a measure of total dissolved solids (TDS)), total suspended solids (TSS) concentration, radioactivity deposited on the solid phase, fractions of gravimetric and colloidal suspensions in ARW (if these are present).

Equipment and working conditions. In this experimental investigation the pH was measured with Hanna HI 4222 model pH-meter, conductivity and TDS were performed with Schott Lab960 model conductivity meter equipped with two conductivity cells, standard cell (LF413T), with $0.475 \text{ cm}^{-1} \pm 1,5\%$ cell constant and very low conductivity cell (LF313T) with $0.100 \text{ cm}^{-1} \pm 2\%$ cell constant, respectively. Both cells have incorporated temperature probes.

Radioactivity deposited on the solid phase was determined by gamma spectrometry; the gravimetric content of solid in ARW suspensions has been determined by normal vacuum filtration with filter membrane having on $0.45 \mu\text{m}$ mean pore diameter and the colloids presence in ARW suspensions was determined by vacuum ultrafiltration on 50 nm membranes.

Chemical characterization methods. The bulk composition and chemical properties of the waste should be known to the extent that any chemical hazards or challenges posed by the waste can be assessed. By examining chemical and physical properties, the required processing limits may be defined. Usually, in ARW, radioactive substances form only a minor component. Other components, the majority, are non-radioactive and harmless.

Equipment and working conditions. Total organic carbon (TOC) was determined by sample digestion with sulphuric acid and peroxodisulfate at 120°C for 2 h, when it occurs the oxidation

of compounds containing carbon to carbon dioxide. The released CO₂ quantity was measured by molecular absorption spectrophotometry and then converted into the corresponding O₂ quantity necessary for the CO₂ formation. Was used an UV-Vis Spectrophotometer, type Pharo 300 (fig. 1.5) and Spectroquant® analytic kits manufactured by Merck.



Figure 1.5. UV-Vis Spectrophotometer, model Pharo 300

The Li⁺, K⁺, Na⁺, Ca²⁺, Mg²⁺, NH₄⁺, F⁻, Cl⁻, Br⁻, NO₃⁻, SO₄²⁻, PO₄³⁻ concentrations were determined by ion-chromatography using a Dionex ICS-5000 chromatography system (fig. 1.6). For anion separation was used a Dionex™ IonPac™ AS22 IC analytic column in which the stationary phase consisted of a hyper-branched polymer, electrostatically attached to the surface of a polymeric substrate.



Figure 1.6. Ion-chromatography system model Dionex ICS-5000

The anions were desorbed onto a separation column using isocratic carbonate/bicarbonate eluent and identified by the retention time, RT, with a conductivity detector with eluent chemical suppression. Conductivity signal intensity is directly proportional to the respective analyte concentration. The concentrations were determined with the aid of the calibration curves obtained using a Combined Seven Anion Standard Solution (F^- , Cl^- , NO_2^- , Br^- , NO^{3-} , SO_4^{2-} , PO_4^{3-}), certified and NIST traceable (National Institute of Standards and Technology, USA).

For cation separation was used a Dionex™ IonPac™ CS12A IC packed column with ethylvinylbenzene/divinylbenzene functional polymer. For removal of cations adsorbed onto the column was used methanesulphonic acid as eluent. Detection was performed with a conductivity detector with eluent chemical suppression. Conductivity signal intensity is directly proportional to the respective analyte concentration. The concentrations were determined with the aid of the calibration curves obtained using a Combined Six Cation Standard Solution (Li^+ , NH_4^+ , Na^+ , Mg^{2+} , Ca^{2+} , K^+), certified and NIST traceable (National Institute of Standards and Technology, USA).

In the eluent chemical suppression working technique, the eluent that exists in the separation column passes through a suppressor containing an ion-exchange membrane. This retains the eluent ions in order not to influence the conductivity signal of the analyte.

Heavy metals concentrations were determined by inductively coupled plasma optical emission spectrometry using the Spectroblue model manufactured by SPECTRO (fig. 1.7).



Figure 1.7. Inductively coupled plasma optical emission spectrometer model Spectroblue

The analyte, in liquid state, is pulverized and the resulted aerosole is carried by a gas flow (Argon) towards the plasma torch where the sample elements are ionised and the resulting ions

are excited. When the excited atoms return to low energy position, an energy quanta is emitted as a characteristic atomic emission spectral line. These spectral lines are recorded as a single spectrum that is dispersed by the spectrometer slits and the spectral lines intensity is monitored by detectors. From here, the signals are controlled and processed by a computerised system.

The radiation intensity, proportional to the concentration of the sample element, is internally recalculated from the stored calibration curve and is directly indicated as percentage concentration. The calibration curve was traced using standard mono or multielement solutions, certified and NIST traceable.

The CN⁻, Cr⁶⁺, total N, S²⁻, SO₃²⁻ concentrations were measured by molecular absorption spectrophotometry, UV and VIS range, using a UV-Vis Pharo 300 spectrophotometer (fig. 1.5) and Spectroquant® analytical kits manufactured by Merck.

Laboratory tests using real samples of the radioactive waste to be treated were performed to establish the correct conditions for operation. Tables 1.4-1.6 show an example of an analysis of one initial ARW effluent, proposed to be treated with the device from IFIN-HH. These tables contain physical characteristics, radioactivity and chemical parameters of the ARW to be processed.

Table 1.4. Physical characteristics of an ARW batch

Nr. crt	Physical characteristic	u.m	Value
1	pH	pH units	7.1
2	Conductivity	µS/cm	1240
3	Salinity	conventional	0.5
4	TDS	mg/L	720
5	TSS	mg/L	60
6	Gross SS	mg/L	32.9
7	Fine SS	mg/L	27.1

Table 1.5. Radioactive characteristics of an ARW batch

γ emitting radionuclides sorbed on coarse particles	⁶⁰ Co	Bq/L	0.11
	¹³⁴ Cs		< AMD
	¹³⁷ Cs		0.41
	¹⁹² Ir		< AMD
	²³⁵ U		< AMD
	²³⁸ U		< AMD
	²⁴¹ Am		0.93
γ emitting radionuclides sorbed on fine particles	⁶⁰ Co	Bq/L	< AMD
	¹³⁴ Cs		< AMD
	¹³⁷ Cs		3.23
	¹⁹² Ir		< AMD
	²³⁵ U		< AMD
	²³⁸ U		< AMD
	²⁴¹ Am		< AMD

γ emitting radionuclides dissolved in liquid phase	^{60}Co	Bq/L	1.82
	^{134}Cs		< AMD
	^{137}Cs		17.9
	^{192}Ir		< AMD
	^{235}U		< AMD
	^{238}U		< AMD
	^{241}Am		< AMD
H ³ concentration in liquid phase	-	Bq/L	35 700
Gross β *	-	Bq/L	34.7
Gross α **	-	Bq/L	0.11

* Gross β activity is equivalent ^{90}Sr ; ** Gross α activity is equivalent ^{241}Am

Table 1.6. Chemical characteristics of an ARW batch

Nr. crt	Ionic species	u.m	value
1	NH_4^+	mg/L	< 0.01
2	NO_3^-		3.56
3	NO_2^-		< 0.01
4	SO_4^{2-}		137.10
5	Cl^-		100
6	Br^-		< 0.01
7	F^-		0.39
8	PO_4^{3-}		3.43
9	Ca^{2+}		76.13
10	Mg^{2+}		35.61
11	Na^+		238.86
12	K^+		14.64
13	Li^+		0.03
14	Al^{3+}		< 0.01
15	S^{2-}		< 0.10
16	SO_3^{2-}		< 1.00
17	As^+		< 0.01
18	Pb^{2+}		< 0.01
19	Cd^{2+}		0.09
20	$\text{Cr}^{3+}, \text{Cr}^{6+}$		0.02
21	$\text{Fe}^{2+}, \text{Fe}^{3+}$		0.48
22	Cu^{2+}		0.46
23	Ni^{2+}		0.34
24	Zn^{2+}		0.16
25	Hg^{2+}		< 0.01
26	Ag^+		< 0.01
27	Se^{2+}		< 0.01
28	Mn^{2+}		0.21
29	CO_2		0.59
30	COD		72.60

REFERENCES

- [1] A Report by the International Nuclear Safety Advisory Group, *Basic Safety Principles for Nuclear Power Plants: 75-INSAG-3 Rev. 1*. Vienna, International Atomic Energy Agency, 1999.
- [2] Food and Agriculture Organization of the United Nations, International Atomic Energy Agency, International Labour Organization, Nuclear Energy Agency of the Organisation for Economic Co-Operation and Development, Pan American Health Organization, World Health Organization, *International Basic Safety Standards for Protection against Ionizing Radiation and for the Safety of Radiation Sources, Safety Series No. 115*, Vienna, International Atomic Energy Agency, 1996
- [3] IAEA Safety Standards - *Classification of Radioactive Waste for protecting people and the environment, General Safety Guide No. GSG-1*, Vienna, International Atomic Energy Agency, 2009
- [4] *Standardization of Radioactive Waste Categories; TRS No. 101*, Vienna, International Atomic Energy Agency, 1970
- [5] *Review of the Factors Affecting the Selection and Implementation of Waste Management Technologies; IAEA-TECDOC-1096*, Vienna, International Atomic Energy Agency, 1999
- [6] *Handling and Processing of Radioactive Waste from Nuclear Applications; TRS No. 402*, Vienna, International Atomic Energy Agency, 2001
- [7] R.O. Abdel Rahman, H.A. Ibrahium, Y.T. Hung, *Liquid Radioactive Wastes Treatment: A Review*, Water, **3**, 551-565, 2011
- [8] International Atomic Energy Agency, Strategy and Methodology for Radioactive Waste Characterization, IAEA-TECDOC-1537, Vienna, 2007
- [9] *Chemical Precipitation Processes for the Treatment of Aqueous Radioactive Waste, TRS No. 337*, Vienna, International Atomic Energy Agency, 1992
- [10] *Guidelines for Low Level GammaSpectrometry – Air Filters, Water, and Soils*, <https://www.ortec-online.com/-/media/ametekortec/application%20notes/guidelines-low-level-gamma-spectrometry.pdf?la=en>
- [11] A. Luca, B. Neacsu, A. Antohe, M. Sahagia, *Calibration of the High and Low Resolution Gamma-ray Spectrometers*, Rom. Rep. in Phys., **64(4)**, 968–976, 2012
- [12] M. Sahagia, L. Grigorescu, *Water equivalent solid standard sources*, Nucl. Instr. and Meth. in Phys. Res. A, **312**, 236–239, 1992
- [13] M. Sahagia, A.C. Razdolescu, A. Luca, R. Macrin, *Volume standard sources in soil matrix*, Rom. J. Phys., **42(9-10)**, 659-663, 1997

CHAPTER 2. AQUEOUS RADIOACTIVE WASTE (ARW) TREATMENT BY COMBINED METHODS IN MODULAR INSTALLATIONS

In modern practice, the ARW processing can be carried out in modular low or medium capacity installations [1]. They are mobile, meaning the installation is shiftable to the ARW source, or fixed, when the ARW is brought to the installation. A modular design is more flexible and adequate for the relatively small volumes of waste having a variety of characteristics. A modular ARW processing installation contains a collection of autonomous treatment modules (three to six) that can be combined in a technological arrangement. The components of the modular system can be supplemented, changed, decreased to meet technical requirements for adequate purification.

ARW treatment using modular approach presents multiple advantages, as: 1) rapid delivery and assembly compared to fixed plant installation; 2) minimization of site infrastructure requirement and disruption; 3) integration of best available technology and use of commercially available items where available/applicable; 4) reduction of the risks related to the design of process; 5) full assembly, testing and inactive commissioning can be completed in the factory; 6) shortest possible installation and commissioning programme on site; no risks for site based activities; 8) simplified opportunities to develop/augment plant should operational requirements dictate; 9) simplified decommissioning by process and/or module; 10) opportunity to redeploy. This chapter contains considerations on some unit operations and on some technical procedures, which are present in the modular installation for ARW treatment from IFIN HH Bucharest.

2.1. General considerations

Liquid radioactive waste (LRW) represents any heterogenous system that has radioactive material suspended in liquid and/or distributed in liquid as solution. The LRW liquid phase can be aqueous or organic solutions (for example, spent extraction agents). Radioactive aqueous solutions make up more than 99% of LRW, therefore, further LRW is considered only aqueous solution.

Radionuclides and impurities are found in various forms in aqueous radioactive waste (ARW) solution. The following main forms of impurities an ARW can contain as radionuclides are: i) suspended particles or emulsified oil products (particle sizes from 10^{-7} m up to several millimeters), ii) colloidal particles or micelles (particle sizes from 10^{-8} m up to 10^{-7} m), iii)

dissolved organic compounds and/or surfactants (particle sizes from 10^{-9} m up to 10^{-8} m), iv) ions (particle sizes from 10^{-10} m up to 10^{-9} m).

It is important to understand that treatment of radioactive liquids always has as result the formation of a radioactive concentrate. Efficiency of ARW purification is determined not only by the purification factor from radionuclides, K_{pur} , but also by the radionuclides concentrating factor in the final volume, K_{con} [2]. For i -th radionuclide, purification factor can be determined by the equation (2.1):

$$K_{pur,i} = \frac{C_{i,0}}{C_{i,f}} \quad (2.1)$$

where

$C_{i,0}$ and $C_{i,f}$ – concentrations of i -th radionuclide in initial solution and treated solution accordingly.

The concentrating factor of the same radionuclide is expressed by relation (2.2):

$$K_{con,i} = \frac{C_{i,k}}{C_{i,0}} \quad (2.2)$$

where

$C_{i,k}$ – concentration of i -th radionuclide in concentrate.

It is obvious that the higher factor of radionuclides concentrating, the less secondary radioactive waste is obtained, which require further conditioning and disposal. ARW purification factor should make up to such values, that the treated water could be discharged into the environment, according to regulations. Liquid radioactive waste treatment does not always require the complete extraction of all impurities. In a number of cases, when there is the possibility to selectively extract the toxic impurities (including radionuclides), and the chemical composition of treated water is similar in composition to the surface waters of the region, the developed technological treatment scheme can be simplified and hence, quantity of the secondary radioactive waste decreased. One of constitutive parts of ARW treatment technology is the further fate of the secondary radioactive waste, therefore, besides quantity of the secondary radioactive waste are also important properties such as: type, physical state and chemical composition, feasibility of their transformation in a solid monolith state following transportation and storage or disposal.

A large part of liquid radioactive waste that requires treatment, is low level radioactive waste. Specific radioactivity of these radioactive waters by β - and γ -radionuclides, as a rule, does not exceed 10^5 Bq/L, and by α -radionuclides – 10^3 Bq/L, therefore, factors of ARW purification

from separate radionuclides should be no more than 1000 – 10000. Such methods as filtration, sorption, microfiltration, ion-exchange, reverse osmosis, electrodialysis, coagulation, ultrafiltration and several others are often used for the purification of low level radioactive liquid waste. Taking into account a great variety of chemical and radiochemical compositions of radioactive waters, in each separate case should be developed an individual technological scheme for ARW treatment. Some features and limitation of different aqueous liquid treatment options were presented with table 1.3, in the first chapter.

ARW treatment generates secondary radioactive waste with high concentration of radionuclides, as liquid concentrates (ion exchange regenerants, ultrafiltration concentrate, concentrated solution from reverse osmosis, etc.) and/or strongly radioactive solids (deep filtration layer, depleted ion exchange resins, destroyed membranes, etc.). So, the problem of radioactive depollution must be seen in its entirety. In this sense, the table 2.1, presents an overview regarding the choosing of a processing technology, whether modular or not, of an ARW with their generated secondary radioactive wastes [3].

Table 2.1. Recommended procedure for radioactive wastes treatment upon state and source

Technology for:		Liquid and wet solid waste						Solid wastes			
Nr. crt.	Waste stream	ChT	IEx	ROs	TFI	CFl	BSI	Enc	LFC	UB	MHC
1	ARW low volumes						X				
2	ARW high volumes	X	X	X	X	X	X				
3	Organic LRW				X	X	X				
4	Sludge type RW (SRW)						X				
5	Ion exchange resins						X				
6	Compactable solid							X	X	X	
7	Non-compactable solid							X		X	
8	Disused sealed source (Short lived isotope $t_{1/2} < 30$ years)							X		X	
9	Disused sealed source (Long lived isotope $t_{1/2} > 30$ years)							X		X	
10	Disused sealed source (high and very high activity)										X
11	Biodegradable radioactive solids						X				

ChT-chemical treatment, IEx-ion exchange, ROs- reverse osmosis, TFI –tangential filtration, CFl – classic filtration , BSI-block solidification, Enc –encapsulation, LFC–low force compresion, UB- unshielded booth, MHC-mobile hot cells

It is worth noting that the solution of fixing radionuclides in blocks of solid materials namely cement blocking (BSI) or cement encapsulation (Enc) appears with high frequency in Table 2.1. It is also important to mention that sometimes radionuclides in liquid or solid wastes,

appear in unexpected ways in some widely used technologies. For example, can be mentioned the case of phosphogypsum wastes that have been tested in Romania as basic material for producing of BCA bricks. The excessively high radioactivity of this type of BCA allowed to see how, in phosphorus fertilizer technology, the radioactive impurities from basic phosphorite or apatite ores were concentrated in phosphogypsum. The recycling of wastes which have as radioactive origin building materials is being overseen with great attention all over the world [4].

Returning now to the problem of ARW treatment it should be noted that ARW can have a complicated chemical composition and a great variety of radionuclide types. So, the combination of various water-treatment methods is usually used in a concrete case. Practically, the treated water is consequently pumped through several different water-treatment equipments. A cascade of various water-treatment equipments, connecting pipelines, pumps, controlling and measuring apparatus and storage tanks make together a water-treatment installation. Water-treatment installations can be stationary or mobile. It is reasonable to use stationary installations in the presence of constantly forming liquid waste, which is characterized by a stable chemical and radiochemical composition. Mobile installations (especially of modular type) are characterized by flexibility of technological schemes, and hence, allow fast decisions in case of spontaneous liquid waste formation.

Often, compositions of liquid radioactive waste in neighboring storage-tanks is different. For the treatment of liquid radioactive waste and changing from one storage-tank to another it is usually required to change the technological treatment scheme. In this case mobile modular type installations are more useful. Such installation can be easily delivered to the site of ARW processing, and by means of combining water-purifying modules it is easy to assemble any optimal technological scheme in a short time. One of the main conditions of water-treatment modules compatibility is standardization of jointing units and productivity correspondence. Design experience of such installations has shown that the optimal productivity of a water-treatment module, providing its transportability, is about $0.2\text{--}1.5 \text{ m}^3/\text{h}$. At higher productivity the dimension of some water-treatment modules does not allow their placement in standard transport containers, and weight issues do not allow using them without an additional foundation and special load-lifting devices. At lower productivity the installation is not suitable for industrial use.

It can be noted that a number of the waste processing technologies could be applied to several different waste streams, therefore, it may not be necessary to have a different process module for each waste stream.

2.2. Modular installation for low and intermediate level aqueous radioactive waste treatment at IFIN-HH, Magurele, Romania

The modular ARW treatment system, used at IFIN-HH by the Radioactive Waste Management Department, consists of four individual modules: filtration module, ultrafiltration module, reverse osmosis module and adsorption on inorganic sorbent module [5].

The modular installation from IFIN-HH, named Aqua-Express (fig. 2.1), is a low and intermediate level liquid radioactive treatment unit designed for medium size research centers and other institutions, which have an activity that leads to the formation of a quantity up to 500 m³/year of low and intermediate level radioactive waters. It consists in four modules designed for treatment by filtration, ultrafiltration, reverse osmosis and adsorption methods. Each module contains different separation materials, corresponding pumps, measuring and control instruments. The purpose of ARW treatment process is the minimisation of volume of radioactive effluents obtaining a physico-chemical stable form and radioactive waste packages suitable for disposal. ARW volume minimisation is achieved by their separation into two streams: the concentrate stream that includes radionuclides and toxic impurities, and the purified effluent stream, whose content does not exceed environmental standards. Concentrates (as a solution), used washing solution, slurries, sorbents which have exhausted their capacity for adsorption, filtration materials and fouled membranes are considered secondary waste and they are sent to conditioning. The purified effluent, after radionuclidic and physico-chemical characterization confirming the fulfillment of legislation requirements, is discharged in the environment or is reused in the treatment facility.

Aqua Express installation was purchased from MosNPO "Radon" from Russia. It was integrated in the treatment plant and, in order to avoid leakage, flexible hoses were replaced by stainless steel pipes and modules were bolted to the floor. But, although it became stationary, it kept its flexibility, because a network of pipes was set-up and it still allows the possibility to combine the modules in different technological schemes addressed to the waste characteristics. Both separation materials and assembled configurations depend on initial ARW characteristics, on quality requirements of the final product and acceptance criteria for secondary waste disposal.

The basic characteristics of ARW accepted for treatment with Aqua Express installation are as follows: i) total γ -activity up to $1 \cdot 10^6$ Bq/L; main contaminants: $^{134}, ^{137}\text{Cs}$ ($1 - 5 \times 10^6$ Bq/L), ^{60}Co , corrosion products; ii) total β -activity mostly ^{90}Sr (up to 1×10^5 Bq/L); iii) total α -activity (up to 1×10^3 Bq/L); iv) pH 1–10; v) moderate salinity of waste (1–10 g/L, it can be a little higher in special cases).

The modular installation Aqua-Express is connected through a pipes network to the fixed part of the aqueous radioactive effluent treatment plant (STERAJMA). This part acts as a collection and storage of radioactive waste liquid and, also for the collection of by-products and the final product resulting from this system. Technological flow sheet of STERAJMA is presented in fig. 2.2.



(a) (b)
Figure 2.1. Filtration, ultrafiltration, reverse osmosis modules (a) and adsorption module (b) of Aqua Express installation

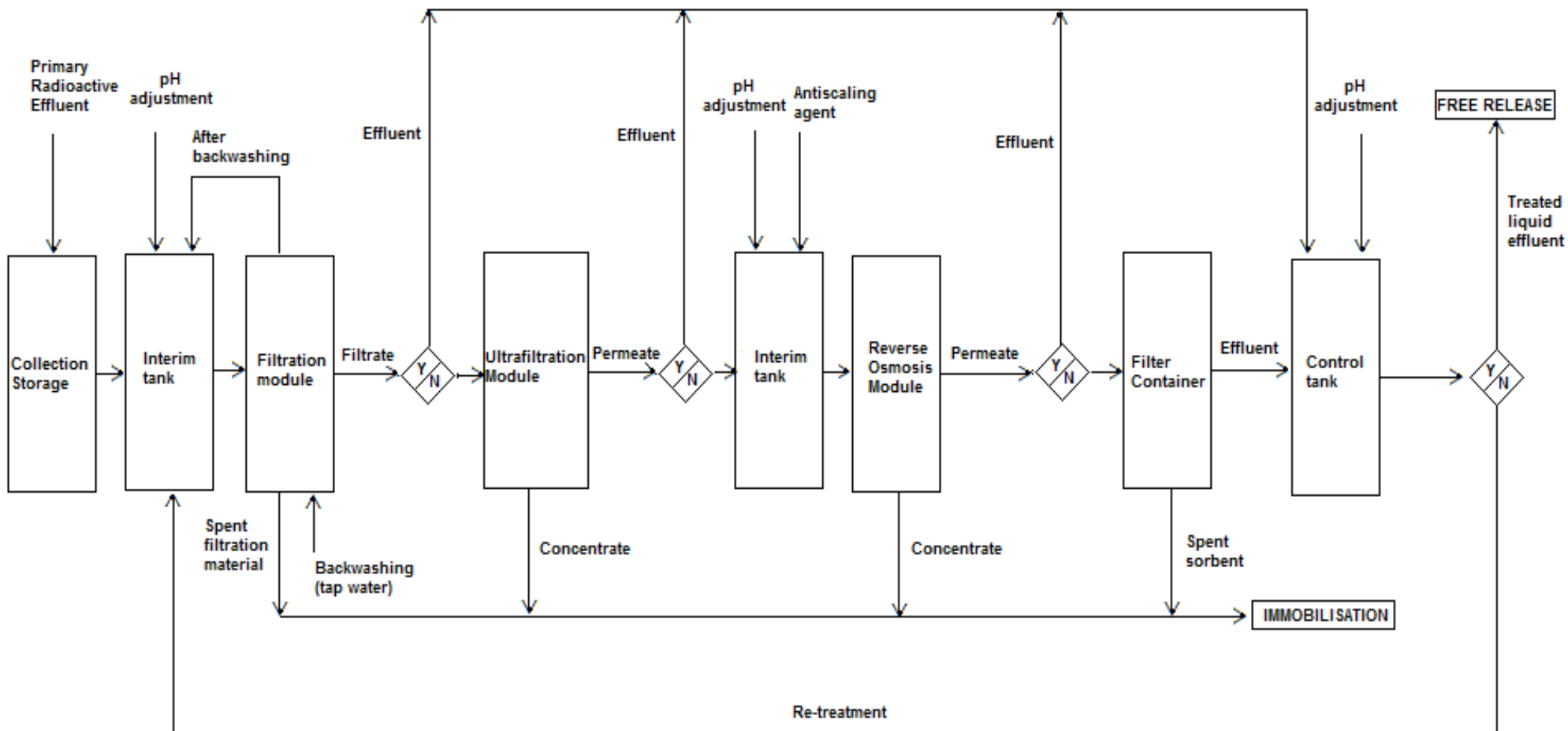


Figure 2.2. Technological flow sheet of aqueous radioactive effluent treatment plant (STERAJMA)

The Filtration Module (figs. 2.3, 2.4) includes 3 filter containers for ARW purification when it contains micro suspended particles, petroleum products and/or dissolved organic substances bearing radionuclides. The separation occurs by passing the ARW through different filtration units filled with granular materials (ex. sand, activated charcoal, crushed natural zeolites, ion exchange resins, synthetic inorganic sorbents).

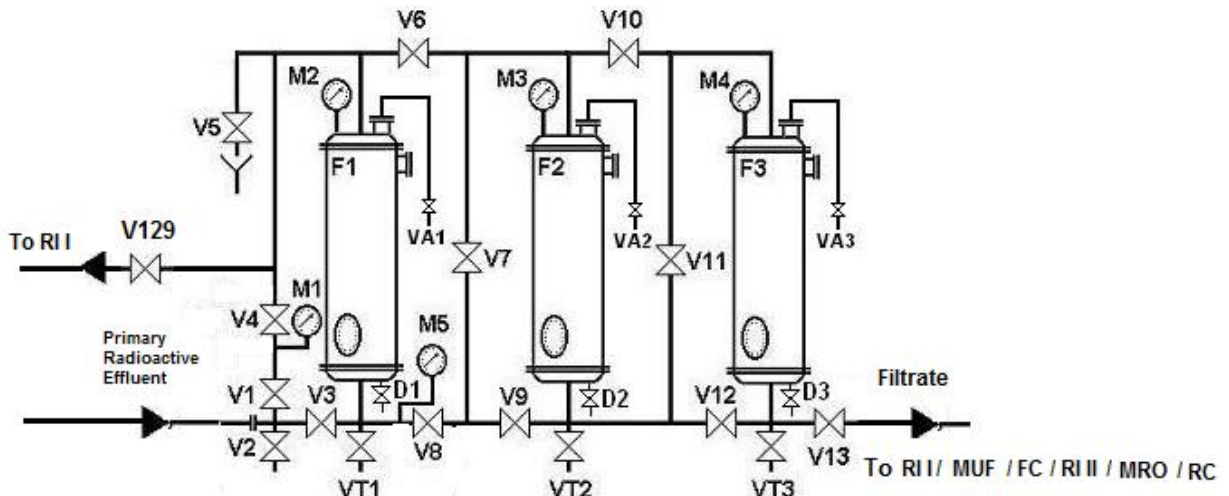


Figure 2.3. Hydraulic line diagram of Filtration Module (F1-F3 – poured filters, V1-V13 – ball-valves, VA1-VA3 - valves for air, VT1-VT3 – ball-valves for sampling, D1-D3 - ball-valves for hydraulic unloading, M1-M5 – manometers



Figure 2.4. Filtration Module

Filtration Module consists of three poured filters (pos. F1-F3), a pump (pos. P1), five manometers (pos. M1-M5), pipelines, a bed frame, equipped for the module loading-unloading, stainless steel tray intended for leakage collection and able to accommodate the whole volume of ARW from module equipment.

The Ultrafiltration (UF) Module (figs. 2.5, 2.6) is intended for further purification of ARW containing solid microprties, colloidal particles, and large polymeric molecules bearing or not radionuclides. In the ultrafiltration module does not occur radionuclides separation. As it results from fig. 2.5 the conception of module is for unsteady state operation.

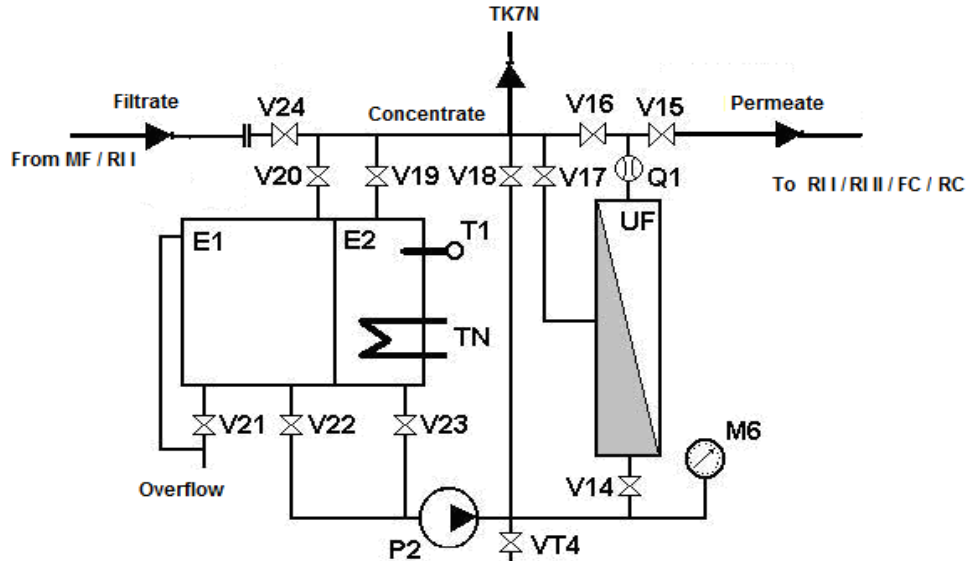


Figure 2.5. Hydraulic line diagram of Ultrafiltration Module (UF – ultrafiltration apparatus, E1-E2 – tanks of processed waste and flushing solution accordingly, P2 – drowned pump, V14-V24 – ball-valves, VT4 – ball-valve for sampling, M6 – manometer, Q1 – flowmeter, T1 – thermometer, TN – electric heating unit.

Ultrafiltration Module consists of an ultrafiltration apparatus (pos. UF), a rotary pump (pos. P2), drowned pump (pos. P3), tanks (pos. E1-E2), a manometer (pos. M6), a flowmeter (pos. Q1), a thermometer (pos. T1), an electric heating unit (pos. TN), pipelines, a bed frame, equipped for the module loading-unloading, a stainless steel tray for leakage collection and able to accommodate the whole volume of ARW from module equipment.



Figure 2.6. Ultrafiltration Module

The Reverse Osmosis (RO) Module (figs. 2.7, 2.8) is intended for deep purification of ARW from all admixtures (ions, non-charged organic molecules, salts, suspensions and etc) except tritium and cesium ions. The cesium ion is the alkali metal ion with lowest charge density and is weakly hydrated with only a single shell of water molecules [6]. Consequently, cesium hydrated ions can penetrate the reverse osmosis membrane pores. For a preliminary cleaning of radioactive water from suspended particles, in order to protect the membranes, a bag filter with bag filtration element (pore size less than 5 μm) is used.

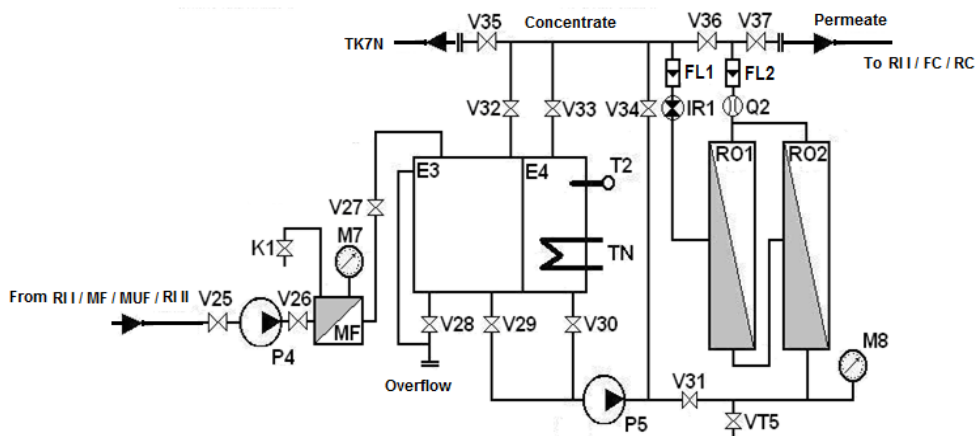


Figure 2.7. Hydraulic line diagram of Reverse Osmosis Module (RO1 and RO2 – reverse osmosis apparatus, MF - bag filter, E3-E4 – tanks of processed waste and flushing solution accordingly, P4 – rotary pump, P5 - three-plung pump, IR1 – needle valve, V25-V37 – ball-valves, VT5 – ball-valve for sampling, K1 - air through off valve, M7-M8 – manometers, Q2 – flowmeter, FL1, FL2 – rotameters, T2 – thermometer, TN – electric heating unit).



Figure 2.8. Reverse Osmosis Module

RO Module consists of two reverse osmosis apparatus (pos. RO1-RO2), bag filters (pos. MF), a rotary pump (pos. P4), three-plunge pump (pos. P5), drowned pump (pos. P6), tanks (pos. E3-E4), a manometer (pos. M7-M8), a flowmeter (pos. Q2), rotameters (pos. R1-R2), a thermometer (pos. T2), an electric heating unit (pos. TN), pipelines, a bed frame,

equipped for the module loading-unloading, a stainless steel tray, used for leakage collection and able to accommodate the module whole volume of ARW.

The membranes used in the UF and RO modules are of spirally wound type, made from composite polyamide. They have pore dimensions as low as 10 nm in ultrafiltration module and 1 nm in reverse osmosis module. The spiral geometry is used in order to ensure a larger membranes surface. A spirally wound membrane element is simply a flat sheet assembly rolled into a central core. The element contains two layers of spirally wound polymeric membrane with a porous woven fabric support sandwiched in between. The envelope formed by sealing the three sides contains the porous support. The remaining open fourth side is embeded to a perforated central tube. The separate spirally wound membrane sections that make up the membrane envelope along with a sheet of plastic mesh are then wrapped around and introduced in cylindrical pressure vessel so that a complete membrane element is obtained. The feed solution enters the first element at one end and flows through the inter-membrane gap created by the mesh. Schematic views of a spiral membrane element are given in fig. 2.9.

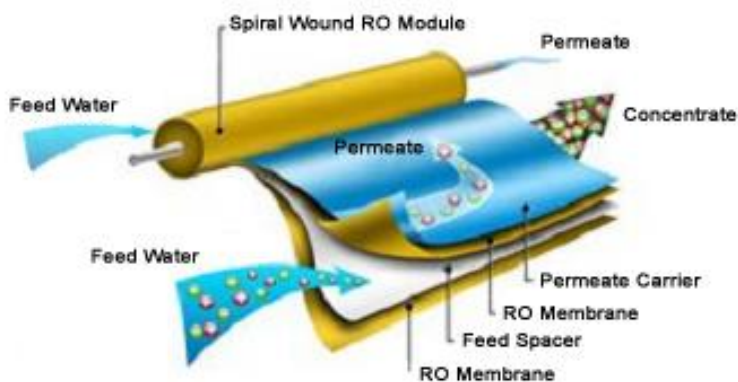


Figure 2.9. Schematic view of a RO spirally wound membrane

The main advantage of this design is the obtaining of a large membrane surface area packed into a relatively small volume of the cylindrical membrane element [5 , 7]. The volume of liquid hold-up is small, which is an advantage since radiation fields can be better controlled. Moreover, the membrane configuration allows easy chemical cleaning. Nevertheless, the narrow flow channels are sensitive to fouling by turbid feed solutions. That is why, determining which UF membrane materials resist best to fouling is a very important task for performance of membrane separation processes. Presently polymers are the most widely used because this are available and economically feasible materials for membrane

preparation, which achieve tailored properties. Vulnerability to fouling is a major problem in membrane technology, so mathematical modelling of membrane fouling is very interesting in process analysis. On the other hand when using a combined treatment method for a given ARW is useful to know when there is a need to change operating variables in the process. Mathematical models can help to predict permeate fluxes under different operating conditions (feed characteristics, feed concentration, transmembrane pressure, cross-flow velocity, temperature, etc.) so that can be predicted the coupled operation of a plant's modules and be avoided time-consuming experiments without modelling. Mathematical modelling of membrane fouling also reduces the number of experiments that are necessary to select the best operating conditions for minimizing membrane fouling in industrial and environmental applications. They can help select the optimal operating parameters and they also have environmental implications due to a significant save in membrane replacement. Therefore, fouling models increase the efficiency of the UF and RO process.

It is important to show that, for filter elements for UF or RO, the high hydraulic resistance of these spirally wound membrane elements compared to other designs is a disadvantage. Sometimes the element itself can break down if high pressure causes the element to come apart in a telescope-like fashion. Another disadvantage is that the entire element has to be replaced in the event of membrane damage or irreversible fouling. As one of the least expensive and compact configurations they are commonly used in reverse osmosis applications. They are rarely used without pretreatment of the feed water to remove suspended solids [7].

Regeneration of the spiral ultrafiltration and reverse osmosis elements is possible by washing them with regenerating solutions.

The Sorption Module (figs. 2.10, 2.11) is intended for retention of Cs radioisotopes and includes a stainless steel filtration cartridge fixed in a standard 200-liters drum, poured with cement grout, which plays the role of a biological shielding. It can be loaded with a synthetic inorganic sorbent selective for Cs radioisotopes (ex. transitional metal ferrocyanide based composite material, deposited onto a matrix).

From
MF / MUF / MRO
To
RC

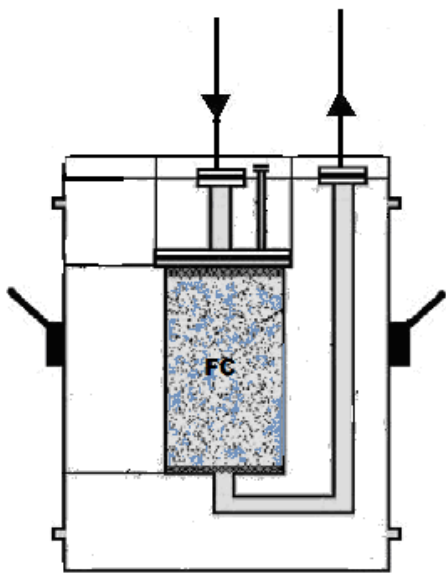


Figure 2.10. Hydraulic line diagram of Sorption Module (FC - filter-container) with synthetic inorganic sorbent



Figure 2.11. Sorption Module

As it will be shown in the following chapters, in this module takes place a fixed bed sorption process when Cs ions from the treated ARW are fixed on the sorbent particles.

When using a combined treatment method for radioactive waste is very important to know when there is a need to change operating variables in the process. Mathematical models can allow the prediction of permeate fluxes under different operating conditions (feed characteristics, feed concentration, transmembrane pressure, cross-flow velocity, temperature,

etc.) so that time consuming experiments can be avoided. Regarding membrane fouling, mathematical modelling reduces the number of experiments that are necessary to select the best operating conditions, very important issue in radioactive waste management for the reason that the exposure of worker is minimized. Mathematical models can help to select the optimal operating parameters and therefore, fouling models increase the efficiency of the UF and RO process.

All modules were considered and evaluated as components of a single system and their interactions and interrelations were streamlined for optimised performance of the system as a whole. The understanding of how the process driven parameters (pressure, flow rate, contact time, composition and pH of ARW) act on the dynamic regime and on the mass transfer mechanisms through the membrane, in terms of polarization, allows control of the treatment process and the effective control of technology leading to treatment optimisation and efficiency improvement in using materials that will become secondary radioactive waste.

REFERENCES

- [1] I. Crabbe, R. Keep, *The Design and Construction of a Modular, Transportable, Liquid Effluent Treatment Plant for Use in a NPP Undergoing Decommissioning -14562* , WM2014 Conference, March 2 – 6, 2014, Phoenix, USA
- [2] *Management of low and intermediate level radioactive wastes with regard to their chemical toxicity*, IAEA-TECDOC-1325, Vienna, International Atomic Energy Agency, 2002
- [3] P. Ivanov, *Modular Design Approach for Processing for Small Volumes of Solids and Liquid LLW and Disused radioactive Sources*, ICTP/IAEA Workshop, November 2-6, 2015, ICTP-Trieste, Italy
- [4] D. Isopescu, M.B. Robu, I. Cretescu, *Studiu privind evaluarea caracteristicilor radioactive pentru produse de constructii*, Univ. Gh. Asachi Iasi, Facultatea de Constructii si Instalatii, Noiembrie 2015
- [5] *Aqua Express Technical Book*, IFIN – HH Service Book, 2010
- [6] J. Mahler, I. Persson, *A Study of the Hydration of the Alkali Metal Ions in Aqueous Solution*, Inorg. Chem., **51(1)**; 425-438, 2012
- [7] *Combined methods for liquid radioactive waste treatment*, IAEA-TECDOC-1336, Vienna, International Atomic Energy Agency, 2003

CHAPTER 3. CHARACTERIZATION AND MODELLING THE ULTRAFILTRATION PROCESS IN LIQUID RADIOACTIVE WASTE TREATMENT

The modular installations for low and intermediate level liquid radioactive waste treatment at IFIN-HH, Magurele, Romania contains an ultrafiltration device, which can be used in designing a technology for a given radioactive waste water. The basic of ultrafiltration, experimental measurements for testing and characterization of the operation procedure with the ultrafiltration device having a given ARW and respectively the clogging modelling and the device modelling define the content of this chapter.

3.1. Ultrafiltration – general description. Specific membranes.

Ultrafiltration (UF) is a pressure-driven membrane separation process recommended for separation, especially from liquids, of small particles (solid, gel and big molecular association (biopolymers)) with mean diameter between 0.001 and 0.1 μm (membranes with pore sizes are in this range). This process implies the passing through the membrane of dissolved compounds, while colloid and suspended matters are rejected. Typically, UF membranes will remove high molecular-weight substances, colloidal materials, and organic and inorganic polymeric molecules. In the nuclear industry domain, UF can be used for removal of substances present in radioactive waste in colloidal or suspended form. Ultrafiltration is also an efficient pretreatment step before reverse osmosis. For a good operation, the membranes of an ultrafilter must be protected against the action of particles larger than 0.1 mm which must be removed, generally by regular pre-filtration. Moreover, feed flows, pH and temperature conditions must be compatible with the membrane material.

As general rule in the case of liquid radioactive waste treatment using membrane processes (ultrafiltration, reverse osmosis, dialysis, etc) there exist a number of advantages like high decontamination factors, significant volume reduction of polluted water and an acceptable energy consumption. Membrane systems are simple and may operate under moderate temperature and pressure conditions. They are flexible, easy to up-scale and can be efficiently combined with other treatment methods. They have already found various applications in the nuclear industry domain. Membrane treatment units can be used at the site of waste generation, which has as consequence the obtaining of small volumes of concentrates that have to be transported to the treatment facility. The main issue in radioactive waste treatment using membrane methods is choosing the appropriate membrane that comes into contact with the radioactive solutions for a long time. The membrane may change its characteristics under the action of ionizing radiation. The features related to separation and

permeation could be altered, especially in the case of membranes manufactured from polymers that suffer various structural changes. The membrane resistivity and stability should be tested before selecting it for a specific application [1]. Various research groups have carried out several studies for effects of radiation on membrane stability; the estimation of threshold value for membrane operation in a specific application [2 – 5] is the aim of this studies. The occurrence of resistivity problems can be prevented by using inorganic membranes like ceramic or metallic. They are stable to an aggressive chemical environment and to all kinds of radiation (γ , β and α). Appropriate chemical and structural modifications can enhance the membranes resistance. The commercially available polymeric membranes can be modified to change their permeation behavior and separation characteristics by introducing functional groups, incorporating additives into membrane matrix or other modifications.

Even though they present several advantages, the implementation of membranes at full-scale has been restricted because of two main problems commonly faced during operation: concentration polarization (CP) and fouling (clogging (C)). CP involves an increase in the concentration of contaminants (solute) close to the membrane surface that creates supplementary resistance to separation. Consequently, CP increases operating costs while also adversely affecting product water quality. The concentration of membrane rejected species determines the amplitude of CP. Membrane fouling (clogging) means the long-term decline in the permeate flux with time. Clogging is a complex phenomenon with a number of affecting factors such as pore plugging, chemical degradation and bacterial growth [6]. Clogging is generally increased by CP as a result of the increase in contaminants concentration near the membrane surface which amplifies this phenomenon. CP was studied from a theoretical view and its effects could be incorporated in membrane design and operation. Due to the simultaneous or separate action of CP and C the permeate flux declines. This phenomena can be divided in: i) fouling (irreversible and long term phenomena) and respectively ii) concentration polarization (reversible and directly occurring phenomena).

In addition to these phenomena, other effects can appear when the solutes show mutual interactions with the solvent. Especially, the difference in charge of the solutes can make one's contribution to an inconsistent behavior of the solution.

Using various numerical methods, most of these studies had the objective to solve the solute mass balance equation with relevant fluid velocity profiles [7] .

3.2. Modelling UF processes

UF flux decline is provoked by several phenomena in, on and near the ultrafiltration membrane. These phenomena can also induce a loss in selectivity and the rationale for the flux decline will be unique in each case. Altogether, the decline of the flux is caused by the decrease of driving force and/or the increase of resistance.

The flux J_V can be described by the following relationship:

$$J_V = \frac{dV}{Adt} = \frac{\text{driving force}(e.g \Delta p, \Delta C, \Delta T)}{\text{viscosity * total resistance}} \quad (3.1)$$

Resistance is defined in correlation with its effect on flux decline and pressure increase as it is shown in Table 3.1 [8]. Resistance types as concentration polarisation, gel formation, and membrane resistance cause a decline that reaches a maximum limiting flux (specific flow rate) asymptote (J_∞), while others, as pore blocking, adsorption, and cake formation cause a continuously decreasing flux with time, tending to zero. Fig. 3.1 illustrates the difference among these two types of flux decline.

Table 3.1. Short description of flux limiters type

Constant flux limiters	
Type	Definition
Membrane resistance	Resistance caused by friction at fluid passage through a membrane
Concentration polarisation	Retained solutes accumulated at the membrane surface
Gel layer	Some solutes concentrate on the membrane surface building a gel
Continuously decreasing flux limiters	
Type	Definition
Cake layer	Similar to a gel layer, but fouling continuously increases with pressure, finally complete clogging of membrane and no flux occur
Pore blocking	Big particles, too large for a pore, will be lodged on/in membrane
Chemical adsorption	Some macromolecules have a chemical affinity for pore walls

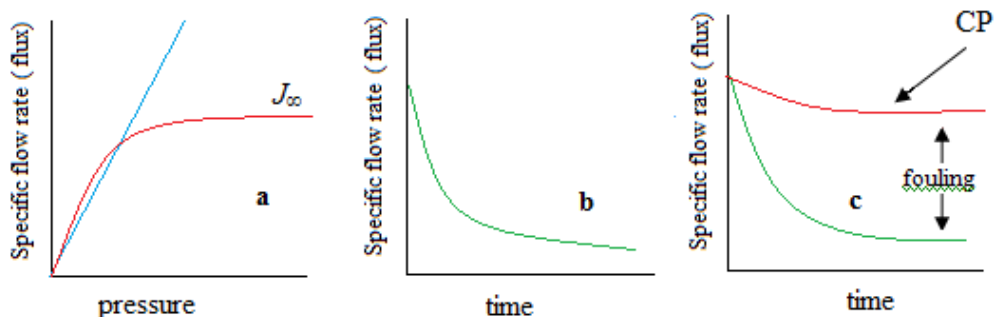


Figure 3.1. Comparison of flux decline caused by asymptotic concentration polarisation and fouling: a) plot of flux vs. pressure cases, b) pure fouling (clogging), c) plot of flux vs. time in a practical case (CP – pure polarization by concentration)

The hydraulic resistances which can occur during ultrafiltration processes are schematically represented in fig. 3.2. The terms *gel* and *cake* describe portions of the same

layer, but each of them has different contributions to flux decline [8]. A *gel* causes flux decline to the J_∞ asymptote. With pressure increasing, the gel resistance increases at a similar rate, issuing zero flux change. The gel is considered as a portion of concentration polarisation. A *cake* describes the component with reversible fouling that continuously thickens, decreasing flux. For an adequate selection of membrane, the gel and the cake volumes increase during ultrafiltration and that produces the concentrate flux decreasing. In an ultrafiltration process the resistances that can occur are [9]: i) resistance of the membrane, R_m , which is always present; ii) resistance of pores being blocked by the solute, R_p ; iii) resistance due to adsorption of the solute onto the walls of the pores of the membrane, R_a , which will result in a less permeable membrane; iv) resistance caused by phenomenon of concentration polarization, R_{CP} (this phenomenon will lead to a higher osmotic pressure $\Delta\pi$ at the membrane interface); v) resistance corresponding to cake/gel layer, R_g .

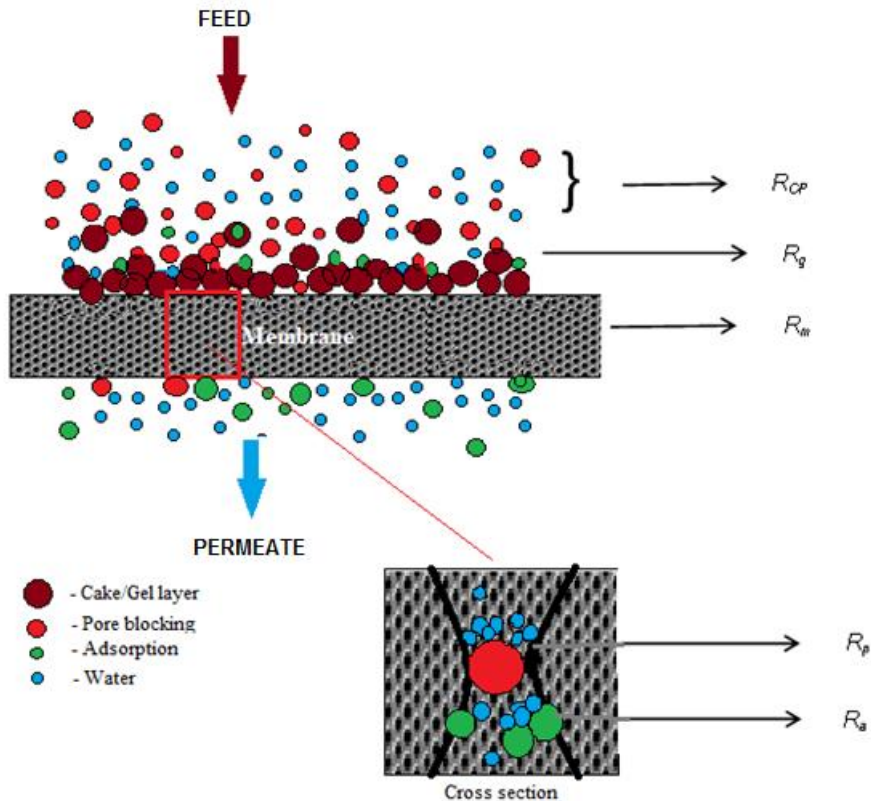


Figure 3.2. Hydraulic resistances for permeate flow in ultrafiltration processes

The total resistance can be considered as sum of all components as it is shown by relation (3.2). Is important to note that during process evolution all the resistances, except R_m , increase with time, resulting a permeate flux decline.

$$R_{TOT} = R_m + R_g + R_p + R_a + R_{CP} \quad (3.2)$$

Permeate flux decline can be also a result of the decrease of driving force. So, if adjacent to the membrane surface is a solute accumulation, then a concentration difference

between the feed side and permeate side appears. This difference leads to an osmotic pressure, and if the accumulation increases, the resistance will arise and the osmotic pressure difference across the membrane will be higher. Consequently, the flux will be lowered.

The concentration of solute near the membrane surface can be described as follows: either by the **cake-filtration** theory or according to the **film** theory.

The **cake-filtration theory** assumes a constant concentration of the deposit near the membrane, whose thickness increases with increasing permeate volume and depends on the applied pressure [9]. The concentration of membrane retained species in the boundary layer can be estimated from the mass balance (for unstirred dead-end filtration conditions) as it results from relation (3.3)

$$C_b \cdot R_{obs} \cdot V_p = \delta \cdot A \cdot C_{bl} \quad (3.3)$$

Here C_b is the concentration of retainable species in the bulk, R_{obs} represents the observed retention efficiency, defined by $R_{obs} = [1 - (C_p/C_b)]$, V_p shows the total permeate volume, A is the active membrane area, δ is the thickness of the layer where occurs by the species retention, C_p gives the concentration of retainable species in permeate and C_{bl} represents the concentration of retained species in membrane boundary layer.

In equation for permeate flux (3.4), where, η_0 represents the viscosity of the solvent (water in case of polluted aqueous radioactive waters) and R_{bl} is the resistance of cake concentrated boundary layer, it is used, for cake resistance, the relation (3.5). The result of processing is in relation (3.6), where are mentioned, separately, the membrane and the cake resistance. In this relation, r_{bl} shows the specific resistance of cake and J_w the pure water flux (flux when through membrane passes only water, so when no cake is present):

$$J_V = \frac{\Delta P}{\eta_0(R_m + R_{bl})} \quad (3.4)$$

$$R_{bl} = \delta \cdot r_{bl} \quad (3.5)$$

$$\frac{1}{J_V} = \frac{1}{J_w} + \frac{\eta_0 C_b R_{obs}}{\Delta P} \cdot \frac{r_{bl}}{C_{bl}} \cdot \frac{V_p}{A} \quad (3.6)$$

Introducing in Eq. (3.6) $J_v = \chi dV_p / Adt$, where χ is the volumetric ratio of water in processed suspension, it is obtained the classical differential filtration equation with coupled support and cake resistances . The integral expression of this model is in equation (3.7)

$$t = \frac{1}{J_w} \left(\frac{V_p}{A} \right) + \frac{\eta_0 C_b R_{obs}}{\Delta P} \cdot \frac{r_{bl}}{C_{bl}} \cdot \left(\frac{V_p}{A} \right)^2 \quad (3.7)$$

This formula leads to the well-known relationships for unstirred dead-end filtration showing that collected permeate or collected cake on membrane linearly depends on the square root of time:

$$V_P \sim t^{0.5} \text{ or } J_{V^-} \sim t^{0.5} \quad (3.8)$$

The **film theory** assumes that the rejection of particles develops a thin fouling layer on the surface of membrane overlapped by a CP layer. In CP layer, particles diffuse from the membrane surface to the bulk phase. Taking into consideration that solute concentration is higher in CP layer than in bulk phase, a concentration gradient is generated. A steady state is assumed so the balance between convection of particles to membrane surface and diffusion away from the membrane is produced [10] and it is characterized by relation written in the form (3.9). The exit of retained species from CP layer is characterized by J_S flux, which is controlled by diffusion coefficient (D) and concentration gradient $\frac{dC}{dx}$ in a CP layer as it can be seen in relation (3.10):

$$J_S = J_V C_b \quad (3.9)$$

$$J_S = D \frac{dC}{dx} \quad (3.10)$$

In a steady state situation, which is reached after some time, the two mechanisms will balance each other and Eqs. (3.9) and (3.10) can be equalized and integrated over boundary layer. The result is the well-known film-theory relationship (3.11) where C_m shows the concentration of retained species at the membrane interface and D/δ is called the mass transfer coefficient k , which is solute and equipment dependent.

$$J_V = \frac{D}{\delta} \cdot \ln \frac{C_m - C_P}{C_b - C_P} \quad (3.11)$$

When the permeate flux is known (see fig. 3.1(c), at large time in CP state), the concentration function for the boundary layer can be expressed with relation (3.12).

$$C_{(\delta-x)} = C_b \cdot \exp \frac{J_V \cdot (\delta - x)}{D} \quad (3.12)$$

Several relationships developed to correlate the mass transfer coefficients ($k=D/\delta$) with physical properties and working parameters have been reported in literature [11 - 14], but they fit generally specific applications. As every application could be unique due to specific local conditions, different processing and various other factors, each operator has to develop his own method to measure mass transfer coefficients in ultrafiltration systems.

The models above presented consider a steady state for specific cake hydraulic resistance (r_{bl}), respectively, on polarization concentration gradient ($\frac{dC}{dx}$). Different models exist in literature to cover the effect of the concentration polarization phenomena for both the cake-filtration type of description and for the dynamic description according to the film theory. These models can be subdivided in: i) resistance models, ii) gel-polarization models and iii) osmotic pressure models.

The resistance models

Generally, the hydraulic resistance models are developed using the series resistance equation based on the electric–hydraulic analogy. There are two types of resistance models: filtration models and boundary layer resistance models.

In most cases, the ***filtration models*** use the consecrated Kozeny-Carman relationship to determine the specific resistance of a cake with a constant concentration and the total resistance R_{bl} . R_{bl} , as needed in Eq. (3.4), is calculated from the thickness of the boundary layer δ and the specific resistance r_{bl} [15]. Total resistance will be equal to $r_{bl} \cdot \delta$ in the the cake-filtration theory and is given as an integral media over the cake thickness (3.13):

$$R_{bl} = \int_0^\delta r_{bl} dx \quad (3.13)$$

The specific hydraulic resistance is expressed by Kozeny-Carman relationship (3.14), where ε is the porosity of the concentrated layer (cake layer) and d_s is a measure for diameter of particles retained by the membrane:

$$r_{bl} = 180 \cdot \frac{(1-\varepsilon)^2}{d_s^2 \cdot \varepsilon^3} \quad (3.14)$$

The influence of the applied pressure on the specific hydraulic resistance can be described by Eq. (3.15) with n as compressibility factor.

$$r_{bl} = r_{bl,0} \cdot \Delta P^n \quad (3.15)$$

Regarding the cake compressibility factor n , it is possible to measure it experimentally, in literature being reported to be 0.5 - 0.7 for solutes like BSA and silica [16, 17], 0 for 100 KDa PES membranes, 0.16 for 0.2 μm TE membranes and 0.29 for 0.22 μm PVDF membranes [18]. The filtration model concept is used for all kinds of filtration (for cross-flow UF [19 , 20], for describing stirred and unstirred dead-end filtration of several solutes [16, 21]).

The basic principle of ***boundary layer resistance models (BLR models)*** [22] is the establishing of a correlation for solvent (permeate) permeability in a concentrated layer (cake agglomeration) near a membrane interface. It is considered that this permeability depends on permeate viscosity (η_0), concentration of retained species in processed suspension (C)

sedimentation coefficient characterizing the deposition of retained species on membrane or on cake ($s(C)$) and on volumetric fractions of cake and permeate in cake agglomeration (ν_1, ν_0). This following relationship can be used.

$$p = \frac{\eta_0 s(C)}{C(1-\nu_1/\nu_0)} \quad (3.16)$$

The specific hydraulic resistance r_{bl} is equal to the reciprocal permeability p^{-1} . In combination with Eq. (3.13) results the total resistance, which is needed in Eq. (3.4) to describe the flux. The sedimentation coefficient is strongly dependent on the concentration. The following formula, where K_1 , K_2 and K_3 are constants characterizing the permeate, underlines the decreasing of this coefficient with increasing concentration of membrane retained species.

$$s^{-1} = (s_0)^{-1} \cdot (1 + K_1 \cdot C + K_2 \cdot C^2 + K_3 \cdot C^3) \quad (3.17)$$

Determination of s^{-1} is tedious and limited to a rather low range of solute concentration.

The cross-flow variant of the BLR model uses Eqs. (3.12), (3.13), (3.16) and (3.17) to obtain the relation (3.18):

$$R_{bl} = \frac{D}{J_V} \frac{(1-\nu_1/\nu_0)}{\eta_0 s_0} [C_m - C_b + \frac{K_1}{2}(C_m^2 - C_b^2) + \frac{K_2}{3}(C_m^3 - C_b^3) + \frac{K_3}{4}(C_m^4 - C_p^4)] \quad (3.18)$$

Expression (3.18) can be used to calculate the total resistance of the boundary layer when the concentration at the membrane interface, C_m , is known. Assuming $R_{obs} = 1$ (CP = 0) the Eq.(3.11) can be re-written as (3.19) from which C_m can be calculated if k is known.

$$J_V = k \cdot \ln \frac{C_m}{C_b} \quad (3.19)$$

Unfortunately, the mass transfer coefficient, k , can not be easily determined from process parameters. Many relationships have been suggested to be used, but none of them can predict the exact mass transfer coefficient [23]. Corrections can be made taking into consideration concentration dependence on certain factors like the increased diffusion coefficient, the increased viscosity and/or the increased density of the solution [24].

The integral boundary layer model was used also to predict the local permeate flux along the membrane, but, the calculation procedure of this model is quite difficult. Hence, the models can be derived to calculate the mean permeate flux in specific, practical applications of ultrafiltration [25].

The gel-polarization model

Many investigators [26 - 30] found that as the applied ultrafiltration pressure is increased, permeate flux first increases and then remains more or less pressure independent.

At the end, a limiting flux is reached where subsequent increase in applied pressure will result in slight increase in permeate flux. Such flux action was not explained well by the film model of concentration polarization [31]. This phenomenon was first explained by Michaels [32] and Blatt [26] who have commented about the gel polarization model. They found that while the solute concentration at the membrane surface increases to its solubility limit, precipitation occurs on the membrane surface to form solid gels. Furthermore, they concluded that if the pressure increases to a value above a certain limit, this transitory increase in flux will lead to a gel layer formation at the membrane surface. Steady state is attained when the hydraulic resistance of the gel layer determines a fall in the permeate flux to the limiting value. The gel concentration depends on the shape, size and chemistry of interaction between solvent and solute, and it is independent of the bulk solution concentration, applied pressure and membrane characteristics [33].

The ***gel-polarization model*** assumes that as the applied pressure is increased further, the flux will increase temporarily, but in turn, will lead to bringing more solute to the gel layer and increasing its thickness, thereby the flux begins to drop below its original level due to the formation of gel layer of rejected particles on the membrane surface [32]. Due to concentration polarization, the concentration of the solute at the membrane surface, C_m , is much higher than that in the bulk solution and when C_m achieves a certain level, a gel layer is formed with a gel layer concentration, C_g . Under the following assumptions: (i) a complete solute rejection of 100% is realised, (ii) the influence of concentration profile and permeate flux on the mass transfer coefficient, k , is negligible, the film-theory relationship (3.11) can be simplified to the ***gel layer model*** equation for limitative permeate flux (3.20).

$$J_{\lim} = k \ln \frac{C_g}{C_b} \quad (3.20)$$

The Eq. (3.20) can be used to evaluate the limiting flux (J_{\lim}) when the gel layer is formed. Later, many investigators [34 - 37] have conducted ultrafiltration experiments to measure the limiting flux at different conditions supported by the gel – polarization model. From Eq. (3.20), the following findings about the limiting flux can be directly drawn: i) J_{\lim} is independent of applied pressure, ii) J_{\lim} varies semi-logarithmically with C_b , iii) J_{\lim} tends to zero at a limiting bulk concentration $C_{b,\lim}$ which is equal the gel concentration C_g (or the cake-concentration in the case of colloidal dispersions) and iv) J_{\lim} may be changed by factors which remodel the overall mass transfer coefficient.

The gel polarization model has been broadly used in the analysis of experimental data obtained for ultrafiltration of macromolecular solutions [38 - 40]. The model fits experimental data very well in numerous cases, and thus, it is suitable for practical purposes.

Osmotic pressure model

As mentioned previously, the membrane rejected solutes accumulate near the membrane surface and this is known as the concentration polarization. The effect of this phenomenon is an extra hydraulic resistance to the solvent (permeate) flow and the development of an osmotic pressure that acts against the applied transmembrane pressure.

The **osmotic pressure model** assumes that the flux decline is a function of all operating variables including the transmembrane pressure, p . The osmotic pressure at the membrane surface diminishes the transmembrane pressure so for J_V can be used the relation (3.21) where R_m is the membrane resistance and $\Delta\pi$ represents the difference in osmotic pressure across the membrane (i.e. $\Delta\pi = \pi(C_m) - \pi(C_p)$) [41].

$$J_V = \frac{(\Delta p - \Delta\pi)}{\eta_0 R_m} \quad (3.21)$$

This approach is different from the gel polarization model which describes the flux decline as a function of mass transport coefficient across the membrane and solute concentration at the membrane surface, meanwhile, the influence of pressure drop across the membrane is neglected. Generally, a polynomial expression describes more confidently the dependence of osmotic pressure upon concentration of retained species. The relation (3.22) where a is a constant and n an exponential factor, with a value greater than 1, considers this dependence.

$$\pi = a \cdot c^n \quad (3.22)$$

Supposing complete rejection ($C_p = 0$), the osmotic pressure π can be expressed as in relation (3.23):

$$\Delta\pi = \pi(C_m) = a \cdot C_m^n \quad (3.23)$$

The easier way to determine C_m is the use of film theory. Hence, combining with Eq.(3.11), is obtained:

$$J_V = \frac{[\Delta p - a(C_b)^n \cdot \exp(nJ_V/k)]}{\eta_0 R_m} \quad (3.24)$$

The derivatives of Eq.(3.24) with respect to Δp and C_b provide other filtration characteristics and also, give insight into the ultrafiltration process [42]. Thus, the flux-pressure derivative is given by relation (3.25):

$$\frac{\partial J_V}{\partial \Delta p} = \left[\eta_0 \cdot R_m + \frac{n}{k} \cdot \Delta\pi \right]^{-1} = \frac{\left(1 + \Delta\pi \cdot \frac{n}{\eta_0 \cdot R_m \cdot k} \right)^{-1}}{\eta_0 \cdot R_m} \quad (3.25)$$

It can be observed that we have two extremes: $\frac{\partial J_V}{\partial \Delta p} \rightarrow (\eta_0 R_m)^{-1}$ for $\Delta p \rightarrow 0$ or $\Delta \pi \rightarrow 0$

and, respectively, $\frac{\partial J_V}{\partial \Delta p} \rightarrow 0$ for $\Delta p \rightarrow \infty$ or $\Delta \pi \rightarrow >> J_V \eta_0 R_m$. Thus, the flux - pressure

profile commences at low Δp with a slope similar to pure solvent flow and as Δp increases, the slope declines and approaches zero at high pressure, which is similar to the gel-polarization model. Rearranging Eq. (3.24), the relationship flux-concentration could be reconsidered by taking the logarithm and differentiating to obtain the derivative from relation (3.26):

$$\frac{\partial J_V}{\partial \ln C_b} = - \left[\frac{1}{k} + \frac{1}{n \left(\frac{\Delta p}{\eta_0 R_m} - J_V \right)} \right]^{-1} = -k \left[1 + \frac{\eta_0 R_m k}{n \cdot \Delta p} \right]^{-1} \quad (3.26)$$

Analysis of this derivative shows that when polarization is significant, the following observations have to be taken into account: $\Delta p \gg J \eta_0 R_m$ or $\frac{n \cdot \Delta \pi}{\eta_0 R_m k} \gg 1$ then

$\frac{\partial J_V}{\partial \ln C_b} \rightarrow -k$. The limiting concentration $C_{b,\lim}$ is obtained for $J \rightarrow 0$ into Eq. (3.24).

Is obtained that transmembrane pressure becomes equal with osmotic pressure (3.27):

$$\Delta p = a C_{b,\lim}^n = \pi(C_{b,\lim}) \quad (3.27)$$

The conclusion from theoretical analysis is [42]: 1) as the membrane resistance, R_m , decreases this will cause a more pronounced osmotic pressure effect, that is flux limitation at lower applied pressures; 2) as the osmotic pressure increases, the bulk concentration will increase too, hence the osmotic pressure limitation will be expected in ultrafiltration of medium macrosolutes.

Statistical model

Currently, statistical modelling of processes has become a very effective method and it is most commonly used to create a model for a process. A statistical model is a class of mathematical models, which combines a set of hypothesis concerning the generation of some sample data, and similar data from a larger population. A statistical model can be viewed as a data-generating process, in a considerably idealized form, of course. The assumptions incorporated by a statistical model describe a set of probability distributions, many of them being assumed to adequately approximate the distribution from which a particular data set is sampled. The role of statistical modelling in the development of the best overall estimate for

the system behavior is extremely important in developing the system and its productivity understanding.

The statistical models are built based on the experimental measurements of one actual process. Proper models can be developed only based on the obtained experimental results and processed from a statistical analysis. Statistical modelling includes all the statistical and mathematical methods that use measured data of y_i ($i=1, P$) and x_j ($j=1, N$) conjunctively to obtain the manifold interdependences between dependent (y_i) and independent (x_j) variables. The relation that represents the statistical model of a process is [43]:

$$y_i = f_i(x_1, x_2 \dots x_n), i=1, p \quad (3.28)$$

In designs where there are multiple parameters, each with discrete possible values or "levels", the full listing of all combinations of factor levels is appointed as a full factorial design. For majority of factorial experiments each factor takes only two levels, generally a low and a high level, so the design is known as a 2^k experiment. A factorial design of an experiment determines the response of every potential combination of factors and factor levels. The responses obtained are investigated to achieve information about every effect and every interaction effect. Before starting the experimental research is needed a plan of the experiments that for the mentioned conditions are well-known as *complete factorial experience (CFE) or plan 2^k* [43]. The factors levels are established taking into consideration the frontiers of the investigated process domain.

A full factorial design is a useful tool when are involved less than five factors, otherwise, testing of all combinations of factor levels becomes too expensive and time-consuming. If the number of combinations is too high to be logically feasible, a fractional factorial design may be considered in which at least half of the possible combinations could be omitted. Each factor is an independent variable, while the level is the subdivision of a factor. The 2^k factorial design involves designs with k factors, each factor with just two levels. These designs are set up to investigate a great number of factors which have two levels, two being the minimal number of levels. By measuring the response, the effect produced by a change in the level of a factor as change in response can be defined and, in this context, it can be decided which factors are important. The simplest factorial design has two factors, each with two levels, 2×2 , or 2^2 , producing $2^2 = 4$ factorial points or experimental conditions. A design denoted as 2^3 factorial means: the number of factors is 3, each factor has 2 levels and in the design are $2^3 = 8$ experimental conditions, and a 2^43^1 design involves five factors, four factors with two levels and one factor with three levels, and has $16 \times 3 = 48$ experimental conditions. Fig. 3.3 shows the factors state in a two-level design with 2 and 3 factors.

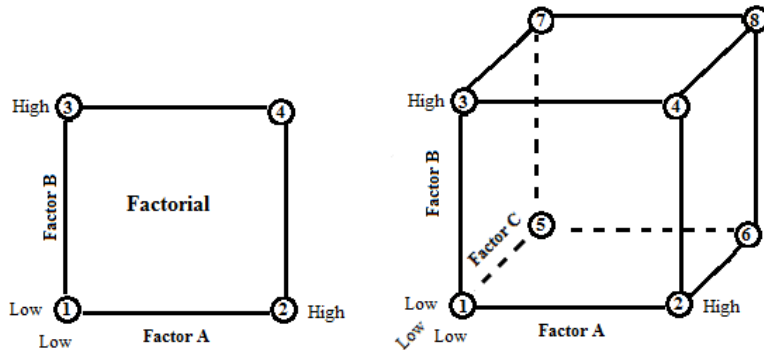


Figure 3.3. Graphical representation of a two-level design with 2 (left) and 3 factors (right)

The results of a factorial experiment can be processed using various software. Between them can be mentioned ANOVA, which can estimate the main effect on response for each factor. To compute the main effect of a factor "A", is deducted the average response of all experimental runs with A at its low level from the average response of all experimental runs with A at its high level. Other exploratory analysis tools can be used for factorial experiments to estimate factors effects.

3.3. Experimental investigation of UF in ARW treatment

The experimental investigation of untreated, pretreated and simulated ARW ultrafiltration was conducted at IFIN-HH, DMDR, in AQUA-EXPRESS installation (shown in fig. 2.1), using a spiral-wound polysulphonamide membrane. The actual untreated and pretreated by sand filtration ARW were subject to treatment in order to evaluate the influence of various parameters on membrane productivity and efficiency. Membrane productivity expressed by permeate volumetric flux, j_P ($\text{L}/\text{m}^2 \cdot \text{h}$), and separation efficiency evaluated as permeate total suspended solids, TSS_P (mg/L), were measured at different values of process factors, i.e., feed flow rate, operating pressure and feed total suspended solids, TSS_F . The influence of process factors on ultrafiltration efficiency was quantified using a 2^3 factorial plan [44]. A second experiment type with a concentrated ARW having high TSS (that promotes an accelerated concentration polarization process) was developed in order to investigate the influence of feed quality and membrane clogging dynamics.

3.3.1. Module description

Ultrafiltration module of this installation (see figs. 2.5, 2.6) is equipped with an ERU-100-1016 membrane element (producer JSC STC Vladipor, Russia) shown in fig. 3.4. According to reference [45], schematic and general views of a spiral membrane element are given in fig. 3.5.



Figure 3.4. Ultrafiltration membrane element type ERU-100-1016

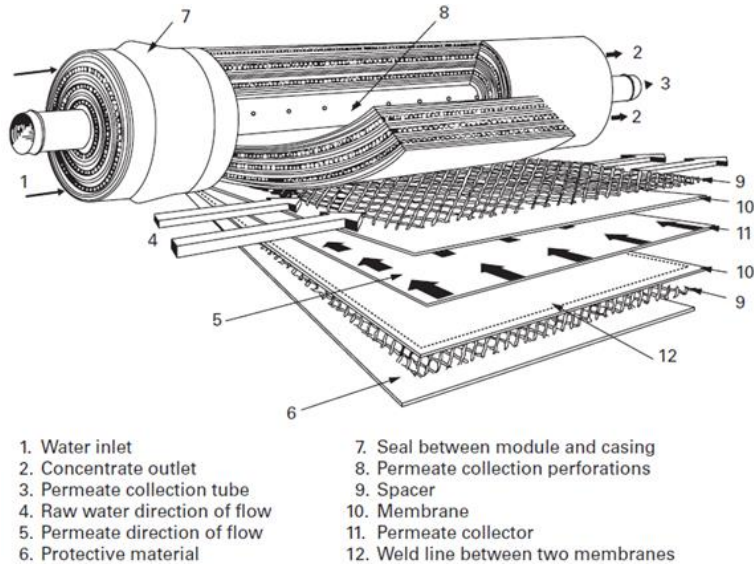


Figure 3.5. Schematic view of a spirally wound membrane section [45].

The individual spirally wound membrane sections are inserted into a cylindrical pressure vessel (7) to form a complete membrane element. The main item of a spirally wound membrane element is a sandwich structure that contains a porous sheet (11) inserted between two membranes (10) and sealed on three sides (12). The open side is welded to a cylindrical collector tube (3). Several such sandwich structures, separated by a spacer (9) are rolled around to the cylindrical collector tube (3) whose role is to collect the permeate. Product water permeates the membrane inside the sandwich in a cross-flow fashion and follows the flow channels (5) in the porous support that directs the permeate to the perforated (8) central tube for collection, while the liquid that does not permeate through the membrane continues to flow over the membrane surface, becoming more and more concentrated with rejected contaminants (2). This concentrated stream leaves the ultrafiltration element parallel to the central tube through the other end from which the feed water entered. Main characteristics of the ultrafiltration element ERU-100-1016 are summarized in Table 3.2.

Table 3.2. Main characteristics of the ERU-100-1016 membrane element

1	Configuration	Spiral Wound
2	Nominal Membrane Area	5 m ²
3	Membrane Polymer	Polysulphoneamide
4	L	1016 mm
5	D _i	100 mm
6	Cut-off	100 KD = 0.05 µm = 50 nm

7	Flow mode	Tangential (crossflow)
8	Water permeability	210 – 240 L/m ² h
9	Circulating flow (cross velocity):	1-1.5 m/s

The drowned pump P2, shown in figs. 2.5, 2.6, used to reach the required working pressure was a rotary type pump JTX 0810 with the following hydraulic properties: H up to 0.45 MPa at Q=5.4 m³/h, N=1.1 kW.

3.3.2. Working procedure

In this experiments was used the technological scheme shown in fig. 3.6. Operating pressures, p , from 0.1 to 0.4 MPa, were applied while TSS_F values were 15 mg/L and 60 mg/L at two feed flow rates, G_V , 7 m³/h and 10 m³/h. The permeate (water passed through the ultrafiltration membrane) was collected in the intermediate tank 2 and the volumetric flux, j_P , was continuously monitored. After each purification experiment, samples of treated waste were taken and the values for TSS_P were measured. The high value of TSS_F corresponds to the ones of untreated ARW, whereas its low level characterizes the waste pretreated by sand filtration. TSS was performed by vacuum filtration using a 50 nm Whatman membrane and a vacuum pump Varian model DS102.

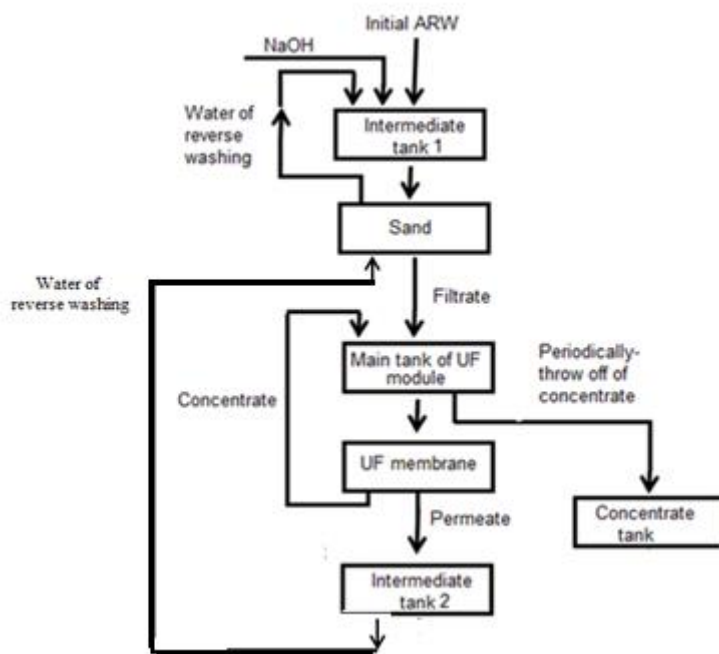


Figure 3.6. Technological scheme for experiment with ultrafiltration membrane element type ERU-100-1016

In the second experiment, the feed tank was filled with concentrated ARW: actual ARW in which clay powder was added, TSS_F becoming 140 mg/L. This clay – ARW mixture was treated by ultrafiltration, working pressure being 0.25 MPa and feed flow rate 10 m³/h.

From the feed, permeate and the concentrate streams, sampling was performed every 15 min. A fixed volume of each sample was filtered via vacuum for determining the TSS_P . The permeate volumetric flux was continuously observed and the variation of permeate TSS was carried out.

3.3.3. Experimental results and discussion

Influence of process factors on membrane productivity and efficiency

Tables 3.3 - 3.4 and fig. 3.7 show the results of experimental measurements for the first experiment type (dependence of j_p and TSS_P on pressure (p), flow rate (G_v) and initial TSS in ARW) for untreated and treated ARW.

Table 3.3. Experimental measurement results for untreated ARW at different feed flow rates

	Feed flow rate = 10 m ³ /h				Feed flow rate = 7 m ³ /h			
	0.1	0.2	0.3	0.4	0.1	0.2	0.3	0.4
p , MPa	0.1	0.2	0.3	0.4	0.1	0.2	0.3	0.4
j_p , L/m ² *h	53	99.6	158	182	42	70	137	164
TSS_F , mg/L	60	60	60	60	60	60	60	60
TSS_P , mg/L	17.2	16.8	14.1	11.6	33.2	30.7	19.8	18.4

Table 3.4. Experimental measurement results for pretreated ARW at different feed flow rates

	Feed flow rate = 10 m ³ /h				Feed flow rate = 7 m ³ /h			
	0.1	0.2	0.3	0.4	0.1	0.2	0.3	0.4
p , MPa	0.1	0.2	0.3	0.4	0.1	0.2	0.3	0.4
j_p , L/m ² *h	56	80	150	200	53	105	176	196
TSS_F , mg/L	15	15	15	15	15	15	15	15
TSS_P , mg/L	0.6	0.6	< 0.1	< 0.1	2.4	2.1	1.7	1.8

As shown in Tables 3.3 - 3.4 and fig. 3.7, the permeate volumetric flux and TSS strongly depend on operating pressure. It can be observed, also, that permeate volumetric flux increased with operating pressure and feed flow rate, and decreased with an increase of TSS_F . When the feed flow rate increased the TSS_P decreased in all cases. Was noted also that when the TSS_F increased, the permeate quality diminished, TSS_P being higher at all tested pressures. At pressure value of 0.4 MPa there appears to be a higher convective flux to the membrane, resulting in a higher concentration of impurities on the membrane surface. Thus, as the flux is higher, a bigger amount of impurities can be pushed through the membrane, which leads to a constant flux. Also, the TSS_P reached a constant value.

Fig. 3.7 highlights also the effects of process factors on permeate performances in terms of its volumetric flux ($j_p = 42 - 200$ L/m²·h) and TSS ($TSS_P = 0.1 - 33.2$ mg/L). Depicted data emphasize the following issues:

- (i) j_p increases with operation pressure ($p = 0.1 - 0.4$ MPa) up to about 4 times, whereas TSS_P decreases with an increase in p (up to 1.8 times for untreated and up to 6 times for pretreated ARW);

- (ii) j_P increases with feed flow rate ($G_V = 7, 10 \text{ m}^3/\text{h}$), i.e., 1.1-1.4 times for untreated and up to 1.1 times for pretreated ARW, whereas TSS_P decreases with an increase in G_V (1.4 - 1.9 times for untreated and 4 - 18 times for pretreated ARW);
- (iii) j_P is 1.1 - 1.5 higher and TSS_P is 11 - 141 lower (up to 15 times for $G_V = 7 \text{ m}^3/\text{hr}$ and over 28 times for $G_V = 10 \text{ m}^3/\text{h}$) for pretreated ($TSS_F = 15 \text{ mg/L}$) than for untreated ($TSS_F = 60 \text{ mg/L}$) ARW. Accordingly, j_P increases with p and G_V as well as it decreases with an increase in TSS_F , whereas TSS_P exhibits an opposite trend.

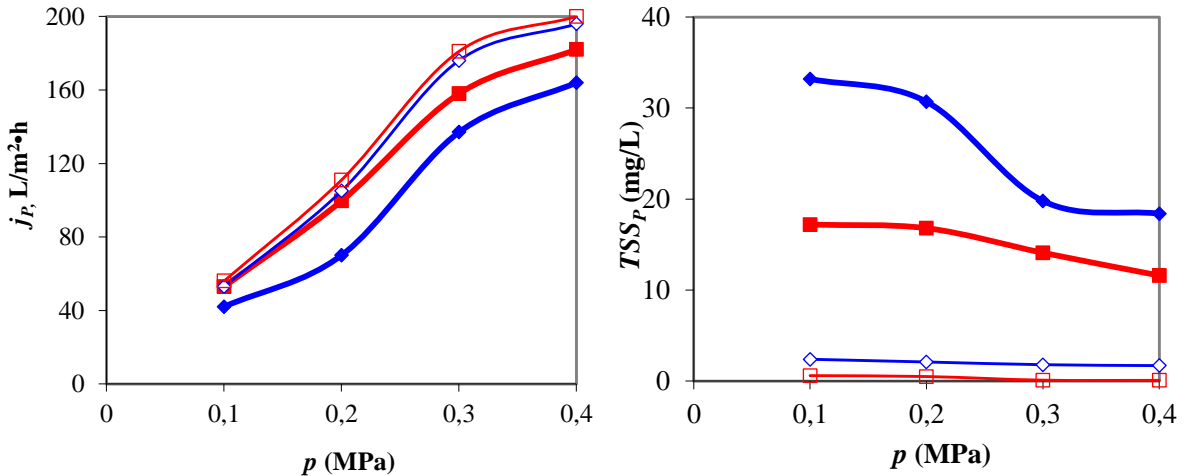


Figure 3.7. Permeate volumetric flux and TSS vs. operating pressure for different feed flow rates of untreated ($TSS_F = 60 \text{ mg/L}$) and pretreated ($TSS_F = 15 \text{ mg/L}$) ARW (untreated: $\blacklozenge G_V = 7 \text{ m}^3/\text{h}$, $\blacksquare G_V = 10 \text{ m}^3/\text{h}$; pretreated: $\blacksquare G_V = 7 \text{ m}^3/\text{h}$, $\blacklozenge G_V = 10 \text{ m}^3/\text{h}$)

Considering these results, a 2^3 factorial plan was used to establish correlations between dependent and independent variables of ultrafiltration process. Permeate flux, j_P ($\text{L}/\text{m}^2 \cdot \text{h}$), and permeate TSS, TSS_P (mg/L), were selected as process dependent variables (responses). Their final values, as well as dimensionless values of process factors determined by Eqs. (3.29 - 3.31), are given in Table 3.5. Tabulated data were processed using the procedure recommended for a 2^3 factorial plan resulting in Eqs. (3.32) and (3.33).

$$x_1 = \frac{G_V - 8.5}{1.5} \quad (3.29)$$

$$x_2 = \frac{p - 0.25}{0.15} \quad (3.30)$$

$$x_3 = \frac{TSS_F - 37.5}{22.5} \quad (3.31)$$

$$j_P = 118.25 + 4.50x_1 + 67.25x_2 - 8x_3 + x_1x_2 + 2.75x_1x_3 - 4.50x_2x_3 + 0.75x_1x_2x_3 \quad (3.32)$$

$$TSS_P = 10.662 - 3.287x_1 - 2.688x_2 + 9.438x_3 + 1.163x_1x_2 - 2.413x_1x_3 - 2.413x_2x_3 + 1.138x_1x_2x_3 \quad (3.33)$$

Statistical models described by Eqs. (3.34) and (3.35) were obtained after eliminating insignificant regression coefficients in Eqs. (3.32) and (3.33) [46 - 48].

$$j_P = 118.25 + 4.50x_1 + 67.25x_2 - 8x_3 + 2.75x_1x_3 - 4.50x_2x_3 \quad (3.34)$$

$$TSS_P = 10.662 - 3.287x_1 - 2.688x_2 + 9.438x_3 - 2.413x_1x_3 - 2.413x_2x_3 \quad (3.35)$$

Regression equations (3.34) and (3.35) reveal the following issues:

(i) permeate flux (j_P) increases with feed flow rate (x_1), operation pressure (x_2), and x_1x_3 interaction, decreases with an increase in feed TSS (x_3) and x_2x_3 interaction, as well as it is heavily affected by x_2 factor;

(ii) permeate TSS (TSS_P) decreases with an increase in x_1 , x_2 , and x_1x_3 interaction, whereas it increases with x_3 and x_2x_3 interaction; moreover, x_3 factor has a more significant effect on TSS_P .

Statistical models expressed by Eqs. (3.34) and (3.35) may be applied to predict the values of permeate flux and permeate TSS at levels of process factors in the ranges considered in the study, *i.e.*, $G_V = 7 - 10 \text{ m}^3/\text{h}$, $p = 0.1 - 0.4 \text{ MPa}$, and $TSS_F = 15 - 60 \text{ mg/L}$.

Table 3.5. Experimental matrix of 2^3 factorial experiment

Exp.	G_V (m^3/hr)	p (MPa)	TSS_F (mg/L)	x_1	x_2	x_3	j_P ($\text{L}/(\text{m}^2 \cdot \text{hr})$)	TSS_P (mg/L)
1	7	0.1	15	-1	-1	-1	53	2.4
2	7	0.1	60	-1	-1	1	42	33.2
3	7	0.4	15	-1	1	-1	196	1.8
4	7	0.4	60	-1	1	1	164	18.4
5	10	0.1	15	1	-1	-1	56	0.6
6	10	0.1	60	1	-1	1	53	17.2
7	10	0.4	15	1	1	-1	200	0.1
8	10	0.4	60	1	1	1	182	11.6

Influence of feed quality on membrane productivity and efficiency

The results obtained in the first experiment suggest that operating at 0.4 MPa and at higher concentrations, the flux does not increase significantly with pressure. A more important influence exert the feed flow rate and feed solid concentration.

To investigate the influence of feed quality on membrane productivity and efficiency, 1000 L ARW containing clay powder were ultrafiltrated at 0.25 MPa pressure and 10 m^3/h feed flow rate. The concentrate was returned in the feed tank and mixed with fresh feed, so, the TSS_F increased permanently, as it can be seen in fig. 3.8. In the experimental conditions mentioned, the permeate volumetric flux, j_P , and TSS_P were measured for 60 min. The characteristics of feed, permeate and concentrate are presented in Table 3.6 and their variations in fig. 3.9.

Table 3.6. Characteristics of feed, permeate and concentrate

Time, min	15	30	40	50	60
TSS_F , mg/L	167	243	468	576	786
j_p , L/m ² *h	180	144	136	124	96
TSS_P , mg/L	18,3	11,4	9,8	0,8	<0,1
TSS_C , mg/L	198	277	512	623	895

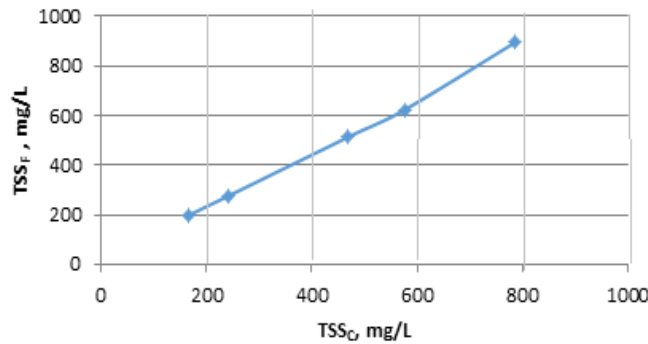


Figure 3.8. Variation of TSS_F with TSS_C at 0.25 MPa pressure and 10 m³/h feed flow rate

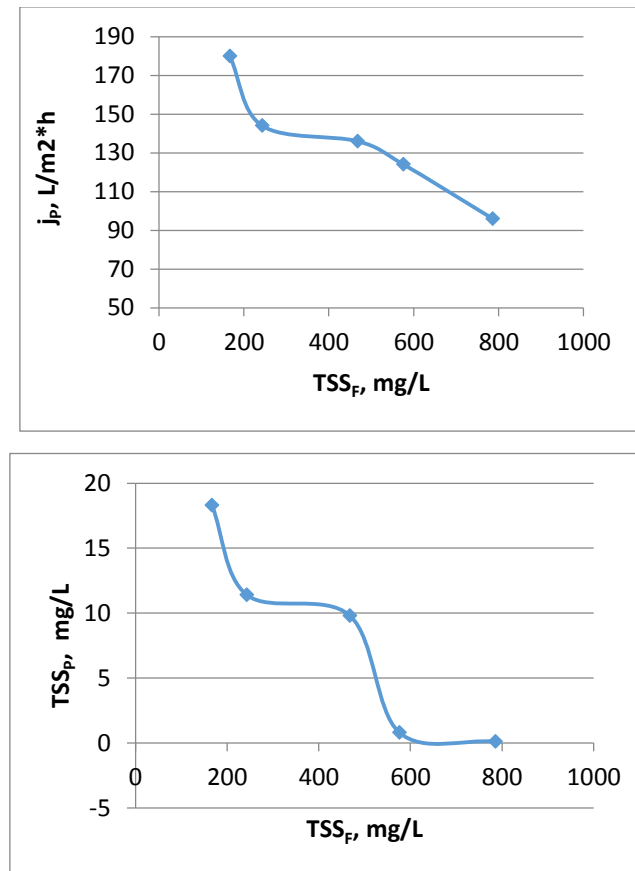


Figure 3.9. Variation of j_p and TSS_P with TSS_F at 0.25 MPa pressure and 10 m³/h feed flow rate

It appears that an important decrease in permeate flux occurs in time, as it is reduced to about half if the concentration of solid particles in feed increases 4 times. The performance of ultrafiltration membrane is still very good, though, as described above, feed liquid is more

and more concentrated and the concentration on the membrane surface would also be larger. But, a higher feed concentration could cause the appearance of larger particles, incapable of penetrating the membrane and, therefore, easier to remove, so, the permeate quality increased, solid particles being almost totally removed.

Both depositional attachment probability and coagulation attachment probability increased with increases in the feed solid concentration.

3.3.4. Use of j_p , TSS_F and TSS_C in modelling of ultrafiltration system with membrane clogging

Ultrafiltration is a separation technique which employs a pressure difference across a membrane which drives the transport of solvent and solute. As it has been shown the flux depends on the properties of the system formed by membrane (specific resistance), solute (concentration, size of suspended particles and size of macro or biomacromolecules from the liquid) and the liquid phase (viscosity). Regardless of the ultrafiltration application [27 – 31], a gel forms on membrane surface and the properties of this gel will also affect the performance of the separation in a significant manner [27]. Normally, the critical flux of a membrane decreases because the membrane has smaller pore size that can be easily clogged. This paragraphe proposes the use of two ultrafiltration units disposed in series to separate an initial ARW into three streams each of which should be rich in small, medium and large molecules or suspended solids. This setup is analyzed by performing a simulation in certain conditions which will be discussed. The simulation is based on three systems of differential-algebraic equations solved using Matchad solvers. From the below description it is not difficult to observe that can be considered the derived ultrafiltration schema (only one unit, two coupled units etc.). The species which are found in the feed are made of small (soluble salts and soluble small organic molecules), medium (soluble polymers or biopolymers and solid microprticles) and large (big soluble polymers or biopolymers, big microparticles etc.). The main reason for which different solutes have different yields of separation is related to difference in size between them. In this way, if a particle is much smaller than the pores of the membrane it will not be retained as much as another particle [28] which has a size comparable to that of the pore size distribution of the porous membrane which is used. When the solid is added to the processed water a sorption process appears between the soluble species and the added solid. This sorption is active until the equilibrium is reached. In this case the ARW processed by deep bed filtraton is suplemented with clay (no more than 80 μm in diameter) before treatment by ultrafiltration (see paragraphs 3.3.2 and 3.3.3).

Stochastic modelling of membrane clogging

Fig. 3.10 describes the possibilities for ultrafiltration membrane clogging evolution. Looking at the microparticles in tangential flow over membrane, two elementary states are identified, as determinant, for the global process evolution [46 - 48]:

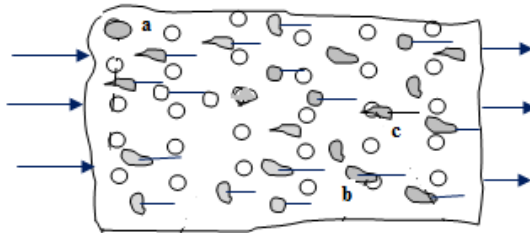


Figure 3.10. Elementary process states of the membrane clogging made of surface pores coverage (a-pore blocked, b-pass over the pore, c-the pore open up)

The type 1 state process characterizes the situation when a pore is covered by a dispersed particle that adheres to the surface (case a in fig. 3.10). The type 2 state process expresses the case when a covered pore that has previously conserved its state as blocked pore is opened up owing to departure of the dispersed particle (case c in fig. 3.10). The case expressed by the fact that the dispersed particle passes over the pore (case b in fig. 3.10) is not an elementary process because it does not have a direct action on the pore coverage or release. It can be deduced that it is the case of stochastic process where the process characteristic random variables are represented by the blocked pores number at membrane surface, $N(\tau)$. Usually, $N(\tau)$ is noted as n . The frequency transition for the state 1 to state 2 related with n is λ_n and the transition probability from the state 2 to state 1 when n pores are blocked is μ_n . The Markov connexion states process can be easily accepted to express partly the process probabilities. The probability to have at the time τ n blocked pores is here noted by $p_n(\tau)$. More correctly, we must write that $p_n(\tau) = P[N(\tau) = n], n = 0, 1, \dots$. If considered two time intervals $(0, \tau)$ respectively $(0, \tau + \Delta\tau)$ for the balance of probabilities, that gives $p_n(\tau + \Delta\tau)$, and the following possibilities can be considered: i) in the interval $(0, \tau)$ n pores are blocked and for the time interval $(\tau, \tau + \Delta\tau)$ no pore is blocked. The occurrence probability of this way is $p_n(\tau)[1 - \lambda_n \Delta\tau - \mu_n \Delta\tau]$; ii) in the interval $(0, \tau)$ $n-1$ pores are blocked and for the interval $(\tau, \tau + \Delta\tau)$ one pore is to be blocked. The probability of this possibility is $p_n(\tau)\lambda_{n-1} \Delta\tau$; iii) in the interval $(0, \tau)$ $n+1$ pores are blocked and for the interval $(\tau, \tau + \Delta\tau)$ one pore is to be released. The happening probability of this event is $p_n(\tau)\mu_{n+1} \Delta\tau$. The assumption of a Markov connexion of the process states arises from probabilities balance the possibilities: a) $n-j$ pores blocked in the time interval $(0, \tau)$ and j pores are blocked in the

interval from $(\tau, \tau + \Delta\tau)$, and respectively; b) $n+j$ pores blocked in the time interval $(0, \tau)$ and j pores are released in the interval from $(\tau, \tau + \Delta\tau)$. In these conditions the probability balance for $p_n(\tau)$ gives to differential equations (3.36), (3.37):

$$\frac{dp_n(\tau)}{dt} = \lambda_{n-1} p_{n-1}(\tau) - (\lambda_n + \mu_n) p_n(\tau) + \mu_{n+1} p_{n+1}(\tau) \quad n \geq 1 \quad (3.36)$$

$$\frac{dp_0(\tau)}{dt} = \lambda_0 p_0(\tau) + \mu_1 p_1(\tau) \quad (3.37)$$

For a simple model, a linear relationship between λ_n , respectively μ_n and n it is considered. So, these transition frequencies are expressed as in relation (3.38); consequently, the relations (3.36) and (3.37) take the forms (3.39) respectively (3.40). With relation (3.41), which shows that at beginning of ultrafiltration all pores are opened, the initial conditions of the model are found:

$$\lambda_n = \alpha(n_0 - n), \quad \mu_n = \beta n, \quad n = 0, 1, 2, \dots, n_0 \quad (3.38)$$

$$\frac{dp_n(\tau)}{d\tau} = \alpha[n_0 - (n-1)]p_{n-1}(\tau) - [\alpha(n_0 - n) + \beta n]p_n(\tau) + \beta(n+1)p_{n+1}(\tau), \quad n \geq 1 \quad (3.39)$$

$$\frac{dp_0(\tau)}{dt} = -\alpha n_0 p_0(\tau) + \beta p_1(\tau) \quad (3.40)$$

$$p_n(0) = 0, \quad p_0(0) = 1, \quad n = 1, 2, 3, \dots, n_0 \quad (3.41)$$

The time evolution of the mean number of the blocked pore is the interest in capitalizing of this model. For this purpose we can use the property of generator function associated to a random variable. Using this function, the relation (3.42) it can be written for the mean number of blocked pores at time τ ,

$$\bar{n} = \sum_{n=0}^{n_0} n p_n(\tau) = E[N(\tau)] = \left[\frac{\partial G(s, \tau)}{\partial s} \right]_{s=1} \quad (3.43)$$

For building the generator function of random variable n can be used the definition formula

$$G(s, t) = \sum_{n=0}^{n_0} s^n p_n(t). \quad \text{Concretely, by multiplying each term of the relations (3.39) and}$$

(3.40) with s^n respectively s^0 it is obtained, after a summation process, the partial differential equation for $G(s, \tau)$ (3.44). As a result of s transformation, the relation (3.41) becomes the univocity conditions (3.45) associated with differential equation of generator function of random variable n .

$$\frac{\partial G(s, \tau)}{\partial t} = \frac{\partial G(s, \tau)}{\partial s} \left[\beta + (\alpha - \beta)s - \alpha s^2 \right] + G(s, \tau) [\alpha n_0 (s-1)] \quad (3.44)$$

$$G(s, 0) = 1, \quad G(1, \tau) = 1 \quad (3.45)$$

If a form of $G(s, \tau)$ obtained by combination of two independent functions depending of s , respectively of s and τ is considered then the relations (3.46) and (3.47) are directly obtained. Using relationships (3.44) and (3.45) it is developed the mathematical problem expressed through relations (3.48) – (3.51).

$$G(s, \tau) = [f(s) + g(s, \tau)]^{n_0} \quad (3.46)$$

$$\frac{\partial g(s, \tau)}{\partial \tau} = \left[\beta + (\alpha - \beta)s - \alpha s^2 \right] \left[\frac{df(s)}{ds} + \frac{\partial g(s, \tau)}{\partial s} \right] + [\alpha(s-1)] [f(s) + g(s, \tau)] \quad (3.47)$$

$$\left[\beta + (\alpha - \beta)s - \alpha s^2 \right] \frac{df}{ds} + [\alpha(s-1)] f(s) = 0 \quad (3.48)$$

$$f(1) = 1 \quad (3.49)$$

$$\frac{\partial g(s, \tau)}{\partial \tau} = \left[\beta + (\alpha - \beta)s - \alpha s^2 \right] \frac{\partial g(s, \tau)}{\partial s} + [\alpha(s-1)] g(s, \tau) \quad (3.50)$$

$$g(s, 0) = 1 - f(s), \quad g(1, \tau) = 0 \quad (3.51)$$

Solving the mentioned mathematical problem leads to relation (3.52) for $G(s, t) = \sum_{n=0}^{n_0} s^n p_n(t)$. This relation immediately implies the relation (3.53) for the mean number \bar{n} of membrane blocked pores.

$$G(s, \tau) = \left[\frac{(\alpha s + \beta) - \alpha(s-1)e^{-(\alpha+\beta)\cdot\tau}}{\alpha + \beta} \right]^{n_0} \quad (3.52)$$

$$\bar{n} = E[N(\tau)] = \left[\frac{\partial G(s, \tau)}{\partial s} \right]_{s=1} = \alpha n_0 \left[\frac{1 - e^{-(\alpha+\beta)\tau}}{\alpha + \beta} \right] \quad (3.53)$$

Using the relation that gives \bar{n} is expressed the time evolution of the permeate flow rate for filtration at constant pressure difference. Because here the permeate flow rate is proportional with the non-blocked pores number it can be written the relation (3.54)

$$\frac{G_{vp}}{G_{vp0}} = \frac{k_p (n_0 - \bar{n})(p - p_{ex})}{k_p n_0 (p - p_{ex})} = F(c_{vs}, p, \tau) = \frac{n_0 - \bar{n}}{n_0} = 1 - \alpha \left[\frac{1 - e^{-(\alpha+\beta)\tau}}{\alpha + \beta} \right] \quad (3.54)$$

There is not a theoretical possibility to establish α and β values and consequently so it must be appealed, for their identifications, to experimental measurements (see data from table 3.6).

Mathematical model of ultrafiltration device

The flowsheet for the ultrafiltration separation process, described inside of subparagraph **Influence of feed quality on membrane productivity and efficiency**, is concentrated in fig. 3.11. It consists of one ultrafilter connected with feed tank and permeate storage tank. The feed taken from a fixed initial volume of ARW with added clay (see table 3.7 for composition of processed ARW) is driven to the concentrate side of the membrane module where it is subjected to the difference in pressure that is driving the flow of liquid through the membrane. The product from this operation is obtained on the permeate side from where it goes to tank 2. The membrane concentrate is recirculated to the feed tank. Here occurs the concentration of ARW in solids and at the same time the transfer of some species (^{60}Co , ^{137}Cs and ^{241}Am respectively). The mathematical model associated to the working of this device consists of one system of differential-algebraic equations (DAE), which can be solved by an integration procedure. For mathematical model building it is considered an unsteady state species mass balance on tanks of volumes V_1 and V_2 , unsteady state mass transfer between solid particles (clay) and liquid phase for ^{60}Co , ^{137}Cs and ^{241}Am species and basic relations characterizing the operation of ultrafilter having membrane area A_1 . In order to consider the clogging of membrane in time, the relation (3.54) is used as in (3.55) where j_{p0} comes from relation (3.34), with α and β are established based on data from table 3.6.

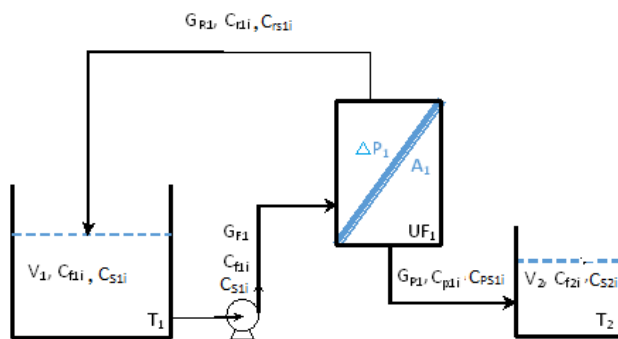


Figure 3.11. Flowsheet for ultrafiltration device for processing of ARW resulted from deep bed filtration

$$\frac{j_p}{j_{p0}} = 1 - \alpha \left[\frac{1 - e^{-(\alpha + \beta)\tau}}{\alpha + \beta} \right] \quad 3.55)$$

Table 3.7 shows that the identification of α and β clogging parameters follows the minimizing of mean quadratic deviation between the experimental permeate specific flow rate and the calculated one, according to relationship (3.55). The segmentation of data from table 3.7 in a two set highlights a linear dependence of α and β upon concentration of total suspended solid in processed media.

Table 3.7. Computation of α and β with data from table 3.6 using Matchad soft

No.	Computation action
1.	Is given the basic experimental conditions of ultrafiltration clogging test: $p = 0.25 \text{ MPa}$; $t = 25^\circ\text{C}$; $c_{TSS0} = 200 \text{ mg/L}$
2.	Are selected the data showing the membrane clogging (first line: current number, second line: time in min, third line specific permeate flow rate in $\text{L/m}^2\text{h}$, fourth line c_{TSS} in mg/L) from table 3.6: $\text{Data := } \begin{pmatrix} 1 & 2 & 3 & 4 & 5 & 6 \\ 0 & 15 & 30 & 40 & 50 & 60 \\ 205 & 180 & 144 & 136 & 124 & 96 \\ 110 & 198 & 277 & 512 & 623 & 895 \end{pmatrix}$
3.	Is defined the function containing the clogging parameters: $f(\alpha, \beta, \tau) := 1 - \alpha \cdot \left[\frac{1 - \exp[-(\alpha + \beta) \cdot \tau]}{\alpha + \beta} \right]$
4.	Are established α and β values for two range of solid concentration in the processed ARW: $F(\alpha_1, \beta_1) := \left[\sum_{i=0}^2 \left[\frac{(\text{ML}^{(2)})_i}{\text{ML}_{0,2}} - f[\alpha_1, \beta_1, (\text{ML}^{(1)})_i] \right] \right]^2$ $\alpha_1 := 0.01; \quad \beta_1 := 0.02 \quad R_1 := \text{Minimize}(F, \alpha_1, \beta_1) \quad R_1 = \begin{pmatrix} 0.013 \\ 0.018 \end{pmatrix}$ $F(\alpha_2, \beta_2) := \left[\sum_{i=3}^5 \left[\frac{(\text{ML}^{(2)})_i}{\text{ML}_{3,2}} - f[\alpha_2, \beta_2, (\text{ML}^{(1)})_i] \right] \right]^2$ $\alpha_2 := 0.01 \quad \beta_2 := 0.02 \quad R_2 := \text{Minimize}(F, \alpha_2, \beta_2) \quad R_2 = \begin{pmatrix} 4.935 \times 10^{-3} \\ 0.025 \end{pmatrix}$
5.	Is found the linear dependence of α and β upon solid concentration in the processed ARW: $Y_1 := \begin{pmatrix} R_{1,0} \\ R_{2,0} \end{pmatrix}, \quad Y_2 := \begin{pmatrix} R_{1,1} \\ R_{2,1} \end{pmatrix}, \quad X := \begin{pmatrix} \sum_{i=0}^2 (\text{ML}^{(3)})_i \\ 3 \end{pmatrix}$ $\sum_{i=3}^5 (\text{ML}^{(3)})_i \\ 3$ $m_1 := \text{slope}(X, Y_1), \quad n_1 := \text{intercept}(X, Y_1), \quad n_1 = 0.017, \quad m_1 = -1.762 \times 10^{-5}$ $m_2 := \text{slope}(X, Y_2), \quad n_2 := \text{intercept}(X, Y_2), \quad n_2 = 0.016, \quad m_2 = 1.32 \times 10^{-5}$
6.	Are written the obtained expressions showing the α and β dependence upon solid concentration of processed ARW: $\alpha = n_1 + m_1 c_{TSS}, \quad \beta = n_2 + m_2 c_{TSS} \quad (c_{TSS} \text{ as mg/L})$

The relations (3.56) and (3.57) show the final expression of α and β .

$$\alpha = 0.017 - 1.762 * 10^{-5} c_{TSS} \quad (3.56)$$

$$\beta = 0.016 + 1.321 * 10^{-5} c_{TSS} \quad (3.57)$$

The composition of ARW processed with the specified ultrafiltration arrangement shown in fig. 3.11 is given in table 3.8. Adding of fresh clay was used to estimate the effect of solid concentration of processed ARW on membrane clogging.

Table 3.8. Physical characteristics of processed ARW

pH	8.35
Electrical conductivity ($\mu\text{S}/\text{cm}$)	1140
TDS (mg/L)	710
TSS (mg/L)	
- $d_p > 8 \mu\text{m}$	0
- $d_p < 8 \mu\text{m}$	10
Mean concentration of γ radionuclides	
- in suspended particles (Bq/g)	^{60}Co 2.2 1.12
- in liquid phase (Bq/L)	^{137}Cs 2.2 17.5
^{241}Am	18 0.21
Fresh added clay (mg/L) mean $d_p < 80 \mu\text{m}$	100
variance $d_p < 8 \mu\text{m}$	

Taking into account the composition of ARW (see table 3.8) a mass transfer currently occurs from liquid to solid (fresh added clay) for ^{60}Co , ^{137}Cs and ^{241}Am . So this fact is considered in modelling. At the same time it is considered that the ultrafiltration membrane adsorption of mentioned radioactive species is not important. From table 3.6 it can be observed that membrane rejection of solid shows an important decrease of solid presence in permeate when the concentration of solids in ultrafiltration feed increase. The processing of data from the mentioned table leads to the relation (3.58) for the degree of solid separation by membrane (p subscript appears for permeate and R for retentate (concentrate)). For species ^{60}Co , ^{137}Cs and ^{241}Am it is assumed that the concentration in the permeate and in the retentate (concentrate) is the same (the membrane does not separate small species (ionic species) from the liquid).

$$T_{RSS} = 1 - \frac{c_{pTSS}}{c_{RTSS}} = 1 - 0.003 * \exp(-0.00002 * c_{RTSS}) \quad (3.58)$$

With the above considerations the mathematical model of ultrafiltration arrangement (fig. 3.11) contains the following equations: mass balance for reservoir T₁ (3.59), expression for permeate volumetric flow rate (3.60), total mass balance for ultrafilter (3.61), expressions for initial specific flow rate ((3.29)-(3.31) and (3.34)), definition of T_{RSS} for a link of solid concentration in permeate and retentate (3.58), the equality of concentration in retentate and permeate for ^{60}Co , ^{137}Cs and ^{241}Am species (3.62), the species mass balance for ^{60}Co , ^{137}Cs and ^{241}Am and T₁ reservoir (3.63), the solid mass balance for the reservoir 1 (3.64), the

accumulation of ^{60}Co , ^{137}Cs and ^{241}Am on solid in reservoir 1 (3.65), the solid mass balance for ultrafilter (3.66), total mass balance (3.67) and species (^{60}Co , ^{137}Cs and ^{241}Am and TSS) balance ((3.68) and (3.69)) for permeate collecting reservoir, initial conditions for all time process variables (3.70)).

$$\frac{dV_1}{dt} = G_{R1} - G_{F1} \quad (3.59)$$

$$G_{p1} = J_p * A_1 \quad (3.60)$$

$$G_{R1} = G_{F1} - G_{p1} \quad (3.61)$$

$$c_{v1Ri} = c_{pi}, \quad i = Co, Cs, Am \quad (3.62)$$

$$\frac{d(V_1 c_{v1Ri})}{dt} = G_{R1} c_{v1Ri} - V_1 c_{v1TSS} \sigma_s k_{ti} (1 - k_{di}) c_{v1Ri} \quad (3.63)$$

$$\frac{d(V_1 c_{v1TSS})}{dt} = G_{R1} c_{v1RTSS} - G_{F1} c_{v1TSS} \quad (3.64)$$

$$\frac{d(V_1 c_{v1si})}{dt} = V_1 c_{v1TSS} \sigma_s k_{ti} (1 - k_{di}) c_{v1Ri}, \quad i = Co, Cs, Am \quad (3.65)$$

$$c_{v1RTSS} = \frac{G_{F1} c_{v1TSS} - G_{p1} c_{pTSS}}{G_{R1}} \quad (3.66)$$

$$\frac{dV_2}{dt} = G_{p1} \quad (3.67)$$

$$\frac{d(V_2 c_{v2pi})}{dt} = G_{p1} * c_{pi}, \quad i = Co, Cs, Am \quad (3.68)$$

$$\frac{d(V_2 c_{v2TSS})}{dt} = G_{p1} * c_{pTSS} \quad (3.69)$$

$$\begin{aligned} \tau &= 0, & c_{v1TSS} &= c_{v1TSS0}, & c_{v2TSS} &= 0, & V_1 &= V_0, & V_2 &= 0, & c_{v1TSS} &= c_{v1TSS0}, \\ c_{v2TSS} &= 0, & c_{v1pi} &= c_{v1pi0}, & c_{v2pi} &= 0, & c_{v2TSS} &= 0, & i &= Co, Cs, Am \end{aligned} \quad (3.70)$$

A summary of presented model shows that it is composed by a system with 13 differential equations completed with algebraic equations which fix the concrete action of units of ultrafiltration arrangement.

For numerical process simulation is used the data from table 3.8, which indicates the values of some of initial species concentration for ARW, proposed for processing by ultrafiltration. Other operating factors are as follows: temperature: 25°C, ultrafiltration pressure: 0.25 MPa, pump flow rate: 5 m³/h, ultrafilter area: 5 m², capacity of reservoir 1 and of reservoir 2: 10 m³. A good correlation between the experimental and numerical data was observed and the full technical details of the numerical process simulation will be published elsewhere.

3.3.5. Conclusions

ARW ultrafiltration was performed using an installation containing spiral-wound polysulphonamide membrane modules in order to evaluate the influence of process factors and waste quality on membrane productivity and efficiency.

Permeate volumetric flux (j_P) and permeate TSS (TSS_P) were measured at different values of feed flow rate (G_V), operating pressure (p) and feed TSS (TSS_F). Permeate flux increased with feed flow rate and operating pressure, as well as decreased with an increase in TSS_F . Permeate TSS exhibited an opposite trend, *i.e.*, it increased with TSS_F and decreased with an increase in G_V and p . The influence of process factors on its performances was quantified using a 2^3 factorial plan. Regression equations which were obtained could be applied to predict the values of permeate flux and TSS at levels of process factors in the ranges considered in the experimental study.

For ARW with high solid particles concentration, ultrafiltration membrane performance is still very good, although permeate volumetric flux decreased.

A stochastic model composed by a system with 13 differential equations completed with algebraic equations which fix the concrete action of units of ultrafiltration arrangement was developed and a numeric process simulation was initiated.

The results obtained in this experimental study are very useful in establishing the performance criteria for ARW treatment by ultrafiltration, related to acceptable limits for variability in productivity and efficiency so that the system could be able to treat a large range of waste, and effective even with fluctuating ARW loadings and different required flow rates.

REFERENCES

- [1] G. Zakrzewska-Trznadel, *Advances in membrane technologies for the treatment of liquid radioactive waste*, Desalination **321**, 119-130, 2013
- [2] V. Ramachandhran, B.M. Misra, *Studies on the radiolytic degradation of cellulose acetate membranes*, J. Appl. Polym. Sci. **30**(1), 35-43, 1985
- [3] V. Ramachandhran, B.M. Misra, *Studies on the radiation stability of ion exchange membranes*, J. Appl. Polym. Sci. **32** (7), 5743-5747, 1986
- [4] A.G. Chmielewski, M. Harasimowicz, *Influence of gamma and electron irradiation on transport properties of ultrafiltration membranes*, Nukleonika **37**(4), 61-70, 1992
- [5] A.G. Chmielewski, M. Harasimowicz, *Influence of gamma and electron irradiation on transport properties of nanofiltration and hyperfiltration membranes*, Nukleonika **42**(4), 857-862, 1997
- [6]. D.E. Potts, R.C. Ahlert, S.S. Wang, *A critical review of fouling of reverse osmosis membranes*, Desalination, **36**, 235-264, 1981
- [7]. C.R. Bouchard, P.J. Carreau, T. Matsuura, S. Sourirajan, *Modelling of ultrafiltration: prediction of concentration polarization effects*, J. Membr. Sci., **97**, pp. 215-229, 1994
- [8]. M. Mulder, *Basic Principles of Membrane Technology*, Kluwer Academic Publishers, Dordrecht, Netherlands, 416-464, 1996
- [9] G.B. Van Den Berg, C.A. Smolders, *Flux Decline in Ultrafiltration Processes*, Desalination, **77**, 101-133, 1990
- [10] T. Varzakas, C. Tzia, *Food Engineering Handbook: Food Process Engineering - Models which describe the CP phenomenon by the film theory*, CRC Press, 16-17, 2014
- [11] R. Ruby-Figueroa, J. Saavedra, N. Bahamonde, A. Cassano, *Permeate flux prediction in the ultrafiltration of fruit juices by ARIMA models*, J. Membr. Sci., **524**, 108-116, 2017
- [12] S. De, S. Bhattacharjee, P.K. Bhattacharya, *Development of Correlations for Mass Transfer Coefficients in Ultrafiltration Systems*, Asia-Pacific Journal of Chemical Engineering, **3(3-4)**, 187-206, 1995
- [13] S. Bhattacharjee, *Estimation of Mass Transfer Coefficient and Gel Concentration During Ultrafiltration of PEG Solution in A Tangential Flow Ultrafiltration Module*, International Journal of Engineering Research & Technology (IJERT), **2(8)**, 1893-1895, 2013
- [14] M.N. de Pinho, V. Geraldes, *Mass transfer coefficient determination method for high-recovery pressure-driven membrane modules*, Desalination, **195**, 69-77, 2006
- [15] W.R. Bowen, F. Jenner, *Theoretical descriptions of membrane filtration of colloids and fine particles: an assessment and review*, Adv. Colloid. Interfac., **56**, 141-200, 1995
- [16] M.W. Chudacek, A.G. Fane, *The dynamics of polarisation in unstirred and stirred ultrafiltration*, J. Membr. Sci., **21**, 145-160, 1984
- [17] P. Dejmek, *Concentration polarization in UF*, Ph.D. Thesis, The University of Lund, Sweden, 1975
- [18] S. Bleich, *Pressure relaxation flux recovery in filtration of Alginate solutions by Ultrafiltration and Microfiltration membranes*, M.Sc. Thesis, The Hebrew University of Jerusalem, Israel, 2011

- [19] J.A. Howell, O. Velicangil, *Theoretical considerations of membrane fouling and its treatment with immobilized enzymes for protein ultrafiltration*, *J. Appl. Polym. Sci.*, **27**, 21–32, 1982
- [20] R.J. Baker, A.G. Fane, C.I.D. Fell and B.H. Yoo, *Factors affecting flux in crossflowfiltration*, *Desalination*, **53**, 81-93, 1985
- [21] A.G. Fane, *Ultrafiltration of suspensions*, *J. Membr. Sci.*, **20**, 249-259, 1984
- [22] G.B. Van Den Berg, C.A. Smolders, *The boundary layer resistance model for unstirred ultraliltration. A new approach*, *J. Membr. Sci.*, **40**, 149-172, 1989
- [23] V. Gekas, B. Hallstrom, *Mass transfer in the membrane concentration polarization layer under turbulent cross flow. I. Critical literature review and adaption of existing Sherwood correlations to membrane operations*, *J. Membr. Sci.*, **30**, 153-170, 1987
- [24] G.B. Van Den Berg, I.G. Racz, C.A. Smolders, *Mass transfer coefficients in cross-flow ultrafiltration*, *J. Membr. Sci.*, **47**, 25-51, 1989
- [25] T. W. Cheng, J.G. Wu, *Modified Boundary Layer Resistance Model for Membrane Ultrafiltration*, *Tamkang Journal of Science and Engineering*, **4(2)**, 111-117, 2001
- [26] W.F Blatt, A. Dravid, A.S. Michaels and L. Nelson, *Solute polarization and cake formation on membrane ultrafiltration: causes, consequences, and control techniques*, J.E. Flinn (Ed.), *Membrane Science and Technology*, Plenum Press, New York, 47-97, 1970
- [27] M.C. Porter, *Concentration polarization with membrane ultrafiltration*, *Ind. Eng. Chem. Prod. Res. Dev.*, **11**, 234-248, 1972
- [28] M.C Porte, *Ultrafiltration of colloidal dispersions*, *AIChE Syrup. Ser.*, **68**, 21-30, 1972
- [29] A.A. Kozinski, E.N. Lightfoot, *Protein ultrafiltration: A general example of boundary Layer filtration*, *AIChE J.*, **18**, 1030-1040, 1972
- [30] A.G. Fane, C.I.D., Fell, A.G. Waters, *The relationship between membrane surface pore characteristics and flux for ultrafiltration membranes*, *J. Membr. Sci.*, **9**, 245-262, 1981
- [31] G.Jonsson, *Boundary layer phenomena during ultrafiltration of dextran and whey solutions*, *Desalination*, **51**, 61-77, 1984
- [32] A.S. Michaels, *New separation technique for the CPI*, *Chem. Eng. Prog.*, **64**, 31-43, 1968
- [33] M. Mulder, *Basic Principles of Membrane Technology 2nd edition*, Kluwer Academic Publishers Dordrecht/Boston/London, 416-464, 1996,
- [34] H.M. Yeh, *Modified Gel-Polarization Model for Ultrafiltration in Hollow-Fiber Membrane Modules*, *Sep. Sci. Technol.*, **31(2)**, 201-211, 1996
- [35] R. Paulen, G. Foley, M. Fikar, Z. Kov'acs, P. Czermak, *Minimizing the process time for ultrafiltration/diafiltration under gel polarization conditions*, *J. Membr. Sci.*, **380(1-2)**, 148-154, 2011
- [36] S.K. Pawar, K.V. Marathe, *Validation of Multiple Solute Model for Application to Micellar Enhanced Ultrafiltration and Comparison with Modified Resistance in Series Model*, *J. Appl. Sol. Chem. Model.*, **2**, 110-121, 2013
- [37] H. Nabetani, M. Nakajima, S.Hagiwara, A. Watanabe, S. Nakao, S. Kimura, *Solute Adsorption and Gel Layer Formation during Ultrafiltration of Ovalbumin*, *Food Sci. Technol. Res.*, **15(3)**, 225 – 232, 2009
- [38] B. Elysee-Collen, R.W. Lencki, *Protein ultrafiltration concentration polarization layer flux resistance I. Importance of protein layer morphology on flux decline with gelatin*, *J. Membr. Sci.*, **129(1)**, 101-113, 1997

- [39] S. Ma, S.C. Kassinos, D. Kassinos, *Direct simulation of the limiting flux: I. Interpretation of the experimental results*, J. Membr. Sci., **337(1-2)**, 81–91, 2009
- [40] M. Yazdanshenas, A. Tabatabaeenezhad, R. Roostazaad, A. Khoshfetrat, *Full scale analysis of apple juice ultrafiltration and optimization of diafiltration*, Sep. Purif. Technol., **47(1-2)**, 52–57, 2005
- [41] O. Kedem, A. Katchalsky, *Thermodynamic analysis of the permeability of biological membranes to non-electrolytes*, Biochim. Biophys. Acta, **27**, 229-246, 1958
- [42] J.G. Wijmans, S. Nakao, C.A. Smolders, *Flux limitation in ultrafiltration: osmotic pressure model and gel-layer model*, J. Membr. Sci., **20**, 115-124, 1984
- [43] T. Dobre, J.M. Sanchez, *Chemical Engineering Modelling, Simulation and Similitude*, Wiley VCH, 308-419, 2007
- [44] L. R. Zicman, E. Neacsu, F. N. Dragolici, C. Ciobanu, Gh. Dogaru, O. C. Parvulescu, T. Dobre, *Experimental and Modelling of Aqueous Radioactive Waste Treatment by Ultrafiltration*, Rev. Chim., **69(5)**, 1149-1151, 2018
- [45] SUEZ's degremont® Water handbook, digital edition, 2016
- [46] Litwiniszyn, J., *Colmatage with reference to the Model of a Random Walking*, Bull. Acad. Pol. Sci., Ser. Sci. Tech., 15, 6, 345-351, 1967
- [47] T. Dobre, J. Sanchez, *Chemical Engineering –Modelling and Simulation*, Wiley VCH, 2007
- [48] T. Dobre, J. Sanchez Marcano, I. Gustav, *Modeling of a filtration unit where clogging occurs II. Stochastic modeling of the clogging function*, Rev Chim - Bucharest, **56**, 8, 866-872, 2005.

CHAPTER 4. CHARACTERIZATION AND MODELLING OF FIXED BED SORPTION PROCESS IN LIQUID RADIOACTIVE WASTE TREATMENT

The fixed bed sorption process is one of the most used sorption procedure for species (target species in industrial applications, pollutants, etc.) separation from gases or liquid media. The fluidised bed and the moving bed procedures are also frequently employed in this type of separations because they confer the capacity to work in continuous steady state regime. Fixed bed sorption procedure works in an unsteady state regime, normally with two steps corresponding to adsorption and desorption. The first part of this chapter contains literature data on sorbents, fluid-sorbent equilibrium and dynamics for fixed bed separation. The second part presents the obtained experimental data and modelling for the case of ^{137}Cs species separation using nickel ferrocyanide fixed on silicagel sorbent.

4.1. Sorbents and their specificity

Sorption is a separation process in which specific components can be distributed between two phases. There are three types of sorption, that can be classified depending on the type of bonding between solute species and sorbent:

(a) Physical sorption. In this case, no exchange of electrons occurs, only intermolecular attractions between valent sites. The heat of adsorption, or activation energy, is low and thus this type of process is stable only at low temperature (it not known a sorption proces of this type operating over 100°C).

(b) Chemical sorption. Also known as chemisorption represents the case of formation of strong bonds (chemical bonds) between active surface sites and the adsorbate. In comparison with physical adsorption, chemisorption has a stronger adsorption energy and thus the bond is more stable at elevated temperature.

(c) Electrostatic sorption (ion exchange sorption). This involves the adsorption of ions by Coulombic attractive force and is more commonly classified as ion exchange. Besides being ion exchangers, these materials can also act as sorbents. When they come in contact with an electrolyte solution the dissolved ions are concentrated on both the surface and in the pores of the ion exchange media. In a solution of weak electrolytes or non-electrolytes, sorption by ion exchangers is similar to that of non-ionic adsorbents. In a solution of strong electrolytes a sorption equilibrium results, owing to the electrostatic attraction between the ions in solution and the fixed ionic groups on the ion exchange media.

In all cases and thus also for ion exchange sorption, the sorption equilibrium is represented by sorption isotherm curves [1], which shows at constant temperature the equilibrium state of solute species in fluid and solid phases.

Ion exchangers are solid materials which have the capability to adsorb positively or negatively charged ions from an electrolyte solution and release an equivalent amount of equal charge sign ions into the solution. Ion exchange materials exchange the mobile ions of an external solution for ions bound by electrostatic forces to the functional groups existing in a solid matrix (the ion exchange material). Ion exchange materials usually have greater affinity for certain ionic species than for others, allowing the possibility to capture the higher-affinity species from solution in exchange for lower-affinity species (e.g., H). Organic and inorganic ion exchange materials have been developed and are available in a variety of forms with widely different chemical and physical properties. In general, choosing an ion exchanger is directly dependent on the suitability for a given application. Applications of ion exchange in nuclear engineering are important and undergoing continuous development [1].

4.1.1. Organic ion exchange resins

An organic ion exchange resin consists of a resin or polymer acting as medium for ion exchange. Typically, is an insoluble matrix (or support structure) made up of microparticles (0.25 - 0.75 mm radius), manufactured from an organic polymer substrate. These particles are porous, which provide a good surface area for the ion exchange, both onto and inside their structure. Some ions are released while other ions are trapped thus the ion exchange process occurs. The ion exchange resins are of various types, including polystyrenes, phenolic resins, polysaccharides (such as cellulose), proteins (such as casein, keratin and collagen) and carbonaceous materials (such as charcoals, lignites and coals). The use of organic ion exchangers in nuclear engineering presents a lot of advantages and disadvantages. As *advantages* of organic ion exchange resins can be mentioned the following: they are available on large scale at reduced cost, present good mechanical properties and are suitable for treatment or stabilization with other additives in order to enhance their uniformity, stability, or sorption selectivity. For instance, charcoals can be treated with different chemical substances that help improve their capacity or selectivity, also cellulose can undergo changes and incorporate phosphate, carbonic functional groups. As *disadvantages* of organic ion exchangers can be mentioned: a decreased exchange capacity compared to inorganic exchangers, sensitivity to swelling and peptide formation. They also exhibit lower radiation and thermal stabilities than their inorganic equivalents. Moreover, many organic exchangers do not have a good selectivity and stability outside the neutral pH range. Ultimately, radiation damage makes it impossible to sufficiently recharge the material after elution of radioisotopes so they cannot be used for subsequent capture/release cycles.

4.1.2. Inorganic ion exchange adsorption materials

Inorganic materials having a structure with an electrical excess charge can function as ion exchangers. There is a very large number of inorganic materials capable of ion exchange. In general, a very interesting property is their high selectivity, so it is possible to use ion exchange in the event when very high concentrations of competing ions are present. Moreover, they are more stable from thermal and radiation point of view when compared to organic exchangers. Zeolites, in particular, can be manufactured/engineered with a wide variety of chemical properties and pore sizes and are stable at high temperatures. Titanates are especially good for absorbing Sr^{2+} in highly alkaline solutions with extremely high salt concentrations such as those found in nuclear waste [2, 3]. Inorganic media exhibit better mechanical and chemical stability compared to their organic counterparts. Synthetic zeolites, in particular, are rather costly, with limited chemical stability when exposed to extreme pH ranges, and also their ion specificity is sensitive to interference from ions with similar sizes. Titanates and silicotitanates have lower efficiency in acidic conditions ($\text{pH} < 4 - 5$) as protons interfere with the ion exchange [4]. Only doped antimony silicates have been proven effective at a pH level lower than 1 or other highly acidic conditions [5].

4.1.3. Short considerations on solute ion exchange equilibrium

As a rule, ion exchange equilibrium can be defined by any of the following terms [6]:

- i) the ion exchange isotherm, ii) the separation factor, iii) the selectivity coefficient, iv) the sorption capacity and respectively v) the distribution coefficient.

The adsorption in ion exchange process follows sorption isotherms like Langmuir, Freundlich and Dubinin-Radushkevitch (D-R) models. Sorbent selectivity is defined by **separation coefficient** $K_{A/B}$ of microcomponent A and macrocomponent B (4.1)

$$K_{A/B} = \frac{K_{dA}}{K_{dB}} = K_{dA} \cdot \frac{C_B}{E_B} \quad (4.1)$$

Here K_{dA} is the distribution coefficient of microcomponent A, C_B represents the concentration of B macrocomponent in fluid and E_B shows the content of sorbent by macrocomponent B.

The sorbent chemical stability depends on solution composition, and on the chemical nature of the sorbent. Better chemical stability in a wide pH domain exhibit the organic ion exchange resins while inorganic sorbents (based on phosphates and oxyhydrates of non-ferrous metals) as well as synthetic and natural zeolites are not stable in acid media (at $\text{pH} < 3$). Sorbents based on ferrocyanides of transitional metals are not stable in alkaline media (at $\text{pH} > 10$).

Breakthrough properties of an ion for different adsorption materials are described by the **breakthrough curves** in various conditions.

It must be taken into consideration the fact that **selectivity coefficients** are not constant and vary with the experimental parameters such as concentration, temperature and presence of other ions in the solution. It should be noted that the determination of selectivity coefficients is an elaborate issue and is usually not performed in the design of waste treatment systems as the majority of these parameters can be obtained from manufacturers' data or literature research respectively experimental research. For general design purposes a few orientative rules can be applied: for cationic organic ion exchange resins (considering low concentrations and normally encountered temperatures in waste processing), the affinity typically increases with an increasing charge on the exchanging cation (a) and an increasing atomic number (decreasing hydrated ionic radii) of the exchanging cation(b), for example the following affinity series: (a) $\text{Li}^+ < \text{H}^+ < \text{Na}^+ < \text{K}^+ < \text{Cs}^+ < \text{Mg}^{2+} < \text{Co}^{2+} < \text{Ca}^{2+} < \text{Sr}^{2+} < \text{Ce}^{3+} < \text{La}^{3+} < \text{Th}^{4+}$ and respectively (b) $\text{Li}^+ < \text{H}^+ < \text{Na}^+ < \text{K}^+ < \text{Cs}^+$.

In the above specification Li^+ is an exception, due to its high hydration energy.

To determine **the distribution coefficient** for ions in aqueous phase and one solid sorbent the following equation is used (4.2). That is obtained from the static batch equilibration technique and here C_i and C_f are the concentrations of the aqueous phase before and after equilibration with the solid sorbent matrix, V is the volume of the aqueous phase and m represents the weight of the matrix.

$$K_d = \frac{C_i - C_f}{C_f} \times \frac{V}{m} \text{ (mL/g)} \quad (4.2)$$

4.2. Modelling of sorption process

An ion exchange system is made up of an aqueous solution in which is found the water swollen ion exchange material. As it is a heterogeneous process, the ion exchange is carried out by ions movement to and from the boundary between interphases. The processes occurring during ion exchange are ion diffusion inside the solid material, ion surface chemical reaction and counter ion diffusion in solution. Moreover, should also be taken into consideration the formation of a thin film at the surface of the solid material. This thin film has different properties than the surrounding solution and its formation cannot be avoided even under strict agitation conditions, but only reduced thickness can be achieved.

4.2.1. Batch systems

In batch systems, the liquid and solid phases, forming an heterogenous system, are brought into intimate contact by mixing. As noted in literature the time of phases contacting

follows the approach of thermodynamic equilibrium. Equilibrium condition is attained when the concentration of the solute remains constant, as a result of zero net transfer of solute sorbed and desorbed from sorbent surface. The equilibrium sorption isotherms depict the connection between the equilibrium concentration, at constant temperature, of the sorbate in the solid and liquid phase. From experimental data can be obtained different isotherm shapes. As it is shown in fig. 4.1 is possible to have linear, favorable, strongly favorable, irreversible and unfavorable [7] equilibrium situations.

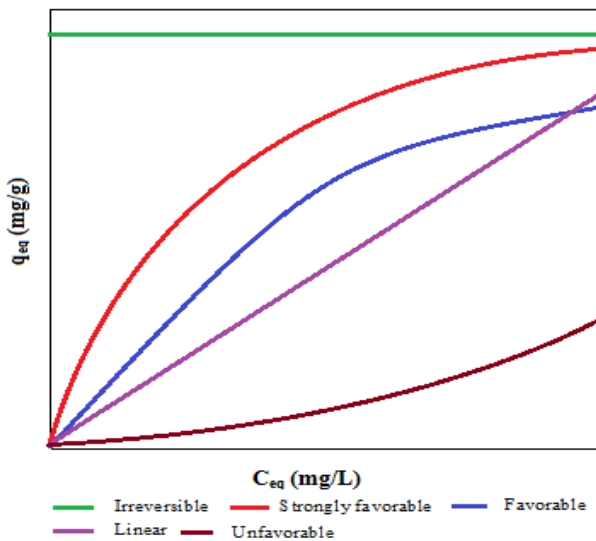


Figure 4.1. Adsorption isotherms

As in all equilibrium cases, the linear isotherm starts from the origin. Sometimes, the sorbent related to this type of isotherm, is selected because the column modelling is easier, especially when equilibrium data is added to the phenomenological dynamic model [8]. Sorbents from which convex upward curvature isotherms are obtained are entitled favorable and strongly favorable. These shapes are chosen for studies in dynamic conditions as they indicate the selectivity of the sorbent to the sorbate of interest. The Langmuir model is suitable for strongly favorable isotherms because it forms a plateau that generally depicts the monolayer adsorption. Sometimes the Langmuir model represents the experimental data even though there are different sites involved in the sorption process such as the ones located in the supercages or in the sodalite cages of NaX zeolite [9]. On the contrary, the sorbent may be highly heterogeneous and in this case, only one type of site may be effective in the sorption process. The irreversible adsorption, represented by a horizontal line, describes the restriction of the extremely favorable isotherm, when exists a constant amount of sorbed compound. When an irreversible isotherm is obtained, no regeneration can occur.

The **Langmuir adsorption model** [10] explains adsorption starting from the assumption that the adsorbate behaves as an ideal gas in isothermal conditions. In these

conditions the adsorbate's partial pressure, p_A , is related to the volume, V , adsorbed onto a solid adsorbent. It is assumed that the adsorbent is an ideal solid surface made up of a series of particular sites where the adsorbate may bind itself. The binding process is considered to be a chemical reaction between the adsorbate molecule A_g and an empty site, S . From this reaction is obtained an adsorbed complex A_{ad} with an associated equilibrium constant, K_{eq} . From these assumptions the Langmuir isotherm can be derived as it is shown by relation (4.4) where θ_A represents the fractional occupancy of the adsorption sites by solute A and V_m expresses the volume of the monolayer from A on sorbent surface.



$$\theta_A = \frac{V}{V_m} = \frac{K_{eq}^A p_A}{1 + K_{eq}^A p_A} \quad (4.4)$$

The adsorption model is constructed on the premiss that a continuous monolayer of adsorbate molecules surrounds a homogeneous solid surface [11]. This particular model presents some disadvantages because it does not consider the adsorbent surface roughness (rough non-homogeneous surfaces have multiple site-types available for adsorption, and also some parameters may be different from site to site, eg. heat of adsorption) and the interactions that occur between adsorbates. Direct interactions happen between neighboring adsorbed molecules, influencing the high-coverage behavior. In the case of indirect interactions, the adsorbate modifies the surface around the adsorbed site, which influences the adsorption of other adsorbate molecules found in the vicinity.

The model revisions take into consideration the points mentioned before, like surface roughness, inhomogeneity, and adsorbate-adsorbate interactions and some of them are presented in the following.

The **Freundlich isotherm** [12] has been extensively used to characterise multisite adsorption process for rough surfaces. With θ_A and p_A as measure of solute species concentration in solid and liquid respectively, the Freundlich isotherm is expressed with relation (4.5) where α_F and C_F are fitting parameters.

$$\theta_A = \alpha_F p_A^{C_F} \quad (4.5)$$

The Freundlich isotherm has two parameters while Langmuir's equations has only one. Freundlich isotherm generally fits the data on rough surfaces much better than the Langmuir's equation.

A related equation is the **Toth equation** [13]. By rearranging the Langmuir equation, one can obtain the below relations between θ_A and p_A . As it is shown by relation (4.7), Toth has modified the equilibrium equation (4.6) by adding two parameters, α_{T0} and C_{T0} .

$$\theta_A = \frac{p_A}{\frac{1}{K_{eq}^A} + p_A} \quad (4.6)$$

$$\theta_A = \frac{\alpha_{T_0} p_A^{C_{T_0}}}{\frac{1}{K_{eq}^A} + p_A^{C_{T_0}}} \quad (4.7)$$

The **Temkin Adsorption Isotherm** accounts for indirect adsorbate-adsorbate interactions on adsorption isotherms [14]. Temkin determined experimentally that the decrease of heats of adsorption is more often than the increase with increasing sorbent coverage. By ignoring the extremely low and large values of concentrations, the model assumes, as above mentioned, that heat of adsorption (function of temperature) of all molecules in the layer would decrease linearly rather than logarithmic with coverage. As implied in the equation, its derivation, characterized by a uniform distribution of binding energies (up to some maximum binding energy), was carried out by plotting the quantity sorbed q_e against $\ln C_e$ and the constants were determined from the slope and intercept. The model is given by expresions (4.8)-(4.12) where A_T is Temkin isotherm equilibrium binding constant (L/g), b_T -Temkin isotherm constant. R expresses the value of universal gas constant (8.314J/mol/K), T introduces isotherm temperature and B is a constant related to heat of sorption (J/mol).

$$q_e = \frac{RT}{b_T} \ln(A_T C_e) \quad (4.8)$$

$$q_e = \frac{RT}{b_T} \ln(A_T) + \frac{RT}{b_T} \ln(C_e) \quad (4.9)$$

$$B = \frac{RT}{b_T} \quad (4.10)$$

$$q_e = B \ln(A_T) + B \ln(C_e) \quad (4.11)$$

In more adsorption studies has been obtained that the Temkin model is most suitable and the applicability follows the order: Temkin > Freundlich > Langmuir adsorption model. When A_T is subunit is possible to use Temkin isotherm in simplified form.

BET equation may describe more accurately the adsorption process where the adsorbate exceeds a monolayer. In 1938, Stephen Brunauer, Paul Hugh Emmett and Edward Teller made a remarkable contribution to surface science by formulating an isotherm for the adsorption of gasses in multimolecular layers, published in *Journal of the American Chemical Society* [15]. This article was the most frequently cited article and was the only one article

with more than 10,000 citations in adsorption research field. Brunauer's model of multilayer adsorption considers a random distribution of sites covered by one, two, three, etc., adsorbate molecules. Brunauer Emmet and Teller has carried out derivation of the isotherm equation for multimolecular adsorption by a method that is a generalization of Langmuir's treatment of a unimolecular layer. For pure gas sorption they obtained an isotherm equation as it is shown by relation (4.12) where v is the total volume, v_m is the volume of gas adsorbed when the entire adsorbent surface is covered with a complete unimolecular layer, c is a constant, p is the pressure, p_S is the saturation pressure of gas. When a species is adsorbed from a gas mixture, p is its' partial pressure.

$$\frac{p}{v(p_S - p)} = \frac{2}{v_m c} + \frac{c-1}{v_m c} \frac{p}{p_S} \quad (4.12)$$

The BET isotherm form for solid-solution system is given by relation (4.13). The relation (4.13) becomes the normal BET equilibrium expression for sorption in liquid media when $n \rightarrow \infty$. For Langmuir equilibrium, $n = 1$. It is observable that this equilibrium expression contains three parameters (q_m , k_l and respectively k_s).

$$q_e = q_m \frac{k_s C_e [1 - (n+1)(k_l C_e)^n + n(k_l C_e)^n]}{(1 - k_l C_e)[1 + (k_s / k_l - 1)k_l C_e - k_s / k_l (k_l C_e)^{n+1}]} \quad (4.13)$$

The design of dynamic sorption processes also considers the multicomponent effluent, meaning that studies of batch competitive systems may be relevant. Sorbents with affinities to different sorbates may be less effective in removing the one of interest. In these cases, higher packed beds are necessary. Multicomponent equilibrium data are obtained considering the initial multicomponent solution. Many models have been proposed, some of them being derived from the single Langmuir model. As it happens with the single sorption, even when the ion exchange phenomenon is involved, release of the out-going ion is neglected [16 - 17].

4.2.2. Dynamic systems

All procedures performed in an unsteady state mode are called sorption dynamic systems. The fixed bed is one of this operation mode. Because the breakthrough curve synthetically characterizes this operation mode in the following are presented literature considerations on this aspect.

The breakthrough curve

The majority of ion-exchange operations, either occurring in laboratory or being a plant-scale process, are realised in columns with fixed bed. A solution flows through a bed of sorbent particles and during this process its composition is changed by transfer of some species via the sorbent particles. The change in time of effluent composition is dependent on

the sorbent properties, the feed composition and the operating conditions (flow rate, temperature etc.). The evolution of the ratio C/C_0 (outlet sorbate concentration/sorbate feed concentration) versus time is known as **breakthrough curves**.

When the fluid phase passes through a fixed sorbent bed, the exchange process occurs until in the effluent are detected amounts of the component which is retained or until its concentration reaches a certain value. So, at time τ is considered that the sorption occurs only in a certain zone of the ion exchange layer named mass transfer zone. A characteristic bed length is associated to the mass transfer zone (height of mass transfer zone). In this situation the layer before the mass transfer zone is saturated by the interested component while the rest of the layer contains pure sorbent. At this time, the effluent does not contain any traces from the retained component. As the run continues, the solid layer near the inlet is nearly saturated, and the mass transfer occurs further from the inlet. When the axial or radial dispersion of the fluid flow in bed are not considered, sorption occurs homogeneously and this is the ideal case. In reality, the concentration gradient is S shaped. The development of this concentration profile in sorption bed and their state at the bed exit, known as the breakthrough curve, is shown in fig. 4.2.

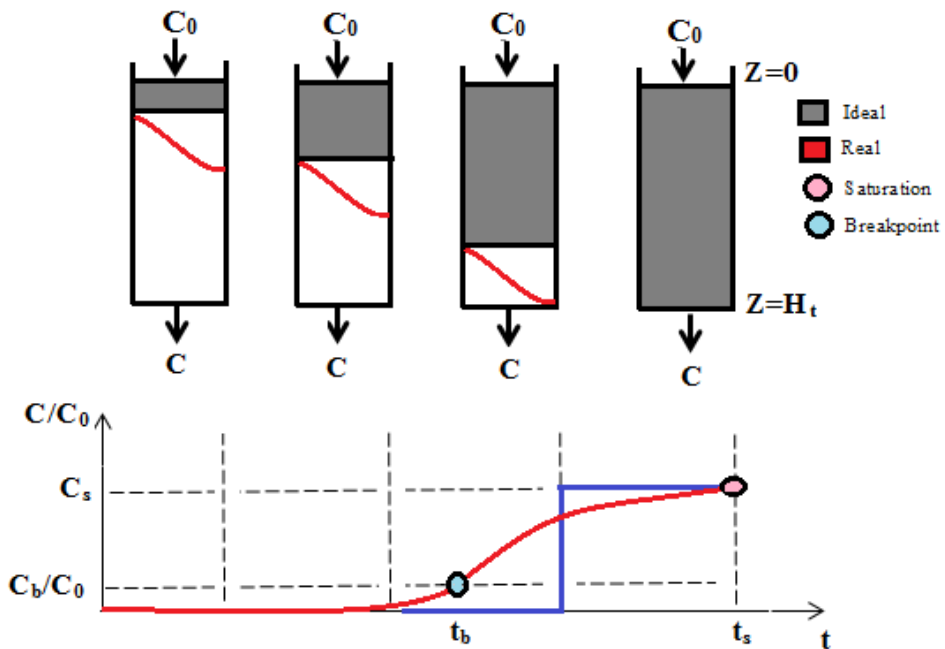


Figure 4.2. Breakthrough curve for the sorption process in fixed beds (C_0 concentration of the inlet solution, C_b concentration of the breakthrough, t_b breakpoint time, t_s saturation time).

The limits of the breakthrough curve are often taken as C/C_0 values of 0.05 to 0.95, unless any other recommendation is fixed. They are related to the breakpoint (t_b , C_b) and saturation point (t_s , C_s), respectively. In most of cases $C_s = C_0$.

When the concentration reaches the fixed limiting permissible value, it is considered that the breakpoint was reached. The flow is stopped, the column is either regenerated or replaced and the inlet concentration is redirected to another fresh sorbent bed.

Mass transfer in fixed beds

In fixed-bed ion exchange, the concentration varies with time and bed position both in the fluid phase and in the solid phase. The transfer process can be described by the overall volumetric coefficient ($K_c a$), which is obtained from a material balance in the column considering irreversible sorption as proposed in [9]. The usual expression of overall volumetric mass transfer coefficient (4.14) contains overall number of transfer units (N) - the length of the bed where the mass transfer is present (H_t) and superficial velocity of the fluid (u_o):

$$K_c a = \frac{N u_o}{H_t} \quad (4.14)$$

Eq. (4.14) can be used for modelling the breakthrough curves, if the batch isotherms can be considered as irreversible.

The overall number of transfer units may be obtained using definition formula, graphically or by numeric integration. In fixed bed sorption process it is used the dimensionless time (T), given here by means of relation (4.15).

$$T = \frac{u_o C_0 (t - \frac{\varepsilon}{u_o} H_t)}{\rho_p (1 - \varepsilon) W_{sat} H_t} \quad (4.15)$$

The term $\frac{\varepsilon}{u_o} H_t$ in Eq. (4.15) is the time required to displace fluid from external voids in the

bed, which is normally negligible. The multiplication from the counter of (4.15) is the total amount of metal fed per unit cross section of the bed up to time. At the denominator $\rho_p (1 - \varepsilon) W_{sat} H_t$ is the capacity of the bed reffering to the time equivalent to total stoichiometric capacity of the packed-bed tower (t_t).

The time equivalent to usable capacity of the bed (t_u) and the time equivalent to total stoichiometric capacity of the packed-bed tower (t_t) if the entire bed reaches equilibrium are provided by a mass balance in the column and they are easily determined [18] by relation (4.16) respectively (4.17), where t_b is the time of breakpoint.

$$t_u = \int_0^{t_b} \left(1 - \frac{C}{C_0}\right) dt \quad (4.16)$$

$$t_t = \int_0^{\infty} \left(1 - \frac{C}{C_0}\right) dt \quad (4.17)$$

With t_u and t_t is possible, as it is shown by relation (4.18), the estimation [17] of the length of unused bed (H_{UNB})

$$H_{UNB} = \left(1 - \frac{t_u}{t_t}\right) H_t \quad (4.18)$$

Different mass transfer parameters may be used for quantitative identification of the lowest resistances condition throughout the investigated working conditions. One of these parameters, referring to the flow mechanism of fluid phase in the bed, is the residence-time distribution (RTD). The average residence time (t_{res}) of the fluid in the column [19], assessed according to relation (4.19), depends on repartition function $F(t)$ (weight fraction of the effluent which stayed in column a shorter time than t) of flowing phase residence time in column. It is interesting to show that $F(t)$ is a curve similar to C/C_o for breakthrough curve.

$$t_{res} = \int_0^{\infty} t dF(t) \quad (4.19)$$

It can be determined how far from the optimum operational condition the column may operate, by the operational ratio, R [18]:

$$R = \frac{|t_{res} - t_u|}{t_u} \quad (4.20)$$

An R value close to zero is an indication that the imposed operational conditions are near the ideal condition, i.e., the optimal region of operation. Therefore, considering this difference one can better select the operational conditions in the column design process. Knowing the average residence time distribution, the variance evaluation in the breakthrough curve is also achievable [19], as in relation (4.21):

$$\sigma^2 = \int_0^{\infty} (t^2 (dF(t) - t_{res}^2)) dt \quad (4.21)$$

The dimensionless variance should be determined as:

$$\sigma_\theta^2 = \frac{\sigma^2}{t_{res}^2} \quad (4.22)$$

Calculation of this parameter is useful in estimating the axial dispersion in the packed bed. Values of σ close to zero represent that the behavior of the velocity profile in packed beds is close to ideal plug-flow with negligible axial dispersion.

Finally, considering a mass balance can be obtained the amount of sorbate retained up to the breakpoint time (U^{t_b}) and up to the saturation time (U^{t_t}).

$$U^{t_b} = t_u \times G_R \times C_0 \quad (4.23)$$

$$U^{t_t} = t_t \times G_R \times C_0 \quad (4.24)$$

In relations (4.23) and (4.24) t_u and t_b are computed according to Eqs. (4.16) and (4.17), G_R is the flow rate and C_0 represents the sorbate concentration at the inlet of fluid phase in the bed.

Minimum mass transfer resistances in the fixed bed

It is quite advantageous to run a process on fixed bed with minimum mass transfer resistances because the sorption process is maximized due to increased availability of sorption sites for the dynamic process. Therefore, it is strongly recommended to optimize the operational conditions. This can be performed by experimenting with a range of different sorbent particle diameters or different flow rates in the column. In special cases, temperature may also be investigated. One can assume to obtain a higher amount of retained sorbate with temperatures increase when the more significant mechanism consists in chemisorption and/or ion exchange. However, if the uptake is due to physisorption phenomenon, an increase in temperature is not so advantageous.

In optimal operational conditions, the mass transfer film around particle and particle resistances are minimised as much as possible while the pore and the solid diffusion are maximized. When the minimisation of film and particle resistances occurs, it is observed that:

- the mass transfer zone length and the operational ratio and the dimensionless variance are minimum;
- the closer the system is to the optimal condition, the closer the breakpoint time is to the saturation time;
- the sorbate uptake up to breakpoint time (U^{t_b}) and up to saturation time (U^{t_u}) are the maximum.

This takes place when there is at least one favorable isotherm and, generally, a steep breakthrough curve is noted.

Competition in sorption

When a feed solution is made up of more than one species, a competition for the sorption on sorbent sites may occur between these species. Uptake of the sorbate of interest is indicated by the dynamic capacity of the column. Thus, the term $U^{t_b}_{i-mix}$ represents the amount of sorbate uptaken at t_b prior to the sorbate i breakpoint [20].

The effect of competitive systems on the sorption process can be well represented by the ratio of the uptake capacity for the sorbent i in multicomponent solution, respectively in single solution, known as removal ratio [21]:

$$\frac{U^{t_b}_{i-mix}}{U^{t_b}_{i-single}} \quad (4.25)$$

Related removal ratio (4.25) the following situations are identified: $R_r > 1$: sorption is promoted if other sorbates are present; $R_r = 1$: there is no interaction between the sorbates; R_r

< 1 : sorption is not promoted if other sorbates are present. Therefore, investigating the effect of different sorbates on the uptake of an i sorbate is useful for evaluating the removal rate at a certain time equivalent to usable capacity of the bed t_u for sorbate i [22].

Isotherms importance in dynamic separation

In the majority of separation and purification processes using the sorption technology are employed continuous-flow columns. For a better understanding and modelling of the dynamic process, is necessary to have an extensive knowledge of the equilibrium in the fixed bed. In order to completely comprehend the entire process, information regarding equilibrium and process kinetics must be correlated with the mass balance. In a column, kinetic studies are almost exclusively limited to the processes where equilibria can be represented either by a linear or Langmuir isotherm or satisfy the mass action law. However, the results of this study including commercial products that have an industrial use have indicated that the above equilibria usually do not fit the experimental results adequately. Furthermore, the conventional procedures of determining the equilibria in batch systems are not, in general, applicable to all types of sorbents [23]. The apparent dynamic isotherm seems to help describe in a more efficient manner the sorption mechanisms occurring in a dynamic process where kinetics and equilibrium act in the same time. In fixed beds, solution is fed without interruption and, at equilibrium, concentration and pH values are equal to their respective feed ones. This does not occur in batch isotherms. This is based on the breakthrough data. Each run up to saturation is related to one point of such data, that is, the amount of sorbate retained up to saturation plotted against the inlet concentration [24]. What is advantageous about the apparent dynamic isotherm is the control of the fluid-phase concentration. Results of the column dynamic simulations depend greatly on the choice of an appropriate mathematical relation used to represent the equilibrium. Therefore, in order to model the dynamic sorption, is better to consider apparent dynamic isotherms instead of the widely used batch isotherms as they better represent equilibrium in fixed bed [25].

Modelling of the breakthrough curve

The mathematical models of phenomenological type are significant instruments in designing the sorption process occurring in fixed bed columns. The validation of this type of model is done by experimental data obtained in laboratory scale. Mathematical models are useful tools for designing and optimizing purposes in industrial scale. Mass transfer has an important effect on the breakthrough curves, even more if the isotherms are expressed by non-linear mathematical equations. The concentration of the sorbate in contacting fixed bed phases

depends on the position and time. Therefore, the phenomenological model is represented by partial differential equations, which are difficult to be solved analytically. Due to their complex nature, the phenomenological mathematical models have suffered many simplifications to obtain an analytical solution. Bohart and Adams (1920) developed one of the first mathematical models [26]. This model was firstly used to describe the dynamic sorption of chlorine in columns packed with activated carbon and is still widely used by several researchers [27 - 34].

The Bohart Adams model considers that the limiting step of the mass transfer is controlled by the kinetics of sorption process which is represented by a second-order reaction. The respective equation is given by Equation 4.26:

$$\frac{C_{out}}{C_F} = \begin{cases} 0, & t < t_F \\ \frac{1}{(e^A + e^{-B} - 1)e^B}, & t > t_F \end{cases} \quad (4.26)$$

The significance of notations in (4.26) is $A = \frac{L \times \beta}{u_0}$, $B = \frac{(-tu_0 + L)\beta}{\alpha u_0}$, $\alpha = \frac{\rho_{bed} q^*}{C^F \varepsilon}$,

$\beta = k_a C^F \alpha$ and $t_F = \frac{L}{u_0}$, where L is the bed length and u_0 gives the superficial flow rate of fluid phase.

Bohart and Adams model considers only one adjustable parameter, the rate constant k_a . The parameter q^* has also been reported as an adjustable parameter. However, its value can be determined as mean species concentration in solid phase (sorbent) at saturation point of the breakthrough curves.

The **model developed by Thomas** has also an analytical solution [35]. The sorption rate is defined by Langmuir adsorption kinetics.

The Thomas mathematical model is obtained by defining the mass balances of the sorbate in the fluid phase and in the solid phase. From these mass balances is derived an equation that describes the system equilibrium. The mass balance in the fluid phase results in the following equation:

$$\frac{\partial C}{\partial t} + \rho_{bed} \frac{(1-\varepsilon)}{\varepsilon} \frac{\partial q}{\partial t} = -u_0 \frac{\partial C_j}{\partial z} + D_L \frac{\partial^2 C_j}{\partial z^2} \quad (4.27)$$

with the following initial and boundary conditions:

$$C(0,z) = 0 \quad (4.28)$$

In the inlet sample in the column ($z = 0$):

$$D_L \frac{\partial C}{\partial z} = u_0 (C(t,0) - C^F) \quad (4.29)$$

In the outlet sample in the column($z = L$):

$$\frac{\partial C}{\partial z} = 0 \quad (4.30)$$

Normally, Fick's second law considers the variation of the adsorbate concentration within the particle in order to have $\partial q / \partial t$. Unfortunately, in these cases, the solution of equations that need to be solved are of increased complexity so, in order to reduce the computational effort, the Fick's Law can be replaced by the simplified kinetics equation [36]. The most used is the **LDF model (Linear Driving Force)**. It applies the $\partial q / \partial t$ expression as a first order kinetics (more precisely as mass transfer rate), represented by Equation (4.31):

$$\frac{\partial q}{\partial t} = -K_s(q - q_{eq}) \quad (4.31)$$

The LDF model has as premise the fact that the driving force for mass transfer varies linearly with the concentration of the sorbate in the solid. In an adsorption process, the equilibrium is generally represented by adsorption isotherms, such as: Langmuir, Freundlich, Tóth, Sips. Fig. 4.3 illustrates the mechanism of the external mass transfer that occurs around the surface of the particle. The mass transfer occurs at interface solid-fluid and is represented by following equation:

$$-K_s(q - q^*) = \frac{K_F \alpha \varepsilon}{\rho_{bed}} (C - C_{eq}) \quad (4.32)$$

The mathematical model that takes into account both mass transfer resistances (external and intraparticle) is called **double resistance model**. This model is composed by the set of Eqs. (4.27) - (4.32). When the mass transfer occurs predominantly intraparticle, that is ($C_{eq} \approx C$), the equilibrium concentration of the sorbate in the solid is directly related to the concentration in bulk phase. When mass transfer resistance occurs in the film, the rate of sorption can be expressed by the following relation:

$$\frac{\partial q}{\partial t} = \frac{K_F \alpha \varepsilon}{\rho_{bed}} (C - C_{eq}) \quad (4.33)$$

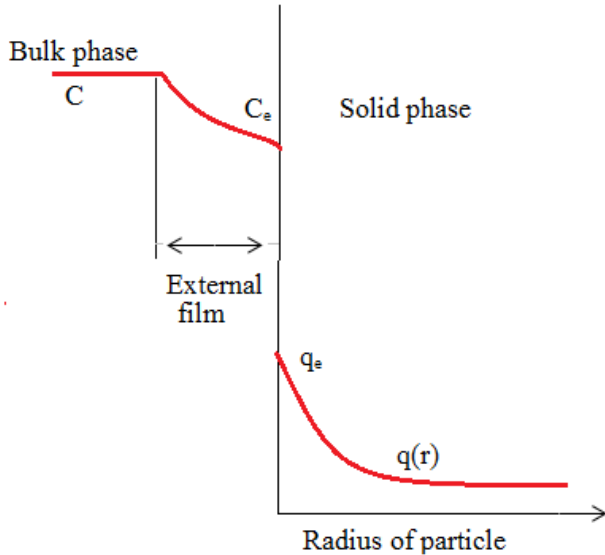


Figure 4.3. Mass transfer in adsorption process

When the working condition is improved after experimental research, the film and intraparticle resistances of the sorption processes (adsorption, ion exchange or adsorption + ion exchange) are reduced to a minimum in the experimental range investigated. This means that the film thickness is as thin as possible and there is no significant steric resistance of the sorbate in the particle pores.

Axial dispersion coefficient (D_L) and external mass transfer coefficient of the model can be determined from the current correlation, referring to fixed bed phases contacting. The relationship for computing the axial dispersion is usually expressed from the dimensionless groups: Reynolds (Re), Peclet (Pe), Schmidt (Sc). Several correlations for calculating of axial dispersion of gases and liquids in packed beds are presented in [37]. There are many correlations for calculating external mass transfer coefficients in porous media, usually expressed in terms of Reynolds (Re_p), Schmidt and Sherwood (Sh_p). For $3 < Re_p < 2000$ in [38]

the authors use the correlation (4.34) where $Sh_p = \frac{K_F d_p}{D}$, $Re_p = \frac{u_0 d_p}{\nu}$ and $Sc = \frac{\nu}{D}$ (d_p

fixed bed particle diameter, K_F fluid phase species mass trasfer coefficient, D diffusion coefficient of interphases transferred species)

$$Sh_p = 1 + 1.1 Re_p^{0.6} Sc^{1/3} \quad (4.34)$$

The mass transfer coefficient in the solid (K_S) is an adjustable parameter of the model that can be obtained from the experimental breakthrough curves.

The **Yoon-Nelson model** is based on the assumption that the decrease in the probability of each adsorbate to be adsorbed is proportional to the probability of its adsorption and breakthrough on the adsorbent [39]. Strictly reffering to breakthrough curve it can be

represented by relation (4.35) where K_{YN} is the Yoon – Nelson rate constant, $t_{1/2}$ gives the time at the middle of the breakthrough curve and C_F is the species concentration in the fluid at bed input.

$$\ln \frac{C}{C_F - C} = K_{YN}t - t_{1/2}K_{YN} \quad (4.35)$$

By plotting $\ln[C/(C_F-C)]$ versus t , K_{YN} and theoretical $t_{1/2}$ are determined. The Yoon-Nelson model not only has a more simple form than other models, but also requires no detailed data concerning the characters of adsorbate and adsorbent, as well as for the parameters of the fixed bed [40]. But as limited by its rough form, the Yoon-Nelson model is less valuable or convenient to obtain process variables and to predict adsorption under variety conditions.

Wang model [41] is a mass transfer model describing the breakthrough curve of solutions containing Co or Zn ions in the fixed bed. It is based on the following assumptions: 1) the adsorption process remains isothermal, 2) the mass transfer equation is written in the form (4.36) where k_w is a kinetic constant, y is the fraction of the adsorbed metal ions, x gives the fraction of metal ions passing through the fixed bed, with $x+y = 1$, 3) the breakthrough curve presents a symmetry and 4) the axial dispersion in the column is negligible.

$$-\frac{\partial y}{\partial t} = k_w xy \quad (4.36)$$

Presuming $y = y_w$ at $t = t_w$ and integrating Eq. (4.36), one can obtain (4.37). If $w = 0.5$, then $y_w = y_{1/2} = x_{1/2}$, $t_w = t_{1/2}$ and from (4.37) is produced the relation (4.38) where x can be expressed as in relation (4.39):

$$\ln[x(1-x_w)/(x_w(1-x))] = k_w(t_w - t) \quad (4.37)$$

$$t = t_{1/2} - \frac{1}{k_w} \ln \frac{1}{1-x} \quad (4.38)$$

$$x = C/C_F \quad (4.39)$$

Substituting Eq. (4.39) into Eq. (4.38), t should be indirectly proportional to $\ln[(C_F/C)-1]$. A plot of $\ln[(C_F/C)-1]$ vs. t produces the slope and intercept values as $1/k_w$ and $t_{1/2}$, respectively. Then the entire breakthrough curve can be obtained based on Eq. (4.38). This model was successfully applied in some cases [42 , 43].

Meanwhile, similar to the Yoon-Nelson model, it cannot provide sufficient information of an adsorption system.

Other models have been developed to fit particular cases.

4.3. Treatment of Aqueous Radioactive Wastes containing Cs by sorption method

The process selection for a liquid radioactive waste treatment depends exclusively upon its radiological and physico-chemical properties. The selection must have a practical understanding regarding the important properties concerning actual working conditions in the plant/installation and also the future conditions that may arise. Removal of radioactive contaminants from radioactive liquid waste is one of the basic methods of radioactive waste management. Different methods such as chemical precipitation, adsorption, and ion exchange are applied for radioactive wastes treatment [44 – 50]. Ion exchange technique in which various type of ion exchangers have been widely used is an attractive method because of its simplicity, selectivity, and efficiency [51 - 58]. Selecting the appropriate separation technology is typically specific to the application as much as the selection of an appropriate sorbent medium is specific to the needs of the system.

For treatment of liquid radioactive waste using sorption process, is available a wide range of materials. These can be found in a variety of forms, have widely differing chemical and physical properties and can be naturally based or synthetic. Sorbent materials can be classified according to their applicability for different practices, like when treating liquids from primary circuits or fuel pools, nuclear grade organic sorbent resins are mostly used. The selection of material to be used is based on its capacity of impurities and undesirable ions removal and pH control. Nuclear grade sorbent resemble commercial grade resins but are more specific regarding particle size and composition. There are two types of resins that can be used as follows: i) organic resins, usually used for a series of treatment cycles, first eluting the sorbed radioisotopes with suitable solutions and then restoring the sorbent to its original ionic form before its reuse, ii) inorganic resins, typically used for the treatment of liquid waste streams for which is not required a high chemical cleaning level; for instance, inorganic sorbent media may be used in systems where the contaminated liquid is purified for recirculation purposes or for reducing the level of radionuclide concentration in the liquid to allow its reclassification. Highly selective inorganic materials also allow the use of sorption method in case that very high concentrations of competing ions are present [59].

The sorbent media must be compatible with the chemical nature of the waste (such as the pH and type of present ionic species), as well as the operating parameters, notably temperature and pressure.

Organic ion-exchangers use molecular recognition to selectively bind and effectively remove caesium. However, in spite of their advantages, these organic ion-exchangers must be synthesized using multi-step organic synthesis processes, and typically have lower exchange capacity compared with their inorganic counterparts. These characteristics can seriously limit

the scope of applications for these materials. An alternative to organic ion-exchangers is emerging for nuclear waste remediation. Inorganic ion-exchangers offer a superior chemical, thermal and radiation stability that is simply not achievable with organic compounds. They can be used to remove both caesium and strontium with a high level of selectivity under a broad pH range. Inorganic ion-exchangers can operate at acidic pH where protons inhibit ion exchange in alternative technologies such as crystalline silicotitanate.

Thermal, chemical, hydromechanical and radiation stability of the major part of inorganic sorbents is by 1 – 3 orders of magnitude greater in comparison with organic ion-exchangers, however, radiation and chemical properties of sorbent are not determinant for purification of intermediate and low level radioactive waters.

When using granulated sorbents for liquid radioactive waste purification, both in static and dynamic conditions, the hydromechanical resistance is important. It determines a loss of sorbent due to a mechanical attrition of granules. Polymeric ion exchange resins have the highest hydromechanical durability. Inorganic sorbents generally have low hydromechanical durability. Attrition stability of a sorbent can be increased due to its granulation with use of an organic and/or inorganic binding agent.

The sorbents proposed for liquid radioactive waste purification must be available, have low cost and be simple to produce. For this purpose, there must exist a technology for its mining (for natural sorbents) or synthesis (for synthetic sorbents), which allows producing the considered sorbent in the required quantities. The ferrocyanide sorbents are prepared in the form of composites with appropriate matrix materials: silica gels, zeolites, etc in order to improve their characteristics.

Duration of the institutional controls is dependent on the disposal of radioactive waste containing ^{137}Cs . This is of major importance as it remains in the environment for up to 300 years (10 half lives), it is a highly radioactive element (by its disintegration a strong gamma ray is emitted) and bioaccumulates through the trophic chain [60].

Cesium (Cs) has 40 known isotopes with atomic masses ranging from 121 to 151. Only one isotope, ^{133}Cs , is stable. The longest-lived radioisotopes are ^{135}Cs with a half-life of 2.3 million years, ^{137}Cs with a half-life of 30.1671 years and ^{134}Cs with a half-life of 2.0652 years. All other isotopes have half-lives less than 2 weeks, most under an hour. The most important caesium isotopes with regard to their impact on human health are cesium-134 and cesium-137. Both ^{137}Cs and ^{134}Cs emit beta radiation and gamma radiation. Beta radiation has a short travel path, can penetrate the skin and superficial body tissues while gamma radiation is the most penetrating and can travel long distances.

Cesium is a difficult metal to remove from wastewater through standard precipitation practices since most cesium salts are very soluble. However, precipitation/co-precipitation processes have been used for industrial-scale radiochemical separations [61 - 63], using different chemical agents. Selective removal of caesium isotopes through ion exchange is a common and proven treatment method for liquid waste, yet various aspects of existing technologies leave room for improvement with respect to both cost and effectiveness.

Extensive research and worldwide practice indicated that, for cesium radionuclides, the most specific sorbents are mixed transition metal ferrocyanides. Different procedures for preparing these ferrocyanides have been mentioned in the literature: precipitation followed by freeze granulation or drying, deposition of thin ferrocyanide films onto the surface of inert (glass, polyethylene terephthalate, Millipore polypropylene membranes) or sorption-active (clinoptilolite, glauconite) supports, preparation of composite sorbents consisting of transition metal ferrocyanides and silica gel, alumina gel, ion-exchange resins, or Taunit carbon nanostructured materials, and sol-gel method [64].

It is emphasised in almost all previously published papers that every synthesis step strongly affects the sorption kinetic and other important characteristics of the sorbents (chemical composition, pore structure, and degree of perfection of the sorbent crystal lattice) which influence the properties of the prepared sorbents. It is also possible to control and upgrade the sorption properties by varying the pore structure of the material or the chemical nature of the sorbent surface.

Column processes utilizing sorbents are somewhat superior to the other techniques. Different inorganic materials that are very selective for cesium have been used for ^{137}Cs adsorption from numerous liquid wastes [65].

Different studies found that ^{137}Cs can be removed from nuclear waste using zirconium and titanium phosphate [66], crystalline silicotitanates [67], ammonium molybdophosphate [68 , 69] and various forms of insoluble ferrocyanides, mainly cobalt, zinc, nickel and titanium ferrocyanide [70 - 73].

The inorganic sorbent suggested for a treatment process must have a high Cs^+ selectivity in the presence of other cations which have a much greater concentration. It must also be very resistant to chemical decomposition caused by radiation and furthermore, to increased temperatures resulting from heat generated by the decay process.

Finally, the compound after ^{137}Cs fixation must allow an easy transformation to the form required for final disposal [74]. However, the sorbents proposed up to now are not suitable as matrices for long-term storage of ^{137}Cs as they are easily submitted to decompositon by

oxygenation, heat, radiolytic processes and also interact with alkaline conditions of cement materials [75].

4.4. Experimental investigation of Ni ferrocyanides deposited onto silicagel beds in ARW treatment

Usually, an ion exchange system comprises a water swollen ion exchange material and the aqueous solution around it. Ion exchange is a heterogeneous process which is attained when ions are transferred to and from the interphase boundary; in other words, the ion exchange is accomplished by a chemical reaction, diffusion inside the sorbent and diffusion in the solution. Also, must not be dismissed the fact that is also obtained a thin film of solution at the exchanger surface. The properties of this thin film must be regarded as separate issue as they are different from the ones of the surrounding solution. The formation of this thin film cannot be adverted, only reduced to some extent by strong agitation.

The sorption capacity of different sorbents depends very much on the available surface area, polarity, contact time, pH and the degree of hydrophobic nature of the adsorbent and adsorbate [76]. Therefore, the selection of the sorbent is the first step in such investigation.

Ferrocyanides (FCN) of transitional metals have been widely and successfully used in the nuclear technology for removal of cesium because of their high selectivity. Other advantages worth mentioning are the high radiation and chemical stability over a wide range of pH and low solubility. However, many ferrocyanides are available in the form of a fine powder and can not be used for column applications. To overcome this drawback, the best way to obtain ferrocyanides is by precipitation on a suitable support or by embedding in another matrix thus obtaining composite sorbents. For the precipitation process, silica gel is generally used as support while for the embedding one, must considered the following issues: the matrix support must fix ferrocyanides, must be chemically inert and must enable the preparation of composite sorbents with a high content of active sorbent. Several applications of these resins to remove radioactive caesium ions have been reported [77 – 80].

Seeing that ^{137}Cs is among the *most problematic radionuclides* present in LL&ILRW, a study regarding removal of 134 , ^{137}Cs from radioactive waters using a synthetic inorganic sorbent was performed [81 - 82]. Nickel ferrocyanide, precipitated on silica gel (PNF-SG), the size of granules 0.5 - 0.8 mm was used as sorbent. Composite sorbent based on nickel ferrocyanide embedded in silica gel matrix was characterised by powdered X-ray diffraction analysis and electron microscopy.

4.4.1. Working procedure and equipment

The effect of different parameters such as pH, contact time, sorbent/waste mass ratio, temperature and initial concentration on the adsorption process was investigated. The adsorption process was evaluated from kinetic, isotherm, and thermodynamic aspects. Also, the decontamination factors in terms of separation yield were determined.

The study continued with investigation of cesium sorption on nickel ferrocyanide, precipitated on silica gel (PNF-SG), on a fixed-bed column. Fixed-bed column performance is usually described through the concept of the breakthrough curve. Breakthrough is said to have occurred when the effluent concentration crosses a set value (typically 5% of influent concentration) and evacuation from the bed occurs when the effluent concentration is equal to another set value (typically 95% of the influent concentration) [83]. Complete evacuation occurs when the effluent concentration is equal to the influent concentration [84 - 85], which might take a long time.

Column performance of Cs ion-exchange on PNF-SG was studied at different Cs concentrations, bed heights and flow rates and the breakthrough characteristics of the ion-exchange system were determined.

Mathematical models were applied to the experimental data obtained from column studies to predict the breakthrough curves and to determine the kinetic parameters.

All the reagents used in this work were of AR grade chemicals and were used without further purification. Cesium was as cesium chloride from Sigma–Aldrich Company. Work solutions were prepared by dissolving inactive CsCl in radioactive water containing 3000 Bq/L ^{137}Cs , that was used as tracer. PNF-SG, was supplied as granules, 0.5 - 0.8 mm size, from SIA “Radon” Moscow, Russia.

Cesium concentration was determined by gamma spectrometry using a high resolution gamma-ray spectrometer, Canberra type, GENIE 2000 version 3.2 software and Laboratory SOurceless Calibration Software (LabSOCS), with 47.5% relative efficiency.

4.4.2. Results and discussion

Cesium species sorbent characterization by SEM/ XRD

The granular particle from silica gel with precipitated nickel ferrocyanide, used as cesium species sorbent, was analyzed by surface electronic microscopy (SEM) and by Xray difraction (XRD). In fig. 4.4 is shown the SEM image at scales between 10 - 100 μm . At this level of magnification it can be observed the basic structure of silica gel support and other species surfaces, probably not only nickel ferrocyanide. Are also identified surface cracks (fig. 4.4 a), small agglomerations on local surface (fig. 4.4b), apparent porosity on *large*

surface area (fig. 4.4c) and crevices with inclusions from others species (fig. 4.4d). This level of magnitude does not allow visualisation of nickel ferrocyanide sites, so the field of view was narrowed to 1 – 2 μm and 0.1 - 1 μm scales. Figure 4.5 presents the scans obtained with different scanner positions at a 1-2 μm scale. Different types of small particles on the sorbent surface (fig. 4.5a) are visible. Nickel ferrocyanide sites (figs. 4.5b,c and d) are majority. It is possible to appreciate that these sites do not exceed the dimension of 2 μm (fig. 4.5d). Also, it can be observed that the nickel ferrocyanide sites do not have an uniform surface distribution. Figure 4.6 showing the microscopic analysis at very fine resolution (100 nm – 1 μm), supports this observation and supplementary shows that these sites of nickel ferrocyanide are dominant in the dimensional range 0,1 μm - 1 μm (fig. 4.6d).

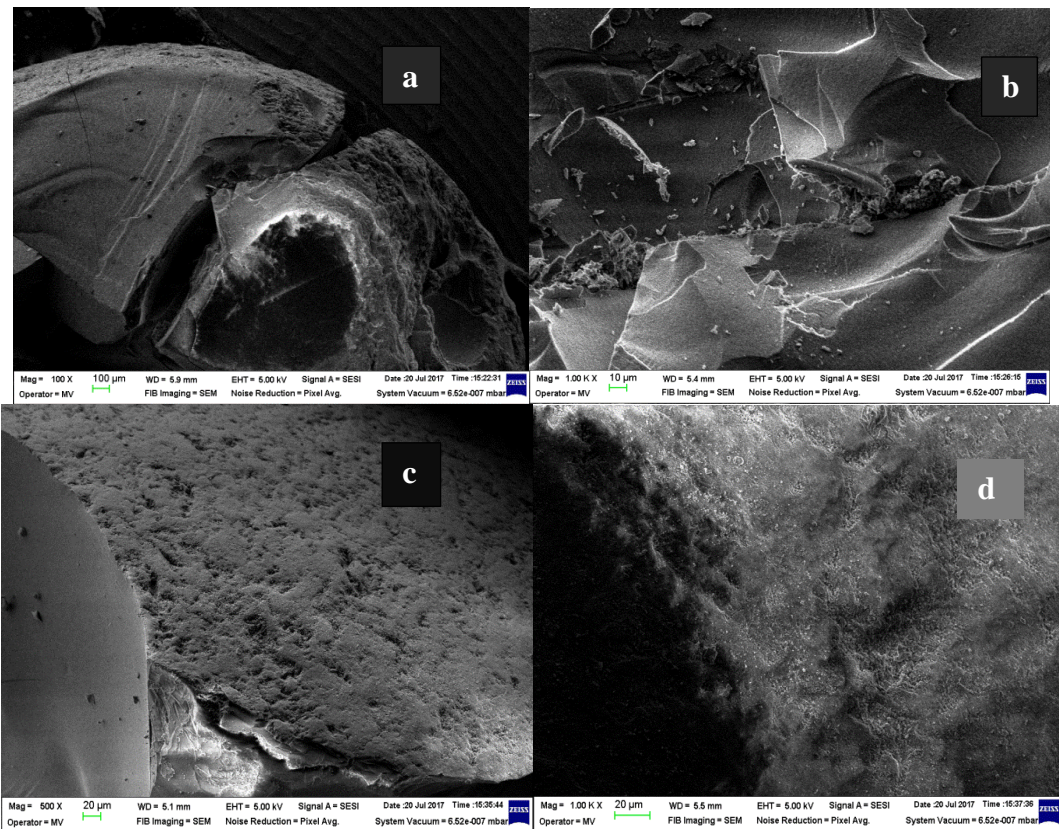
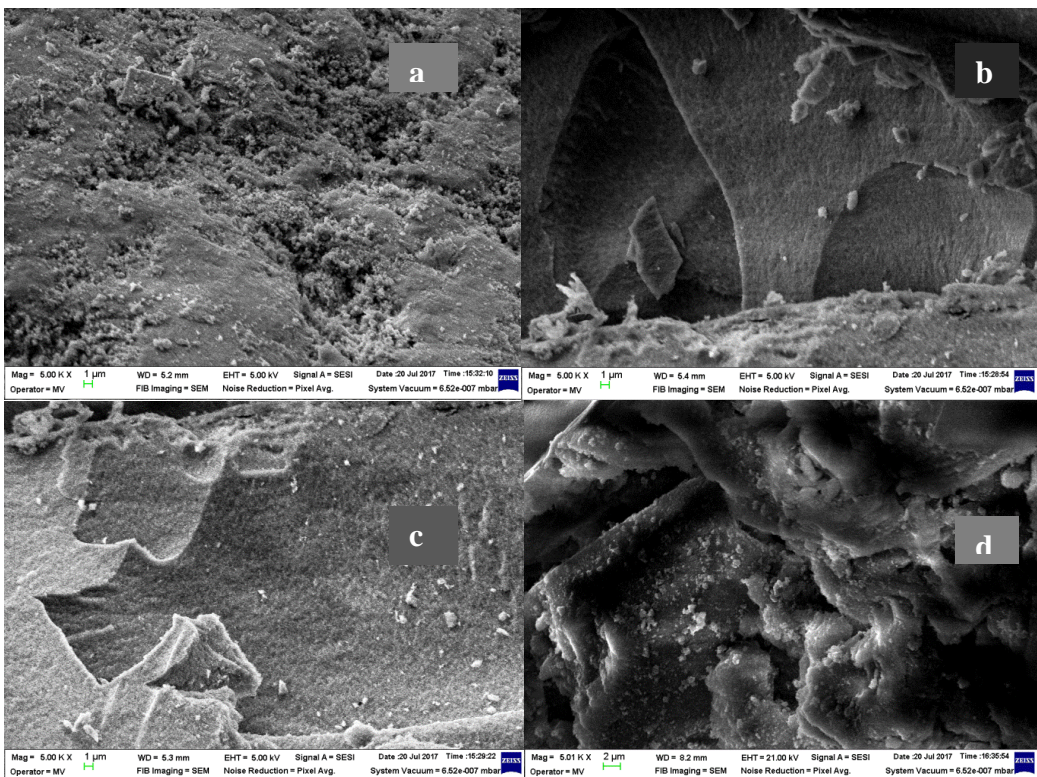
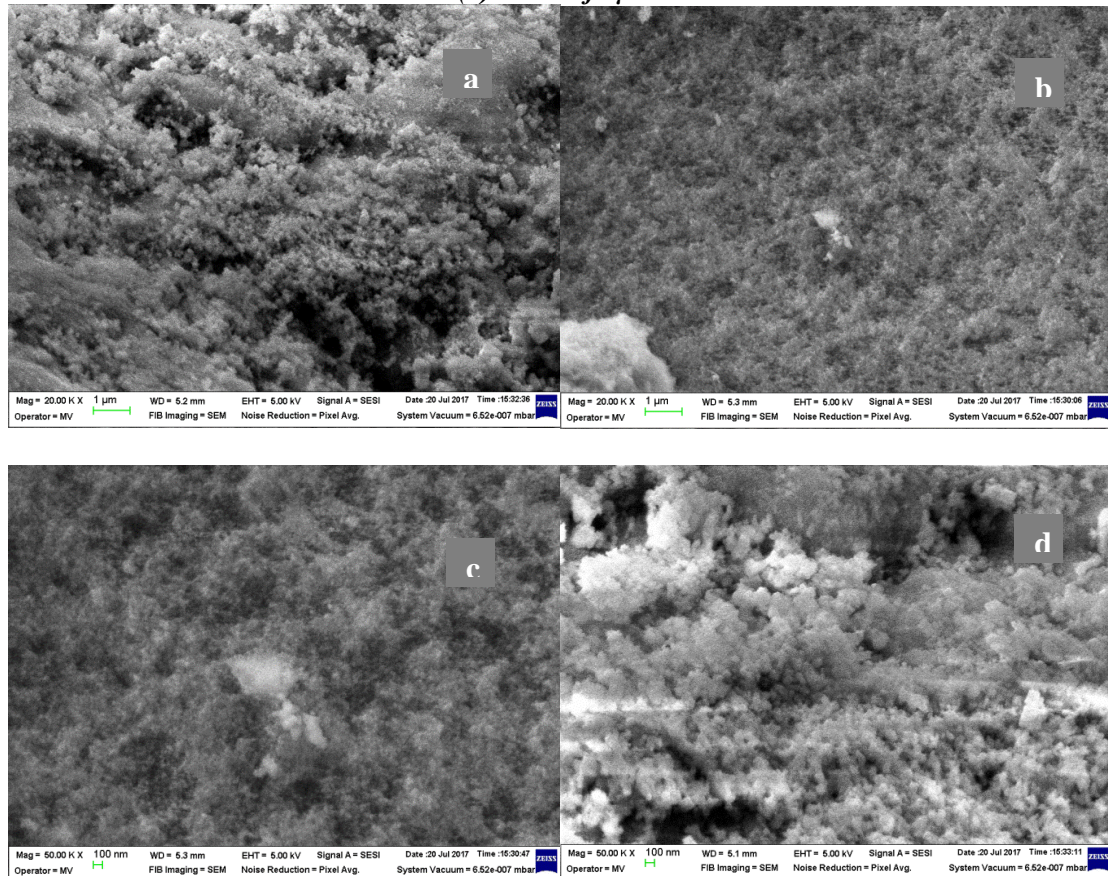


Figure 4.4. SEM images of PNF-SG sorbent. (a) Scale of 100 μm . (b) Scale of 10 μm . (c), (d) Scale of 20 μm .



**Figure 4.5. SEM images of PNF-SG sorbent. (a), (b), (c) Scale of 1 μm .
(d) Scale of 2 μm .**



**Figure 4.6. SEM images of PNF-SG sorbent. (a), (b) Scale of 1 μm .
(c), (d) Scale of 0.1 μm .**

Fig. 4.7 contains the XRD analysis of PNF-SG sorbent. Here appear the XRD spectral lines, coded after elements of identified crystalline species. This analysis is interpreted in the

sense of estimating the participation of the identified elements (less C and N that can not be detected) in the formation of the analyzed structure. Tables 4.1 and 4.2 centralize this estimation.

Table 4.1. Estimation of elements participation at PNF-SG composition (normalized values without C and N elements)

E	Z	Concentration	Intense spectral line	Intensity	Statistical error	Detection limit	Analyzed layer thickness
Si	14	62.76 %	Si KA1-HR-Tr	94.40	0.583 %	105.1 ppm	4.0 μm
Ni	28	17.10 %	Ni KA1-HR-Tr	101.9	0.561 %	61.3 ppm	38 μm
Fe	26	9.75 %	Fe KA1-HR-Tr	185.1	0.417 %	39.8 ppm	33 μm
K	19	7.52 %	K KA1-HR-Tr	21.38	1.23 %	77.2 ppm	6.7 μm
Ca	20	2.21 %	Ca KA1-HR-Tr	6.534	2.23 %	110.4 ppm	7.7 μm
S	16	0.67 %	S KA1-HR-Tr	1.753	4.47 %	81.3 ppm	2.53 μm

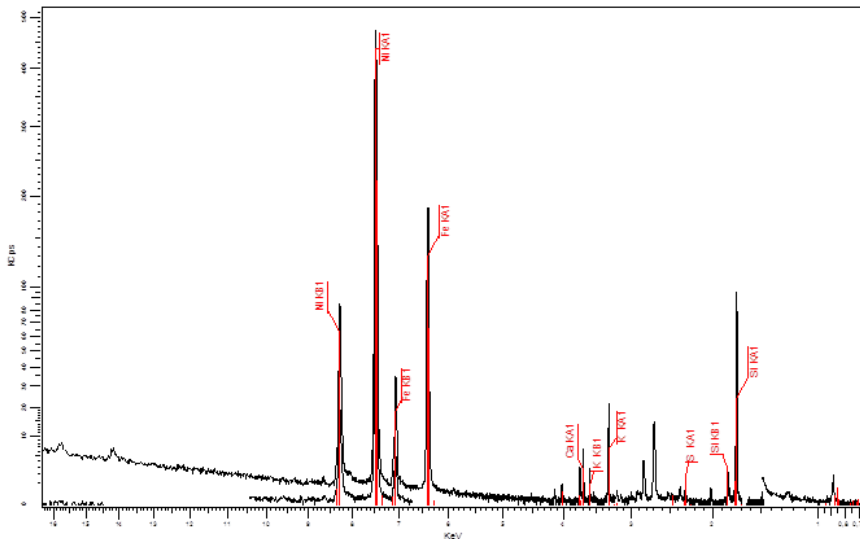


Figure 4.7. The XRD analysis of PNF-SG sorbent.

Table 4.2. Estimation of elements participation at PNF-SG composition (natural values without C and N elements)

E	Z	Concentration	Intense spectral line	Intensity	Statistical error	Detection limit	Analyzed layer thickness
Si	14	23.05 %	Si KA1-HR-Tr	94.40	0.583 %	35.8 ppm	12.4 μm
Ni	28	5.14 %	Ni KA1-HR-Tr	101.9	0.561 %	21.7 ppm	107 μm
Fe	26	3.73 %	Fe KA1-HR-Tr	185.1	0.417 %	14.1 ppm	97 μm
K	19	2.57 %	K KA1-HR-Tr	21.38	1.23 %	27.2 ppm	19.5 μm
Ca	20	0.78 %	Ca KA1-HR-Tr	6.534	2.23 %	33.8 ppm	22.5 μm
S	16	0.22 %	S KA1-HR-Tr	1.753	4.47 %	28.7 ppm	7.3 μm

The data in tables 4.1 and 4.2 gives an estimated composition, due to the fact that a single region was investigated, as fig. 4.8 shows.

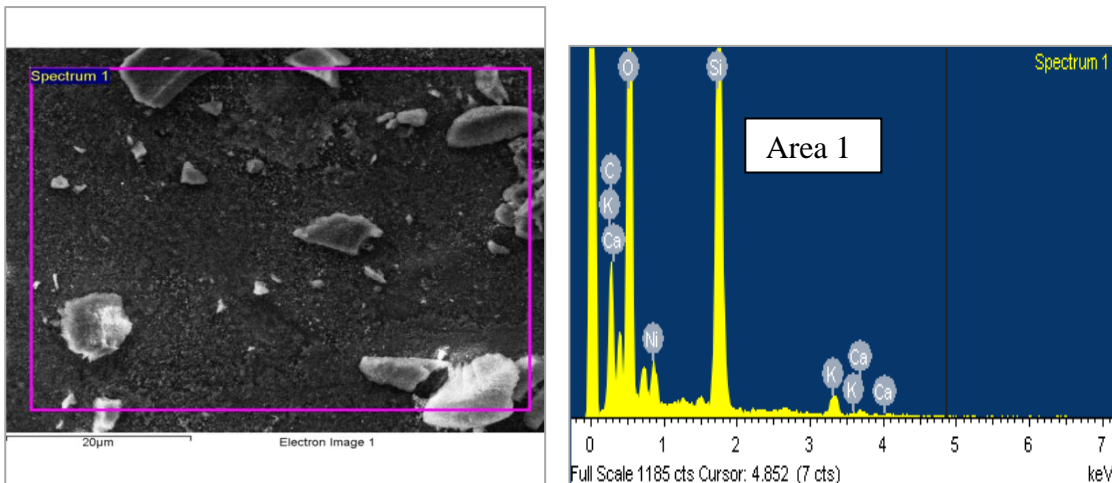


Figure 4.8. Local spectrum in an area and intensity of identified species (major species: SiO_2 type 1 -52.45%, SiO_2 type 2- 10.25%).

Identification of the Cs species sorption characteristic parameters

Two types of experiments were performed in the investigation of cesium species sorption on PNF-SG: i) batch sorption with interest in establishing the sorption equilibrium, ii) fixed bed sorption where the basic aim was the identification of process model parameters.

Batch sorption studies

Batch experiments were performed under kinetic and equilibrium conditions. To determine the pH range at which the maximum uptake of Cs^+ ions would take place on PNF-SG, a series of 250 mL polypropylene Erlenmeyer flasks, each containing 1 g, 3 g and 5 g of PNF-SG was filled with 250 mL of 1000 mg/L Cs^+ solution. The initial pH was adjusted to values ranging from 3.0 to 10.0 using dilute solution of hydrochloric acid or sodium hydroxide. The flasks were shaken for 2 h to attain equilibrium (fig. 4.9). Preliminary investigations showed that the sorption process of each studied ion was completed after 2 h. The suspension obtained was filtered to separate the solid from the liquid phase. The radioactivity of clear liquid phases obtained was measured in order to obtain quantitative data of Cs^+ adsorption.

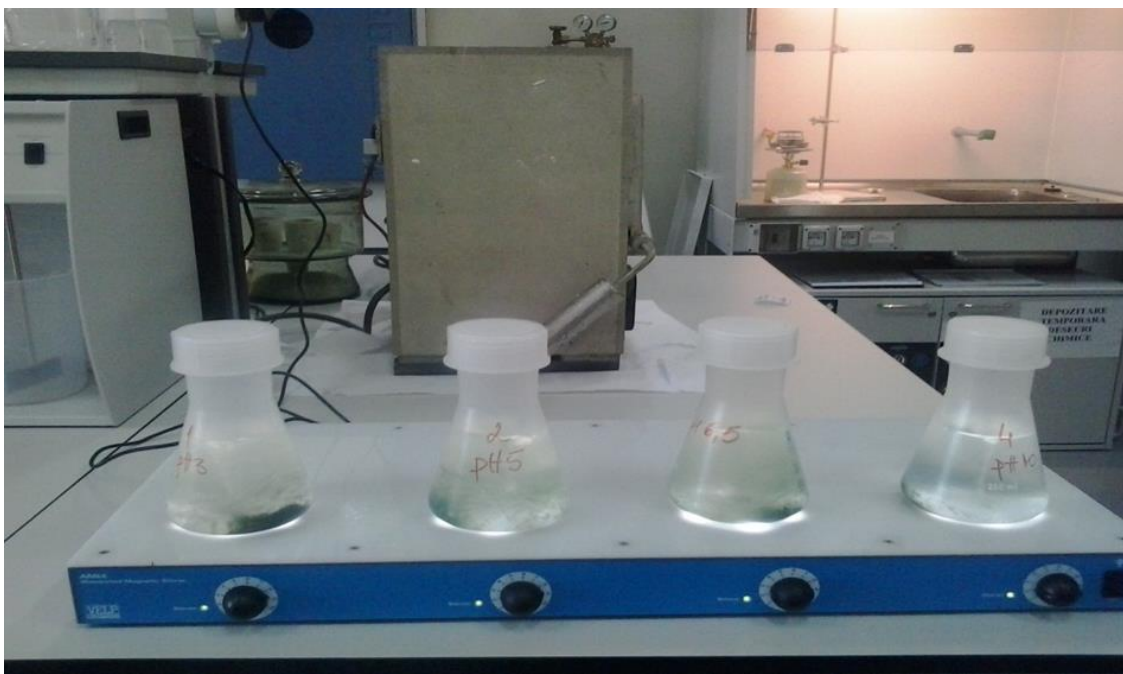


Figure 4.9. Erlenmeyer flasks containing PNF-SG and 1000 mg/L Cs^+ solution on shaker mixer

Kinetic experiments

Kinetic studies were performed at four different temperatures (298, 308, 318 and 328 K) using an initial ion concentration of 1000 mg/L. Also, to study the process kinetics, the adsorption capacity of the PNF-SG was measured at different time intervals, in the range 30 – 120 min. For these investigations, sorbent/ liquid phase mass ratio of 0.02 g/mL was used and the solution was kept stirred in a thermostat shaker adjusted at the desired temperature. The amount of ion sorbed at a time t , q_t (mg/g), and the distribution coefficient, k_d (mL/g) were calculated using cesium balance relation (4.40) and distribution coefficient definition (4.41)

$$q_t = (C_0 - C_t) \frac{V}{m} \quad (4.40)$$

$$k_d = \frac{(C_0 - C_t)}{C_t} \times \frac{V}{m} \quad (4.41)$$

In the above relations C_0 and C_t represent the initial and at time t concentrations (mg/L) of Cs^+ in solution, V is the solution volume (L) and m the weight (g) of the PNF-SG sorbent.

Sorption equilibrium experiments

For experiments of sorption isotherm measurements, 250 mL of the metal ion solution, of varying Cs^+ concentrations (100–1000 mg/L), were agitated with 5 g of PNF-SG at different temperatures (298, 308, 318 and 328 K) and at initial pH of 3.0. After the established contact time (2 h) was reached, the suspension obtained was filtered and the amount of the metal ion retained in the PNF-SG phase (mg/g) was calculated. All batch experiments were carried out in duplicate and the mean values are presented.

Effect of experimental conditions on adsorption process: Dosage effect

The removal percentage of Cs^+ increased with increasing of solid to liquid ratio, r from 0.004 to 0.02 g/mL and the maximum uptake was achieved at 0.02 g/mL (fig. 4.10). Therefore, the optimized solid to liquid ratio of 0.02 g/mL was selected for further experiments.

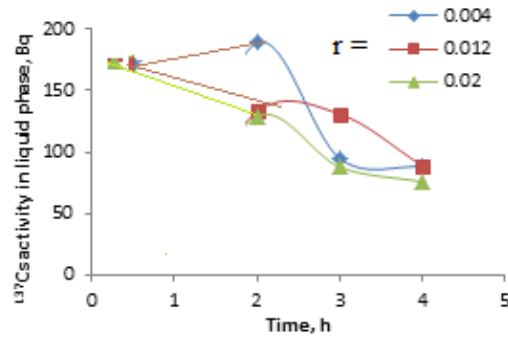


Figure 4.10. Effect of solid/liquid ratio on Cs^+ activity in liquid phase ($\text{pH} = 3, t = 25^\circ\text{C}$)

Effect of experimental conditions on adsorption process: Effect of contact time

The amount of adsorbed ions onto PNF-SG at different contact times, τ is shown in fig. 4.11. The uptake of ions increased with time and reached equilibrium after 90 min. The sorption process was initially very fast and between 80% and 90% of the maximal capacity was obtained within 30 min. This quite rapid removal was due to the porous structure of the composite which allows the facile diffusion of the ions to the exchange sites. The adsorption of ions gradually decreased with time until saturation was attained. The two stage sorption mechanisms with the first rapid and quantitatively predominant and the second slower and quantitatively insignificant, has already been reported [86].

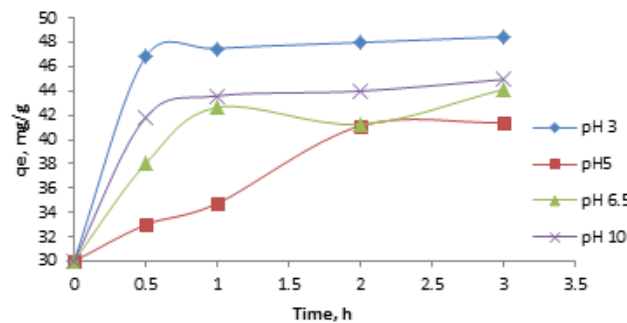


Figure 4.11. Effect of contact time on Cs content in sorbent ($r = 0.02 \text{ g/mL}, t = 25^\circ\text{C}$)

Effect of experimental conditions on adsorption process: Effect of initial pH

Metal sorption from aqueous solutions can be greatly affected by the solution pH, which impacts not only the binding sites (e.g., degree of protonation) but also the metal chemistry (e.g., speciation and precipitation). The amount of Cs^+ uptake as a function of initial

pH is shown in fig. 4.12 and also in fig. 4.11. It was concluded that acidic and alkaline media are favorable for uptake process. This could be attributed to: a) in acidic media Cs is present completely as soluble Cs^+ ; b) in alkaline solutions formation of mixed precipitates of transition metal ferrocyanides (nickel in this case) and hydroxides occurs [87], and this fact favors the removing of Cs species from liquid phase.

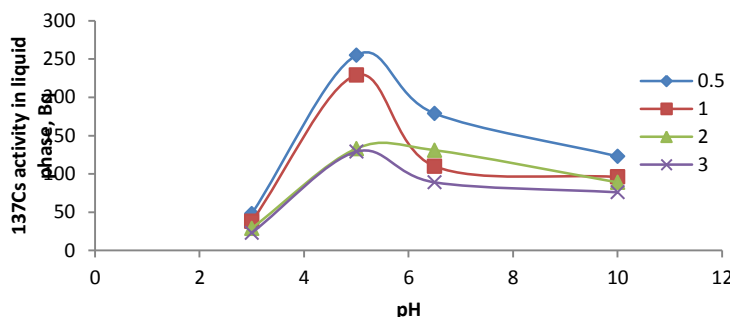


Figure 4.12. Effect of initial pH on Cs^+ activity in liquid phase ($r = 0.02 \text{ g/mL}$, $t = 25^\circ\text{C}$)

The highest uptake was observed at pH 3 and pH 10. Since it has been reported dissolution of transition metal ferrocyanides at $\text{pH} > 10$ [87], all future sorption experiments in this work were carried out at initial pH value of 3.

Effect of experimental conditions on adsorption process: Effect of temperature

The adsorption removal of Cs^+ onto PNF-SG at four different temperatures, namely 298, 308, 318, 328 K, was examined (fig. 4.13). The adsorption capacity increased with increasing the temperature, confirming the adsorption process was endothermic. The data were used to estimate the thermodynamic parameters.

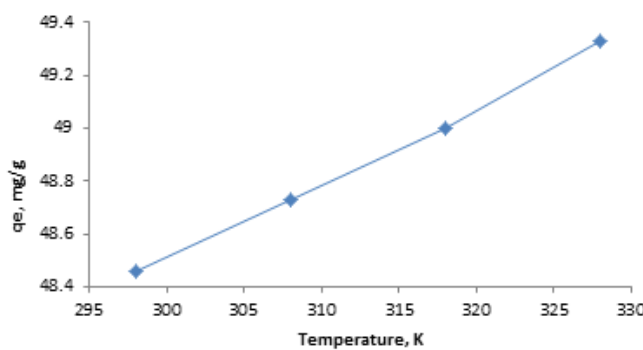


Figure 4.13. Effect of temperature on PNF - SG Cesium sorbent ($\tau = 2 \text{ h}$, $r = 0.02 \text{ g/mL}$, $\text{pH} = 3$)

Kinetic sorption modelling

Two kinetic models including pseudo-first-order and the pseudo-second-order were used to estimate the kinetic parameters for dynamics of Cs content in solid (PNF – SG sorbent). The integrated pseudo-first-order model expressed as Lagergren's equation [88]:

$$\ln(q_e - q_t) = \ln q_e - k_1 t \quad (4.42)$$

where q_e and q_t are, respectively, the amount of ions adsorbed per unit mass of PNF – SG at equilibrium and at any time t (mg/g); k_1 is the rate constant of pseudo-first-order sorption model (min^{-1}). The slope and intercept of the plot of $\ln (q_e - q_t)$ against t is shown in fig. 4.14, and they were used to calculate k_1 and q_e (Table 4.3).

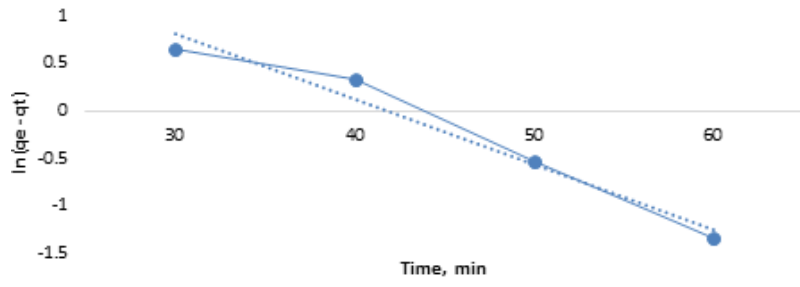


Figure 4.14. Pseudo first-order kinetic plots for the sorption of Cs^+ onto PNF – SG at 298 K, $\text{pH} = 3$, $r = 0.02 \text{ g/mL}$

The pseudo-second-order model and initial sorption rate (h) are written [87] as it shows the relation (4.43) and (4.44). Here k_2 is the rate constant of pseudo second-order equation (g/mg min) and v_{r0} represents the initial sorption rate (mg/g min).

$$\frac{t}{q_t} = \frac{1}{k_2 q_e^2} + \frac{1}{q_e} t \quad (4.43)$$

$$h = v_{r0} = k_2 q_e^2 \quad (4.44)$$

The values of t/q_t were linearly correlated with t as it can be seen in fig. 4.15. The important parameters including pseudo-second-order rate constant, k_2 (g/mg min), the equilibrium sorption capacity, q_e and the initial sorption rate, v_{r0} (mg/g min) were determined from the slope and the intercept of the plot (Table 4.3).

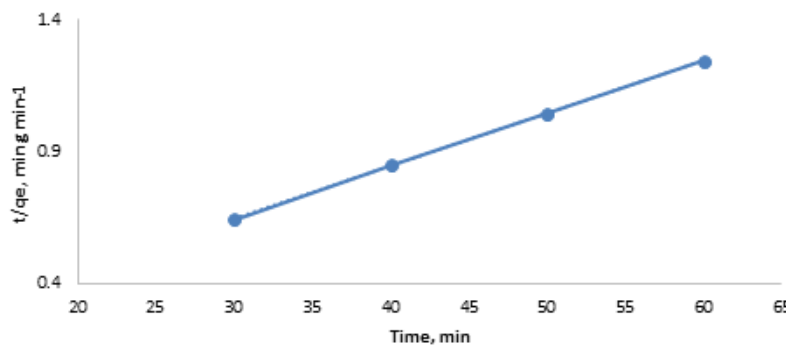


Figure 4.15. Pseudo second-order kinetic plots of Cs^+ sorption onto PNF – SG at 298 K, $\text{pH} = 3$, $r = 0.02 \text{ g/mL}$

Table 4.3. The calculated parameters of the pseudo first-order and pseudo second-order kinetic models for Cs^+ ions sorbed onto PNF – SG at 298 K, pH = 3, $r = 0.02 \text{ g/mL}$

First-order kinetic parameters			Second-order kinetic parameters				$q_e, \text{exp}, (\text{mg/g})$
k_1 (min ⁻¹)	$q_e, \text{calc},$ mg/g	R^2	k_2 (g/mg min)	$q_e, \text{calc},$ mg/g	v_{r0} (mg/g min)	R^2	
0.683	4.406	0.965	0.0087	50	21.74	0.999	48.46

The value of the correlation coefficients (R^2) and agreement of calculated q_e with experimental data (see table 4.3) revealed that sorption process can be described well by pseudo-second-order equation. It is possible to control the ion exchange process by film diffusion, by particle diffusion or by chemical exchange (chemisorption). It is reported that the rate of ion exchange is controlled by chemical exchange if experimental data are fitted to pseudo-second-order equation [89]. Data showing effect of temperature increasing on initial sorption rate (v_{r0}) and on rate constant (k_2) are not presented. The correlation coefficient R^2 has an extremely high value (> 0.99), and its calculated equilibrium sorption capacity (q_e) is consistent with the experimental data. Therefore, the overall rate constant of both sorption process appear to be controlled by the chemical sorption process.

In this case the reaction is said to be of second-order kinetic and for estimating the activation energy (chemisorption of Cs^+ on PNF – SG sorption), E_a , was used the Arrhenius equation (4.45), where k_2 and A (g/mmol min) are the rate constant and temperature independent factor, respectively E_a is the activation energy of the adsorption (J/mol), R is the gas constant (8.314 J/molK) and T represents the absolute temperature (K).

$$\ln k_2 = \ln A - \frac{E_a}{RT} \quad (4.45)$$

The plot of $\ln k_2$ against $1/T$ given in fig. 4.16 shows that experimental data are pertinent for activation energy identification at Cs^+ chemisorption onto PNF – SG sorbent.

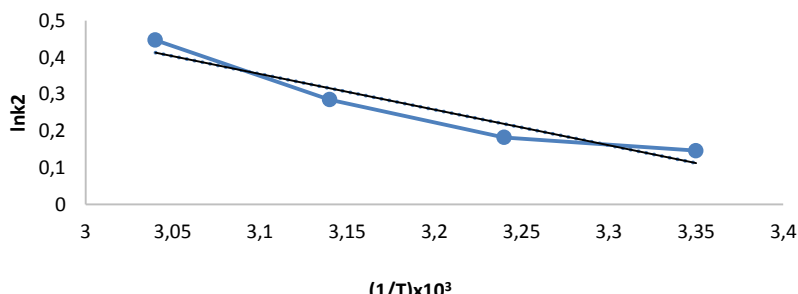


Figure 4.16. Linear least square plots for obtaining E_{ad} for Cesium species sorption onto PNF – SG sorbent ($r = 0.02 \text{ g/mL}$, $pH = 3$, $\tau = 2 \text{ h}$)

Adsorption of Cs^+ was followed with low potential energy as show in Table 4.4 (E_a was less than 42.0 J/mol) [90].

Evaluation of thermodynamic parameters

The values of enthalpy change (ΔH°) and entropy change (ΔS°) were determined using linear plot of Van't Hoff equation (4.46)

$$\ln k_d = -(\Delta H^\circ / RT) + (\Delta S^\circ / R) \quad (4.46)$$

The notations significance in Van't Hoff equation are as follows: k_d - the distribution coefficient, R - the gas constant, T - the absolute temperature. A plot of $\ln k_d$ versus $1/T$, shown in fig. 4.17, has enthalpy in the slope and entropy in the intercept. The value of free energy change (ΔG°) was calculated from (4.47). The calculated thermodynamic parameters are listed in Table 4.4.

$$\Delta G^\circ = \Delta H^\circ - T \Delta S^\circ \quad (4.47)$$

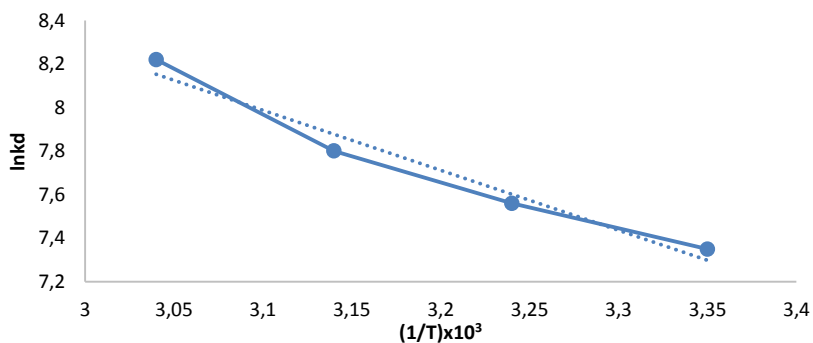


Figure 4.17. Van't Hoff plot of Cs^+ adsorption on PNF – SG sorbent
($r = 0.02 \text{ g/mL}$, $pH = 3$, $\tau = 2 \text{ h}$)

Table 4.4. Computed thermodynamic parameters of Cs^+ adsorption on PNF – SG sorbent ($r = 0.02 \text{ g/mL}$, $pH = 3$, $\tau = 2 \text{ h}$)

E_a (kJ/mol)	ΔH° (kJ/mol)	ΔS° (kJ/mol ^0K)	ΔG° (kJ/mol)			
			298 K	308 K	318 K	328 K
8.06	22.92	0.137	-17.91	-19.28	-20.65	-22.02

The positive values of ΔH° revealed the endothermic nature of the adsorption process. The positive values of ΔS° indicated that randomness of the system increased during the sorption process. The ΔG° values, negatives and decreasing with temperature, indicate a spontaneously process for Cs^+ adsorption of on PNF – SG sorbent.

Sorption isotherms

As it is shown in the opening chapter, the Langmuir, Freundlich, Temkin or Brunauer-Emmett-Teller isotherms can be used in equilibrium data processing. The relationship between the amount of ions adsorbed by unit mass of the PNF – SG and the concentration of remaining ions in solution represents the sorption isotherm [91] (fig. 4.18).

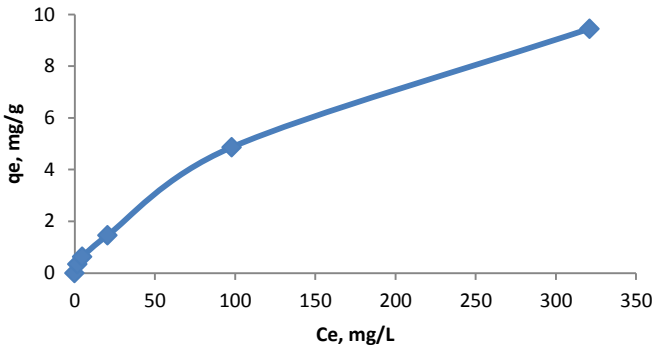


Figure 4.18. Sorption isotherm of Cs^+ on PNF – SG sorbent at 298 K and $\text{pH} = 3$

The isotherm is regular, positive, and concave to the concentration axis. Here two isotherm models including Langmuir and Freundlich, were used to describe the equilibrium experimental data. The linearized form of the Langmuir equation [10] is written by relation (4.48) where Q_0 (mg/g) represents the saturation adsorption capacity and b the constant related to the free energy of adsorption.

$$\frac{C_e}{q_e} = \frac{1}{Q_0 b} + \frac{C_e}{Q_0} \quad (4.48)$$

The Langmuir isotherm parameters were calculated from the slope and the intercept of plot of (C_e/q_e) against C_e (fig. 4.19).

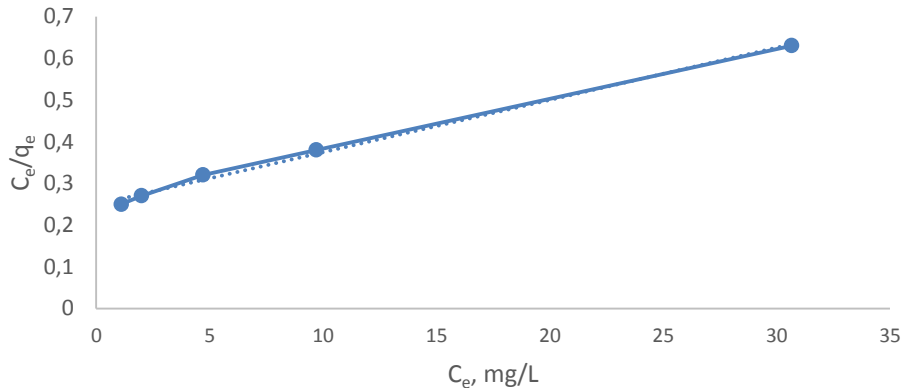


Figure 4.19. Langmuir plots of data from fig. 4.18

By means of Langmuir isotherm can be computed the separation factor (R_L), defined by relation (4.49), where C_0 (mg/L) is the initial Cs ions concentration.

$$R_L = \frac{1}{1 + bC_0} \quad (4.49)$$

As it has been shown, the sorption process may be irreversible ($R_L = 0$), favorable ($0 < R_L < 1$), linear ($R_L = 1$), and unfavorable ($R_L > 1$) [92]. Table 4.5 contains the values Q_0 , b and R_L .

In the case of the Freundlich isotherm, the linearized form is written [12] with relation (4.50), where K_f is the Freundlich constant related to the adsorbent capacity and n is a constant indicating the intensity of the adsorption process.

$$\log q_e = \log K_f + \frac{1}{n} \log C_e \quad (4.50)$$

The plot of $\log q_e$ versus $\log C_e$ is shown in fig. 4.20. The values of the constant n and K_f were calculated from the slope and the intercepts of the plot and listed in Table 4.5.

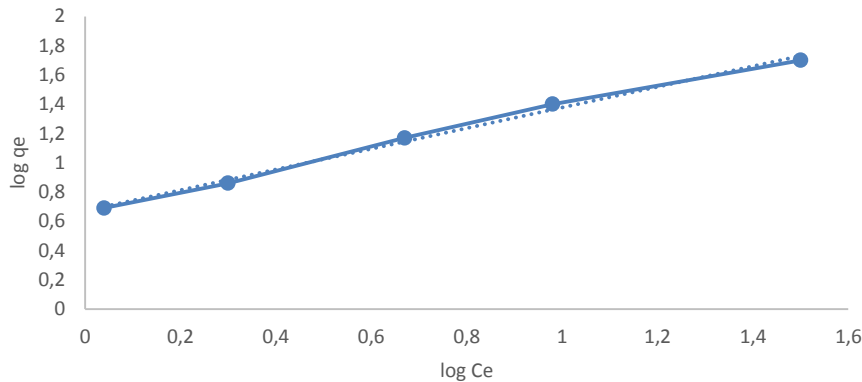


Figure 4.20. Characteristic Freundlich plots of data from fig. 4.18

Table 4.5. Adsorption isotherm parameters for Cs^+ on PNF – SG sorbent
($r = 0.02 \text{ g/mL}$, $\text{pH} = 3$, $\tau = 2 \text{ h}$)

Isotherm	Model parameter			
	Q_0 (mg/g)	B (L/mg)	R_L	R^2
Langmuir	80	0.05	0.019	0.9955
	n	K_f (mg/g)	-	R^2
Freundlich	1.4	4.7	-	0.9946

The adsorption data obey both Langmuir and Freundlich isotherms. The R_L values for Cs^+ is 0.019, indicating a favorable sorption process. The Freundlich intensity constant n is greater than unity indicating an increase in sorption tendency at increasing of Cs species concentration.

Comparison of R^2 values determines which model best represents the adsorption behavior of the adsorbent. In this case it cannot be selected but can be accepted that Langmuir isotherm honourable covers experimental data. In this situation it can be accepted that adsorption behavior of Cs species onto PNF – SG sorbent appears to be homogeneous rather than heterogeneous.

Decontamination factor

Decontamination factor (DF) was calculated in terms of separation yield as the ratio of initial Cs^+ concentration to final concentration resulting from a separation process. In order to establish acceptable limits for variability in separation process performance

isolated and synergic effects of parameters were determined by calculating DFs (fig. 4.21, 4.22 and 4.23).

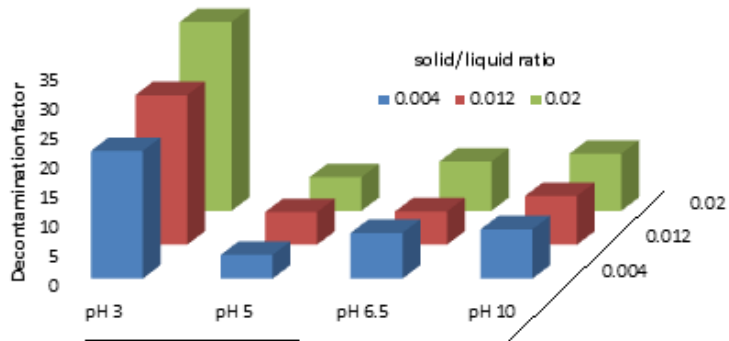


Figure 4.21. DF versus pH and solid/liquid ratio ($\tau = 2 \text{ h}$, 298 K , $C_0 = 1000 \text{ mg/L}$)

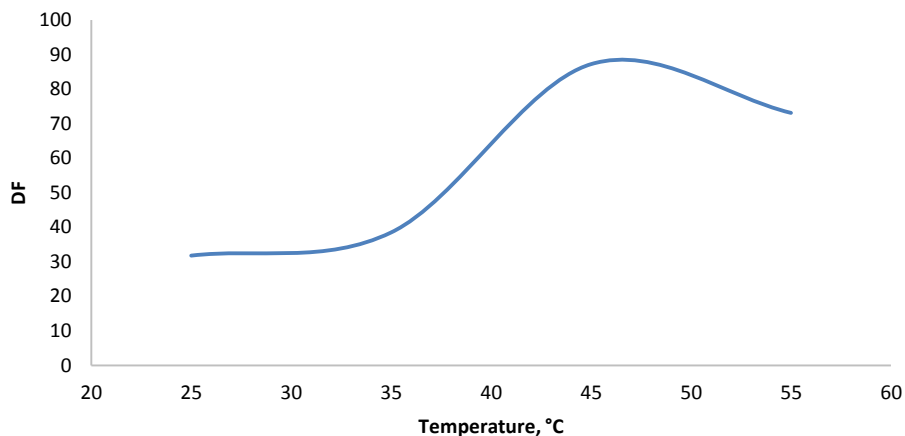


Figure 4.22. DF versus temperature ($\tau = 2 \text{ h}$, $r = 0.02 \text{ g/mL}$, pH 3 and initial $C_0 = 1000 \text{ mg/L}$)

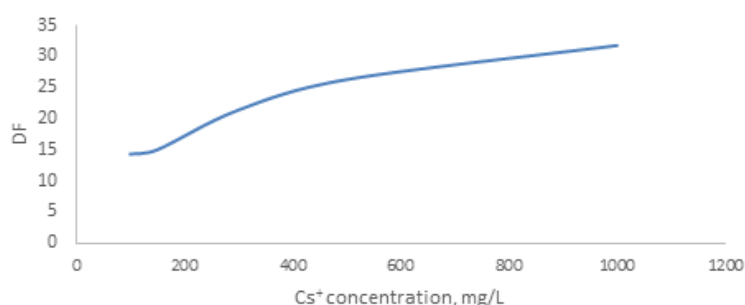


Figure 4.23. DF versus initial Cs^+ concentration ($\tau = 2 \text{ h}$, $r = 0.02 \text{ g/mL}$, pH 3 and 298 K)

As it can be seen from these figures, DF is strongly affected by all process parameters. The parameter that has the most influence is temperature. By increasing the process temperature up to 50°C DFs could reach 100. Moreover, acidic medium promotes the achievement of values up to 40, and DFs increase with increasing initial Cs^+ concentration up to 800 mg/L. A further increase in initial Cs^+ concentration had a

negligible effect on the DFs. That may be caused by the decrease of number ratio of vacant sites with respect to the number of Cs^+ ions on the surface of sorbent. According to initial radioactive waste characteristics, the best combination of influencing parameters can be chosen and acceptable limits for variability in separation process can be established.

Fixed-bed column study

Fixed-bed column experiments were conducted at temperature of 25°C using a glass column with an internal diameter of 20 mm and a height of 25 cm. The column was packed with PNF-SG on supporting layers of glass–wool to prevent the loss of the sorbent. The initial pH was adjusted at 3 (determined in batch investigation) using dilute solution of hydrochloric acid.

Breakthrough and exhaustion are respectively taken as $C/C_0 = 0.05$ and 0.95.

Effect of influent concentration

The breakthrough curves were obtained for different influent Cs species concentrations ($C_0 = 50, 100$ and 150 mg/L) at 3 mL/min and following conditions: column diameter, \varnothing , 20 mm, column height, H , 20 mm, PNF-SG sorbent weight, m , 5 g, flow rate in column, Q , 3 mL/min , initial radioactive concentration from ^{137}Cs 3300 Bq/L and pH = 3. The effect of influent Cs species concentration on the state of breakthrough curves results from fig. 4.24a. It can be observed that whereas the Cs species appeared in effluent after 315 min for 50 mg/L, the breakthrough occurred at 180 and 150 min for 100 and 150 mg/L. For the same flow rate and bed height, when the influent concentration of Cs species was increased, sharper breakthrough curves were obtained and a steep breakthrough curve was obtained at 150 mg/L. This is due to increase in the concentration gradient, which affects the exchange rate.

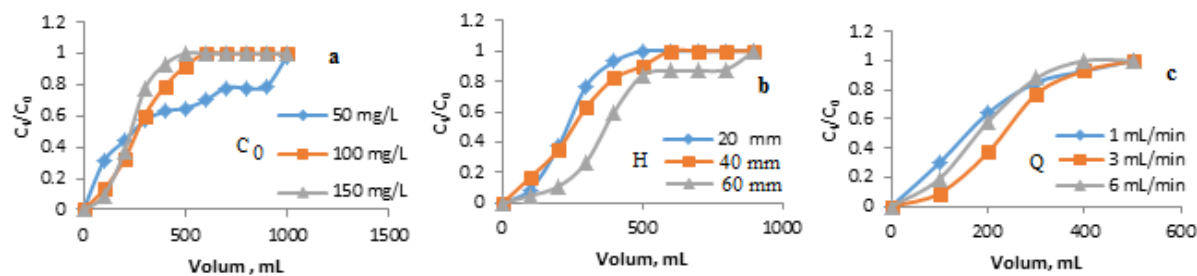


Figure 4.24. Breakthrough curves for sorption of Cs species on PNF – SG sorbent : a) the effect of influent concentrations ($Q = 3 \text{ mL/min}$; $H = 20 \text{ mm}$); b) the effect of bed heights ($C_0 = 150 \text{ mg/L}$; $Q = 3 \text{ mL/min}$); c) the effect of flow rates of feed ($C_0 = 150 \text{ mg/L}$; $H = 20 \text{ mm}$)

Effect of bed height.

Effect of bed height on process dynamics given by breakthrough curve was studied by operating the adsorption column at three different bed heights ($H = 20, 40$ and 60 mm) by

charging 5, 10 and 15 g of PNF-SG, respectively. Work conditions were: flow rate, Q 3 mL/min, Cs species concentration in column input $C_0 = 150$ mg/L, initial radioactive concentration of $^{137}\text{Cs} - 3300$ Bq/L and pH = 3. As it can be seen from fig. 4.24b, the volume of solution treated increased with the increase in bed height, due to increased availability of exchange sites. The exhaust time increased from 150 to 190 min and 295 min, when the bed height was increased from 20 mm to 40 mm and 60 mm, respectively. An increase in column length (the other parameters being kept constant) increases both the breakthrough and the overall capacity. Amount of PNF-SG sorbent in the column increases and consequently, availability of ion exchange sites increases linearly with the height of the column.

Effect of feed flow rate

To study the effect of flow rate, the column were charged at flow rates of 1, 3 and 6 mL/min with initial Cs species concentration maintained at 150 mg/L. Other data characterizing this experiments sorts are: column diameter, $\emptyset = 20$ mm, column height, $H = 20$ mm, mass of PNF-SG sorbent in experiment, $m = 5$ g (corresponds to bed height $H = 20$ mm), initial radioactive concentration of ^{137}Cs 3300 Bq/L and pH = 3. Since the flow rate is varying, breakthrough curves are shown in fig. 4.24c. The experimental characteristic breakthrough times were observed to be 157, 150 and 123 min when flow rate is increased from 1 to 3 mL/min and 6 mL/min. Earlier breakthrough and exhaustion were observed with increase in flow rate. This reduction is due to insufficient contact time in the bed. At higher flow rates, slope of the curve decreased showing high volume of unsaturated zone as a result of insufficient contact.

Application of dynamic models for breakthrough curve

In designing of a fixed bed sorption exchange process, breakthrough curves for different operating conditions are required. In the absence of experimental data, these curves can be generated if a suitable model is available and the model constants are known. Solving the differential equation based models of proposed rate mechanisms is a difficult process and also they cannot be solved for all the operating conditions. Simple models which would predict the breakthrough behavior of an adsorption process are suitable for analyzing the column studies. Here the analysis of the breakthrough curve was done using two of these models, the Thomas model and the Yoon–Nelson one.

Thomas model: Thomas model is based on the assumption that the process follows Langmuir kinetics with no axial dispersion; the rate driving force follows second order reversible reaction kinetics. The expression of the Thomas model for a column operation is [93]:

$$\frac{C}{C_0} = \frac{1}{1 + \exp[K_{Th}q_0m/Q - K_{Th}C_0t]} \quad (4.51)$$

and its linearized form is:

$$\ln\left(\frac{C_0}{C} - 1\right) = \frac{K_{Th}q_0m}{Q} - K_{Th}C_0t \quad (4.52)$$

The meaning of notations from the relations (4.51) and (4.52) is: K_{Th} - the Thomas rate constant (L/min mg), q_0 - the maximum solid-phase concentration of Cs (mg/g), m - the amount of the PNF-SG in the column (g), Q - the flow rate (L/min), C - effluent concentration in cesium (mg/L), C_0 - influent concentration in cesium (mg/L). Thomas model was applied to the data at C/C_0 values between 0.05 and 0.95, for different operating conditions. The values of K_{Th} and q_0 , which are the model parameters, were obtained from the plot of $\ln(C_0/C - 1)$ versus time. The result of parameters identification is given in Table 4.6. It can be seen that R^2 values ranged from 0.9470 to 0.9996, indicating the suitability of Thomas model.

Table 4.6. Thomas model parameters for Cs uptake of PNF-SG for different experimental conditions

Flow rate Q , (mL/min)	Initial conc. C_0 , (mg/L)	Bed height H , (cm)	Thomas constant K_{Th} , (L/min mg) $\times 10^{-4}$	q_0 (model) (mg/g)	R^2
1	150	2	1.14	5.51	0.9996
3	150	2	3.31	7.02	0.9983
6	150	2	4.60	4.91	0.9833
3	50	2	2.68	2.89	0.9470
3	100	2	3.2	5.44	0.9994
3	150	2	3.31	7.02	0.9983
3	150	2	3.31	7.02	0.9983
3	150	4	1.92	3.87	0.9922
3	150	6	1.73	4.16	0.9654

Thomas rate constant (K_{Th}) increased from 2.68×10^{-4} to 3.31×10^{-4} with increasing the influent concentration from 50 to 150 mg/L. The rate constant was observed to be increasing with increasing the flow rate and decreased with increasing the bed height. The model or theoretical breakthrough curves for Cs ion exchange on PNF-SG were obtained using the parameters K_{Th} and q_0 determined from the available experimental data for different operating conditions. The experimental and model breakthrough curves are shown in fig. 4.25. The breakthrough curves confirm the applicability of this model in describing the experimental data.

Yoon–Nelson model: This model was based on the assumption that the rate of decrease in the probability of adsorption for each adsorbate molecule was proportional to the probability of

adsorbate sorption and the probability of adsorbate breakthrough on the adsorbent. The Yoon–Nelson model is not only less complicated than other models, but also requires no detailed data concerning the characteristics of sorbate, the type of adsorbent, and the physical properties of sorption bed.

The Yoon–Nelson equation for sorption of single component is expressed [93] by relation (4.53) where K_{YN} is a rate constant (h^{-1}), τ represents the time required for 50% sorbate breakthrough and t is the current time (h).

$$\frac{C_t}{C_0 - C_t} = \exp(K_{YN}t - \tau K_{YN}) \quad (4.53)$$

For a symmetric breakthrough curve the quantity of solute sorbed at time τ equals half of the removal capacity, and it is calculated relative to the initial concentration and flow rate. The uptake capacity q can be calculated with equation (4.54) where m is the mass of the sorbent (g) and Q is the flow rate (mL/min).

$$q = \frac{C_0 Q \tau}{m} \quad (4.54)$$

From the intercept and slope of the plot of $\ln[C/(C_0 - C)]$ against sampling time (t), values of K_{YN} and τ were determined. The values of K_{YN} and τ determined for different operating conditions are listed in Table 4.7. It was observed that the rate constant K_{YN} increased from 1.72×10^{-2} to 6.98×10^{-2} with increasing Cs inlet concentration from 50 to 150 mg/L. When the bed height increased from 2 to 6 cm, the values of K_{YN} decreased. As the flow rate increased, also K_{YN} increased.

Table 4.7. Yoon Nelson model parameters for Cs uptake of PNF-SG for different experimental conditions

Flow rate Q , (mL/min)	Initial conc. C_0 , (mg/L)	Bed height H , (cm)	Yoon–Nelson rate constant K_{YN} , (L/min mg) $\times 10^{-4}$	$q_{0(\text{model})}$ (mg/g)	τ (min)	R^2
1	150	2	0.75	2.97	50	0.9415
3	150	2	3.21	5.42	69	0.9994
6	150	2	4.98	7.01	57	0.9983
3	50	2	1.72	5.52	70	0.9996
3	100	2	4.98	7.01	71	0.9983
3	150	2	6.98	4.92	69	0.9831
3	150	2	4.98	7.01	69	0.9983
3	150	4	2.88	3.87	72	0.9924
3	150	6	2.59	4.16	130	0.9654

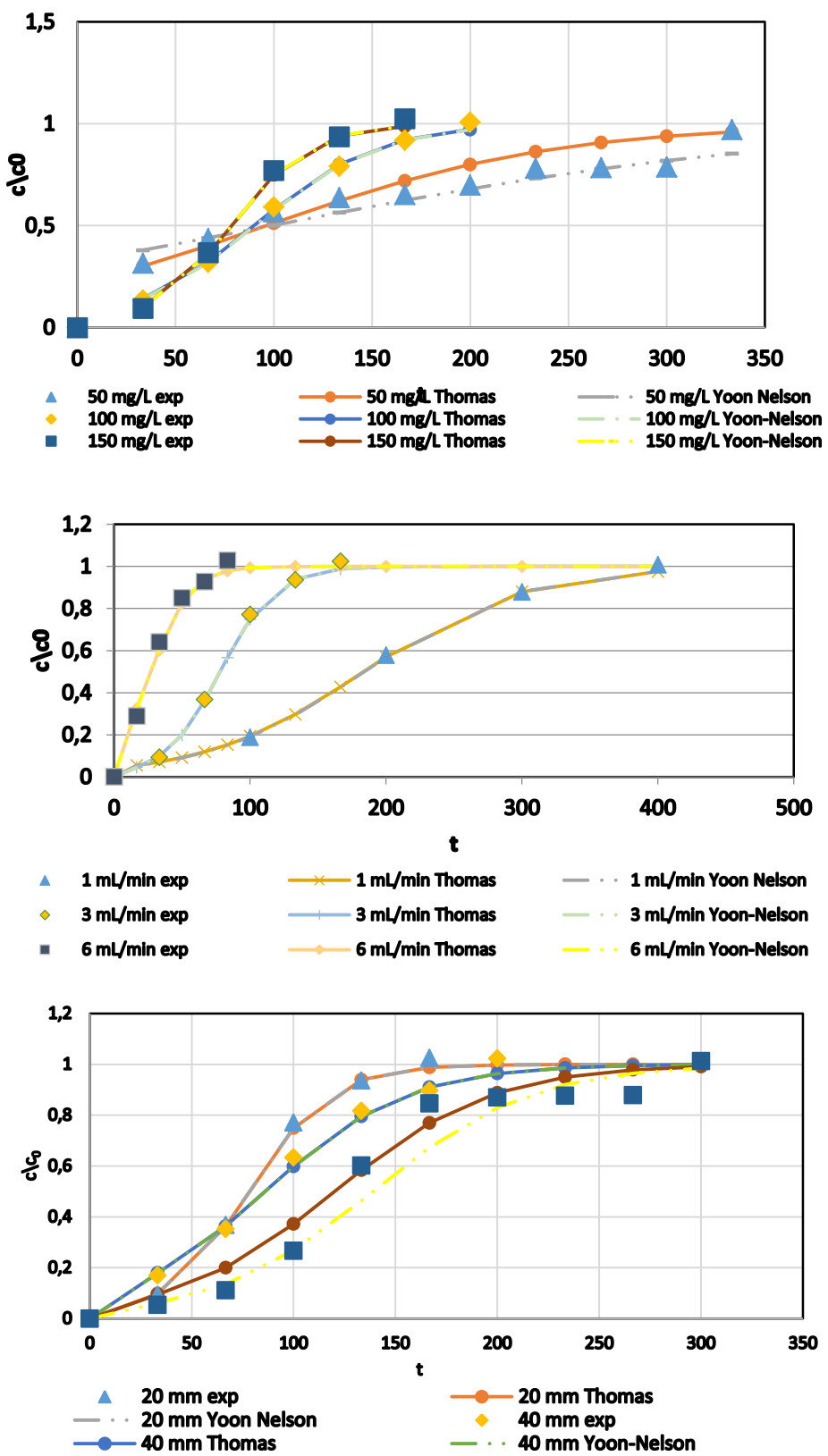


Figure 4.25. Comparison of experimental and model breakthrough curves for different feed concentrations (a), feed flow rates (b) and bed heights (c)

Table 4.7 indicates that the model and experimental uptake capacities were comparable and the regression coefficient (R^2) varies between 0.9415 and 0.9996. The model curves were compared with the experimental curves as shown in fig. 4.25. This model

provided a good fit of the experimental data for all the effects studied with good correlation coefficients.

4.4.3. Conclusions

Potassium nickel ferrocyanide, precipitated on silica gel particles was tested as inorganic ion exchange material for the removal of cesium ions from aqueous solutions. The kinetic was experimentally studied and the obtained rate data were analyzed using simple kinetic models. Results explained that the pseudo second-order sorption mechanism is dominant and the overall rate constant of sorption process appears to be controlled by a chemical sorption process. Equilibrium isotherms have been determined and tested for different isotherm expressions and the sorption data were successfully modeled using Langmuir and Freundlich approaches. The values of thermodynamic parameters indicated the endothermic and spontaneous nature of this sorption process. Analysis of the kinetic data showed that the pseudo-second-order model fitted well with the experimental data confirming that the chemical sorption was the determining step.

On the basis of the experimental results of fix-bed column investigation, the following conclusion can be drawn: the adsorption of PNF-SG was found to be dependent on the flow rate, the initial Cs concentration and bed height. All investigated experimental conditions show that the prediction of whole breakthrough curve is effective with Thomas and Yoon–Nelson models. Comparing the values of R^2 of the breakthrough curves, both models can be used to describe the behavior of Cs ion exchange on PNF-SG in a fixed-bed column. The behavior of the PNF-SG and the determined coefficients of the models for different operating conditions can be used to scale up the process.

Decontamination factors were calculated in order to identify all influencing parameters and acceptable limits for variability in separation process.

REFERENCES

- [1] J.D. Joshi, *An Overview of '3d' and '4f' Metal Ions: Sorption Study with Phenolic Resins in Ion Exchange Technology II: Applications*, D. Inamuddin, M. Luqman, (Eds.), Springer Science & Business Media, 351-354, 2012
- [2] R.G. Anthony, R.G. Dosch, D. Gu, C.V. Philip, *Use of Silicotitanates for Removing Cesium and Strontium from Defense Waste*, Ind. Eng. Chem. Res., **33**, 2702 – 2705, 1994
- [3] E.A. Behrens, P. Sylvester, A. Clearfield, *Assessment of a Sodium Nonatitanate and Pharmacosiderite-Type Ion Exchangers for Strontium and Cesium Removal from DOE Waste Simulants*, Environ. Sci. Technol., **32**, 101 – 107, 1998
- [4] A.I. Bortun, L.N. Bortun, A. Clearfield, *Evaluation of Synthetic Inorganic Exchangers for Cesium and Strontium Removal from Contaminated Ground Water and Wastewater*, Solvent. Extr. Ion. Exch., **15**, 909 – 929, 1997
- [5] T. Moeller, et al., *Uptake of ^{85}Sr , ^{134}Cs and ^{57}Co by Antimony Silicates Doped with Ti^{4+} , Nb^{5+} , Mo^{6+} and W^{6+}* , J. Mater. Chem., **11**, 1526 – 1532, 2001
- [6] *Application of Ion Exchange Processes for the Treatment of Radioactive Waste and Management of Spent Ion Exchangers*, TRS No. 408, Vienna, International Atomic Energy Agency, 2002
- [7] W.L. McCabe, J.C. Smith, P. Harriot, *Unit Operations of Chemical Engineering*, McGraw-Hill International Ed., 6th ed., New York, USA, 802, 2001
- [8] F. Helfferich, *Ion Exchange*, Dover Publications Inc., New York, Vol. 7, 134-140, 1995
- [9] M.A. Barros, A.S. Zola, P.A. Arroyo, E.F. Sousa-Aguiar, C.R.G. Tavares, *Binary Ion Exchange of Metal Ions in Y and X Zeolites*, Braz. J. Chem. Eng., **20(4)**, 413-421, 2003
- [10] I. Langmuir, *The adsorption of gases on plane surfaces of glass, mica and platinum*, J. Am. Chem. Soc., **40**, 1361–1403, 1918
- [11] D.A.H. Hanaor, M. Ghadiri, W. Chrzanowski, Y. Gan, *Scalable Surface Area Characterization by Electrokinetic Analysis of Complex Anion Adsorption*, Langmuir **30(50)**, 15143–15152, 2014
- [12] H. Freundlich, *Adsorption in solution*, Phys. Chem., **57**, pp. 384–401, 1906
- [13] J. Toth, *State equations of the solid gas interface layer*, Acta Chem. Acad. Hung., **69**, 311-317, 1971
- [14] M.J. Temkin, V. Pyzhev, *Recent modifications to Langmuir isotherms*, Acta Physiochim., **12**, 217-222, 1940
- [15] S. Brunauer, P.H. Emmett, E. Teller, *Adsorption of Gases in Multimolecular Layers*, J. Am. Chem. Soc., **60(2)**, 309–319, 1938
- [16] N.Z. Misak, *Some aspects of the application of adsorption isotherms to ion exchange reactions*, React. Funct. Polym., **43**, 153-164, 2000
- [17] M. Sprynskyy, B. Buszewski, A.P. Terzyk, K. Namiesnik, *Study of the selection mechanism of heavy metal (Pb^{2+} , Cu^{2+} , Ni^{2+} and Cd^{2+}) adsorption on clinoptilolite*, J. Colloid. Interface Sci., **304**, 21-28, 2006
- [18] C.J. Geankoplis, *Transport Processes and Unit Operations*, 3rd edition, PTR Prentice Hall, 703, 1993
- [19] C.G. Hill, *An Introduction to Chemical Engineering Kinetics and Reactor Design*, John Wiley & Sons, New York, 388-425, 1977

- [20] E. Valdman, L. Erijman, F.L.P. Pessoa, S.G.F. Leite, *Continuous Biosorption of Cu and Zn by Immobilized Waste Biomass Sargassum sp.*, Process Biochemistry, **36**, 869-873, 2001
- [21] D. Mohan, S. Chander, *Single Component and Multi-component Adsorption of Metal Ions by Activated Carbons*, Colloids and Surfaces A, **177(2-3)**, 183-196, 2001]
- [22] M.A.S.D. Barros, A.S. Zola, C.R.G. Tavares, E.F. Sousa-Aguiar, *Chromium uptake from tricomponent solution in zeolite fixed bed*, Adsorption, **12**, 229-248, 2006
- [23] K. Klamer, D.W. Van Krevelen, *Studies on Ion Exchange-I*, Chem. Eng. Sci., **7(4)**, 197-203, 1958
- [24] M.A.S.D. Barros, E.A. Silva, P.A. Arroyo, C.R.G. Tavares, R.M. Schneider, M. Suszek, E.F. Sousa-Aguiar, *Removal of Cr(III) in the fixed bed column and batch reactors using as adsorbent zeolite NaX*, Chem. Eng. Sci., **59**, 5959 – 5966, 2004
- [25] M.A.S.D. Barros, A.S. Zola, P.A. Arroyo, E.F. Sousa-Aguiar, C.R.G. Tavares, *Equilibrium and dynamic ion exchange studies of Cr³⁺ on zeolites NaA and NaX*, Acta Scientiarum, **24(6)**, 1619-1625, 2002
- [26] G.S. Bohart, E.Q. Adams, *Some aspects of the behavior of charcoal with respect to chlorine*, J. Am. Chem. Soc., **42**, 523-544, 1920
- [27] K.H. Chu, E.Y. Kim, X. Feng, *Batch Kinetics of Metal Biosorption: Application of the Bohart-Adams Rate Law*, Separ. Sci. Technol., **46(10)**, 1591-1601, 2011
- [28] C.E. Borba, E.A. Silva, M.R. Fagundes-Klen, A.D. Kroumov, R. Guirardello, *Prediction of the copper (II) ions dynamic removal from a medium by using mathematical models with analytical solution*, J. Hazard. Mater., **152(1)**, 366-372, 2008
- [29] A. Chatterjee, S. Schiewer, *Biosorption of Cadmium(II) Ions by Citrus Peels in a Packed Bed Column: Effect of Process Parameters and Comparison of Different Breakthrough Curve Models*, Clean Soil Air Water, **39(9)**, 874-881, 2011
- [30] M.A. Martin-Lara, F. Hernainz, G. Blazquez, G. Tenorio, M. Calero, *Sorption of Cr (VI) onto Olive Stone in a Packed Bed Column: Prediction of Kinetic Parameters and Breakthrough Curves*, J Environ Eng-ASCE, **136 (12)**, pp. 1389 - 1397, 2010;
- [31] H. Muhamad, H. Doan, A. Lohi, *Batch and continuous fixed-bed column biosorption of Cd²⁺ and Cu²⁺*, Chem. Eng. J., **158(3)**, 369-377, 2010
- [32] K.S. Rao, S. Anand, P. Venkateswarlu, *Modelling the kinetics of Cd(II) adsorption on Syzygium cumini L leaf powder in a fixed bed mini column*, J. Ind. Eng. Chem., **17(2)**, 174-181, 2011
- [33] A. Singh, D. Kumar, J. P Gaur, *Continuous metal removal from solution and industrial effluents using Spirogyra biomass-packed column reactor*, Water Res., **46(3)**, 779-788, 2012
- [34] M. Trgo, N.V. Medvidovic, J. Peric, *Application of mathematical empirical models to dynamic removal of lead on natural zeolite clinoptilolite in a fixed bed column*, Ind. J. Chem. Techn., **18(2)**, 123-131, 2011
- [35] H.C. Thomas, *Heterogeneous ion exchange in a flowing system*, J. Am. Chem. Soc., **66**, 1664–1666, 1944
- [36] H.K. Hsuen, *An improved linear driving force approximation for intraparticle adsorption*, Chem. Eng. Sci., **55**, 3475-3480, 2000
- [37] J.M.P.Q. Delgado, *A critical review of dispersion in packed bed*, Heat Mass Transfer, **42**, 279-310, 2006

- [38] N. Wakao, T. Funazkri, *Effect of fluid dispersion coefficients on particle-to-fluid mass transfer coefficients in packed beds*, Chem. Eng. Sci. **33**, 1375-1384, 1978
- [39] Y.H. Yoon, H.N. James, *Application of gas adsorption kinetics I. A theoretical model for respirator cartridge service life*, Am. Ind. Hyg. Assoc. J., **45(8)**, 509-516, 1984
- [40] O. Hamdaoui, *Dynamic sorption of methylene blue by cedar sawdust and crushed brick in fixed bed columns*, J. Hazard. Mater., **138(2)**, 293-303, 2006
- [41] Y.H. Wang, S.H. Lin, R.S. Juang, *Removal of heavy metal ions from aqueous solutions using various low-cost adsorbents*, J. Hazard. Mater., **102(2-3)**, 291-302, 2003
- [42] C. Araneda, C. Basualto, J. Sapag, C. Tapia, D. Cotoras, F. Valenzuela, *Uptake of copper (II) ions from acidic aqueous solutions using a continuous column packed with microcapsules containing a β -hydroxyoximic compound*, Chem. Eng. Res. Des., **89(12)**, 2761-2769, 2011
- [43] A.M. Mahmouda, F.A. Ibrahima, S.A. Shaban, N. A. Youssefa, *Adsorption of heavy metal ion from aqueous solution by nickel oxide nano catalyst prepared by different methods*, Egyptian Journal of Petroleum, **24(1)**, 27–35, 2015
- [44] K. Shakir, M. Sohsah, M. Soliman, *Removal of cesium from aqueous solutions and adioactive waste simulants by coprecipitate flotation*, Sep. Purif. Technol., **54**, 373–381, 2007
- [45] E. Bascetin, G. Atun, *Adsorptive removal of strontium by binary mineral mixtures of montmorillonite and zeolite*, J. Chem. Eng. Data, **55**, 783–788, 2010
- [46] M.V. Balarama Krishna, S.V. Rao, J. Arunachalam, M.S. Murali, S. Kumar, V.K. Manchanda, *Removal of ^{137}Cs and ^{90}Sr from actual low level radioactive waste solutions using moss as a phyto-sorbent*, Sep. Purif. Technol., **38**, 149–161, 2004
- [47] Z. Cheng, Z. Gao, W. Ma, Q. Sun, B. Wang, X. Wang, *Preparation of magnetic Fe_3O_4 particles modified sawdust as the adsorbent to remove strontium ions*, Chem. Eng., J., **209**, 451–457, 2012
- [48] C. Zhang, P. Gu, J. Zhao, D. Zhang, Y. Deng, *Research on the treatment of liquid waste containing cesium by an adsorption-microfiltration process with potassium zinc hexacyanoferrate*, J. Hazard. Mater., **167**, 1057–1062, 2009
- [49] G. Lujaniene, S. Meleshevych, V. Kanibolotskyy, J. Sapolait, V. Strelko, V. Remeikis, O. Oleksienko, K. Ribokaite, T. Sciglo, *Application of inorganic sorbents for removal of Cs, Sr, Pu and Am from contaminated solutions*, J. Radioanal. Nucl. Chem., **282**, 787–791, 2009
- [50] M.C. Duff, D.B. Hunter, D.T. Hobbs, S.D. Fink, Z. Dai, J.P. Bradley, *Mechanisms of strontium and uranium removal from high-level radioactive waste simulant solutions by the sorbent monosodium titanate*, Environ. Sci. Technol., **38**, 5201–5207, 2004
- [51] G.M. Walker, J.-A. Hanna, S.J. Allen, *Treatment of hazardous shipyard wastewater using dolomitic sorbents*, Water Res., **39**, 2422–2428, 2005
- [52] A.M. Puziy, *Cesium and strontium exchange by the framework potassium titanium silicate $\text{K}_3\text{Ti}_4\text{O}_4(\text{SiO}_4)_{34}\text{H}_2\text{O}$* , J. Radioanal. Nucl. Chem., **237**, 73–80, 1998
- [53] E.I. Shabana, M.I. El-Dessouky, *Sorption of cesium and strontium ions on hydrous titanium dioxide from chloride medium*, J. Radioanal. Nucl. Chem., **253**, 281–284, 2002
- [54] T.A. Todd, K.N. Brewer, D.J. Wood, P.A. Tullock, N.R. Mann, L.G. Olson, *Evaluation and testing of inorganic ion exchange sorbents for the removal of cesium-137 from Idaho chemical processing plant acidic tank waste*, Sep. Sci. Technol., **36**, 999–1016, 2001
- [55] A.M. El-Kamash, *Evaluation of zeolite A for the sorptive removal of Cs^+ and Sr^{2+} ions from aqueous solutions using batch and fixed bed column operations*, J. Hazard. Mater., **151**, 432–445, 2008

- [56] A. Ghaemi, M. Torab-Mostaedi, M. Ghannadi-Maragheh, *Characterizations of strontium (II) and barium (II) adsorption from aqueous solutions using dolomite powder*, J. Hazard. Mater., **190**, 916–921, 2011
- [57] P.A. Hass, *A Review of Information on Ferrocyanide Solids for Removal of Cesium from Solutions*, Separ. Sci. Technol., **28(17-18)**, 2479-2506, 1993
- [58] Y. Lin, G.E. Fryxell, H. Wu, M. Engelhard, *Selective sorption of cesium using self-assembled monolayers on mesoporous supports*, Environ. Sci. Technol., **35(19)**, 3962-3968, 2001
- [59] *Application of ion exchange processes for the treatment of radioactive waste and management of spent ion exchangers TRS No. 408*, Vienna, International Atomic Energy Agency, 2002
- [60] C. Bucur, M. Olteanu, N. Dulama, M. Pavelescu, *Cesium Sorption/Desorption on Saligny Geologic Formations*, Rom. Journ. Phys., **56(5-6)**, 769–783, 2011
- [61] W.W. Schulz, L.A. Bray, *Solvent Extraction recovery of Byproduct 137Cs and 90Sr from HNO₃ Solutions—A Technology Review and Assessment*, Sep. Sci. Technol., **22**, 191-202, 1987
- [62] A.E. Savkin, Y.T. Slastennikov, O.G. Sinyakin., *Processing NPP bottoms by ferrocyanide precipitation*, 2002 International Waste Management Conference (WM'02 Conference), February 24-28, 2002, Tucson, USA
- [63] D.D. Walker, M.J. Barnes, C.L. Crawford, R.A. Peterson, R.F. Swingle, S.D. Fink., *In Tank Precipitation with Tetraphenylborate: Recent Process and Research Results*, in Science and Technology for Disposal of Radioactive Tank Wastes, W. W. Schulz, N. J. Lombardo (Eds.); Plenum, New York, 219 - 230; 1998
- [64] J. Lehto, E. Pukko, T. Jakkola, *Separation of Cesium from a Nuclear Waste Solution by Precipitation with Sodium Hexanitrocobaltate and Tungstophosphoric*, Radiochimica Acta, **38**, 53-56, 1985
- [65] A.V. Voronina, V.S. Semenishchev, E.V. Nogovitsyna, N.D. Betenekov, *A study of ferrocyanide sorbents on hydrated titanium dioxide support using physicochemical methods*, Radiochemistry, **54(1)**, 69-74, 2012
- [66] V.N. Lebedev, N.A. Mel'nik, A.V. Rudenko, *Sorption of cesium on titanium and zirconium phosphates*, Radiochemistry, **45**, 149–151, 2003
- [67] K.A. Venkatesan, V. Sukumaran, M.P. Antony, T.G. Srinivasan, *Studies on the feasibility of using crystalline silicotitanates for the separation of cesium-137 from fast reactor high-level liquid waste*. J. Radioanal. Nucl. Chem., **280**, 129–136, 2009
- [68] T.J. Tranter, R.S. Herbst, T.A. Todd, A.L. Olson, H.B. Eldredge, *Evaluation of ammonium molybdophosphate-polyacrylonitrile (AMP-PAN) as a cesium selective sorbent for the removal of Cs-137 from acidic nuclear waste solutions*, Adv. Environ. Res., **6**, 107–121, 2002
- [69] G.S. Murthy, M.V. Sivaiah, S.S. Kumar, V.N. Reddy, R.M. Krishna, S. Lakshminarayana, *Adsorption of cesium on a composite inorganic exchange zirconium phosphate–ammonium molybdophosphate*, J. Radioanal. Nucl. Chem., **260**, 109–114, 2004
- [70] J. Narbutt, J. Siwiniski, B. Bartos, A. Bilewicz, *Studies on new titanium hexacyanoferrate sorbents for radiocesium removal from primary coolant of pressurized water reactors*, J. Radioanal. Nucl. Chem., **101**, 41-49, 1986;

- [71] C. Loos-Neskovic, S. Ayrault, V. Badillo, B. Jimenez, E. Garnier, M. Fedoroff, D.J. Jones, B. Merinov, *Structure of copper-potassium hexacyanoferrate (II) and sorption mechanisms of cesium*, J. Solid. State Chem., **177**, 1817–1828, 2004
- [72] J. Orechovska, P. Rajec, *Sorption of cesium on composite sorbents based on nickel ferrocyanide*, J. Radioanal. Nucl. Chem., **242**, 387-390, 1999
- [73] A.V. Voronina, N.D. Betenekov, E.V. Nogovitsyna, V.S. Semenishchev, A.F. Nikiforov, *Statics and kinetics of caesium sorption by the nickel-potassium ferrocyanides based on hydrated titanium and zirconium dioxides from aqueous media*, Russian Journal of Construction Science and Technology, **1**, 52-56, 2015
- [74] *Treatment of low- and intermediate-level liquid radioactive wastes*, TRS No. 236, Vienna, International Atomic Energy Agency, 1984
- [75] F. Xiaogui, J. Shan, W. Qiulin, C. Jing, S. Chongli, *Thermal decomposition of potassium titanium hexacyanoferrate(II) loaded with cesium in a fixed bed calciner*, Chin. J. Gem. Eng., **15**, 184-189, 2007
- [76] M. Suzuki, *Adsorption Engineering*, Elsevier Science Publishers B.V., 172, 1990
- [77]. H.J. Won, J.K. Moon, C.H.Y. Chung, *Evaluation of ferrocyanide anion exchange resins regarding the uptake of cs+ ions and their regeneration*, Nuclear Engineering and Technology, **40(6)**, 489-496, 2008
- [78] K. Watari, K. Imai, Y. Ohmomo, Y. Muramatsu, Y. Nishimura, M. Izawa, L.R. Baciles, *Simultaneous Adsorption of Cs-137 and I-131 from Water and Milk on Metal Ferrocyanide-Anion Exchange Resin*, J. Nucl. Sci. Techn., **25(5)**, 495-499, 1988
- [79] T.R. Folsom, N. Hansen, T.J. Tatum, V.F. Hodge, *Recent Developments in Method for Concentrating and Analyzing Radiocesium in Sea Water*, J. Radiation. Res., **16**, 19-27, 1975
- [80] D.R. Mann, S.A. Casso, *In Situ Chemisorption of Radiocesium from Sea Water*, Marine Chem., **14(4)**, 307-328, 1984
- [81] L.R. Zicman, E. Neacsu, L. Done, L. Tugulan, F. Dragolici, B.T. Obreja, T. Dobre, *Removal of ¹³⁷cs ions from aqueous radioactive waste using nickel ferrocyanide, precipitated on silica gel*, Bulletin of Romanian Chemical Engineering Society, **2(1)**, 84-99, 2015
- [82] L.R. Zicman, E. Neacsu, L. Done, L.C. Tugulan, C. Alexandru, F.N. Dragolici, M. Nicu, L.F. Ionacsu, B.T. Obreja, G. Dogaru, T. Dobre, *Investigation and modelling of fixed bed cesium sorption on nickel ferrocyanide, precipitated on silica gel*, Rom. J. Phys. **62**, 806, 2017
- [83] K. Naddafi, R. Nabizadeh, R. Saeedi, A.H. Mahvi, F. Vaezi, K. Yaghmaeian, A.Ghasri, S. Nazmara, *Biosorption of lead (II) and cadmium (II) by protonated Sargassum glaucescens biomass in a continuous packed bed column*, J. Hazard. Mater., **147(3)**, 785-791, 2007
- [84] O. Hamdaoui, *Dynamic sorption of methylene blue by cedar sawdust and crushed brick infixed bed columns*, J. Hazard. Mater. **138(2)**, 293–303, 2006
- [85] O. Hamdaoui, *Removal of copper (II) from aqueous phase by purolite C100-MB cation exchange resin in fixed bed columns: Modelling*, J. Hazard. Mater., **161(2-3)**, 737-746, 2009
- [86] M.M. Abd El-Latif, M.F. Elkady, *Kinetics study and thermodynamic behavior for removing cesium, cobalt and nickel ions from aqueous solution using nanozirconium vanadate ion exchanger*, Desalination, **271**, 41-54, 2011
- [87] V.V. Milyutin, S.V. Mikheev, V.M. Gelis, O.A. Kononenko, *Coprecipitation of Microamounts of Cesium with Precipitates of Transition Metal Ferrocyanides in Alkaline Solutions*, Radiokhimiya, **51(3)**, 258-260, 2009

- [88] S. Lagergren, *About the theory of so-called adsorption of soluble substances*, K. Sven. Vetenskapsakad. Handl. **24**, 1-39, 1898
- [89] Y.S. Ho, G. McKay, *Pseudo second-order model for sorption processes*, Process. Biochem., **34**, 451-465, 1999
- [90]. K.G. Scheckel, D.L. Sparks, *Temperature effects on nickel sorption kinetics at mineral water interface*, Soil. Sci. Soc. Am. J., **65**, 719-728, 2001
- [91]. J. Peric, M. Trgo, N.V. Medvidovic, *Removal of zinc, copper and lead by natural zeolite-a comparison of adsorption isotherms*, Water Res. **38**, 1839-1899, 2004
- [92]. D. Mohan, S. Chander, *Single, binary and multicomponent sorption of iron and manganese on lignite*, J. Colloid. Interface Sci., **299**, 57-76, 2006
- [93]. C. Mahendra, P.M. Sathya Sai, C. Anand Babu, K. Revathy, K.K. Rajan, *Analysis and modelling of fixed bed sorption of cesium by AMP-PAN*, J. Environ. Chem. Eng., **3(3)**, 1546-1554, 2015

CHAPTER 5. THE USE OF THE REVERSE OSMOSIS METHOD IN THE COMBINED TREATMENT OF AQUEOUS RADIOACTIVE WASTE (ARW)

Reverse osmosis (RO) as an efficient technology for removing the cesium, strontium, technetium and uranium species from ARW, in order to respect the regulatory limits, was successfully researched and applied in more concrete cases. For a large variety of separation membrane matrices, literature data show that the rejection rates were acceptable at low concentrations of contaminants. However, rejections of ^{137}Cs and ^{90}Sr species at higher concentrations may not be adequate even when using sophisticated membranes. After a short introduction in the theory of reverse osmosis this chapter is oriented on quantitative characterization of RO system from the ARW treatment installation presented in the second chapter of this work.

5.1. Short RO characterization

Due to its high efficiency, easy operation, compact equipment, simplicity in the process control, low capital and operating expenses, membrane technology is being used extensively for various separation and purification processes [1 - 10]. Reverse osmosis (RO) as a feasible separation process is a relatively young technology. It is based on osmosis, which is a natural phenomenon where a solvent (usually water) passes through a semipermeable barrier from the side with lower solute concentration to the one with higher solute concentration (fig. 5.1a). Water continues to flow through the membrane separating the two solutions (fig 5.1a and fig 5.1b) until the solvent chemical potential equilibrium is established (fig. 5.1b). Fig. 5.1b shows that the osmotic pressure of one couple solution-membrane is the pressure required to stop water flow requested by equilibrium.

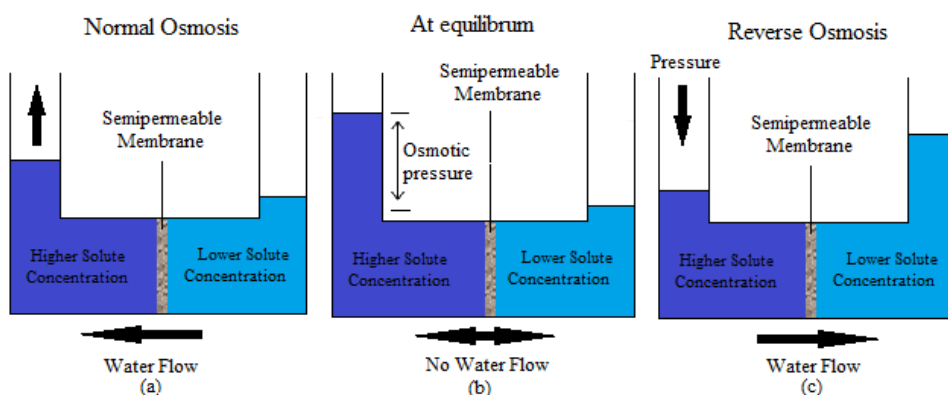


Figure 5.1. Schematic of normal osmosis (a) and reverse osmosis (c) phenomena

If a pressure difference greater than the osmotic pressure difference is applied, the flow of water (solvent) is reversed, as it can be seen in fig. 5.1c; as a result, separation of water from the solution occurs as pure water flowing from the high concentration side to the low concentration side. This phenomenon is termed reverse osmosis (RO).

A RO membrane acts as a semipermeable barrier allowing a selective passage of a particular species (solvent) while partially or completely retaining other species (solute). For solute and solvent, the transport across the membrane and their chemical potential gradients across the membrane provide their driving forces. The solute chemical potential gradient is usually expressed in terms of concentration, whereas the water (solvent) chemical potential gradient is generally expressed as pressure difference across the membrane [11]. Three streams (and associated variables) of the RO membrane process are involved: *the feed water* enters the RO membrane under pressure (enough pressure to overcome osmotic pressure), the water molecules pass through the semi-permeable membrane resulting in the *permeate* (or *product*) *stream* while the salts and other contaminants are not allowed to pass and are discharged through the *concentrate* (or *reject*) *stream*, which goes to drain or can be fed back into the feed water supply to be recycled through the RO system. A few important parameters of RO process are further highlighted.

The water flux through the membrane, J_w , is defined by Eq. (5.1), where G_w is the volumetric or mass flow rate of water and A_m the membrane surface area.

$$J_w = \frac{G_w}{A_m} \quad (5.1)$$

The solute mass flux, J_{ms} , is given by Eq. (5.2), where G_{ms} is the mass flow rate of solute.

$$J_{ms} = \frac{G_{ms}}{A_m} \quad (5.2)$$

The solute rejection coefficient, R , is expressed by Eq. (5.3), where C_P is the permeate solute concentration and C_F the feed solute concentration.

$$R = 1 - \frac{C_P}{C_F} \quad (5.3)$$

The quantity of water that passes through the membrane (the permeate) is evaluated in terms of water recovery coefficient, r , defined by Eqs. (5.4) and (5.5) for a batch and a continuous RO system, respectively. Here V_F is the feed volume, V_P the permeate volume, F_F the feed flow rate, F_P the permeate flow rate and Δt the operating time.

$$r = \frac{\sum J_w A_m \Delta t}{V_F} = \frac{V_P}{V_F} \quad (5.4)$$

$$r = \frac{J_w A_m}{F_F} = \frac{F_p}{F_F} \quad (5.5)$$

The concentration factor, CF , is defined by Eq. (5.6) as the ratio between the solute concentration in the concentrate stream (C_C) and its concentration in the feed stream (C_F).

$$CF = \frac{C_C}{C_F} \quad (5.6)$$

RO is used industrially for the production of drinking water from saline or brackish waters and is increasingly being used for the treatment of wastewaters. RO membranes have been recently applied to process the liquid radioactive waste from commercial nuclear power plants [12 - 14]. With good membranes, nearly all contaminants from a solution (dissolved gases and tritium being two exceptions) are rejected in RO. So it is obtained a permeate with high purity, ie with little radioactive activity, which makes it suitable for discharge into the environment. A RO system in the nuclear industry is usually a part of an integrated liquid waste treatment system and is used to replace or improve the existing evaporation and/or ion exchange technology.

5.2. Modelling RO process

During the past years diffusion controlled membrane processes as reverse osmosis (RO) and nanofiltration (NF) have been used in an increasing number of applications. These treatment processes have become competitive technologies to traditional water treatment processes because they have some advantages: i) high effectiveness in removing most inorganic and organic impurities resulting ultra-pure water which complies with existing requirements and regulations; ii) high capability to treat different water sources: sea water, brackish ground water and surface water, wastewater; iii) good versatility for all purpose of water quality; they can remove heavy metals, pesticides, natural organic matter (NOM), disinfection by-products (DBP), Volatile Organic Chemicals (VOC) and other dissolved species.

In modelling of mass transfer, with respect to water flux and salt transport through the membrane, different theories and numerous models have been developed. A lot of research works have dedicated a great deal of attention to develop more accurate models to asses performance of NF/RO processes in pre-design studies, design, operation and other aspects related to water treatment.

The **diffusion solution models** are used on a large scale in diffusion controlled membrane process. These models are based on several basic principles of diffusion, convection, film theory and electroneutrality. Diffusion solution models contain parameters

that consist in actual operation conditions, which can be precisely and directly monitored. In diffusion solution models, mass transfer coefficients for water and solute are the most important parameters. Hypothetically, solute mass transfer coefficients (SMTCs) can be established by solving the model equations or estimated with other existing theoretical approaches. Actually, it is much more difficult to model these coefficients because:

1. The (SMTCs) vary with feed water quality, operating conditions, and physico-chemical properties of membrane, which may deteriorate in time.
2. Variation of the SMTCs with water quality restricts the model application. A foregoing study [15] proved that SMTCs evaluated with Homogenous Solution Diffusion Model (HSDM) are both stage and site specific. This finding limited HSDM use in providing an accurate prediction of solute concentration in permeate from different systems, using solute and solvent mass transfer coefficients values.
3. Different operating conditions lead to different SMTCs, so, diffusion solution models have a limited accuracy in membrane scale-up prediction. A previous study [16], focused on correlation of productivity and water quality between different users highlighted the difference of inorganic solute mass transfer coefficients between flat sheet membrane, single element and large scale membrane systems.

For a good predictability of solution diffusion model the SMTCs were modified by the incorporation of several factors. The impact of these factors can be reversible or irreversible. The reversible impact does not cause any permanent change on membrane-water film interface or material. Instead, chemical or mechanical instability can produce irreversible variations of solute mass transfer coefficient with respect to changes in membrane material and membrane solvent interface. As for the reversible impact, the SMTCs may be dependent on operating conditions such as flux, recovery, feed water quality and temperature. By incorporation of flux and recovery, model errors are significantly reduced and were able to predict the pesticide rejection in a pilot scale study [17]. Also, HSDM has been integrated over membrane channel in relation to recovery, thus the predictability at high recovery was improved [18]. Other choice is to split theoretically the membrane element into several sub-elements which are identical and had less than 1% recovery and to apply HSDM to each of them [19, 20]. It was obtained a significant correction and this approach allowed a more accurate distribution of feed concentration and improved predictability at high recovery [18].

The effects of many factors, as solute form, osmotic pressure, membrane surface characteristics and flux or recovery on solute mass transfer are not yet considered, so, the solution diffusion model can be still improved. The irreversible impact can be related to numerous factors such as system hydrodynamics, operating conditions, membrane properties,

and feed property (solute). Membrane material may be affected by the interaction with solvent, oxidants, bioorganics etc., resulting chemical or biological degradation. The issues that adversely influence RO system during the operation and affect solute mass transfer coefficient may include but are not limited to: scaling, colloidal, biological and metal oxide fouling (clogging), plugging and membrane shriveling.

Productivity model [21 – 23] was developed to consider these irreversible changes, however currently no solute mass transfer model can assess accurately long term membrane performance and water quality deterioration. The existing diffusion solution models, do not take into consideration the effect of osmotic pressure increment over the membrane channel. To correlate osmotic pressure into net driving force, was considered a particularly linear or log mean concentration approximation of osmosis driving force. Even if it is acknowledged that the solutes from feed water are concentrated continuously in the membrane channel leading to osmotic pressure increase, flux decline and permeate concentration increase, the incorporation of this factor into current diffusion solution model has not yet received enough attention.

For modelling is taken into account that the membrane performance is influenced by surface characteristics. The membrane surface characteristics are typically designed by manufacturers to assure a significant membrane efficiency. In modelling the membrane performance both the membrane surface and solution properties should be taken into consideration. Since a RO membrane has unique surface characteristics, in all existing solution models the coefficients are developed for only that specific membrane. Withal, the concentration polarization can lead to membrane fouling [24]. Solutes as natural organic matter (NOM) and/or surfactants adsorbed to the membrane have complicated influence on the membrane surface properties [24 – 27]. In conclusion, there is a need for a more intense concern regarding the development of models related to membrane surface characteristics along with solute interference.

Artificial neural network model has been used lately in membrane separation ie in the case of RO. Initially these models type were recommended by some current studies dedicated to membrane separation mechanisms. The complexity of solute, solvent and membrane characteristics and their interactions causes difficulties in the accurate identification of physico-chemical phenomena that occur at membrane surface. To simulate membrane separation besides the conventional methods, new approaches such as artificial neural network models have been developed [28 - 30]. An artificial neural network (ANN) is a modelling tool that provide the capability to solve non-linear and linear multivariate regression problems. There is no need for an explicit expression of the physical meaning of

the system or process under study. ANN network model is a black box type correlation method and it makes possible the study of the relationship between the input and output variables of the process with only a limited number of experimental runs [29]. This model does not apply any physical laws thereby the problems of previous complexity are overcome. ANN network models are simple, easy to use, and site specific.

Returning now to the **diffusion models** is important to mention that the research efforts to predict the SMTCs, k_s , *had not* shown promising results. Optical or microelectrode measurements [31] made the determination of k_s possible, while its direct measurements are difficult. Other theoretical approach of extended Nernst-Plank equation only found applications for laboratory scale [32, 33]. Based on solution-diffusion and mass transfer theory, a spiral-wound process model was established by some chinese researchers to achieve accurate prediction of RO separation performance and to accelerate the computing efficacy for real time simulation. The model is expressed by differential and algebraic equations with some inequality and equality constraints related to equipment and water quality [36]

Membrane transport models allow also the determination of membrane mass transfer coefficient. In this approach, membrane SMTCs can be further connected to membrane-solution physico-chemical characteristics. The SMTCs were found corresponding to membrane feed water quality and a model for their prediction has been established using normal distribution and solute charge and molecular weight [34]. SMTCs have been found to change via different solution composition [35]. Multitudinous of these models for membranes separation process (RO/NF) contain fundamental equations that consider: i) mass balance around the membrane element; ii) pressure driven solvent gradient; iii) concentration gradient; iv) recovery imposed degree and v) recycle rate balance. These equations contain basic parameters that constitute the primary basis for development of existing models. Fig. 5.2. shows a single RO/NF element diagram along with the flow, solute concentration and pressure of the feed, permeate and concentrate streams for single element.

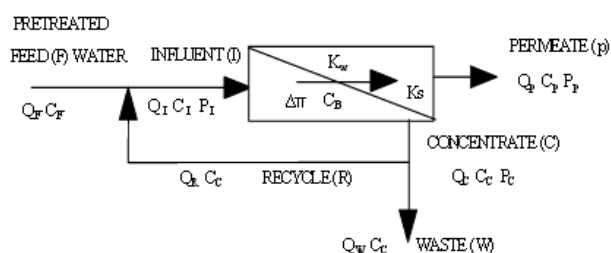


Figure 5.2. Flow diagram for NF/RO unit

Other principles such as film theory, concentration polarization considerations, ion coupling and electro-neutrality of processed liquid system, irreversible thermodynamics application to concrete separation, surface phenomena and fluid transport through pores were applied to improve developed models. Examples of these particularized models and their associated expression equations are briefly presented below.

Irreversible Thermodynamics Models. Models based on the principles of irreversible thermodynamics were among the earliest RO membrane developed models [37, 38]. These irreversible thermodynamics models assume that the membrane is near equilibrium and so fluxes can be written by phenomenological relationships [37, 39 – 41]. One of the earliest model was that derived by Kedem and Katchalsky with equations [39 – 43] for water (J_w) and solute (J_s) flux. Relations (5.7) and (5.8) give these equations. Here L_p , ω , and σ characterise the membrane transport coefficients of filtration, reflection and permeability, respectively σ is defined as the Staverman reflection coefficient $\sigma = (\frac{\Delta p}{\Delta \pi})_{J_w=0}$; the reflection coefficient represents an association of solute and solvent flux through the membrane. The difference $\Delta p = p_1 - p_2$ is the hydrostatic pressure difference and $\Delta \pi$ gives the osmotic pressure difference. According to J.H van't Hoff equation it has the expression $\Delta \pi = RT\Delta c$, with R the gas constant, T thermodynamic temperature and $\Delta c = c_1 - c_2$ the difference between the solution concentrations at both sides of the membrane. By $(C_m)_{avg}$ it is expressed the logarithmic mean solute concentration over the RO membrane.

$$J_w = L_p(\Delta p - \sigma \Delta \pi) \quad (5.7)$$

$$J_s = \omega \Delta \pi + (1 - \sigma)(C_m)_{avg} J_w \quad (5.8)$$

Some models assume that the bulk feed solution concentration is equal to the membrane wall solution concentration while other models propose an expression based on polarization concentration. In these models the solute rejection has the expression [43] written as in relation (5.9)

$$\frac{1}{R} = \frac{1}{\sigma} + \left(\frac{L_\pi}{L_p} - \sigma^2 \right) \left(\frac{L_p}{\sigma} \right) \pi_F \frac{1}{J_w} \quad (5.9)$$

In relation (5.9) L_π is determined from reflexion solute coefficient according to relation $\omega = (\frac{L_\pi}{L_p} - \sigma^2)(C_m)_{avg} L_p$. The coefficients in Eqs. (5.7, 5.8, 5.9), can be functions of concentration [37, 39, 40]. This dependence is a disadvantage of the Kedem-Katchalsky model. To avoid concentration dependence, Spiegler and Kedem, in [45], defined local water (P_w) and solute (P_s) permeabilities and reflection coefficients and then represented the fluxes (water and solute) as in relations (5.10), (5.11).

$$J_w = -P_w \left(\frac{dp}{dz} - \sigma \frac{d\pi}{dz} \right) \quad (5.10)$$

$$J_s = -P_s \frac{dC_m}{dz} + (1-\sigma) C_m J_w \quad (5.11)$$

In terms of permeabilities, the solute rejection coefficient in integrated form [24, 25, 30] is given by relation (5.12).

$$\frac{1}{R} = \frac{1 - \sigma \exp(-(1-\sigma) \frac{\delta J_w}{P_s})}{\sigma [1 - \exp(-(1-\sigma) \frac{\delta J_w}{P_s})]} \quad (5.12)$$

The ***Spiegler-Kedem model***, another thermodynamic based model, was widely applied in describing and analysis of RO membrane separations. Irreversible thermodynamics models can describe RO membrane transport, but they have a major disadvantage, that is the treatment of the membrane is considered a "black box" [40], and that is the reason for what these models do not provide a deep understanding of the transport mechanisms of the membrane. As a result, these models are not useful for optimizing processes based on membrane structure and properties, and, also, do not sufficiently describe the water flux for some solute systems; some dilute organics have water fluxes substantially lower than those described by the basic equation of these class models (Eq. (5.7)).

Diffusion-Based Models. In order to have good results for various RO cases, as it results from the description of this class of models given in the opening of this paragraph, is possible to use various model forms. Some diffusion based models are presented below.

Solution-Diffusion Model. The solution-diffusion (SD) model was proposed, in 1965, by Lonsdale et al. [46]. It is based on diffusion of the solute and solvent through the membrane. The model assumes the following [37, 38, 46]: 1) the RO membrane has a homogeneous, nonporous surface layer; 2) both the solute and solvent arrive in this layer and then each diffuses across it; 3) the solute and solvent diffusion is uncoupled and due to its own chemical potential gradient they diffuse individually across the membrane; 4) the solute and solvent (water in the case of ARW) gradients are the result of concentration and pressure differences across the membrane.

The solute and solvent fluxes through the membrane are strongly influenced by solubilities (partition coefficients) and diffusivities of the solute and solvent in the membrane phase. Afterwards, Lonsdale performed the derivation of the SD model [37, 46] starting with the solvent (water) flux which considers that the water passage through the membrane is only by

diffusion and consequently the flux is expressed, as it is shown by relation (5.13), by Fick's law [47].

$$J_w = D_{wm} \frac{dC_{wm}}{dz} \quad (5.13)$$

In relation (5.13) C_{wm} represents the water concentration in the membrane and D_{wm} is the water diffusivity in the membrane.

Assuming that the water-membrane solution fits Henry's law can be written the relation (5.14). The coupling of (5.14) with (5.13) leads to (5.15).

$$d\mu_w = -R_g T d \ln C_{wm} = -R_g T \frac{dC_{wm}}{C_{wm}} \quad (5.14)$$

$$J_w = \frac{D_{wm} C_{wm}}{R_g T} \frac{d\mu_w}{dz} \approx \frac{D_{wm} C_{wm}}{R_g T} \frac{\Delta\mu_w}{\delta} \quad (5.15)$$

In (5.15) the membrane water chemical potential change is given with relation (5.16) where

\bar{V}_w represents the partial molar volume of water.

$$\Delta\mu_w = R_g T \ln \Delta a_w + \bar{V}_w \Delta p \quad (5.16)$$

Assuming that variation of \bar{V}_w with pressure is not significant, the osmotic pressure is given after (5.17). Now the change of chemical potential of water takes the expression (5.19).

$$\pi = \frac{-R_g T}{\bar{V}_w} \ln a_w \quad (5.17)$$

$$\Delta\mu_w = -\bar{V}_w \Delta\pi + \bar{V}_w \Delta p = \bar{V}_w (\Delta p - \Delta\pi) \quad (5.18)$$

When (5.18) is introduced in Eq. (5.15) the below expression for water flux is obtained (here A represents the water permeability coefficient).

$$J_w = \frac{D_{wm} C_{wm} \bar{V}_w}{R_g T \delta} (\Delta p - \Delta\pi) \equiv A(\Delta p - \Delta\pi) \quad (5.19)$$

The solute flux is expressed, also, from Fick's law. For that it is assumed that chemical potential difference caused by pressure is negligible, therefore the driving force is almost entirely due to differences of concentration. Solute flux [47] is given by relation (5.20) where ΔC_m expresses the solute concentration difference across the membrane and D_{sm} is the solute diffusion coefficient in active membrane layer.

$$J_s = D_{sm} \frac{dC_m}{dz} \approx D_{sm} \frac{\Delta C_m}{\delta} \quad (5.20)$$

The solute membrane concentration is dependent upon the feed and permeate concentration through a partition coefficient, K_{sm} , assumed to be independent of concentration:

$$K_{sm} = \frac{C_{smf}}{C_F} = \frac{C_{smp}}{C_p} \quad (5.21)$$

If this expression is used in the solute expression then Eq. (5.20) becomes (5.22), where B represents the solute permeability coefficient.

$$J_s = \frac{D_{sm} K_{sm}}{\delta} (C_F - C_p) \equiv B(C_F - C_p) \quad (5.22)$$

The relations for solvent and solute flux are used in the expression of solute rejection, so, for the solution-diffusion model, solute rejection can be expressed as in (5.23). It is important to observe that Eq. (5.23) shows that if we have $\Delta P \rightarrow \infty$ then $R \rightarrow 1$. So the complete rejection in RO is not possible.

$$\frac{1}{R} = 1 + \frac{B}{A} \frac{1}{\Delta p - \Delta \pi} \quad (5.23)$$

Comparing SD model Eqs. (5.19) and (5.22) with Eqs. (5.7) and (5.8) of the Kedem-Katchalsky model it can be seen that they are equivalent for a membrane with perfect solute rejection ($\sigma = 1$). The fact that only two parameters are sufficient to characterize the membrane system constitutes the essential advantage of the SD model, and this model has been widely applied to treatment process of inorganic salt and organic solute systems. However in some papers [37] is indicated that the SD model is limited to membranes with low water content. Also, it was pointed out that SD model does not adequately describe water or solute flux for many RO membranes and solutes, particularly organics. These deviations may have as potential causes imperfections in the membrane barrier layer, convection effects (pore flow), and solute-solvent-membrane interactions [37, 48].

Solution-Diffusion-Imperfection Model. An early modification of the solution diffusion model was the **solution-diffusion-imperfection model**. This model tried to include, apart from diffusion of solvent and solute, the pore flow through a membrane as the mechanisms of transport [49]. This model accepts the existence of small imperfections or defects (pores) on the surface of membranes through which transport can occur, so total water flux through the membrane is written [22, 28, 33] as in (5.24) relation where K_2 represents coupling coefficient describing pore flow

$$N_w = A(\Delta p - \Delta \pi) + K_2 \Delta p = J_w + K_2 \Delta p \quad (5.24)$$

The first term in Eq. (5.24) accounts for diffusive flux while the second term is the pore flow contribution to the water flux. The total solute flux is given by

$$N_s = K_3 (C_F - C_p) + K_2 \Delta p = J_s + K_2 \Delta p \quad (5.25)$$

The parameter K_3 is a solute permeability coefficient while the second term in Eq.(5.25) accounts for solute pore flow through the membrane. Rejection for this model can be expressed as:

$$\frac{1}{R} = 1 + \frac{K_3}{A} \frac{1}{\Delta p - \Delta\pi} + \frac{K_2}{A} \frac{\Delta p}{\Delta p - \Delta\pi} \quad (5.26)$$

While some researchers have shown that excellent fits of experimental data with the solution diffusion-imperfection model are possible, the model has two major disadvantages: i) it contains three parameters that must be determined by nonlinear regression in order to characterize the membrane system, and ii) the parameters describing the system are usually functions on feed concentration and pressure [37], both central factors in RO. Also, some dilute organic systems ($\Delta\pi = 0$) have lower water fluxes than those predicted by Eq. (5.24).

Extended Solution-Diffusion Model. Burghoff et al. recognized that the SD model does not explain the negative solute rejections found for some organics and so formulated **the extended-solution-diffusion model** [50]. They pointed out that the SD model does not take into account the possible pressure dependence of the solute chemical potential which, while negligible for inorganic salt solutions, can be important for organic solutes [40, 50, 51]. Including the pressure dependent term, the chemical potential is given by equation (5.27). With this equation the solute flux becomes as in relation (5.28) where L_{sp} represents the parameter responsible for solute transport due to the pressure difference across the membrane

$$\Delta\mu_s = R_g T \ln \frac{C_F}{C_p} + \bar{V}_s \Delta p \quad (5.27)$$

$$J_s = \frac{D_{sm} K_{sm}}{\delta} (C_F - C_p) + L_{sp} \Delta p \quad (5.28)$$

In these conditions the rejection is given by (5.29).

$$\frac{1}{R} \left[1 - \frac{L}{AC_F} \left(1 - \frac{\Delta\pi}{\Delta p} \right) \right] = 1 + \frac{B}{A(\Delta p - \Delta\pi)} \quad (5.29)$$

Comparing Eqs. (5.23), (5.26), and (5.29) it can be seen that these have the same general form; however, these were derived using fundamentally different principles.

In [45] is shown that the negative rejections of phenol by a cellulose acetate membrane were adequately described by the extended-solution-diffusion model. However, this model has not been widely used for modelling RO membranes. Also, it still does not address the substantial decreases in water flux found for some dilute organic systems.

Pore Models. All pore models type consider the separation membrane as a porous structure with very fine pores where at the pore level we have hydrodynamic flow and solute diffusion. Some of these models are outlined here.

Preferential Sorption-Capillary Flow Model. An early pore model was **the preferential sorption-capillary flow (PSCF) model** proposed by Sourirajan [52]; this model assumes that the mechanism of separation is determined by both surface phenomena and fluid transport through pores in the RO membrane. In contrast to the SD model, the membrane is assumed to be microporous [52, 53]. The model states that the membrane barrier layer has chemical properties such that it has a preferential sorption for the solvent or preferential repulsion for the solutes of the feed solution. As a result, a layer of almost pure solvent is preferentially sorbed on the surface and in the pores of the membrane. Solvent transport occurs as solvent from this layer is forced through the membrane capillary pores under pressure.

The water flux according to this model is given by relation (5.30) where A is the pure water permeability constant of the membrane and $\pi(X)$ represents the osmotic pressure of the feed or permeate side with solute molar fraction X .

$$N_w = A\{\Delta p - [\pi(X_F) - \pi(X_P)]\} \quad (5.30)$$

The solute flux is expressed as (5.31) where K_D is the distribution coefficient of the solute from the feed with respect to membrane pore and D_{sp} is the solute diffusivity in the membrane pore. Solute rejection is obtained as it is shown by relation (5.32).

$$N_s = \frac{D_{sp} K_D C_T}{\delta} (X_F - X_p) \quad (5.31)$$

$$\frac{1}{R} = 1 + \frac{D_{sp} K_D C_T}{\delta} \frac{1}{A\{\Delta p - [\pi(X_F) - \pi(X_p)]\}} \quad (5.32)$$

It should be noted that although the forms of Eqs. (5.19) and (5.30) and Eqs. (5.22) and (5.31) appear virtually identical, the conceptual meaning of the parameters is greatly different. These equations were utilized to analyze transport for a large number of solutes and selected membranes [53]. However, as for the SD model, water flux drop caused by some dilute organics as well as rejection for some solutes are not described by these equations.

Finely-Porous Model. The **finely-porous model** was first proposed by Merten [54] and later in a modified form by Jonnson and Boesen [55]. This model assumes that transport of water takes place by viscous flow through uniform membrane pores and that transport of solute occurs by both diffusion and convection in these pores. The derivation is summarized here.

For finely-porous model, a balance of applied and frictional forces acting on solute in a membrane pore with length $\tau\delta$ and radius R_p results in [37, 53 – 55] relation (5.33) where F_s is the driving force for solute transport due to its chemical potential gradient, F_{sw} is the friction force between solute and water and F_{sm} is the friction force between solute and the membrane pore.

$$F_s = -(F_{sw} - F_{sm}) \quad (5.33)$$

The driving force for solute transport due to its chemical potential gradient, defined by (5.34), depends on pore concentration gradient. The specific friction forces F_{sw} and F_{sm} present pure convection expressions ((5.35) – (5.37)).

$$F_s = -\frac{d\mu_s}{dz} = -\frac{d\mu_s}{dC_{pore}} \frac{dC_{pore}}{dz} = \frac{-R_g T}{C_{pore}} \frac{dC_{pore}}{dz} \quad (5.34)$$

$$F_{sw} = -X_{sw}(u_s - u) \quad (5.35)$$

$$F_{sm} = -X_{sm}(u_s - u_m) = -X_{sm}u_s = -X_{sm} \frac{J_s^{pore}}{C_{pore}} \quad (5.36)$$

$$u_s = \frac{J_s^{pore}}{C_{pore}} \quad (5.37)$$

The Eq. (5.36) can be solved for solute flux through a single pore. The result is in (5.38).

$$J_s^{pore} = \frac{C_{pore}}{X_{sw}}(-F_{sw}) + uC_{pore} \quad (5.38)$$

In order to eliminate F_{sw} from the last expression Eqs. (5.34) and (5.36) are combined with Eq. (5.33) and the result is in (5.39).

$$-F_{sw} = \frac{-R_g T}{C_{pore}} \frac{dC_{pore}}{dz} - X_{sm} \frac{J_s^{pore}}{C_{pore}} \quad (5.39)$$

From (5.38) and (5.39) it is obtained for solute pore flux the relation (5.40) where b is expressed by relation (5.41).

$$J_s^{pore} = \frac{-R_g T}{X_{sw}b} \frac{dC_{pore}}{dz} + \frac{uC_{pore}}{b} \quad (5.40)$$

$$b = \frac{X_{sw} + X_{sm}}{X_{sw}} \quad (5.41)$$

Using the observations on pore flux and on equilibrium state of solute at the membrane sides (5.42), it can be noticed that equation (5.40) supports, if b , K_D , and X_{sw} are independent of solute concentration, an analytic integration. The result is in equation (5.43).

$$C_{pore}(\tau\delta) = \frac{J_s^{pore}}{u} \Big|_{z=\tau\delta}, C_{pore}(0) = K_D C_F, C_{pore}(\tau\delta) = K_D C_p \quad (5.42)$$

$$\frac{C_p}{C_F} = \frac{\exp(u\tau\delta \frac{X_{sw}}{R_g T})}{1 + \frac{b}{K_D} [\exp(u\tau\delta \frac{X_{sw}}{R_g T}) - 1]} \quad (5.43)$$

The friction coefficient X_{sw} can be defined as in relation (5.44) and for a similar expression for X_{sm} it produces for b coefficient the expresion (5.45).

$$X_{sw} = \frac{R_g T}{D_{sw}} \quad (5.44)$$

$$b = \frac{D_{sw}}{D_{sm}} \quad (5.45)$$

The parameter b is defined as the ratio of the frictional force acting on the solute moving in a membrane pore to the frictional force experienced by the solute in a free solution. It can be estimated using the Ferry-Faxen equation or a Ferry-Faxen-type equation [55]; these equations were developed by considering the friction experienced by a molecule moving through a narrow pore.

Eq.(5.43) can be rewritten in terms of rejection as in relation (5.46). The pore tortuosity τ appears to be an important parameter in species rejection degree expression (5.46).

$$R = 1 - \frac{\exp\left(u\tau\delta \frac{X_{sw}}{R_g T}\right)}{1 + \frac{b}{K_D} \left[\exp\left(u\tau\delta \frac{X_{sw}}{R_g T}\right) - 1 \right]} \quad (5.46)$$

The viscous flow water flux through the membrane is determined by balancing the effective pressure driving force with the frictional force between the solute and pore wall; the water flux is given [55] by the following relation where ε is the porosity of the membrane and X_{sm} represents the frictional force between the solute and the membrane.

$$J_w = \varepsilon u = \frac{\varepsilon R_p^2 \Delta p}{8\eta\tau\delta} \left[\frac{1}{1 + \frac{R_p^2 X_{sm} C_p}{8\eta}} \right] \quad (5.47)$$

In [37, 56] was pointed out that the finely-porous model can provide valuable insight into parameters such as pore size, solute-membrane interaction (friction parameter), and solute distribution coefficient that affect solute transport; in [40] is indicated that the finely-porous model or modified finely-porous models (which contain different solute distribution coefficients on the feed and permeate side of the membrane) have been successfully used to predict solute separation. However, for some solute systems such as dilute organics, Eq. (5.47) does not adequately describe the decreasing in water flux compared to the pure water flux unless a correction is made in the pore size; it is usually necessary to reduce the pore size

in order to obtain agreement between measured and predicted water flux. This disadvantage limits the finely porous models applicability for water flux prediction for these systems.

Mehdizadeh [57] pointed out an inconsistency in the original finely-porous model and developed a **modified finely-porous model**. The flux condition in Eq.(5.42) is inconsistent with the concept of the finely-porous model in the sense that it ignores the diffusive component of the flux at the pore outlet. The solute flux should be given by relation (5.48).

$$J_s^{pore} \Big|_{z=\tau\delta} = \frac{-R_g T}{X_{sw} b} \frac{dC_{pore}}{dz} \Big|_{z=\tau\delta} + \frac{u C_{pore}}{b} \Big|_{z=\tau\delta} \quad (5.48)$$

From a material balance on solute in the pore at steady state it is obtained the constant solute flux in pore (5.49). The z derivative of relation (5.40), coupled with (5.49), is established for species concentration in pore the relation (5.50)

$$\frac{dJ_s^{pore}}{dz} = 0 \quad (5.49)$$

$$\frac{d^2 C_{pore}}{dz^2} - \frac{u X_{sw}}{R_g T} \frac{dC_{pore}}{dz} = 0 \quad (5.50)$$

With boundary condition from (5.42), the integration of equation (5.50) gives the permeate concentration of solute species (5.51):

$$C_p = C_F - (C_F C_p) \left[\frac{1 - \exp\left(u \frac{X_{sw}}{R_g T} z\right)}{1 - \exp\left(u \tau\delta \frac{X_{sw}}{R_g T}\right)} \right] \quad (5.51)$$

Mehdizadeh solved Eq. (5.51) for the permeate concentration by trial and error; however, this can be avoided with reformulation of the pore boundary conditions [58]. Mehdizadeh compared his model with the original finely-porous model using the same parameters and found that the predicted permeate concentration of the modified finely-porous model was always higher than that of the original finely-porous model; this was expected since taking into account diffusive flux of the solute increases its predicted transport rate through the membrane pore.

However, since both finely-porous models rely on measured separation data in order to determine some of the transport parameters, it is not clear whether one model gives significantly better predictions than the other.

Surface Force-Pore Flow Model. The **surface force-pore flow (SFPF) model** developed by Sourirajan and Matsuura [53, 56] is a two-dimensional extension of the finely porous model. While the finely-porous model considers only axial solute concentration gradients, the SFPF

model recognizes that the solute concentration in a RO membrane pore may be a function of radial as well as axial position [40]. The SFPF model assumes [40, 43, 53]:

1) water transport through the membrane occurs in pores by viscous flow; 2) solute transport takes place by diffusion and convection in the membrane pores; 3) transport of both water and solute through the membrane pores is determined by interaction forces, friction forces, and chemical potential gradients of the water and solute; 4) the pores of the membrane are cylindrical and run the length of the membrane barrier layer; 5) a molecular layer of pure water is preferentially sorbed on the pore wall; 6) a potential field controls the solute distribution of the membrane pore.

A balance on the forces acting on the water in the membrane pore shown in fig. 5.3 (with $\tau = 1$) results in the velocity profile of the solution in the pore as [53]:

$$\frac{d^2u}{dr^2} + \frac{1}{r} \frac{du}{dr} + \frac{1}{\eta} \frac{\Delta p}{\delta} + \frac{1}{\eta} \frac{R_g T}{\delta} (C_p(r)|_{z=\delta} - C_F) [1 - \exp(-\phi(r))] - \frac{1}{\eta} [b(r) - 1] X_{sw} C_p(r)|_{z=\delta} u = 0 \quad (5.52)$$

The boundary conditions of this flow equation are classical (maximum velocity in the pore center $\frac{du}{dr}|_{r=0} = 0$ and zero velocity at the pore wall $u(R) = 0$)

Assuming that the pure water flow rate through the membrane is described by the Poiseuille equation, the ratio of the water flux to the pure water flux is given by relation (5.53).

$$\frac{J_w}{J_{w0}} = \frac{2 \int_0^{R_p} u r dr}{R_p^4 \Delta p} \quad (5.53)$$

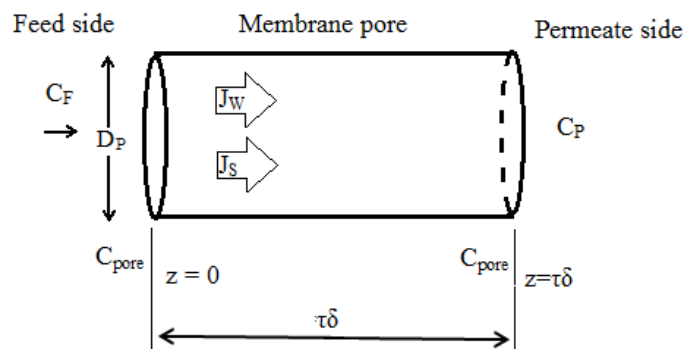


Figure 5.3. Schematic of a Membrane Pore

Similarly, a force balance on the solute in the pore results [53] in expression (5.54), which is similar in form to Eq.(5.43) of the finely-porous model.

$$\frac{C_p(r)|_{z=\delta}}{C_F} = \frac{\exp(u(r)\delta) \frac{X_{sw}}{R_g T}}{1 + \frac{b(r)}{\exp(-\phi(r))} [\exp(u(r)\delta) \frac{X_{sw}}{R_g T} - 1]} \quad (5.54)$$

In this model (SFPF model) it is assumed a Maxwell-Boltzmann distribution of solute on the membrane sides ((5.55) and (5.46))

$$C_{pore}(r,0) = C_F \exp\left(\frac{-\phi(r)}{R_g T}\right) = K_D(r)C_F \quad (5.55)$$

$$C_{pore}(r,\delta) = C_p(r)|_{z=\delta} \exp\left(\frac{-\phi(r)}{R_g T}\right) = K_D(r)C_p(r)|_{z=\delta} \quad (5.56)$$

It is observed that the distribution of solute in the membrane is represented in terms of a radially-dependent partition coefficient. The water velocity is also radially dependent for the SFPF model. The total permeate concentration is determined by averaging Eq. (5.54) over the pore outlet [52]:

$$C_p = \frac{\int_0^{R_p} C_p(r)|_{z=\delta} u(r) r dr}{\int_0^{R_p} u(r) r dr} \quad (5.57)$$

For species rejection degree is obtained the relation (5.58), where the quantity $\phi(r)$ in the water and solute transport equations is given by a coulombic potential function (5.59).

$$R = 1 - \int_0^{R_p} \left(\frac{\exp(u(r)\delta) \frac{X_{sw}}{R_g T} u(r) r}{1 + \frac{b(r)}{\exp(-\phi(r))} [\exp(u(r)\delta) \frac{X_{sw}}{R_g T} - 1]} \right) dr + \int_0^{R_p} u(r) r dr \quad (5.58)$$

$$\phi(r) = \frac{\tilde{A}}{R_p - r} \quad (5.59)$$

For ionized solutes, where \tilde{A} is a measure of the electrostatic repulsion force between the ionic solute and the membrane, a Lennard-Jones potential function is used (5.60)

$$\phi(r) = -\frac{\tilde{B}}{(R_p - r)^3} \quad (5.60)$$

In the case of nonionized organic solutes \tilde{B} is a measure of short range van der Waals forces characterizing the solute interaction with membrane material. The parameters X_{sw} and $b(r)$ are the same as in the finely-porous model; in applications of the SFPF model, b is usually not considered a function of radial pore position.

The transport equations for the SFPF model, expressed in dimensionless form, have been solved using a variety of numerical techniques. Sourirajan and Matsuura [53] used liquid chromatography techniques in order to determine \tilde{A} or \tilde{B} for a solute and then used trial and error to find the membrane pore radius: R_p was varied until the predicted and measured permeate concentrations were in agreement. Alternatively, if R_p was specified, then \tilde{A} or \tilde{B} was varied to produce agreement in the predicted and measured permeate concentrations. Mehdizadeh and Dickson [59, 60] used a similar solution technique. The need for trial and error solution of the transport equations, using measured pore radius values and one experimental data point for permeate concentration, was eliminated by imposing Eq. (5.58) (in differential form) as a condition in the solution of Eq.(5.52) and solving the resulting system of equations by a collocation method [61, 62]; the values of \tilde{A} or \tilde{B} were calculated by this method.

Both solution techniques indicated that the SFPF model gave excellent predictions of solute separation for a wide range of inorganics and organics under varying operating conditions. However, for some dilute organics that cause substantial decrease in water flux, Eq.(5.53) does not adequately predict the water flux ratio. The pore radius must be reduced in order to force the predicted and measured water flux ratios into agreement for these systems.

An important modification of the SFPF model has been formulated to recognize that it is more realistic to assume a distribution of membrane pore sizes [53]. Also, some inconsistencies in the SFPF model similar to those pointed out for the original finely-porous model were evidenced; a modified SFPF correcting these conceptual errors was formulated by Mehdizadeh and Dickson [59, 63]. However, although the inclusion of a pore distribution in the SFPF model or the use of Dickson and Mehdizadeh's modified SFPF model is conceptually more correct, it is not immediately obvious that these provide better solute separation predictions.

Charged Membrane Models. Although water transport for charged RO (i.e., nanofiltration) membranes is usually adequately described by the above models. The charged RO membrane theories must be used to predict ionic solute separations. These models account for electrostatic effects as well as for diffusive and/or convective flow in order to describe the solute separation. Many charged membrane transport theories have been proposed; two conceptually-important models for solute transport are discussed below.

Donnan Equilibrium Models. **Donnan equilibrium models** assume that a dynamic equilibrium is established when a charged membrane is placed in a salt solution [43, 64]. The counter-ion of the solution, opposite in charge to the fixed membrane charge (typically carboxylic or sulfonic groups), is present in the membrane at a higher concentration than that

of the co-ion (same charge as the fixed membrane charge) because of electrostatic attraction and repulsion effects. This creates a Donnan potential which prevents the diffusive exchange of the counter-ion and co-ion between the solution and membrane phase. When a pressure driving force is applied to force water through the charged membrane, the effect of the Donnan potential is to repel the co-ion from the membrane; since electroneutrality must be maintained in the solution phase, the counter-ion is also rejected, resulting in ionic solute separation. A Donnan equilibrium model [64], is used in describing of distribution coefficient between a negatively-charged membrane and the solution phase of a salt M_nN_m which ionizes to M^{m+} and N^{n-} , as in relation (5.61).

$$K = \frac{C_m}{C_{Fi}} = \left[\left(\frac{nC_{Fi}}{C_m^*} \right)^n \left(\frac{\gamma}{\gamma_m} \right)^{m-n} \right]^{\frac{1}{m}} \quad (5.61)$$

It can be approximated the solute rejection with relation (5.62).

$$R = 1 - K \quad (5.62)$$

The model correctly predicted that the solute rejection was a function of membrane charge capacity (C_m^*), ion feed concentration (C_{Fi}), and ion charge (m, n). However, this model does not take into account solute diffusive and convective fluxes which may also be important in charged membrane separations.

Extended Nernst-Planck Model. Extended Nernst-Planck equations was used for the prediction of solute ion fluxes [65 - 68]. The general form of solute flux equation is given by convective, electrostatic (Donan) and diffusive participation (5.63)

$$J_{is} = J_w C_{im} + z_i C_{im} \frac{F \tilde{E}}{R_g T} - D_m \frac{dC_m}{dz} - C_m D_m \frac{d(\ln \gamma_m)}{dz} \quad (5.63)$$

The first term in Eq. (5.63) represents the solute flux contribution due to convection, the second term accounts for solute flux due to the Donnan potential, and the last two terms describe solute transport due to diffusion. In [67] was shown that the **extended Nernst-Planck model** correctly predicts the trends expected for ionic solute rejection, including conditions under which a negative rejection is obtained.

Other RO Membrane Transport Models. Several other transport models for RO membranes have also been proposed in literature. Soltanieh and Gill [37] and Sourirajan and Matsuura [53] discussed the relative free energies of membrane-ion interactions and the relation of these to membrane selectivity. Some success in the use of dimensional analysis to correlate experimental RO membrane data was reported by Garcia and Medina [69]. Mason and Lonsdale [70] presented the general statistical-mechanical theory of membrane transport; they pointed out that most RO membrane transport models (solution-diffusion, diffusion-

convection, etc.) could be derived from statistical-mechanical theory. Bitter [71] also developed a general model based on the solution-diffusion mechanism using Maxwell-Stefan equations to calculate diffusive transport and Flory-Huggins equations to calculate solubility of species in the membrane. Bitter indicated that the procedure he used should be applicable to almost all membrane systems; however, some of the solute, solvent, and membrane properties needed in the model are difficult to obtain.

The extended Stefan-Maxwell equations were used to describe total flux (solute plus solvent) of aqueous-organic solutions through membranes; their model indicated that water flux reduction was in part due to frictional effects caused by the organic. The model use the total flux [71] in the form of relation (5.64), where the term $W_s X_P$ was described as a solute-membrane friction term.

$$N_T = \frac{A\{\Delta p - [\pi(X_F) - \pi(X_p)]\}}{1 + W_s X_P} \quad (5.64)$$

Previously, a similar empirically-derived relationship was used to successfully describe reduction in water flux for aqueous-organic systems [73]. Other investigators were also able to adequately describe fluxes for both water and organic solute by modifying the solution diffusion model; they assumed the water and organic content of the membrane was constant [74, 75]. Williams used an adsorption resistance term to describe flux drop caused by dilute organic solutes with a RO membrane; he assumed the organics adsorbed on the membrane caused more resistance to water flow through it. The water flux in this model [76] was given as in (5.65), where R_m is the membrane resistance and R_{Ads} is the resistance due to solute adsorption.

$$J_w = \frac{\Delta p - \Delta \pi}{R_m + R_{Ads}} \quad (5.65)$$

Similar expressions were also used to describe water fluxes for organic solutes that were adsorbed on the RO membranes [77 – 79]. Forms of Eq.(5.65) have also been applied extensively to describe ultrafiltration membranes [80 – 84].

5.3. Experimental investigation of Reverse Osmosis process in ARW treatment

The experimental studies were conducted at IFIN-HH, DMDR, in AQUA-EXPRESS installation (shown in fig. 2.1). ARW was treated in order to determine the influence of different RO factors, *i.e.*, feed pressure, pH and temperature, on membrane productivity and separation efficiency. Membrane productivity was evaluated by permeate volumetric flux and its efficiency was assessed by measuring permeate conductivity and Co (radioactive species)

concentration in permeate (representing a measure of rejection of all salts and Co, respectively).

5.3.1. Materials and method

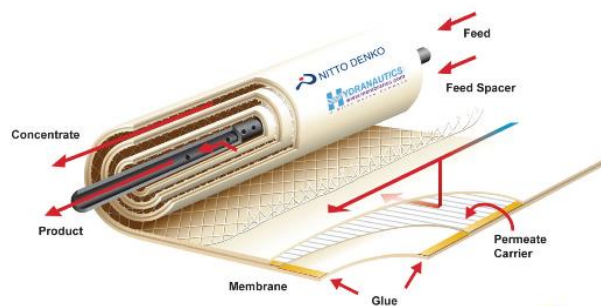
RO membrane element Hydranautics SWC1-4040 – Italy, used in this experiment is presented in fig. 5.4 and its main characteristics are summarized in Table 5.1. Can be observed fixed characteristics (membrane type, membrane material, membrane surface maximum working pressure, etc.), indicative characteristics (salt rejection capacity, feed water turbidity, etc.) and manipulable characteristics (operating temperature, pH, feed flow rate). The membrane consists of a compact base of 30 – 60 nm polyamide (PA), whose microstructure is shown in fig. 5.5. Initial pH of ARW was adjusted using concentrated nitric acid and 30% sodium hydroxide solution.

Table 5.1. SWC1-4040 membrane characteristics

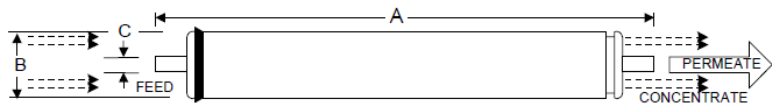
1	Membrane type	Spiral wound
2	Membrane material	Composite polyamide
3	Membrane surface area	6.5 m ²
4	Permeate flowrate	4.5 m ³ /day
5	Salt rejection capacity	Min. 99.5%
6	Working pressure	Max. 6.9 MPa
7	Permeate chlorine concentration	Max. 0.1 ppm
8	Operating temperature	Max. 45 °C
9	pH range	3-10
10	Feed water turbidity	1.0 NTU
11	Concentrate/permeate flow rate ratio	Min. 5/1



(a)



(b)



A, inches (mm) B, inches (mm) C, inches (mm) Weight, lbs. (kg)
40.00 (1016) 3.95 (100.3) 0.75 (19.1) 8 (3.6)

Core tube extension = 1.05" (26.7 mm)

(c)

Figure 5.4. Hydranautics SWC1-4040 RO membrane element (a), system elements and membrane warping (b) and geometric dimensions (c) [85].

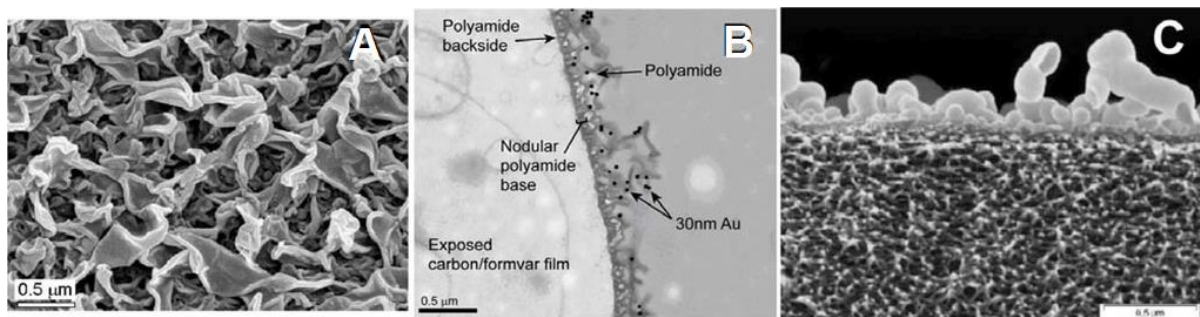


Figure 5.5. Electron micrographs of the polyamide (PA) layer:
(A) structure of the PA surface [86]; (B) TEM cross section of an isolated PA layer [87]; (C) SEM cross section of a PA layer [88].

Feed, permeate and concentrate flow rates were measured with flowmeters. Conductivity was measured with Schott Lab 960 conductivity meter equipped with two conductivity cells, LF413T and LF313T, for high and low values, respectively. Co concentration was measured using ^{60}Co as tracer. The ^{60}Co activity was determined by gamma spectrometry using a high resolution gamma-ray spectrometer, Canberra type, GENIE 2000 version 3.2 software and Laboratory Sourceless Calibration Software (LabSOCS). The RO process studied in this paper is included in the technological scheme shown in fig. 5.6.

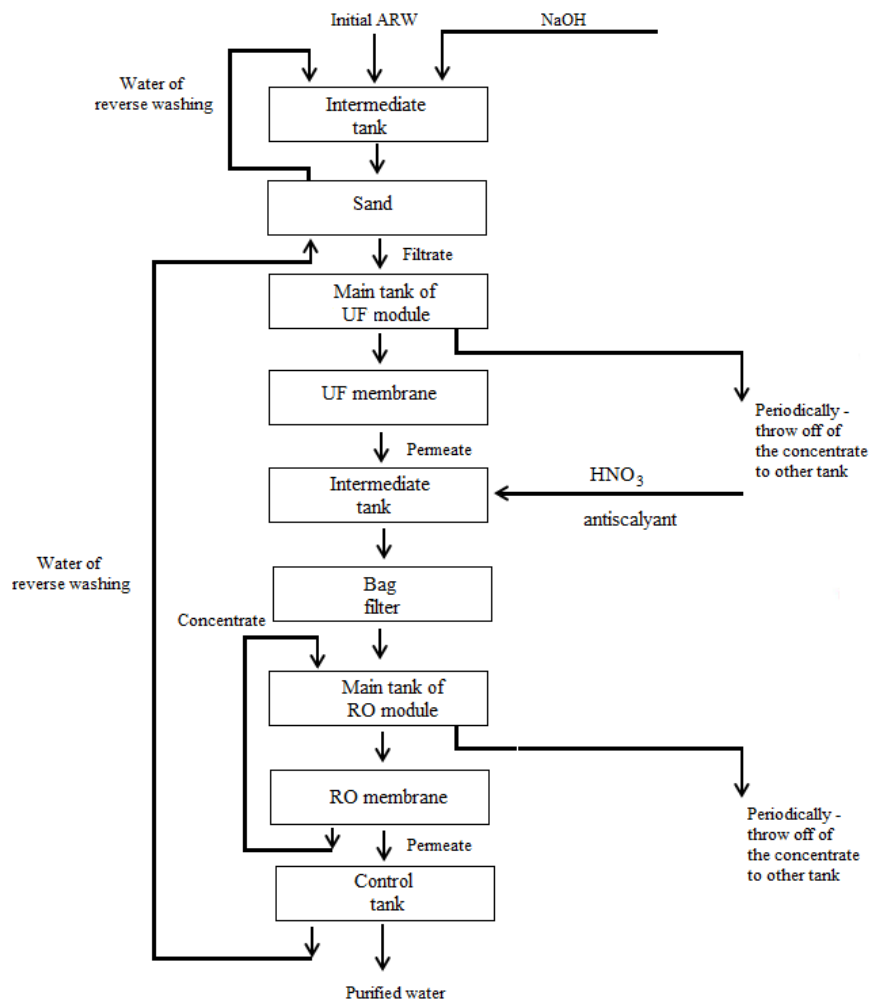


Figure 5.6. Technological scheme for treating the ARW

The permeate obtained after ultrafiltration module represented the RO module feed. As it is shown in Tables 5.2 and 5.3 the RO feed was completely characterized from the point of view of composition and radioactivity.

Table 5.2. Radioactivity concentration of RO module feed

Radionuclide	Activity, Bq/L
^{60}Co	10.68
^{137}Cs	1.62
^{241}Am	1.90

Table 5.3. Physico-chemical parameters of ARW feed in RO module

No.	Parameter	Value	No.	Parameter	Value
1	pH	7.1	17	Al^{3+}	< 0.01 mg/L
2	Conductivity	1240 $\mu\text{S}/\text{cm}$	18	S^{2-}	< 0.1 mg/L
3	TDS	720 mg/L	19	SO_3^{2-}	< 1 mg/L
4	NH_4^+	< 0.01 mg/L	20	As^+	< 0.01 mg/L
5	NO_3^-	3.56 mg/L	21	Pb^{2+}	< 0.01 mg/L
6	NO_2^-	< 0.01 mg/L	22	Cd^{2+}	0.09 mg/L

7	SO_4^{2-}	137.1 mg/L	23	$\text{Cr}^{3+} + \text{Cr}^{6+}$	0.02 mg/L
8	Cl^-	100 mg/L	24	$\text{Fe}^{2+} + \text{Fe}^{3+}$	0.48 mg/L
9	Br^-	< 0.01 mg/L	25	Cu^{2+}	0.46 mg/L
10	F^-	0.39 mg/L	26	Ni^{2+}	0.34 mg/L
11	PO_4^{3-}	3.43 mg/L	27	Zn^{2+}	0.16 mg/L
12	Ca^{2+}	76.13 mg/L	28	Hg^{2+}	< 0.01 mg/L
13	Mg^{2+}	35.61 mg/L	29	Ag^+	< 0.01 mg/L
14	Na^+	238.86 mg/L	30	Mo^{2+}	< 0.01 mg/L
15	K^+	14.64 mg/L	31	Mn	0.21 mg/L
16	Li^+	0.03 mg/L	32	Co^{2+}	1.59 mg/L

The working pressure in the RO module ranged from 2 to 4 MPa, the temperature from 25 to 45°C and the pH values from 4 to 9. The permeate was collected in a tank and its flux was continuously monitored.

After each purification experiment, permeate samples have been taken and the conductivity and radioactivity of ^{60}Co were measured.

5.3.2. Results and discussion

The experiment was organized in order to highlight the effect of different factors (feed ARW pressure, feed ARW pH and feed ARW temperature) on permeate flux and permeate quality. Rejection efficiency was assessed by measuring conductivity and Co (radioactive species) concentration in permeate (representing a measure of rejection of all salts and Co, respectively).

Effect of feed waste pressure. The most important operational parameter in a RO system is the feed pressure. The effect of pressure on the membrane performance was studied keeping all other parameters constant ($\text{pH} = 6.2$, $t = 25^\circ\text{C}$). Plots of permeate flux depending on operating time and pressure are illustrated in fig. 5.7. The influence of feed pressure on conductivity and Co concentration of permeate, as well as on salt and Co rejection is shown in figs. 5.8 and 5.9, respectively.

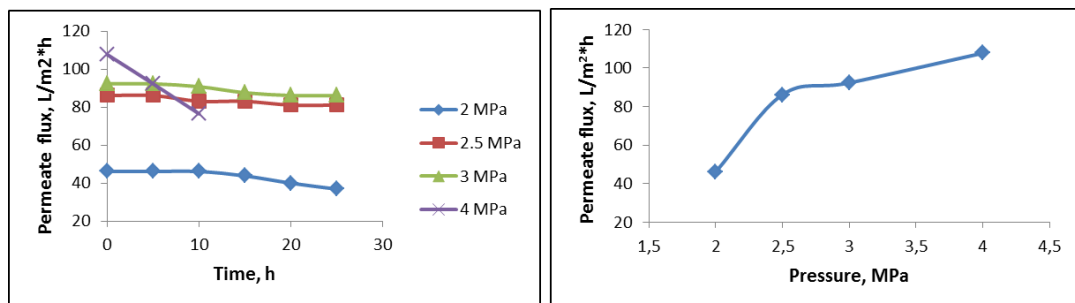


Figure 5.7. Permeate flux versus time and feed pressure at the begining of RO process ($\text{pH}=6.2$, $t=25^\circ\text{C}$)

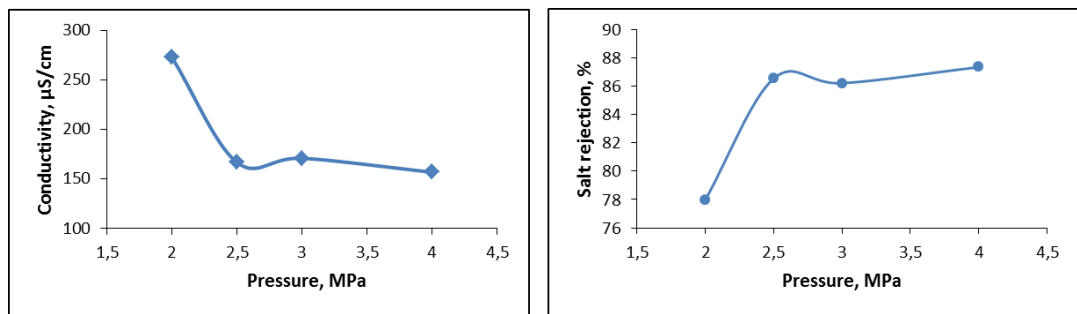


Figure 5.8. Effect of feed waste pressure on permeate conductivity/salt rejection
($pH = 6.2$, $t = 25^{\circ}C$, $\tau = 20\text{ h}$)

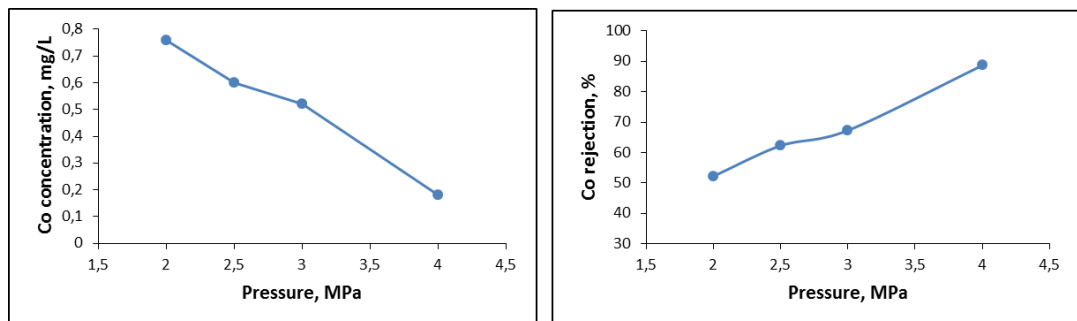


Figure 5.9. Effect of feed waste pressure on Co concentration in permeate/Co rejection
($pH = 6.2$, $t = 25^{\circ}C$, $\tau = 20\text{ h}$)

As depicted in these figures, the permeate flux increases as the work pressure increases, but at higher pressure a more rapid decline in the flux occurs because the higher permeate rates at higher pressures led to enhanced transport of foulants to the membrane, greater compaction of the fouling layer and increased hydrodynamic resistance. Regarding the conductivity and Co concentration of permeate as a measure of salt rejection, their values decreased with an increase in the pressure. Pressure increases the driving force for the solvent and decreases osmotic pressure hence more amount of water can pass through the membrane resulting in an increase in salt rejection [89]. From these graphs it can be seen that maximum flux and salt rejection were obtained at 4 MPa, but the permeate flux decreases rapidly at this pressure value. No considerable effect can be observed if pressure varied in 2.5 - 3 MPa range. RO is a pressure-driven process and the main energy consumers in any membrane desalination plant are the high pressure pumps. An operating pressure of 2.5 MPa was selected in order to reduce the energy required for processing the feed waste.

Effect of feed waste pH. Experiments were conducted at $p = 2.5\text{ MPa}$ and $t = 25^{\circ}\text{C}$ under different pH levels of feed waste. The pH was adjusted with concentrated nitric acid and 30 % sodium hydroxide solution and the feed waste was recirculated 2 h for homogenization. The variations of permeate flux depending on time and initial pH are shown in fig. 5.10. The

effect of pH on conductivity and Co concentration of permeate, as well as on salt and Co rejection is shown in figs. 5.11 and 5.12, respectively.

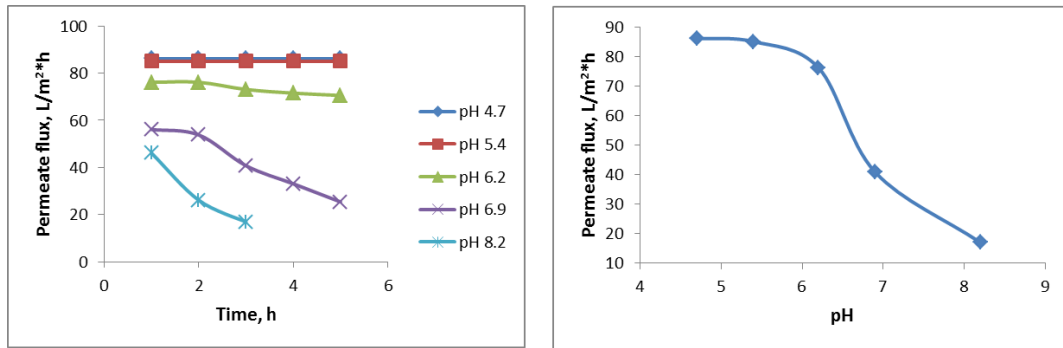


Figure 5.10. Permeate flux versus time and pH of feed ARW ($p = 2.5 \text{ MPa}$, $t = 25^\circ\text{C}$)

The results obtained have shown a decrease in time of the RO module treatment capacity in the case of feed waste with neutral or high pH. For a low pH (acidic conditions), the permeate flux remained almost constant. This finding could be explained by the fact that the low pH conditions prevent the precipitation of Ca^{2+} , SO_4^{2-} and CO_3^{2-} ions.

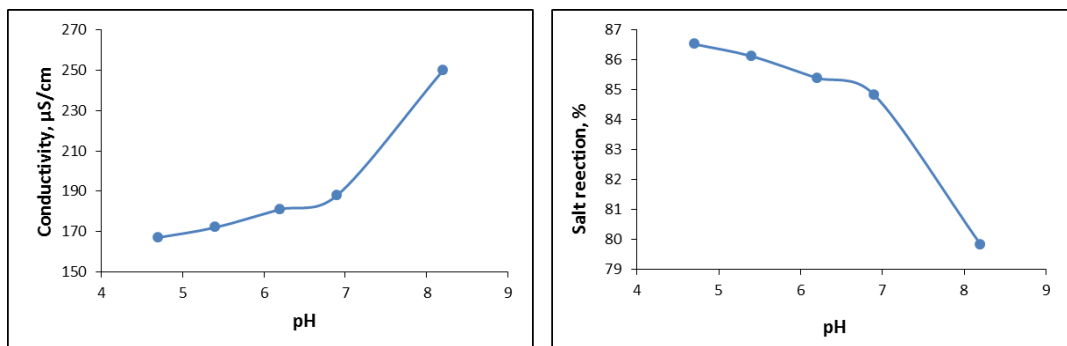


Figure 5.11. Effect of feed waste pH on permeate conductivity/salt rejection

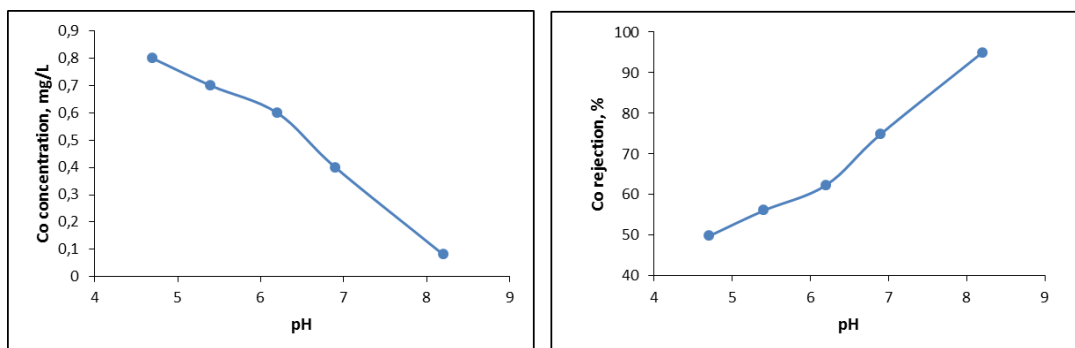


Figure 5.12. Effect of feed waste pH on Co concentration in permeate/Co rejection

It was observed that as feed pH increased, permeate conductivity and Co rejection also increased, while permeate Co concentration decreased.

The pH affects the separation performance by influencing the hydration and absorption capacity of solution on membrane. When a charged membrane is placed in a salt solution, a dynamic equilibrium is established [90 – 92]. The counter-ion of the solution,

opposite in charge to the fixed membrane charge, is present in the membrane at a higher concentration than that of the co-ion (same charge as the fixed membrane charge) because of electrostatic attraction and repulsion effects. This creates a Donnan potential which prevents the diffusive exchange of the counter-ion and co-ion between the solution and membrane phase. When a pressure driving force is applied to force water through the charged membrane, the effect of the Donnan potential is to repel the co-ion from the membrane; since electroneutrality must be maintained in the solution phase, the counter-ion is also rejected and salt rejection occurs. As the fixed charge in polyamide membranes has the isoelectric point of the charged groups at a range of pH 3-4 [93], the membranes are negatively charged at pH>4 and the rejections of positive charged ions (see Table 2) decrease.

The rejection of Co ions at pH = 4 significantly falls compared with pH > 8. Co is present in feed waste as dissolved cobalt (Co^{2+}) and gives Co(OH)_2 at pH > 8. Co(OH)_2 stays in colloidal phase and is easily rejected by membrane. Therefore Co rejection increases at higher pH.

Effect of feed waste temperature. The effect of varying temperature on performance of RO membrane while keeping other parameters constant ($p = 2.5 \text{ MPa}$, pH = 6.2) is shown in graphs from figs. 5.13 – 5.15.

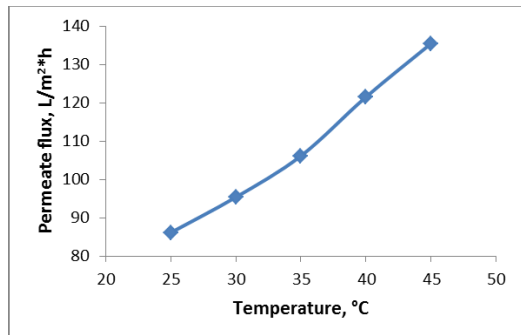


Figure 5.13. Effect of feed waste temperature on permeate flux

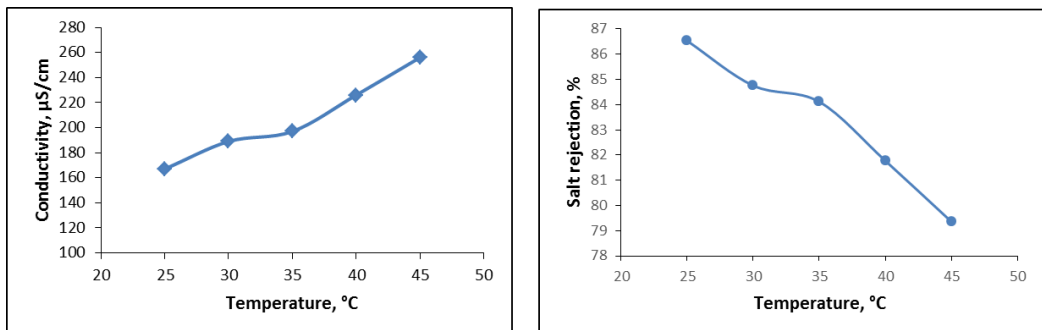


Figure 5.14. Effect of feed waste temperature on permeate conductivity/salt rejection

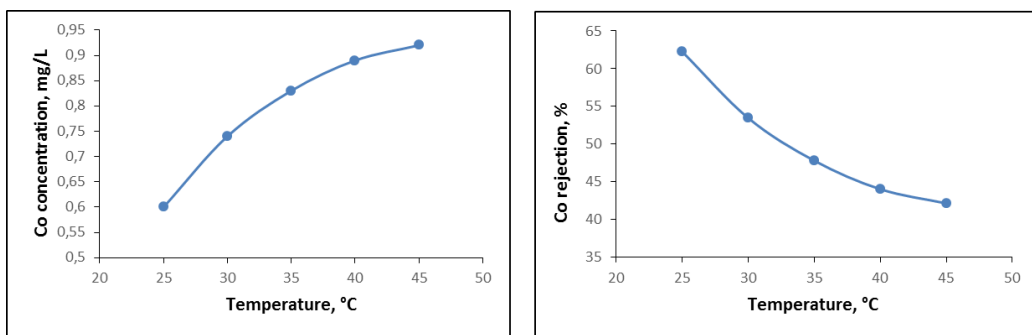


Figure 5.15. Effect of feed waste temperature on Co concentration in permeate/Co rejection

It can be observed from figs. 5.13 – 5.15 that as feed waste temperature increased, the flux, conductivity and Co concentration in permeate increased (salt rejection decreased). As temperature increases, viscosity decreases and water permeation rate through the membrane increases, but, also, the solubility of solute increases and higher diffusion rate of solute through the membrane is possible.

5.4. Conclusions

A widely used method in desalination plants is reverse osmosis. The most important variable of this process is the clean water flux. The clean water or permeate passes through the membranes but trap larger particles and compounds are removed and released as a concentrate.

Membrane permeability, salt concentration on the membrane surface, feed pH, temperature and pressure are parameters that influence the permeate flux. Because is difficult to measure the salt concentration on the membrane surface it should be estimated. During the purification process appears a concentration polarization that leads to an unwanted increase of the salt concentration on the membrane surface. Also, the convective transport of salt molecules to the boundary layer of the membrane creates a polarization effect and leads to membrane blockage. To predict the permeate flux is required a correct estimation of the concentration polarization that allows carrying out a good design and control of the desalination plant. Several models have been proposed in literature to estimate the concentration polarization (or the salt concentration on the membrane surface).

Practical experience in the development and operation of pilot and full-scale facilities utilizing RO process for treatment of liquid radioactive waste is considered to be of particular importance and interest. This research, but also the development and application of different new materials for treatment of liquid radioactive waste, aimed at improving the treatment efficiency.

Hydranautics SWC1-4040 RO membrane was tested for ARW treatment. The membrane was found to be sensitive to various operating parameters such as feed ARW pressure, pH and temperature. RO membranes have shown to be effective in rejecting dissolved species while maintaining higher flux, but the feed ARW requires pretreatment like ultrafiltration and pH adjustment.

Based on membrane performance, during these experiments has been gathered the key technical information and have been determined the acceptable limits for parameters variability for which treatment process meets a good performance. Long-term experiments should be conducted to study the fouling effects on the performance and economy of the process.

REFERENCES

- [1] A.A.A. Al Janabi, O.C. Pârvulescu, T. Dobre, V.A. Ion, *Pervaporation of aqueous ethanol solutions through pure and composite cellulose membranes*, Rev. Chim., **67(1)**, 150-156, 2016
- [2] A.A.A. Al Janabi, O.C. Pârvulescu, B. Trică, T. Dobre, *Effect of process factors on pervaporation dehydration of isopropanol*, Rev. Chim., **68(6)**, 1302-1305, 2017
- [3] R.D. Ambashta, M.E.T. Sillanpää, *Membrane purification in radioactive waste management: a short review*, J. Environ. Radioact., **105**, 76-84, 2012
- [4] T. Dobre, O.C. Pârvulescu, J. Sanchez-Marcano, A. Stoica, M. Stroescu, G. Iavorschi, *Characterization of gas permeation through stretched polyisoprene membranes*, Sep. Purif. Technol., **82**, 202-209, 2011
- [5] Z. Dong, G. Liu, S. Liu, Z. Liu, W. Jin, *High performance ceramic hollow fiber supported PDMS composite pervaporation membrane for bio-butanol recovery*, J. Membr. Sci., **450**, 38-47, 2014
- [6] R.O.A. Rahman, H.A. Ibrahium, Y.-T. Hung, *Liquid radioactive wastes treatment: A review*, Water, **3(2)**, 551-565, 2011
- [7] P. Salehian, W.F. Yong, T.-S. Chung, *Development of high performance carboxylated PIM-1/P84 blend membranes for pervaporation dehydration of isopropanol and CO₂/CH₄ separation*, J. Membr. Sci., **518**, 110-119, 2016
- [8] N. Uzal, A. Jaworska, A. Miśkiewicz, G. Zakrzewska-Trznadel, C. Cojocaru, *Optimization of Co²⁺ ions removal from water solutions via polymer enhanced ultrafiltration with application of PVA and sulfonated PVA as complexing agents*, J. Colloid. Interface Sci., **362**, 615-624, 2011
- [9] Y.M. Xu, N.L. Le, J. Zuo, T.-S. Chung, *Aromatic polyimide and crosslinked thermally rearranged poly (benzoxazole-co-imide) membranes for isopropanol dehydration via pervaporation*, J. Membr. Sci., **499**, 317-325, 2016
- [10] G. Zakrzewska-Trznadel, *Advances in membrane technologies for the treatment of liquid radioactive waste*, Desalination, **321**, 119-130, 2013
- [11] D. Bhattacharyya, M. Williams, *Introduction and Definitions - Reverse Osmosis*, Membrane Handbook, W. Ho and K. Sirkar (Eds.), Van Nostrand Reinhold, New York, 265-268, 1992
- [12] J. Torbitt, *Nine mile point - unit 1 experience with membrane processing of radwaste, 1997 EPRI International LLRW Conference*, July 21–23, 1997, Providence, USA
- [13] J. Freeman, *Wolf Creek's liquid waste processing success where we were and where we are*, 1999 EPRI International LLRW Conference, July 12-14, 1999, East Brunswick, USA
- [14] S.K. Sen Gupta, J.A. Slue, W.S. Tulk, *Liquid Radwaste Processing with Cross-flow Microfiltration and Spiral Wound Reverse Osmosis*, 1995 International Waste Management Conference (WM'95 Conference), February 26 - March 2, 1995, Tucson, USA
- [15] V. Geraldes, V. Semião, M.N. de Pinho, *Flow and mass transfer modelling of nanofiltration*, J. Membr. Sci., **191(1-2)**, 109–128, 2001

- [16] W.A. Lovins, *Correlation and Modelling of Laboratory and Field Scale Integrated Membrane System Productivity and Water Quality*, Ph.D. Thesis, University of Central Florida, USA, 2000
- [17] J.S. Taylor, X.S. Chen, L.A. Mulford, C.N. Norris, *Flat Sheet, Bench, and Plot Testing for Pesticide Removal Using Reverse Osmosis*, Report No. 90808 of AWWA Research Foundation and American Water Works Association, Denver, USA, 2000
- [18] L. A Mulford, *Verification and Modelling of Mass Transfer in Single and Multi-Element Nanofiltration Arrays for Pilot and Full-scale Operation*, Ph.D. Thesis, University of Central Florida, USA, 1999
- [19] S. Chellam, J.S. Taylor *Simplified Analysis of Contaminant Rejection During Groundand Surface Water Nanofiltration Under the Information Collection Rule*, Wat. Res. **35(10)**, 2460-2474, 2001
- [20] S. Chellam, J.G. Jacangelo, T.P. Bonaquisti, *Modelling and experimental verification of pilot-scale hollow fiber direct flow microfiltration with periodic backwash*, Environ. Sci. Technol., **32(1)**, 75–81, 1998
- [21] P. Aimar, V. Sanchez, *A novel approach to transfer limiting phenomena during ultrafiltration of macromolecules*, Ind. Eng. Chem. Fundam., **25**, 789-798, 1986
- [22] C.E. Goodyer, A.L. Bunge, *Mass transfer through membranes with surface roughness*, J. Membr. Sci., **409–410**, 127-136, 2012
- [23] A. Childress, M. Elimelech, *Effect of solution chemistry on the surface charge of polymeric reverse osmosis and nanofiltration membranes*, J. Membr. Sci., **119**, 253-268, 1996
- [24] S. Bhattacharya, S.T. Hwang, *Concentration polarization, separation factor, and Peclet number in membrane processes*, J. Membr. Sci., **132**, 73-90, 1997
- [25] G. Amy, J. Cho, *Interactions Between Natural Organic Matter (NOM) and Membranes: Rejection and Fouling*, Water Sci. Technol., **40(9)**, 131-139, 1999
- [26] E.M. Vrijenhoek, S. Hong, M. Elimelech, *Influence of membrane surface properties on initial rate of colloidal fouling of reverse osmosis and nanofiltration membranes*, J. Membr. Sci., **188(1)**, 115–128, 2001
- [27] N. Her, G. Amy, C. Jarusutthirak, *Seasonal variations of nanofiltration (NF) foulants: identification and control*, Desalination, **132**, 143-160, 2000
- [28] H. Niemi, S. Palosaari, *Calculation of Permeate Flux and Rejection in Simulation of Ultrafiltration and Reverse Osmosis Processes*, J. Membr. Sci., **84**, 123-130, 1993
- [29] M. Khayet, C. Cojocaru, M. Essalhi, *Artificial neural network modelling and response surface methodology of desalination by reverse osmosis*, J. Membr. Sci., **368(1–2)**, 202–214, 2011
- [30] D. Liboteana, J. Giralta, F. Giralta, R. Rallob, T. Wolfec, Y. Cohend, *Neural network approach for modelling the performance of reverse osmosis membrane desalting*, J. Membr. Sci., **326(2)**, 408-419, 2009
- [31] Z.V.P. Murthy, S. K. Gupta, *Estimation of mass transfer coefficient using a combined nonlinear membrane transport and film theory model*, Desalination, **109**, 39-49, 1997

- [32] D. Van Gauwbergen, J. Baeyens, *Modelling reverse osmosis by irreversible thermodynamics*, Sep. Purif. Technol., **13**, 117-128, 1998
- [33] J. Straatsma, G. Bargeman, H.C. van der Horst, J.A. Wesslingh, *Can nanofiltration be fully predicted by a model?*, J. Membr. Sci., **198**, 273-284, 2002
- [34] S.J. Duranceau, *Modelling of Mass Transfer and Synthetic Organic Compound Removal in a Membrane Softening Process*. Ph.D. Thesis, University of Central Florida, USA, 1990
- [35] L. K. Sung, *Film Theory and Ion Coupling Models for a Diffusion Controlled Membrane Process*, PH.D. Thesis, University of Central Florida, USA, 1993
- [36] A. Jiang, Q. Ding, J. Wang, S. Jiangzhou, W. Cheng, C. Xing *Mathematical Modelling and Simulation of SWRO Process Based on Simultaneous Method*, J. Appl. Math., **2014**, 1-11, 2014
- [37] M. Soltanieh, W. Gill, *Review of Reverse Osmosis Membranes and Transport Models*, Chem. Eng. Commun., **12(4-6)**, 279-363, 1981
- [38] B. Baranowski, *Non-equilibrium Thermodynamics as Applied to Membrane Transport*, J. Membr. Sci., **57(2-3)**, 119-159, 1991
- [39] G. Jonsson, *Overview of Theories for Water and Solute Transport in UF/RO Membranes*, Desalination, **35**, 21-38, 1980
- [40] J. Dickson, *Fundamental Aspects of Reverse Osmosis*, in *Reverse Osmosis Technology*, B. Parekh, (Ed.), Marcel Dekker, Inc., New York 1-51, 1988
- [41] G., Van Den Berg, C. Smolders, *Diffusional Phenomena in Membrane Separation Processes*, J. Membr. Sci., **73(-3)**, 103-118, 1992
- [42] O. Kedem, A. Katchalsky, *A physical interpretation of the phenomenological coefficients of membrane permeability*, J. Gen. Physiol., **43**, 143-179, 1961
- [43] D. Bhattacharyya, M. Williams, *Theory - Reverse Osmosis, Membrane Handbook*, W. Ho and K. Sirkar, (Eds.), Van Nostrand Reinhold, New York 269-280, 1992
- [44] W. Pusch, *Determination of Transport Parameters of Synthetic Membranes by Hyperfiltration Experiments*, Ber Bunsenges Phys. Chem., **81(3)**, 269-276, 1977
- [45] K. Spiegler, O. Kedem, *Thermodynamics of Hyperfiltration (Reverse Osmosis): Criteria for Efficient Membranes*, Desalination, **1(4)**, 311-326, 1966
- [46] H. Lonsdale, U. Merten, R. Riley, *Transport Properties of Cellulose Acetate Osmotic Membranes*, J. Appl. Polym. Sci., **9**, 1341-1362, 1965
- [47] Fick, A. (1855). "On liquid diffusion". Poggendorffs Annalen. 94: 59. – reprinted in "On liquid diffusion". J. Membr. Sci., **100**, 33–38, 1995
- [48] M. Mazid, *Mechanisms of Transport Through Reverse Osmosis Membranes*, Separ. Sci. Technol., **19(6-7)**, 357-373, 1984
- [49] T. Sherwood, P. Brian, R. Fisher, *Desalination by Reverse Osmosis*, Ind. Eng. Chem. Fund., **6**, 2-12, 1967

- [50] H. Burghoff, K. Lee, W. Pusch, *Characterization of Transport Across Cellulose Acetate Membranes in the Presence of Strong Solute-Membrane Interactions*, J. Appl. Polym. Sci., **25**, 323-347, 1980
- [51] W. Pusch, *Measurement Techniques of Transport Through Membranes*, Desalination, **59** 105-115, 1986
- [52] S. Sourirajan, *Reverse Osmosis*, Academic Press, New York, 580-620, 1970
- [53] S. Sourirajan, T. Matsuura, *Reverse osmosis/ultrafiltration process principles*, NRCC Press, Ottawa, 802–805, 1985
- [54] U. Merten, *Transport Properties of Osmotic Membranes*, Desalination by Reverse Osmosis, U. Merten, (Ed.) MIT Press, Cambridge, 15-54, 1966
- [55] G. Jonsson, C. Boesen, *Water and Solute Transport Through Cellulose Acetate Reverse Osmosis Membranes*, Desalination, **17**, 145-157, 1975
- [56] T. Matsuura, S. Sourirajan, Reverse Osmosis Transport Through Capillary Pores Under the Influence of Surface Forces, Ind. Eng. Chem. Proc. Dev. Des., 20(2), 273-282, 1981
- [57] H. Mehdizadeh, J. Dickson, *Theoretical modification of the finely porous model for reverse osmosis transport*, J. Appl. Polym. Sci., **42**(4), 1143–1154, 1991
- [58] M. Williams, *Measurement and Mathematical Description of Separation Characteristics of Hazardous Organic Compounds with Reverse Osmosis Membranes*, Ph.D. Thesis, University of Kentucky, USA, 1993
- [59] H. Mehdizadeh, J. Dickson, P. Eriksson, *Temperature Effects on the Performance of ThinFilm Composite, Aromatic Polyamide Membranes*, Ind. Eng. Chem. Res., **28**, 814-824, 1989
- [60] H. Mehdizadeh, J. Dickson, *Solving Nonlinear Differential Equations of Membrane Transport by Orthogonal Collocation*", Comput. Chem. Eng., **14**, 157-160, 1990
- [61] D. Bhattacharyya, M. Jevtitch, J. Schrot, G. Fairweather, *Prediction of Membrane Separation Characteristics by Pore Distribution Measurements and Surface Force-Pore Flow Model*, Chem. Eng. Commun., **42**, 111-128, 1986
- [62] M. Jevtitch, *Reverse Osmosis Membrane Separation Characteristics of Various Organics: Prediction of Separation by Surface Force-Pore Flow Model and Solute Surface Concentration by Finite Element Method*, PhD. Thesis, University of Kentucky, USA, 1986
- [63] H. Mehdizadeh, *Modelling of Transport Phenomena in Reverse Osmosis Membranes*, PhD. Thesis, McMaster University, Canada, 1990
- [64] D. Bhattacharyya, C. Cheng, *Separation of Metal Chelates by Charged Composite Membranes*, Recent Developments in Separation Science, vol. XX, N. Li, J. M. Calo (Eds.), CRC Press, West Palm Beach, 707-730, 1986
- [65] N. Lakshminarayanaiah, *Transport Phenomena in Artificial Membranes*, Chemical Reviews, **65**, 491-565, 1965
- [66] N. Lakshminarayanaiah, *Transport Phenomena in Membranes*, Academic Press, New York, 247-248, 1969

- [67] L. Dresner, *Some Remarks on the Integration of the Extended Nernst-Planck Equations in the Hyperfiltration of Multicomponent Solutions*, Desalination, **10**, 27-46, 1972
- [68] L. Dresner, J. Johnson, *Hyperfiltration (Reverse Osmosis)*, *Principles of Desalination*, 2nd editio., K. Spiegler and A. Laird, (Eds.), Academic Press, Inc., New York, 401-560, 1980
- [69] A. Garcia, G. Medina, *Predicting Membrane Performance by Dimensional Analysis*, T. ASAE, **32**, 2059-2065, 1989
- [70] E. Mason, H. Lonsdale, *Statistical-Mechanical Theory of Membrane Transport*, J. Membr. Sci., **51(1-2)**, 1-81, 1990
- [71] J. Bitter, *Transport Mechanisms in Membrane Separation Processes*, Plenum Press, New York, 35-39, 1991
- [72] S. Thiel, D. Lloyd, *Frictional and Osmotic Effects in the Pressure Driven Membrane Separation of Dilute Solutions*, J. Membr. Sci., **50(2)**, 131-139, 1990
- [73] P. Connell, J. Dickson, *Modelling Reverse Osmosis Separations with Strong Solute-Membrane Affinity at Different Temperatures Using the Finely Porous Model*, J. Appl. Polym. Sci., **35(5)**, 1129–1148, 1988
- [74] R. Rautenbach, A. Gröschl, *Fractionation of aqueous organic mixtures by reverse osmosis*, Desalination, **90(1-3)**, 93–106, 1993
- [75] A. Belkacem, S.E.M.L. Kad, O. Belhamiti, *Mathematical Modelling of Reverse Osmosis Process by the Orthogonal Collocation on Finite Element Method*, Asian J. Appl. Sci. Eng., **1**, 1-18, 2008
- [76] M. Williams, *Separation and Purification of Dilute Hazardous Organics by Ozonation-Low Pressure Composite Membrane Proces*", M.S. Thesis, University of Kentucky, USA, 1989
- [77] M. Williams, R. Deshmukh, D. Bhattacharyya, *Separation of hazardous organics by reverse osmosis membranes*, Environ. Prog., **9**, 118–125, 1990
- [78] R. Deshmukh, *Adsorption of Selected Organics on Reverse Osmosis Membranes and its Effect on Membrane Separation Characteristics*, M.S. Thesis, University of Kentucky, USA, 1989
- [79] A. Kothari, *Concentration and Purification of Hazardous Wastes by Low Pressure Composite Membranes: Treatment of Soil-Wash Rinse Water Leachates*, M.S. Thesis, University of Kentucky, USA, 1991
- [80] C. Bhattacharjee, P. Bhattacharya, *Prediction of Limiting Flux in Ultrafiltration of Kraft Black Liquor*, J. Membr. Sci., **72**, 137-147, 1992
- [81] C. Bhattacharjee, P. Bhattacharya, *Flux Decline Behavior with Low Molecular Weight Solutes During Ultrafiltration in an Unstirred Batch Cell*, J. Membr. Sci., **72**, 149-161, 1992
- [82] M. Cheryan, *Ultrafiltration Handbook*, Technomic Publishing Co., Inc., Lancaster, 171–196, 1986
- [83] S. Kulkarni, E. Funk, N. Li, *Theory and Mechanistic Concepts, Membrane Handbook*, W. Ho, K. Sirkar, (Eds.), Van Nostrand Reinhold, New York, 398-407, 1992

- [84] S. Nakatsuka, A. Michaels, *Transport and Separation of Proteins by Ultrafiltration through Sorptive and Non-sorptive Membranes*, J. Membr. Sci., **69**, 189-211, 1992
- [85] <http://www.membranes.com/pdf/HYDRABrochure.pdf>
- [86] F.A. Pacheco, I. Pinna, M. Reinhard, J.O. Leckie, *Characterization of isolated polyamide thin films of RO and UF membranes using novel TEM techniques*, J. Membr. Sci., **358**, 51-59, 2010
- [87] A.K. Ghosh, B.-H. Jeong, X. Huang, E.M.V. Hoek, *Impacts of reaction and curing conditions on polyamide composite reverse osmosis membrane properties*, J. Membr. Sci., **311**, 34-45, 2008
- [88] K. Gerstandt, K.V. Peinemann, S.E. Skilhagen, T. Thorsen, T. Holt, *Membrane processes in energy supply for an osmotic power plant*, Desalination, **224**, 64-70, 2008
- [89] M. Arora, R.C. Maheshwari, S.K. Jain, A. Gupta, *Use of membrane technology for potable water production*, Desalination, **170**, 105-112, 2004
- [90] D. Berge, H. Gad, I. Khaled, M.A. Rayan, *An experimental and analytical study of RO desalination plant*, Mansoura Engineering Journal, **34**, 71-92, 2009
- [91] D. Bhattacharyya, C. Cheng, *Separation of Metal Chelates by Charged Composite Membranes*, in *Recent Developments in Separation Science vol. IX*, N.N. Li (Ed.), CRC Press, Boca Raton, 707 , 1986
- [92] D. Bhattacharyya, M. Williams, *Theory - Reverse Osmosis*, in *Membrane Handbook*, W. Ho and K. Sirkar (Eds.), Van Nostrand Reinhold, New York, 269-280, 1992.
- [93] N. Hilal, A.F. Ismail, T. Matsuura; D. Oatley-Radcliffe, *Electrokinetic Phenomena for Membrane Charge*, *Membrane Characterization*, Elsevier, 405-422, 2017

CHAPTER 6. CHARACTERIZATION AND MODELLING THE DEEP BED FILTRATION PROCESS IN LIQUID RADIOACTIVE WASTE TREATMENT

6.1. Deep bed filtration – general description

Filtration is a separation process of a solid particle from a fluid and is widely used as an engineering practice for a long time. The separation is performed when a fluid–particle mixture passes through a medium in which particles remain and only the clear fluid passes. Depending on the process conducted and considering factors like particle retention mechanism, the type of medium used, the flow configuration and/or the system treated, in the past years have been used different terminologies such as cake filtration, surface filtration, depth filtration, deep bed filtration, cross-flow filtration, aerosol filtration, water (liquid) filtration, granular filtration, fibrous filtration, fabric filtration, cartridge filtration, membrane filtration, etc. [1].

The deep-bed filter (or as generally denominated „sand filter”) is a clarification filter that has been used for water treatment for over 200 years.

The system involves the operation of a filter having as filter medium a granular material deposited as deep bed and the liquid that usually flows downwards under the influence of its own hydrostatic head. When exhausted, the bed is generally cleaned by flow reversal, which helps the trapped dirt to detach form the bed particles, loosening it. This way, the dirt is washed out of the vessel. Deep-bed filters are commonly filled with sand, but anthracite, coke, garnet and other inert solids can be used also as filter media [2].

The deep bed filtration clarifies suspensions with small solid content by flowing through a granular bed formed by poured particles. By flowing inside the granular bed, interaction forces could appear between one particle from the suspension and one particle from the granular bed. This occurrence determines the attachment of the particle from the suspension to the particle of the bed. This process occurs in more points located between suspension input and bed exit. The quantity of the solid particles retained cannot exceed the quantity determined by the granular bed open spaces hold-up. During filtration appear clogging phenomena, meaning that the retained amount of solid is almost equal to the quantity set up by the bed open spaces. The clogged bed can be regenerated by reversing the flow of water through the filter material causing the filter bed to expand breaking up the compacted filter bed and forcing the accumulated particles to go out from the bed and return them to suspension.

The origins of deep-bed filtration theory can be traced back to over a half-century ago and are related to the works of Iwasaki [3] and Mints [4]. Filtration models are generally classified as phenomenological, stochastic or trajectory ones [5]. Even if the latter are better

justified, their practical application cannot be extended more than to simple geometric representations that relate to clean bed conditions only. These trajectory models can be experimentally validated with only limited success as they require the introduction of different empirical coefficients, used mostly for stochastic and phenomenological models, whereas the latter ones often have some information about the stochastic aspects of mass transfer.

The filtration process is composed of two steps: the initial one, and the transient one. In the initial stage, particle deposition takes place onto a clean filter, the particles are directly deposited onto filter grains. This particle deposition does not have a great effect on the properties of the filter at this stage of the process. The transient stage begins after the initial stage has run its course, and characterises the rest of the filtration process. On the filter grains that are already partially covered by deposited particles takes place supplementary deposition. While this stage runs its course, performance characteristics of the filter are extremely modified: the particle removal can increase or decrease depending on the factors such as available surface area, collection by deposited particles or changes in interstitial (through pores) velocity. This signifies the performance of the filter is dramatically different over the duration of a filter run [6].

The liquid separated from the solids is named filtrate or effluent. As in other separation processes, the separation of phases is never complete: the liquid adheres to the separated solids and the filtrate often contains some amount of solids. The objective of filtration may be clearing of the liquid or solids recovery or both.

The deep bed filtration represents the process of particles removal form a suspension (either liquid or gas) by means of passing the suspension through a granular or fibrous medium. The particles deposited at the surface of the media (granule or fiber) cause a continuous structural change of the medium, which, in turn, affects the filtration rate as well as the flow resistance of the medium. As a consequence, is reported a time variation in the effluent particle concentration and the pressure drop required to maintain a fixed amount of fluid that passed through the bed. In the case of constant pressure operations, the throughput is lower with time. In most deep bed filtration uses, must be attained a standard of effluent quality and a maximum allowable pressure drop so, when the limits are reached the filter must be cleaned. Consequently, the performance of a deep bed filtration process is characterised by the records of the effluent concentration and pressure drop and also by the frequency and conditions used for filter cleaning [5].

The deep filtration occurs because of several mechanisms: the contact of particles with the retention site, the fixation of particle sites and the breaking away of previously retained particles [7].

In the modelling of a process, the focus is upon developing equations that describe the process behavior. So, a model for the bed filtration should describe how the porous medium (bed), as a system responds to the flow of a suspension through it. In deep bed filtration, important variables that describe the performance of the filtration include:

- (1) Effluent concentration of suspended particles that describes the filtrate quality.
- (2) Pressure difference across a porous material through which the suspension is being injected. The duration of the filtration is limited by the pressure drop across the media .

These variables are to be considered in the modelling process, so that the model response can be compared with the experimental results for both effluent concentration and pressure drop.

The flow of suspended particles through a granular media is associated with the deposition and sometimes release of the particles in the pore spaces. Structure changes and pore condition modifications are consequences of the particle deposition and release processes. Thus, the effluent concentration is not constant and is variable with time. Pore geometry changes influence also the pressure gradient which may exhibit a local variation. Therefore it is obvious that the nature of the filtration is unsteady state [8].

6.2. Deep bed filtration modelling

Two categories of models have appeared to explain deep bed filters behavior. Fundamental (or microscopic) models consider the importance of actual transport and attachment mechanisms. Phenomenological (or macroscopic) models attempt to explain the physical progression of the filtration cycle, by ripening, effective filtration, and breakthrough, though this is performed with empirical parameters acquired from experimental studies rather than fundamental mechanisms.

Because of the complexity of filtration mechanisms and the great variety in feed water properties, neither model can predict filter performance without experimental or site-specific pilot studies; however, they provide a good understanding and management of the filtration process.

The models reported in the literature have greatly enhanced our understanding of the mechanisms behind deep-bed filtration and provided useful insights in specific practical applications. The microscopic view is usually presented as a sequence of transport and attachment steps where the transport is discussed in view of five transport mechanisms, namely interception, inertia, diffusion, sedimentation and local turbulence [9] and the attachment is viewed through the van der Waals attraction and electrostatic repulsion of two

entities, a particle and a grain media. This allows obtaining a “filter coefficient” which is then introduced into a macroscopic model [10].

6.2.1. Phenomenological (semi-empirical) modelling of bed filtration

Phenomenological model describes the “overall behavior” of the filtration process by using a set of differential equations including some parameters. The parameters should be determined through the experiments and depend on the type and characteristics of the filter (porous medium) and suspension. The term “macroscopic model” is also used for the phenomenological model since the model does not provide any information regarding the nature or mechanism of the filtration process.

In a phenomenological model the effects of physicochemical characteristics of the filter medium, solution and particles along with some parameters of the flow field and local mass transfer are implicitly incorporated into empirical constants and expressions [11].

The specific deposit σ , gives the amount (volume) of deposited particles per unit medium volume. Therefore, the quantity $\partial\sigma/\partial t$ is the rate of filtration. A simple expression of filtration rate was first suggested by Iwasaki [3], based on his experimental observations. Experimental data for slow sand filters show that the particle concentration profile throughout a filter (c vs. z) can often be described by the logarithmic law, this is,

$$\frac{\partial c}{\partial z} = -\lambda c \quad (6.1)$$

where

c - the suspension particle concentration (vol/vol),

λ - the filter coefficient.

Thus, the filtration rate expression can be written as

$$\frac{\partial \sigma}{\partial t} = \lambda u_s c \quad (6.2)$$

where

u_s – the fluid velocity.

Usually, the logarithmic behavior observed by Iwasaki is applicable only during the initial period of filtration. Because λ does not remain constant but varies with time during filtration process, λ may be expressed as

$$\lambda = \lambda_0 \mathcal{F}(\alpha, \sigma) \quad (6.3a)$$

with

$$\mathcal{F}(\alpha, \sigma) = 1 \quad (6.3b)$$

and the filtration rate expression becomes

$$\frac{\partial \sigma}{\partial t} = u_s \lambda_0 F(\alpha, \sigma) c \quad (6.4)$$

where

λ_0 - the initial value of λ ,

$F(\alpha, \sigma)$ - the correcting factor to account for the deviation from the logarithmic law of the concentration profile,

α - the relevant parameter vector.

Filter coefficient may have two interpretations. Referring to Eq. (6.1), the rate of filtration is first order with respect to the particle concentration of the suspension to be treated. λ , therefore, may be viewed as the first-order reaction rate constant.

Alternatively, λ may be considered as the probability of a particle's being captured (deposited) during a time interval of $1/u_s$ in its flowing through the medium (or traveling a unit distance). In the case of λ being not constant (or varies with σ), it may be considered as a pseudo-first-order rate constant.

The selection of a particular form of expression for F depends, of course, upon the filter medium as well as the suspension to be filtered. If a filter's performance is enhanced with the increase in deposition, then the suspension particle concentration (c vs. z) obtained at different times can be expected to display a systematic downward displacement as time passes. An upward displacement of the concentration profiles corresponding to increasing time implies that the filter's performance deteriorates with deposition. A downward displacement followed by an upward displacement means the filter first improves its performance with deposition and then deteriorates. These different behaviors are shown in fig. 6.1. For $F(\alpha, \sigma)$ various investigators proposed different formula containing different adjustable parameters as a function of specific conditions.

The various behaviors displayed in fig. 6.1 may be explained as follows: as a result of deposition, the geometry and size of filter grains are modified. The flow field near filter grains may be altered, and the magnitude and nature of the particle–filter grain (including deposited particles) interactions may also be changed. The combined effect of these changes may enhance deposition, retard deposition, or have no effect. If the net effect remains favorable (enhancing deposition), the behavior shown in fig. 6.1a is observed. In contrast, fig. 6.1b depicts the situation if the net effect is unfavorable (retarding deposition). The mixed behavior of fig. 6.1c corresponds to the case of transition from favorable to unfavorable (curve 1) or from unfavorable to favorable (curve 2).

Equations (6.2) and (6.4), together with appropriate initial and boundary conditions give a complete description of the particle concentration distributions in the suspension and filter medium as functions of position and time.

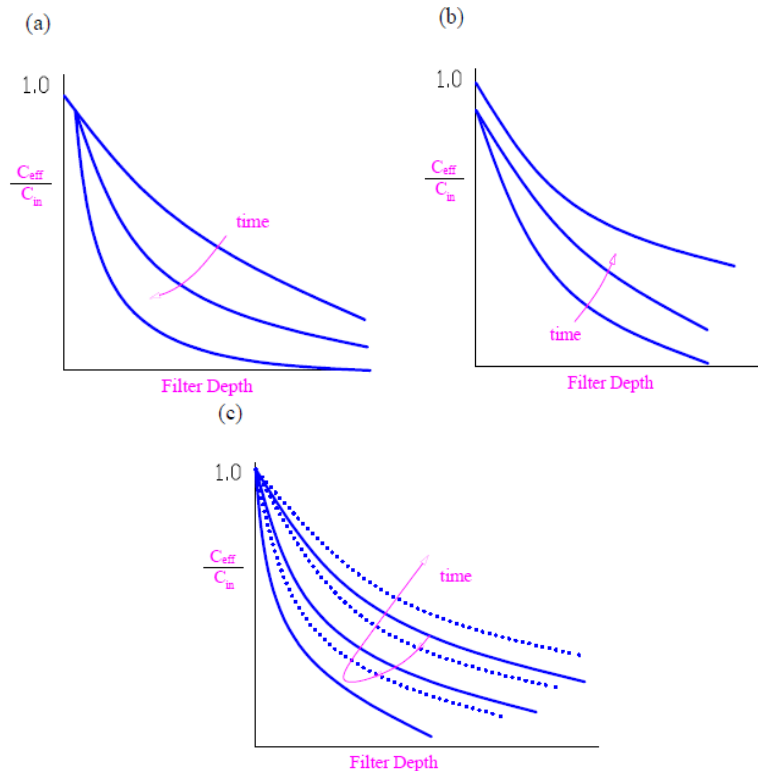


Figure 6.1. Effect of deposition on filter performance (a) performance enhanced with time, (b) performance declined with time, (c) mixed behavior.

Specifically, these results enable the prediction of the effluent concentration history (c at $z = L$ vs. *time*) and the extent of deposition throughout the medium (σ vs. z at various times). This, of course, assumes that the values of λ_0 and the functional form of F are known. The accumulation of deposited particles within a filter medium causes a change of the structure of the medium, which, in turn, results in a decrease of the medium permeability. Since the extent of deposition is not uniform, this implies that the medium permeability during filtration, in general, is not constant, but varies along the z -direction (i.e., the direction of suspension flow).

If the fluid throughput is kept constant, the pressure drop required to maintain a constant throughput varies with time and can be calculated as follows, assuming that the flow of fluid through porous media (either granular or fibrous) may be described by Darcy's law:

$$u_s = -\frac{k}{\mu} \frac{\partial p}{\partial z} \quad (6.5)$$

The pressure drop ($-\Delta p$) across a filter medium of height L , is

$$(-\Delta p) = \mu u_s \int_0^L \frac{dz}{k} \quad (6.6)$$

Initially, the pressure drop is $(-\Delta p)_0$ and the filter permeability, k_0 , is constant throughout the entire medium, or

$$(-\Delta p)_0 = \frac{\mu u_s}{k_0} L \quad (6.7)$$

Dividing Eqs (6.6) by (6.7) yields

$$\frac{(-\Delta p)}{(-\Delta p)_0} = \frac{1}{L} \int_0^L \left(\frac{k_0}{k} \right) dz \quad (6.8a)$$

with the differential form

$$\frac{\left(\frac{\partial p}{\partial z} \right)}{\left(\frac{\partial p}{\partial z} \right)_0} = \frac{k_0}{k} \quad (6.8b)$$

where $\left(\frac{\partial p}{\partial z} \right)$ is the local pressure gradient necessary to maintain a given constant suspension throughput. The change of local permeability (or pressure gradient) results from the accumulation of deposited particles. Similar to Eq. (6.3a), one may write

$$\frac{k_0}{k} = \frac{\left(\frac{\partial p}{\partial z} \right)}{\left(\frac{\partial p}{\partial z} \right)_0} = G(\beta, \sigma) \quad (6.9)$$

and

$$\frac{(-\Delta p)}{(-\Delta p)_0} = \int_0^1 g(\beta, \sigma) d\left(\frac{z}{L}\right) \quad (6.10)$$

As for $F(\alpha, \sigma)$, many investigators proposed for $G(\beta, \sigma)$ several expressions.

The dynamic behavior of deep bed filtration is, therefore, given by Equations (6.8a) or (6.10). The parameters and functions present in this system of equations are λ_0 , k_0 , $F(\alpha, \sigma)$ and $G(\beta, \sigma)$.

A number of predictive models have been presented in the literature. The equations allow for various analytical solutions, which have been used for the treatment of laboratory data and for prediction of porous media contamination and clogging [12 – 21].

Various empirical models were developed based of simplifying assumptions about the specified interaction description. **Mints model** or the filtration coefficient model is the most notorious.

The filter coefficient may be expressed as a function of single collector efficiency and the single collector efficiency may be related to microscopic filtration mechanism [22, 23].

This coefficient noted as λ (λ_0, q_p) is defined as the fraction of the solid retained from the suspension in an elementary length of the granular bed. It is dependent on its initial value (λ_0) and on the local concentration of the retained particles around the bed deposition elements (c_p). It is defined by Eq. (6.11):

$$\lambda(\lambda_0, c_p) = -\frac{dc_p}{c_p} \frac{1}{dx} \quad (6.11)$$

where

λ - filter coefficient, m^{-1} ,

c_p - the mass concentration of particles (suspended solids) in the suspension, kg_p/m^3 ,

x - the space coordinate (bed depth), m.

Fig. 6.2 shows the relationship between local concentration of the particles in suspension and the retained particles in the bed. Here is presented the mass balance of solid with respect to an elementary control volume for the case when the plug flow is assumed for the suspension flow:

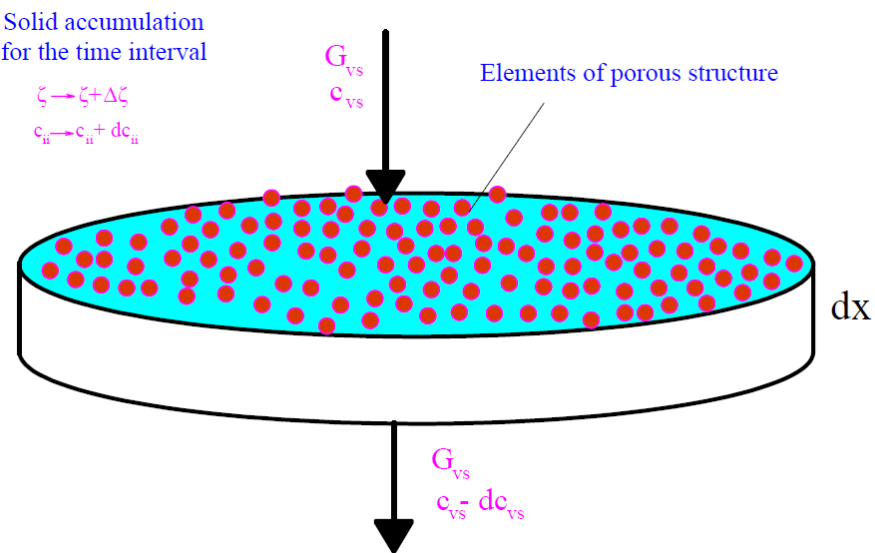


Figure 6.2. The scheme for the retained solid balance in the deep bed filtration

Eq. (6.12) represents the retained solid balance. By coupling this relation with the definition of the filtration coefficient is obtained the mathematical expression of Mints deterministic model. The Eq. (6.13) is written for the filtration start and Eq. (6.14) for other time filtration. Detachment coefficient of the retained particle is introduced by notation α , with T^{-1} as dimension:

$$-\frac{dc_p}{dx} = \frac{A}{G_{vs}} \frac{\partial q_p}{\partial t} = \frac{1}{w} \frac{\partial q_p}{\partial t} \quad (6.12)$$

where

A - the cross-sectional area of granular bed,

G_V - the volumetric flow rate of suspension,

w - the superficial velocity of suspension,

τ - the time.

$$\frac{\partial q_p}{\partial \tau} = w \lambda_0 c_p \quad \tau = 0 \quad (6.13)$$

$$\frac{\partial q_p}{\partial \tau} = w \lambda_0 c_p - \alpha q_p \quad \tau > 0 \quad (6.14)$$

By coupling Eqs. (6.14) and (6.12) the relation (6.15) is obtained. Their derivative with time gives the relation (6.16). Replacing the term $\partial q_p / \partial \tau$ will result the famous Mints model equation (6.17).

The most used univocity conditions of the Mints model, shown by the Eqs. (6.18) and (6.19), are:

a) no retained solid contained in the bed before starting the filtration;

b) constant flow rate and a constant value of the concentration of the retainable solid in the input suspension during the filtration.

$$-\frac{\partial c_p}{\partial x} = \lambda_0 c_p - \frac{\alpha}{w} q_p \quad (6.15)$$

$$-\frac{\partial^2 c_p}{\partial x \partial \tau} = \lambda_0 \frac{\partial c_p}{\partial \tau} - \frac{\alpha}{w} \frac{\partial q_p}{\partial \tau} \quad (6.16)$$

$$\frac{\partial^2 c_p}{\partial x \partial \tau} + \lambda_0 \frac{\partial c_p}{\partial \tau} + \alpha \frac{\partial c_p}{\partial x} = 0 \quad (6.17)$$

$$\tau = 0 \quad x \geq 0 \quad c_p = 0 \quad (6.18)$$

$$\tau \geq 0 \quad x = 0 \quad c_p = c_{v0} \quad (6.19)$$

One solution of the Mints model is provided by the Eqs. (6.20) - (6.22). This solution cannot meet the requirement of the relation (6.13). The obtained solution represents a series with a rapid convergence considering the strong evolution of the chain Q_i . Hence, a good result will be produced by limiting to four or five terms in the sum from relation (6.20).

$$\frac{c_p}{c_{p0}} = \sum_{i=1}^{\infty} \exp(-\lambda_0 x) \frac{(\lambda_0 x)^{i-1}}{(i-1)!} Q_i \exp(-\alpha \tau) \quad (6.20)$$

$$Q_i = Q_{i-1} - \frac{(\alpha \tau)^{i-2}}{(i-2)!} \quad i \geq 2 \quad (6.21)$$

$$Q_1 = \exp(\alpha \tau) \quad (6.22)$$

Eq. (6.23) shows another proposed solution of the Mint model, expressed by help of i -order Bessel functions with real argument $I_i[(\lambda_0 x \alpha \tau)^{1/2}]$:

$$\frac{c_p}{c_{p0}} = (\exp - (\lambda_0 x + \alpha \tau) \sum_{i=1}^{\infty} \left(\frac{\alpha \tau}{\lambda_0 x} \right)^{1/2} I_i \left[(\lambda_0 x \alpha \tau)^{1/2} \right])^{1/2} \quad (6.23)$$

Some considerations of the Mints model are the following:

- a) the initial filtration coefficient λ_0 has a constant value in time and position;
- b) the detachment coefficient is also, a constant parameter;
- c) the quantity of the treated suspension by deep bed filtration is determined by the quantity of the deposited solid in the bed;
- d) an increase of the filtration efficiency does not occur at the start of deep bed.

Some inconsistencies of the Mints model are presented below:

- 1) it is valid principally when the saturation of the fixed bed with retained micro-particles is slow;
- 2) it is not usual when the detachment depends on the retained solid concentration and /or on the flowing velocity;
- 3) it is not usual when the velocity of the mobile phase is not constant in time; this situation is generated by the solid deposition in the bed or by pressure increase when the filtration occurs with constant flow rate.

6.2.2. Stochastic modelling of bed filtration

In the above chapter deep bed filtration is treated as a deterministic process. A specific filtration rate expression is assumed and filtration performance is definitive and predictable. This deterministic treatment has been used, to a large degree, by most workers in the field although studies, which examine deep bed filtration using nondeterministic approach, have also appeared in literature in the past.

Modelling of deep bed filtration as a stochastic process has been applied in a number of different ways [24 – 31]. Randomness is mainly related to the particle size and shape distribution, stochastic heterogeneity of the pore space, surface and stochastic structure of the flow.

If a granular medium is viewed as a large number of interconnected pores, then filtration through the medium causes deposits to accumulate within the pores, ultimately blocking some of them. At the same time, as the pressure drop increases, some of the deposits or parts of them may be reentrained and the blocked pores reopened (or scoured). Thus, the

pressure-drop increase may be viewed as resulting from two processes, blockage and scouring, which occur simultaneously and are stochastic in nature.

A stochastic process consists of, by definition, a collection of random variables, associated with or indexed by a set of numbers, describing an empirical process whose development can be ruled by probabilistic laws. When a fluid containing particles reaches a porous medium, the liquid and the solid phase in the suspension can be separated, either by depositing in the pore or accumulating in front of the surface. This is similar to what happens in the filtration process. Then, the retention process of particles when flowing through a porous media is called Deep Bed Filtration [32].

In treating filtration as a stochastic process, Litwiniszyn [33] considered as the random variable, the number of blocked pores in a unit filter volume at time t , noted $N(t)$. A specific value of $N(t)$ will be expressed by n . Given $N(t) = n$, it is assumed that for the birth-death process,

- (1) $\lambda_n \Delta t + o(\Delta t)$ represents the conditional probability that, during the interval $(t, t + \Delta t)$, a pore will be blocked (a birth event); λ_n is a function of n ;
- (2) $\mu_n \Delta t + o(\Delta t)$ represents the conditional probability that, during the interval $(t, t + \Delta t)$, a blocked pore will be scoured (a death event); μ_n is a function of n ;
- (3) $o(\Delta t)$ is the conditional probability that, in the interval $(t, t + \Delta t)$, more than one event will occur; $o(\Delta t)$ signifies

$$\lim_{\Delta t \rightarrow 0} \frac{o(\Delta t)}{\Delta t} = 0 \quad (6.24)$$

Clearly, probability that there is no change in the interval $(t, t + \Delta t)$ is

$$1 - \lambda_n \Delta t - \mu_n \Delta t - o(\Delta t) \quad (6.25)$$

The probability that exactly n pores are blocked is pointed out as

$$P(t) = P_r[N(t) = n], n = 0, 1, 2, \dots \quad (6.26)$$

For two successive time intervals, $(0, t)$ and $(t, t + \Delta t)$, the blocking of exactly n pores during the interval $(0, t + \Delta t)$ can occur in the following ways:

- (1) During $(0, t)$ all n pores are blocked and none during $(t, t + \Delta t)$. The occurrence probability of this way is $P_n(t)[1 - \lambda_n \Delta t - \mu_n \Delta t - o(\Delta t)]$.
- (2) During $(0, t)$ exactly $(n - 1)$ pores are blocked and one pore is blocked during $(t, t + \Delta t)$. The occurrence probability is $P_{n-1}(t)[\lambda_{n-1} \Delta t + o(\Delta t)]$.
- (3) During $(0, t)$ exactly $(n + 1)$ pores are blocked and one blocked pore is scoured during $(t, t + \Delta t)$. The occurrence probability is $P_{n+1}(t)[\mu_{n+1} \Delta t + o(\Delta t)]$.
- (4) During $(0, t)$ exactly $(n - j)$ pores ($2 \leq j \leq n$) are blocked and j pores are blocked during $(t, t + \Delta t)$. The probability of this event is $o(\Delta t)$.

(5) During $(0, t)$ exactly $(n + j)$, $(2 \leq j \leq (n_0 - n))$, are blocked and j blocked pores are scoured during $(t, t+\Delta t)$. The probability is $\text{o}(\Delta t)$.

Thus, the probability of having n pores blocked during $(t, t+\Delta t)$ is

$$P_n(t+\Delta t) = P_n(t)[1 - \lambda_n \Delta t - \mu_n \Delta t] + P_{n-1}(t)\lambda_{n-1} \Delta t + P_{n+1}(t)[\mu_{n+1} \Delta t + \text{o}(\Delta t)], n \geq 1 \quad (6.27)$$

and

$$P_0(t+\Delta t) = P_0(t)[1 - \lambda_0 \Delta t] + P_1(t)\mu_1 \Delta t + \text{o}(\Delta t) \quad (6.28)$$

By deriving as a function of time are obtained the so-called master equations [34]:

$$\frac{dP_n(t)}{dt} = \lambda_{n-1} P_{n-1}(t) - (\lambda_n + \mu_n) P_n(t) + \mu_{n+1} P_{n+1}(t), n \geq 1 \quad (6.29)$$

$$\frac{dP_0(t)}{dt} = -\lambda_0 P_0(t) + \mu_1 P_1(t) \quad (6.30)$$

Litwiniszyn [33] assumed that

$$\lambda_n = \delta(n_0 - n), n = 0, 1, 2, \dots, n_0 \quad (6.31a)$$

$$\mu_n = \omega_n \quad (6.32b)$$

where

δ, ω – rate constants of the birth and death processes,

n_0 - the total number of open pores in a clean filter.

Eqs. (6.29) and (6.30) become

$$\frac{dP_n(t)}{dt} = \delta[n_0 - (n-1)]P_{n-1}(t) - [\delta(n_0 - n) + \omega_n]P_n(t) + \omega(n+1)P_{n+1}(t), n \geq 1 \quad (6.32)$$

$$\frac{dP_0(t)}{dt} = -\delta n_0 P_0(t) + \omega P_1(t) \quad (6.33)$$

In the case of a clean filter, all the pores are open, so, the initial conditions of these two equations are

$$P_n(0) = 0, n = 1, 2, \dots, n_0 \quad (6.34a)$$

$$P_0(0) = 1 \quad (6.34b)$$

The solution of Eqs. (6.32) and (6.33) with the initial condition of Eqs. (6.34a) and (6.34b) gives the distribution of the pore blockage probabilities. The expected number of blocked pores at time t , $E[N(t)]$, is given as:

$$E[N(t)] = \sum_{n=0}^{n_0} n P_n(t) \quad (6.35)$$

To evaluate this quantity, solving Eqs. (6.32) and (6.33) is unnecessary. Alternatively, can be used the method of probability generating function, defined as

$$g[s, t] = \sum_{n=0}^{n_0} s^n P_n(t) \quad (6.36)$$

The relationship between $g(s, t)$ and $E[N(t)]$ reveals that

$$E[N(t)] = \frac{\partial g(s,t)}{\partial s} \Big|_{s=1} \quad (6.37)$$

By combining Eqs. (6.26), (6.32), (6.33) and (6.36) it can be shown [35] that $g(s,t)$ is the solution to the following equation:

$$\frac{\partial g(s,t)}{\partial t} = \frac{\partial g(s,t)}{\partial s} [\omega + (\delta + \omega)s - \delta s^2] + g(s,t)[\delta n_0(s-1)] \quad (6.38)$$

with the following initial and boundary conditions:

$$g(s,0) = 1 \quad (6.39a)$$

$$g(1,t) = 1 \quad (6.39b)$$

$$g(s,t) = \left[\frac{(\delta s + \omega) - \delta(s-1)e^{-(\delta+\omega)t}}{\delta + \omega} \right]^{n_0} \quad (6.40)$$

Substituting Eqs. (6.40) into Eq. (6.37):

$$E[N(t)] = \delta n_0 \left[\frac{1 - e^{-(\delta+\omega)t}}{\delta + \omega} \right] \quad (6.41)$$

The above results can now be incorporated with the pressure drop-flow rate relationship, namely, the Kozeny–Carman equation. For the reason that the particle deposition leads to the blockage of some pores, the effective cross-sectional area of the filter flow decreases with the increase of the number of blocked pores. Consequently, under the constant flow condition, the effective superficial velocity is inversely proportional to the number of unblocked pores. Eq. (6.41) shows that the pressure-drop across a filter bed is proportional to the number of unblocked pores. Thus, the ratio between the pressure of a clogged filter and a clean filter is

$$\frac{\left(\frac{-\Delta p}{L} \right)}{\left(\frac{-\Delta p}{L} \right)_0} = \frac{n_0}{n_0 - E[N(t)]} = \frac{\delta + \omega}{\omega + \delta e^{-(\delta+\omega)t}} \quad (6.42)$$

It should be mentioned that δ and ω present in Eq. (6.42) are adjustable parameters. The stochastic model discussed above provides no information about the magnitudes of δ or ω nor the relationships between one of them with relevant operating variables.

Numerous models have been used to predict the removal efficiency in deep bed filtration at initial and transient stages. However, studies are still ongoing to develop a model which can describe the entire filter cycle.

Another approach in modelling deep bed filtration is the one that firstly traces the description of the suspension particle trajectory around the deposition particle of the bed, despite the fact that more results obtained applying these models are not, at this time, satisfactory. This fact is a consequence of the simplification related to the nature of the forces

which determine the filtration process. Fig. 6.3 [36] is an indirect presentation of these forces, where it is shown the moving of one particle from the suspension around one particle from the granular bed. The particle capture in porous media can be caused by different mechanisms [36].

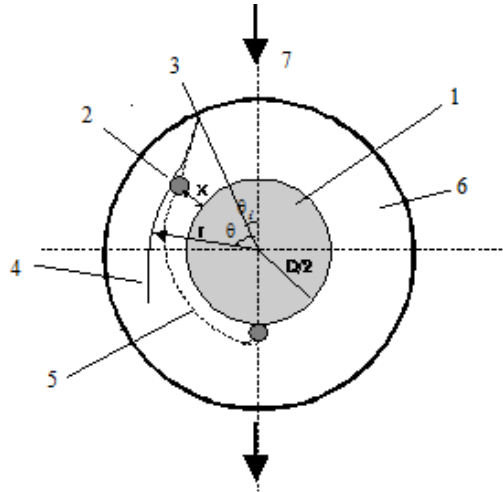


Figure 6.3. Particle retention by a filter grain [36]: (1) filter grain, (2) particle from suspension, (3) particle input in the boundary layer, (4) non-deposition trajectory of particle, (5) deposition trajectory of particle, (6) boundary layer around the filter grain, (7) flow direction of suspension (r and θ are radial coordinates of particle trajectory, θ_i is the input angle of particle, D is the diameter of filter grain, x is the distance between particle and filter grain).

The most important forces, which are taken into account in the deep bed filtration, are:

- *the inertial force* that is caused by the tendency of the micro-particle to move with the fluid stream. If the particle has enough inertia will maintain a hydrodynamic trajectory imposed by the flow around one fixed element. This inertial action is formulated by the dimensionless Stokes number:

$$In = (\rho_p d^2 w) / (18 \eta d_s)$$

where

d - the micro particle diameter,

d_s - the diameter of the element of the granular bed,

ρ_p - the density of the micro particle expected for deposition,

η - the density of the flowing liquid,

w - the real local liquid velocity.

- *the gravitational force* that induces the settling of the micro-particle from the suspension. If the particle is large enough and has a density greater than that of the fluid in which it is suspended, it will settle out of suspension in the direction exerted by the gravitational force.

This behavior is characterized by a gravitational parameter, the Stokes number:

$$St = [g (\rho_p - \rho) d^2] / (18 \eta w)$$

where

g – the gravitational acceleration,

ρ - the density of fluid.

This can be seen as the ratio between the Stokes velocity for the particle and the flowing suspension velocity.

- *the diffusion force* gives the local action of the Brownian motion, due to the thermal energy of water molecules, on the deposition of the micro particle. If the particle is very small, Brownian motion will induce a random movement that increases significantly as the particle size decreases. For particles with $d < 1 \mu\text{m}$ this mechanism becomes consistent and can be characterized in terms of the Peclet number:

$$\text{Pe} = (3 \pi \eta d d_s w_f)/(kT) = d_s w / D$$

where

D – the Stockes-Einstein diffusion coefficient.

This is the ratio of the Stokes and Brownian forces, which together manipulate the micro particle movement.

- *the laminar flow force* characterizes the action of the flowing liquid on the micro particle. The flow through the filter bed is laminar, with a velocity gradient, and consequently a shear field. In the case of an uniform shear field, a spherical particle would suffer a rotation that will cause a deflection path across the shear field. Non-uniform shear field, non-sphericity of particle and non-uniformity of the element of the porous structure will generate an undesired rotation movement for the microparticle that will affect the particle trajectory in an unpredictable manner. The overall effect is considered as the effect of the laminar flow force or hydrodynamic action. It is characterized by means of Reynolds number for the filter bed:

$$(\text{Re} = (w d_s \rho) / \eta)$$

These forces give the mechanisms that, most likely, do not act separately, particles in the suspension will be subject to all of them in different degrees; the approach of the micro particle to the deposition element of the porous body will produce. After transport to the filter grain surface at distances smaller than $1 \mu\text{m}$, other forces emerge and produce the fixation of the micro particle on the element of the porous structure by a variety of mechanisms.

Among these forces are mentioned:

- *the electrostatic force* appears when both micro particle and the deposition element of the bed have electric charges; if they have the same sign of the electric charges, a repulsive force will appear having the value predicted by the relation (6.43):

$$F_R^{(x)} = \frac{\exp\left[-kd\left(\frac{2x}{d}-2\right)\right]}{1+\exp\left[-kd\left(\frac{2x}{d}-2\right)\right]} \quad (6.43)$$

- *the Van der Waals force* acts due to instantaneous dipole moments generated by the temporary asymmetrical distribution of electrons of the constitution material of the micro particle and of the deposition element. This force is largely responsible for particle adhesion and strongly depends on the inter particles distance and on the wavelength ($\bar{\lambda}$) that characterizes the assembly micro particle-deposition element. Since the filter grain is generally larger, at least with two orders of magnitude, than the suspended particle, the surface of the filter grain can be supposed to be flat relative to the particle.

The relation (6.44) describes a qualitative indication of the force arisen between a filter grain (collector) and a suspended particle, with rapid decreasing when the argument increases

$$F_{vw}^{(x)} = \frac{1}{\left(\frac{2x}{d}-2\right)^2} F\left(\frac{\frac{2x}{d}-2}{\bar{\lambda}}\right) \quad (6.44)$$

- *the hydrodynamic adhesion force* is related to the resistance that is present in the case of adhesion of microparticle – deposition element, filter grain or wall, due to the inter parteners liquid that must be eliminated; this force will retard the adhesion of the micro particle and allow for drawing them in the flowing suspension.

- *the detachment force* realizes the separation of the assembly microparticle - deposition element when the number on the retained microparticles to one deposition element is great. Detachment is directly proportional to the specific deposit and is explained by considering that the varying levels of structural strength of the deposit causes the scission of the less firmly attached particles as new particles arrive. Generally, the detachment does occur in reversed-flow, the common method for filter cleaning.

These forces determine a very complicated interaction between the suspended microparticles and the deposition elements of the porous body. Consequently, there is now a general consensus that it is impossible the development of one completely phenomenological model for the deep bed filtration.

For micro-particle evolution in the filtration bed, two elementary processes are taken into account by a deep bed stochastic model [37]:

a) type I process that considers motion of microparticles with the velocity $v_I = v$, induced by the surrounding flowing fluid; this process type reveals the non deposition of the microparticle situation;

b) type II process that shows the situation when exists the possibility of the microparticle to take the deposition way; the motion of microparticles has the velocity $v_2 = 0$.

The stochastic model accepts a Markov type relation between its two elementary states. For that are defined the following items:

- $\beta\Delta\tau$ - the transition probability from the type I process to type II process,
- $\gamma\Delta\tau$ - the transition probability from a type II process to a type I process,
- $P_1(x, \tau)$ – the probability to locate the microparticle at the position x and time τ with a type I evolution,
- $P_2(x, \tau)$ - the probability to locate the microparticle at the position x and time τ .

With these assumptions and notations the general stochastic model gives the following form:

$$\frac{\partial P_1(x, \tau)}{\partial \tau} = -v \frac{\partial P_1(x, \tau)}{\partial x} - \beta P_1(x, \tau) + \gamma P_2(x, \tau) \quad (6.45)$$

$$\frac{\partial P_2(x, \tau)}{\partial \tau} = \beta P_1(x, \tau) - \gamma P_2(x, \tau) \quad (6.46)$$

Considering that the probability to locate the microparticle in the specified position can be formulated as $P(x, \tau) = P_1(x, \tau) + P_2(x, \tau)$, the stochastic model is converted into a form that permits, as the Mints model, the computation of the $c_p(x, \tau) / c_{p0}$. By replacing $P_1(x, \tau)$ and $P_2(x, \tau)$ with $P(x, \tau)$ in Eqs. (6.45) - (6.46) results an important partly differential equation, specified with the relation (6.47)

$$\frac{\partial^2 P(x, \tau)}{\partial \tau^2} + v \frac{\partial^2 P(x, \tau)}{\partial x \partial \tau} + v\gamma \frac{\partial P(x, \tau)}{\partial x} + (\beta + \gamma) \frac{\partial P(x, \tau)}{\partial \tau} = 0 \quad (6.47)$$

A new form of the stochastic model of the deep bed filtration is produced as follows: the mixed partly differential term from the Eq. (6.47) is eliminated assigning the notation $z = x - v\tau / 2$. This transformation has as consequence the obtaining of the hyperbolic partly differential equation (6.48) with its characteristic univocity conditions, (6.49) and (6.50). These univocity conditions set that no suspension is in the bed at the start of filtration process and at the bed input begins the suspension feed, therefore there is a constant probability for the input of the microparticles:

$$\begin{aligned} & \frac{\partial^2 P\left(z + \frac{v\tau}{2}, \tau\right)}{\partial \tau^2} - \frac{v^2}{4} \frac{\partial^2 P\left(z + \frac{v\tau}{2}, \tau\right)}{\partial z^2} + \frac{v}{2}(\beta + \gamma) \frac{\partial P\left(z + \frac{v\tau}{2}, \tau\right)}{\partial z} + \\ & + (\gamma - \beta) \frac{\partial P\left(z + \frac{v\tau}{2}, \tau\right)}{\partial \tau} = 0 \end{aligned} \quad (6.48)$$

$$\tau = 0, x > 0, z = x \quad P(z, \tau) = 0 \quad (6.49)$$

$$\tau > 0, x = 0, z > 0 \quad P(z, \tau) = P_0 \quad (6.50)$$

The jumping frequencies from one state to another have important values and characterize the common deep bed filtration.

The Eq. (6.48) that describes an hyperbolic model is transformed into partly differential Eq. (6.51) that represents a parabolic model. With the univocity conditions (6.49) and (6.50) this model accepts the analytical solution given by the relations (6.52) and (6.53).

$$\frac{v^2}{4(\gamma+\beta)} \frac{\partial^2 P(z+\frac{v\tau}{2}, \tau)}{\partial z^2} = \frac{v}{2} \left(\frac{\gamma-\beta}{\gamma+\beta} \right) \frac{\partial P\left(z+\frac{v\tau}{2}, \tau\right)}{\partial z} + \frac{\partial P\left(z+\frac{v\tau}{2}, \tau\right)}{\partial \tau} = 0 \quad (6.51)$$

$$x - \frac{v\beta}{\gamma+\beta} < 0, \quad \frac{P(x, \tau)}{P_0} = \frac{1}{2} \left\{ 1 + erf \left[\frac{x - \frac{v\beta}{\gamma+\beta}}{\sqrt{\frac{v}{\gamma+\beta}}} \right] \right\} \quad (6.52)$$

$$x - \frac{v\beta}{\gamma+\beta} > 0, \quad \frac{P(x, \tau)}{P_0} = \frac{1}{2} \left\{ 1 - erf \left[\frac{x - \frac{v\beta}{\gamma+\beta}\tau}{\sqrt{\frac{v^2}{\gamma+\beta}}} \right] \right\} \quad (6.53)$$

6.3. Experimental investigation of deep bed filtration in ARW treatment

Deep-bed filtration (DBF) is a method widely used for separation of inorganic and organic particles from suspensions with low levels of suspended solids. When a diluted suspension flows through a filtering granular bed, the particles to be removed approach the filter grains (collectors) by various transport mechanisms (direct interception, inertia, sedimentation, molecular diffusion, electrostatic forces, hydrodynamic action) and they can further adhere to the collector surface (by van der Waals forces, electric double layer interactions, hydrogen bonding, mutual adsorption of polymeric species) [8, 38 -.46]. DBF involves two stages, *i.e.*, an initial (clean bed) one, where the deposition of particles occurs on the clean filter grains, followed by a transient stage, where the particles are deposited on the filter grains which are partially covered by other particles [8, 42]. In the transient stage both attachment and detachment forces should be considered.

DBF performances, usually evaluated in terms of suspended solid concentration in the effluent (filtrate quality) and head loss across the bed, are affected by various process factors. Accordingly, they depend on physical and chemical characteristics of both filtration medium (material, shape, size distribution, density, and surface charge of filter grains, depth and void fraction of fixed bed) and suspension (type, shape, size distribution, surface charge, density

and concentration of particles, age and viscosity of suspension) as well as on the operating conditions (suspension flow rate, operating temperature and pressure).

Sand, anthracite coal, granular activated carbon, garnet, natural zeolites, synthetic inorganic sorbents, ion exchange resins, glass and expanded polystyrene beads, are common granular materials used to remove TSS from a diluted suspension by DBF [38, 40, 41, 44, 45, 47 - 49]. Rapid sand filtration is widely applied to water treatment [41, 50].

In aqueous radioactive waste (ARW) processing, the knowledge that exists on water purification can be applied. However, there are some additional problems referring to the specialized requirements of radioactive waste management. ARW treatment by deep-bed sand filtration (DBSF) could lead to an effluent with an acceptable level of residual radioactivity for discharge or further processing by other separation methods (*e.g.*, ion exchange, fixed-bed adsorption, ultrafiltration, reverse osmosis) as well as a low amount of secondary radioactive waste [48, 51]. The first application of DBSF in nuclear engineering dates from 1948, when this process was used to air purification [52].

The process control based on modelling could offer valuable information that may be applied to reduce the treatment costs and to protect the health of operators. A DBSF model for the removal of radioactive pollutants from medium and low level ARW could be very useful to design and optimize the process, because it determines a decrease in the number of experiments, which can be expensive, may require considerable time and, most important, increase the radiological dose to workers.

The quality of ARW treated by rapid sand filtration was measured and simulated in this paper. Mathematical models were adopted to predict the process performance and their adjustable parameters were fitted based on experimental data.

6.3.1. Models for deep bed filtration of ARW

DBF process can be described by microscopic or macroscopic models, including trajectory analysis, deterministic or stochastic phenomenological ones [8, 9, 17, 34, 38 – 44, 46, 53 - 55]. A physical model associated to a trajectory analysis microscopic approach is presented in fig. 6.2 [34]. The prediction of the trajectory of a particle around a filter grain is very difficult due to a large number of forces involved, *e.g.*, interception, inertial, gravitational, diffusion, electrostatic, hydrodynamic, van der Waals, electric double layer.

In this paper macroscopic approaches were selected for predicting the process performances. A filtration coefficient semiempirical deterministic model and a two-state stochastic model were used to simulate the separation of clay particles ($d_p = 20 \mu\text{m}$) from suspensions as well as of radioactive suspended particles ($d_p > 50 \text{ nm}$) from ARW.

Filtration coefficient (FC) semiempirical deterministic model

A filtration coefficient, λ , can be defined by Eq. (6.11). The basic equations of the filtration coefficient semiempirical deterministic model used are the relations (6.12) – (6.23)

Based on experimental data of suspended solid concentration in the effluent ($x = H$) of DBF device, *i.e.*, $c_{vsk}(H, \tau_k)$, $1 \leq k \leq N$, α and λ_0 adjustable parameters can be determined by minimizing the root mean square error (RMSE) between the experimental and predicted data expressed by Eq. (6.54).

$$F(\lambda_0, \alpha) = \sqrt{\frac{1}{N} \sum_{k=1}^N \left[\frac{c_{pk}(H, \tau_k)}{c_{p0}} - \sum_{i=1}^{\infty} \exp(-\lambda_0 H) \frac{(\lambda_0 H)^{i-1}}{(n-1)!} Q_n \exp(-\alpha \tau_k) \right]^2} \quad (6.54)$$

Two-state (TS) stochastic model

Two elementary processes can be identified for particle evolution in the filtrating granular bed [56], *i.e.*, based on following presumptions:

- (1) the particle moves with the velocity $v_1=v$ determined by the fluid flowing over the filter grains,
- (2) the particle deposition ($v_2=0$).

Accordingly, based on a Markov type connection between (1) and (2) states, the unsteady balance of probabilities to locate the particle at x and τ coordinates, $P_1(x, \tau)$ and $P_2(x, \tau)$ and Eqs. (6.45) – (6.47) was obtained Eq. (6.55). By dividing its terms to v and assuming that $\frac{1}{v} \frac{\partial P_1(x, \tau)}{\partial \tau}$ and $\frac{\gamma}{v} \frac{\partial P_1(x, \tau)}{\partial \tau}$ are negligible in comparison with $\frac{\beta}{v} \frac{\partial P_1(x, \tau)}{\partial \tau}$, Eq. (6.55) became Eq. (6.56).

$$\begin{aligned} \frac{\partial^2 P_1(x, \tau)}{\partial \tau^2} &= -v \frac{\partial^2 P_1(x, \tau)}{\partial x \partial \tau} - \beta \frac{\partial P_1(x, \tau)}{\partial \tau} - \gamma \left(\frac{\partial P_1(x, \tau)}{\partial \tau} + v \frac{\partial P_1(x, \tau)}{\partial x} \right) \quad (6.55) \\ \frac{\partial^2 P_1(x, \tau)}{\partial x \partial \tau} + \frac{\beta}{v} \frac{\partial P_1(x, \tau)}{\partial \tau} + \gamma \frac{\partial P_1(x, \tau)}{\partial x} &= 0 \end{aligned} \quad (6.56)$$

Taking into account the boundary condition expressed by Eq. (6.57), the analytical solution of Eq. (6.56) is given by Eqs. (6.58) and (6.59), where I_i is the modified Bessel function of the first kind [6.57].

$$x=0 \quad \tau>0 \quad P_1(0, \tau)=1, \quad P_2(0, \tau)=0 \quad (6.57)$$

$$\frac{P_1(x, \tau)}{P_1(0, \tau)} = 1 - \exp \left[- \left(\frac{\beta x}{v} + \gamma \tau \right) \right] \sum_{i=1}^{\infty} \left(\frac{\gamma \tau}{\beta x} \right)^{\frac{i}{2}} I_i \left[\left(\frac{\beta \gamma x \tau}{v} \right)^{\frac{1}{2}} \right] \quad (6.58)$$

$$I_i(u) = \sum_{m=0}^{\infty} \left[\frac{\left(\frac{u}{2}\right)^{i+2m}}{m!(m+i)!} \right] \quad (6.59)$$

Based on the similarity between Eqs. (6.17) and (6.56) as well as Eqs. (6.18) and (6.57), β and γ parameters can be adjusted using experimental data ($c_{pk}(H, \tau_k)$, $1 \leq k \leq N$) by minimizing RMSE expressed by Eq. (6.60), where the real velocity of particle (v) is defined by Eq. (6.61) depending on suspension superficial velocity (w) and bed void fraction (ε_b).

$$G(\beta, \gamma) = \sqrt{\frac{1}{N} \sum_{k=1}^N \left\{ \frac{c_{pk}(H, \tau_k)}{c_{p0}} - 1 + \exp \left[- \left(\frac{\beta H}{v} + \gamma \tau_k \right) \right] \sum_{i=1}^{\infty} \left(\frac{w \tau_k}{\beta H} \right)^{\frac{i}{2}} I_i \left[\left(\frac{\beta \gamma H \tau_k}{v} \right)^{\frac{1}{2}} \right] \right\}^2} \quad (6.60)$$

$$v = \frac{w}{\varepsilon_b} \quad (6.61)$$

6.3.2. Experimental set-up

Two experimental studies of DBSF were conducted under various operating conditions using silica sand as a filtering medium. Diluted clay suspensions were processed in the first study, whereas ARW was treated in the second one.

DBSF of clay suspensions

DBSF experiments were performed using a pilot-scale setup (fig. 6.4) consisting of: (i) a metallic column (90 cm height and 5 cm inner diameter) equipped with manometers at its top and bottom, (ii) a pressurized vessel (400 L volume) for suspension storage, (iii) a compressed air supply for maintaining a constant pressure (1.5-2 bar) in the storage vessel, and (iv) flow rate control valves.

Gravel was placed on a sieve at the column bottom to support the granular bed and to distribute uniformly the suspension. Uniform sand grains, either 0.5 or 0.8 mm diameter (D), (fig. 6.4) were packed in the column resulting in bed void fractions (ε_b) of 0.324 and 0.377 m^3/m_b^3 , respectively. Clay suspensions were obtained by adding 200 and 400 g of clay particles (20 μm mean diameter (d_p) and $1400 \text{ kg}_p/m_p^3$ density (ρ_p)), respectively, in 200 L tap water (fig. 6.5). Pressure difference between the bed inlet and outlet ($\Delta p = p_{in} - p_{out}$) was continuously measured.

Effluent samples were collected at regular intervals and mass concentration of particles (c_p) was determined for each sample. A volume of sample was filtered on a Whatman® quantitative filter paper, ashless, Grade 40 (8 μm pore size). The filter paper with solid residue retained was dried into an oven at 105°C for 2 h, placed into a desiccator to cool

to room temperature, and then weighed. The effects of sand grain size ($D=0.5, 0.8$ mm), bed depth ($H = 0.2, 0.4$ m), mass concentration of particles in the influent ($c_{p0}=1, 2 \text{ kg}_p/\text{m}^3$), suspension superficial velocity ($w = 0.015, 0.020 \text{ m/s}$), and operating temperature ($t = 25, 45^\circ\text{C}$) on c_p/c_{p0} were evaluated.

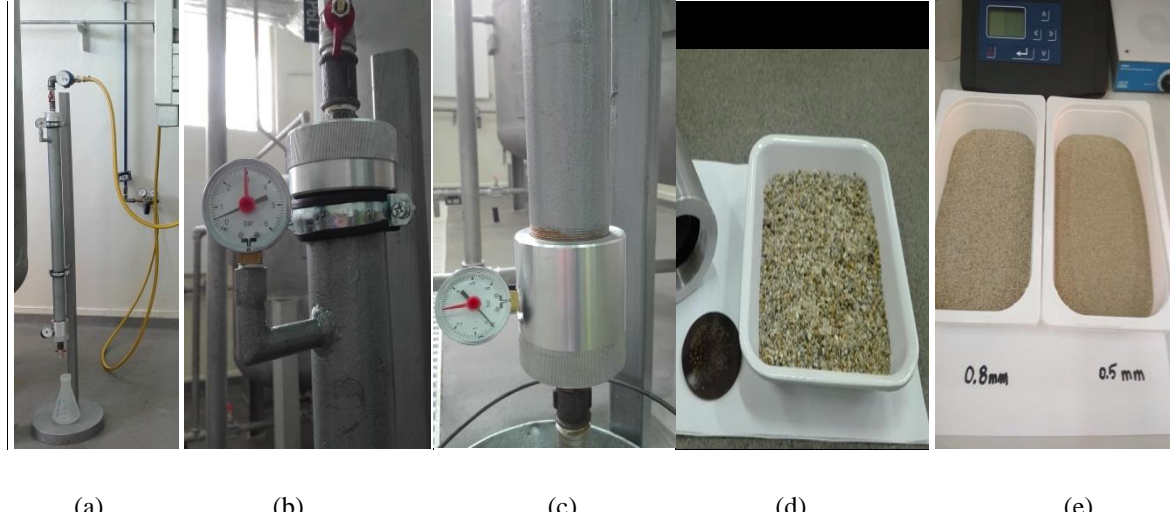


Figure 6.4. Pilot-scale set-up: a) column and filtrate collector bottle, b) valve and manometer at column top, c) column bottom with manometer, d) gravels for supporting the sand bed, e) sand particles before loading into column

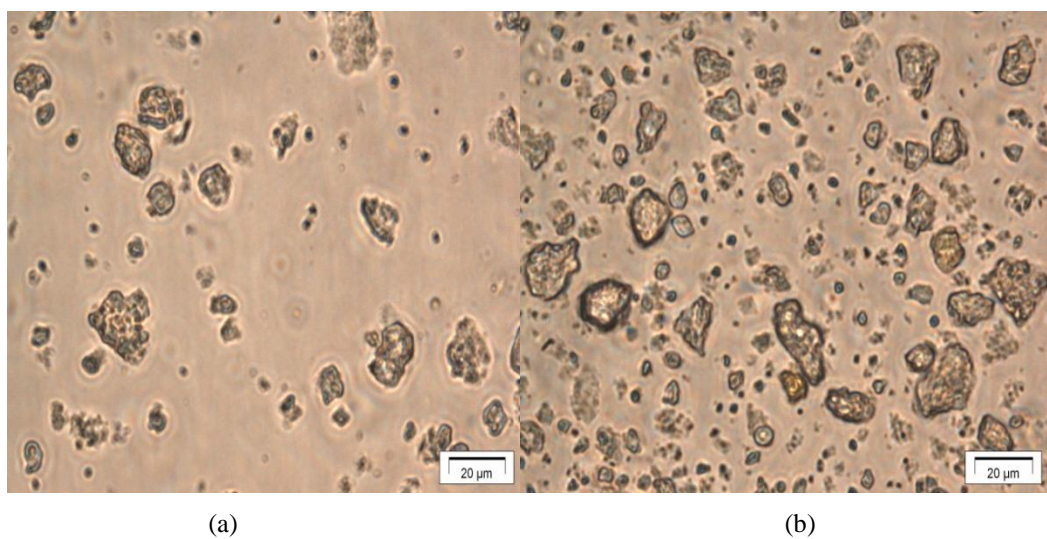


Figure 6.5. Clay micro suspensions 1g/L (a) and 2 g/L (b)

DBSF of ARW

Experiments of DBSF were conducted in a column (fig. 6.6) of a filtration module for ARW treatment. It consisted of three metallic columns (114 cm height and 35 cm inner diameter), tanks for ARW and effluent storage, a submersible pump for feed, piping, measuring and control equipment.



Figure 6.6. Metallic columns for ARW treatment by DBSF

Samples from collecting tank were taken at regular intervals and mass concentration of particles (c_p^c) as well as activity concentration of radionuclides (^{60}Co , ^{137}Cs , ^{241}Am , and ^3H) in suspended particles and liquid phase were measured for each sample. TSS (c_p^c) was determined by filtration on a 50 nm Whatman membrane using a Varian DS 102A vacuum pump (Agilent). The membrane was further dried into an oven at 105°C for 2 h, cooled to room temperature in a dessicator, and then weighed. Activity concentrations of γ -emitting radionuclides (^{60}Co , ^{137}Cs , and ^{241}Am) in the particles and liquid phase were evaluated based on a Laboratory SOurceless Calibration Software (LabSOCS) version 3.2 integrated in a Genie 2000 γ -ray spectrometry system (Canberra Inc.). Activity concentration of β radionuclide (^3H) in the liquid phase was determined using a liquid scintillation analyzer, Tri-Carb 2910 TR type, Perkin - Elmer. The samples used for counting were previously distilled to avoid other interfering β radionuclides and a 20 mL pretreated sample was mixed with liquid scintillation; sample: liquid scintillation ratio was 1:3. The liquid scintillation used for the sample preparation is Ultima Gold type. For the samples chemical quenching parameters determination, the device uses a ^{133}Ba external standard source. The acquisition and processing software is QuantaSmart. The values of process factors for ARW treatment by DBSF were as follows: $D = 0.5$ mm, $H = 0.3$ m, $c_{p0} = 0.223 \text{ kg}_p/\text{m}^3$, $w = 0.003 \text{ m/s}$, and $t = 25^\circ\text{C}$.

6.3.3. Results and discussion

DBSF of clay suspensions

Experimental dynamics of the ratio between the concentration of clay particles in the effluent and that in the influent (c_p/c_{p0}) under various operating conditions are presented in figs. 6.7-6.11, where the bullets represent experimental data and the lines are experimental

data processed by Matchad function *supsmooth(vx, vy)*. Depicted results highlight that all process factors, *i.e.*, D (0.5 and 0.8 mm), H (0.2 and 0.4 m), c_{p0} (1 and 2 kg_p/m^3), w (0.015 and 0.020 m/s), and t (25°C and 45°C), influence the dynamics of c_p/c_{p0} (breakthrough curves). Higher levels of sand grain size (fig. 6.7), suspended solid concentration in the influent (fig. 6.9), suspension superficial velocity (fig. 6.10), and operating temperature (fig. 12) as well as a lower value of bed depth (fig. 6.8) resulted in sharper breakthrough curves, indicating a faster saturation of the bed.

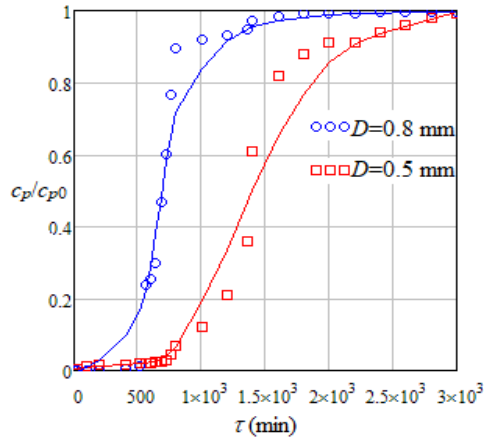


Figure 6.7. Effect of sand grain diameter (D) on c_p/c_{p0} dynamics
($H = 0.4\text{ m}$, $c_{p0} = 2\text{ kg}_p/\text{m}^3$, $w = 0.020\text{ m/s}$, $t = 25^\circ\text{C}$)

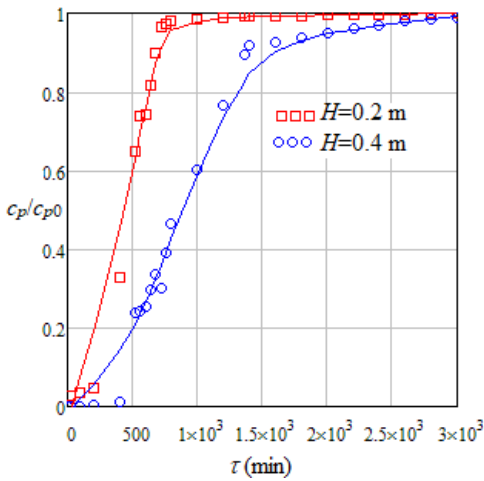


Figure 6.8. Effect of bed depth (H) on c_p/c_{p0} dynamics
($D = 0.8\text{ mm}$, $c_{p0} = 2\text{ kg}_p/\text{m}^3$, $w = 0.020\text{ m/s}$, $t = 25^\circ\text{C}$)

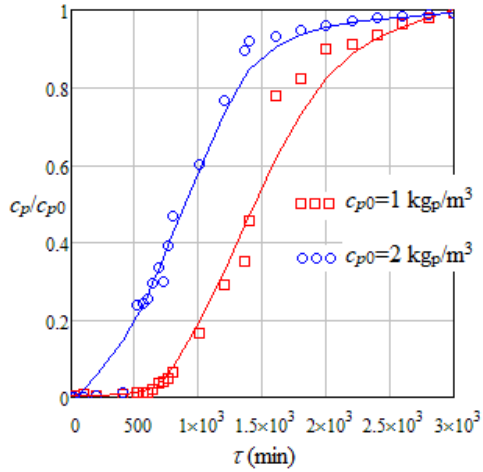


Figure 6.9. Effect of suspended solid concentration in the influent (c_{p0}) on c_p/c_{p0} dynamics ($D = 0.8 \text{ mm}$, $H = 0.4 \text{ m}$, $w = 0.020 \text{ m/s}$, $t = 25^\circ\text{C}$).

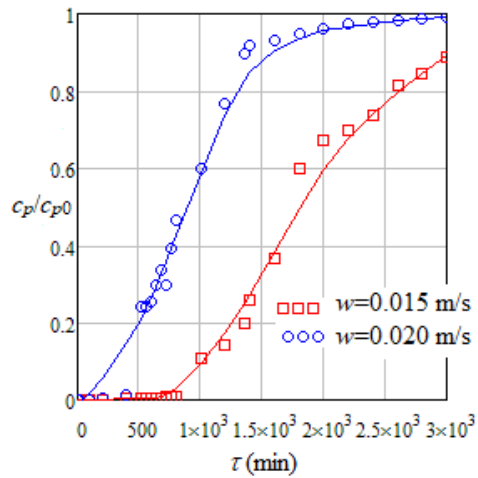


Figure 6.10. Effect of suspension superficial velocity (w) on c_p/c_{p0} dynamics ($D = 0.8 \text{ mm}$, $H = 0.4 \text{ m}$, $c_{p0} = 1 \text{ kg}_p/\text{m}^3$, $t = 25^\circ\text{C}$).

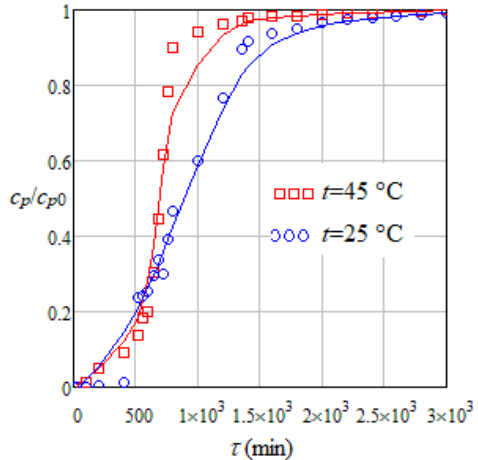


Figure 6.11. Effect of operating temperature (t) on c_p/c_{p0} dynamics ($D = 0.8 \text{ mm}$, $H = 0.4 \text{ m}$, $c_{p0} = 1 \text{ kg}_p/\text{m}^3$, $w = 0.020 \text{ m/s}$).

Based on experimental data shown in figs. 6.7 - 6.11 values of adjustable parameters of FC model (λ_0 , α) and TS stochastic model (β , γ) were determined by minimizing the RMSE expressed by Eqs. (6.54) and (6.60), *i.e.*, $F(\lambda_0, \alpha)$ and $G(\beta, \gamma)$. Table 6.1 contains values of

model parameters under different experimental conditions ($F_{min}(\lambda_0, \alpha) = 0.15 \pm 0.06$ and $G_{min}(\beta, \gamma) = 0.20 \pm 0.02$). By processing the data summarized in Table 6.1, multiple linear relationships (Eqs. (6.62)-(6.65)) were obtained between the model parameters (λ_0 (m⁻¹), α (h⁻¹), β (min⁻¹), and γ (min⁻¹)) and process factors (D (mm), H (m), c_{p0} (kg_p/m³), w (m/s), and t (°C)).

Table 6.1. Effect of process factors (D , H , c_{p0} , w , and t) on characteristic parameters of FC deterministic model (λ_0 , α) and TS stochastic model (β , γ)

No.	D (mm)	H (m)	c_{p0} (kg _p /m ³)	w (m/s)	t (°C)	λ_0 (m ⁻¹)	$\alpha \times 10^3$ (h ⁻¹)	$\beta \times 10^3$ (min ⁻¹)	$\gamma \times 10^3$ (min ⁻¹)
1	0.5	0.4	2	0.020	25	9.19	2.33	3.47	1.01
2	0.8	0.4	2	0.020	25	7.51	3.92	4.87	2.31
3	0.8	0.2	2	0.020	25	13.3	6.54	0.81	3.16
4	0.8	0.4	2	0.020	25	7.84	2.21	1.07	1.76
5	0.8	0.4	1	0.020	25	9.24	2.30	0.77	1.96
6	0.8	0.4	2	0.020	25	7.81	3.21	0.60	1.79
7	0.8	0.4	1	0.015	25	10.4	1.99	0.61	1.53
8	0.8	0.4	1	0.020	25	7.80	3.20	2.19	1.78
9	0.8	0.4	2	0.020	45	7.39	3.96	0.47	2.37
10	0.8	0.4	2	0.020	25	7.79	3.20	2.33	1.79

$$\lambda_0 = 31.6 - 3.60D - 29.1H - 1.73c_{p0} - 212w + 0.01t \quad (6.62)$$

$$\alpha = 0.0004 + 0.0053D - 0.0110H + 0.0016c_{p0} + 0.0660w + 2 \times 10^{-6}t \quad (6.63)$$

$$\beta = -0.0100 + 0.0047D + 0.0200H + 0.0041c_{p0} + 0.0300w - 0.0002 \quad (6.64)$$

$$\gamma = -0.0018 + 0.0043D - 0.0043H + 0.0004c_{p0} + 0.0840w + 3 \times 10^{-6}t \quad (6.65)$$

Tabulated values of model parameters were used to estimate the dynamics of pressure loss for DBSF with a constant filtrate flow rate. In this case the pressure must increase in order to compensate the increase in the pressure loss caused by the deposition of particles in the bed. Dimensionless pressure loss ($\Delta p/\Delta p_0$) was determined using Eq. (6.66) [44], where f (m_p³/m³) is the pore filling degree, ε_b (m³/m_b³) the bed void fraction, ρ_p (kg_p/m_p³) the particle density, and $q_p(x, \tau, \lambda_0, \alpha)$ is given by Eq. (6.67) depending on $c_p(x, \tau, \lambda_0, \alpha)$ (according to Eq. (6.12)).

$$\frac{\Delta p}{\Delta p_0} = \left(1 + \frac{\frac{1}{H} \int_0^H q_p(x, \tau, \lambda_0, \alpha) dx}{f \varepsilon_b \rho_p} \right) \quad (6.66)$$

$$q_p(x, \tau, \lambda_0, \alpha) = w \int_0^\tau \left(-\frac{dc_p(x, \tau, \lambda_0, \alpha)}{dx} \right) d\tau \quad (6.67)$$

Experimental and predicted (FC model) dynamics of $\Delta p/\Delta p_0$ for 2 runs (nos. 7 and 8) in Table 6.1 are presented in fig. 6.12. Suspension superficial velocity was the only process factor that varied in the experimental runs (nos. 7 and 8), *i.e.*, $w_7 = 0.015 \text{ m/s}$ and $w_8 = 0.020 \text{ m/s}$. Measured values of initial pressure loss corresponding to w_7 and w_8 were $\Delta p_{0,7} = 0.28 \text{ bar}$ and $\Delta p_{0,8} = 0.27 \text{ bar}$, respectively. Depicted data reveal an acceptable agreement between experimental and predicted results.

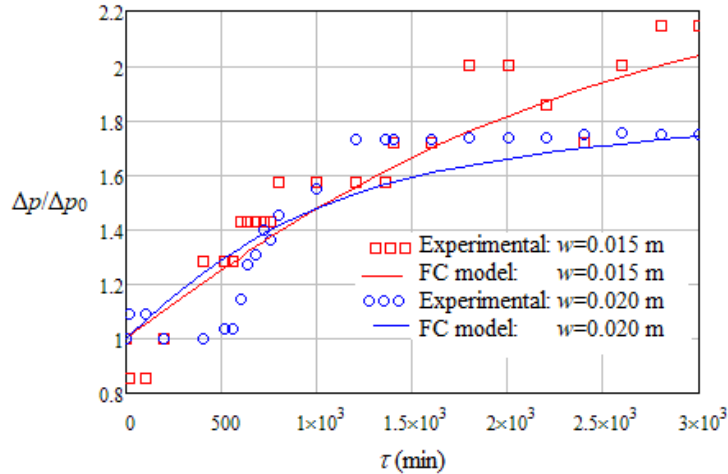


Figure 6.12. Dynamics of pressure loss for DBSF with a constant flow rate ($D = 0.8 \text{ mm}$, $H = 0.4 \text{ m}$, $c_{p0} = 2 \text{ kg}_p/\text{m}^3$, $t = 25^\circ\text{C}$, $f = 0.7 \text{ m}_p^3/\text{m}^3$, $\varepsilon_b = 0.377 \text{ m}^3/\text{m}_b^3$, $\rho_p = 1400 \text{ kg}_p/\text{m}_p^3$)

DBSF of ARW

Physical characteristics of feed and treated ARW, including pH, electrical conductivity, TDS, TSS, activity concentrations of radionuclides (^{60}Co , ^{137}Cs , ^{241}Am , and ^3H) in suspended particles and liquid phase, are summarized in Table 6.2, where MDA represents the minimal detected activity.

Table 6.2. Physical parameters of feed and treated ARW
($D = 0.5 \text{ mm}$, $H = 0.3 \text{ m}$, $w = 0.003 \text{ m/s}$, $t = 25^\circ\text{C}$)

ARW	Feed	Treated
Volume of ARW treated by DBSF (m^3)	0	10
pH	7.10	8.35
Electrical conductivity ($\mu\text{S}/\text{cm}$)	1240	1140
TDS (kg/m^3)	0.720	0.710
TSS (kg_p/m^3)	0.223	0.003
Activity concentration of γ radionuclides in suspended particles (kBq/kg_p)	^{60}Co 9.54 ^{137}Cs 26.85 ^{241}Am 173.62	- - -
in liquid phase (kBq/m^3)	1.49 18.50 0.25	1.12 17.50 0.21
Activity concentration of β radionuclides in liquid phase (kBq/m^3)	^3H 32000	^3H 31900

Values of parameters presented in Table 6.2 highlight an advanced retention of 98.7% (from 0.223 to 0.003 kg_p/m³) of radioactive suspended particles containing γ -emitting radionuclides (⁶⁰Co, ¹³⁷Cs, and ²⁴¹Am) as well as a removal of ⁶⁰Co, ¹³⁷Cs, ²⁴¹Am, and ³H from liquid phase of 24.8, 5.41, 16, and 0.31%, respectively. Bed radioactivities determined by the deposition of radioactive particles loaded with γ -emitting radionuclides and the sorption of radionuclides from the liquid phase were predicted.

Bed radioactivity caused by the deposition of radioactive particles (loaded with γ -emitting radionuclides) on the filtering grains, $r_{b,p}$ (kBq/kg_b), can be expressed by Eq. (6.68), where q_p (kg_p/m_b³) is the mass concentration of particles deposited in the bed, $r_p = 210.01$ kBq/kg_p the particle radioactivity (total activity concentration of γ -emitting radionuclides in the particles), $\rho_b = 1300$ kg_b/m_b³ the bed density, λ_0 (m⁻¹) and α (h⁻¹) the adjustable parameters of FC model estimated by Eqs. (6.62) and (6.63). Space and time variations of bed radioactivity given by Eq. (6.68) are presented in fig. 6.13. Depicted results highlight larger values of $r_{b,p}$ for higher levels of τ and lower levels of x . Moreover, the bed radioactivity is almost constant for $\tau > 2700$ min, indicating that the bed is close to saturation with particles.

$$r_{b,p}(x, \tau, \lambda_0, \alpha) = \frac{q_p(x, \tau, \lambda_0, \alpha)}{\rho_b} r_p \quad (6.68)$$

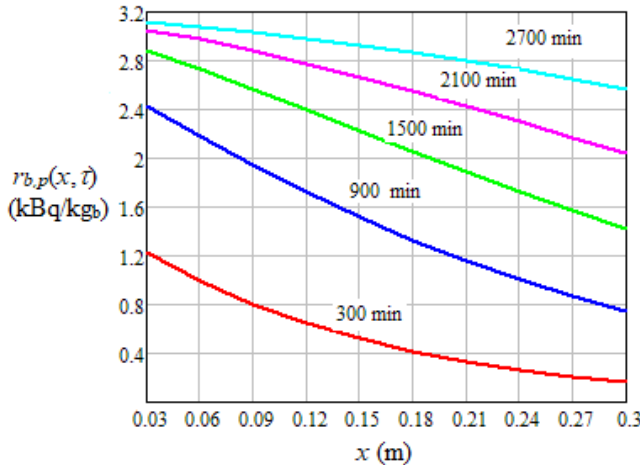


Figure 6.13. Predicted space and time variations of bed radioactivity determined by the deposition of radioactive suspended particles ($d_p > 50$ nm) from ARW on the sand grains ($D = 0.5$ mm, $H = 0.3$ m, $c_{p0} = 0.223$ kg_p/m³, $w = 0.003$ m/s, and $t = 25$ °C).

A deterministic model was developed to describe the sorption of radionuclides (0.1 - 0.3 nm) from ARW on the filtering grains covered by radioactive suspended particles. It consists of equations of mass balance in the filtering bed (Eqs. (6.69)), overall sorption rate (Eq. (6.70)), interface equilibrium (Eq. (6.71)), mass balance in the tank of treated water (Eq. (6.72)), limit and boundary conditions (6.73) - (6.75), where c_j (kBq/m³) and q_j (kBq/m_b³) are the activity concentrations of j radionuclide in the liquid phase and the filtering bed,

respectively, q_p (kg_p/m_b^3) is the mass concentration of particles deposited on the grains, ε_d (m^3/m_d^3) the deposit porosity, ρ_p (kg_p/m_p^3) the particle density, and * superscript denotes the equilibrium state. Adjustable model parameters, *i.e.*, transfer coefficient (k_{tj}) and distribution coefficient (k_{dj}) of j species, were fitted based on experimental dynamics of dimensionless concentration of j radionuclide (^{60}Co , ^{137}Cs , ^{241}Am , and ^3H) in the collecting tank (c_j^c/c_{j0}), which are presented in fig. 6.14.

$$\frac{\partial}{\partial \tau} \left(\varepsilon_b - \frac{q_p}{(1-\varepsilon_d)\rho_p} \right) c_j + w \frac{\partial c_j}{\partial x} = - \frac{\partial q_j}{\partial \tau} \quad (6.69)$$

$$\frac{\partial q_j}{\partial \tau} = \frac{6 \left(1 - \varepsilon_b + \frac{q_p}{(1-\varepsilon_d)\rho_p} \right)}{D} k_{tj} \left(\varepsilon_b - \frac{q_p}{(1-\varepsilon_d)\rho_p} \right) (c_j - c_j^*) \quad (6.70)$$

$$c_j^* = k_{dj} q_j \quad (6.71)$$

$$\frac{dc_j^c}{d\tau} = \frac{c_j(H, \tau)}{\tau} \quad (6.72)$$

$$\tau = 0 \quad 0 \leq x \leq H \quad c_j(0, x) = 0 \quad q_j(0, x) = 0 \quad (6.73)$$

$$\tau > 0 \quad x = 0 \quad c_j(0, \tau) = c_{j0} \quad q_j(0, \tau) = q_{j0}^* \quad (6.74)$$

$$\tau = 0 \quad c_j^c(0) = 0 \quad (6.75)$$

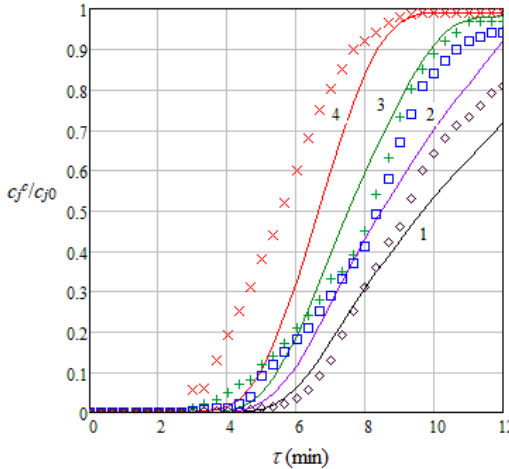


Figure 6.14. Experimental (points) and predicted (line) dynamics of dimensionless concentration of radionuclides ((1) ^{60}Co , (2) ^{137}Cs , (3) ^{241}Am , (4) ^3H) in the collecting tank ($c_{Co,0} = 1.49 \text{ kBq/m}^3$, $c_{Cs,0} = 18.50 \text{ kBq/m}^3$, $c_{Am,0} = 0.25 \text{ kBq/m}^3$, $c_{H,0} = 32000 \text{ kBq/m}^3$, $D = 0.5 \text{ mm}$, $H = 0.3 \text{ m}$, $c_{p0} = 0.223 \text{ kg}_p/\text{m}^3$, $w = 0.003 \text{ m/s}$, and $t = 25^\circ\text{C}$).

A procedure similar to those reported for fixed bed sorption [58 - 62]) was used to identify the model parameters. Algorithm steps were as follows: (i) a set of k_{dj} and k_{tj} values, where k_{tj} value was estimated by assuming $Sh_j = 2$ [63, 64] was selected; (ii) $c_j(H, \tau)$ dynamics

were predicted depending on k_{dj} and k_{tj} values according to Eqs. (6.69) - (6.71); (iii) a logistic function (6.76) was used to express analytically the dependence between c_j and τ ; characteristic parameters of logistic function, *i.e.*, ϕ_j , χ_j , and τ_{sj} , were fitted based on $c_j(H, \tau)$ predicted breakthrough curve; (iv) $c_j^c(\tau)$ dynamics were simulated by integrating Eq. (6.75); (v) it was established the correctness of values by comparing the experimental and simulated data; if they were in a good agreement, k_{dj} value was considered as acceptable; otherwise, another value of k_{dj} was selected and the algorithm was repeated.

$$c_j(H, \tau) = \frac{e^{\phi_j + \chi_j(\tau - \tau_{sj})}}{1 + e^{\phi_j + \chi_j(\tau - \tau_{sj})}} \quad (6.76)$$

Values of k_{dj} , k_{tj} , ϕ_j , χ_j , and τ_{sj} parameters corresponding to the experimental conditions ($c_{Co,0} = 1.49 \text{ kBq/m}^3$, $c_{Cs,0} = 18.50 \text{ kBq/m}^3$, $c_{Am,0} = 0.25 \text{ kBq/m}^3$, $c_{H,0} = 32000 \text{ kBq/m}^3$, $D = 0.5 \text{ mm}$, $H = 0.3 \text{ m}$, $c_{p0} = 0.223 \text{ kg}_p/\text{m}^3$, $w = 0.003 \text{ m/s}$, and $t = 25^\circ\text{C}$) are summarized in Table 6.3. High values of k_{dj} ($300\text{-}2500 \text{ m}_b^3/\text{m}^3$) indicate low equilibrium activity concentrations of radionuclides retained in the filtering bed. Experimental and predicted dynamics of dimensionless radionuclide concentration in the collecting tank (fig. 6.14) highlight an acceptable agreement.

Table 6.3. Characteristic parameters of multicomponent sorption model for ARW processing by DBSF

j	Radioactive species	k_{dj} (m_b^3/m^3)	$k_{tj} \times 10^5$ (m/s)	τ_{sj} (s)	ϕ_j (-)	χ_j (s^{-1})
1	^{60}Co	300	0.95	240	-8.928	0.069
2	^{137}Cs	800	0.98	230	-7.261	0.069
3	^{241}Am	1400	1.05	210	-6.982	0.062
4	^3H	2500	1.15	160	-8.564	0.058

Simulations of activity concentration of j radionuclide in the filtering bed (q_j), which are presented in fig. 6.15, highlight a rapid saturation (after about 10 min) of the bed with radionuclides transferred from the liquid phase. Saturation activity concentrations of radionuclides in the filtering bed, are as follows: $q_{Co,s} = 4.7 \times 10^{-3} \text{ kBq/m}_b^3$, $q_{Cs,s} = 23 \times 10^{-3} \text{ kBq/m}_b^3$, $q_{Am,s} = 0.18 \times 10^{-3} \text{ kBq/m}_b^3$, and $q_{H,s} = 13 \text{ kBq/m}_b^3$. Accordingly, saturation bed radioactivity caused by the sorption of radionuclides on the filtering grains, given by Eq. (6.77), is $r_{b,r} = 0.01 \text{ kBq/kg}_b$. After 600 min, corresponding to a treated ARW volume of 10 m^3 at $w = 0.003 \text{ m/s}$ ($G_V = 1 \text{ m}^3/\text{h}$), this value is significantly lower than those predicted for the bed radioactivity determined by the deposition of radioactive particles (fig. 6.13), *i.e.*, $r_{b,p} = 0.5 \text{ - } 1.8 \text{ kBq/kg}_b$, and it can be considered as negligible.

$$r_{b,r} = \frac{\sum_{j=1}^3 q_{j,s}}{\rho_b} \quad (6.77)$$

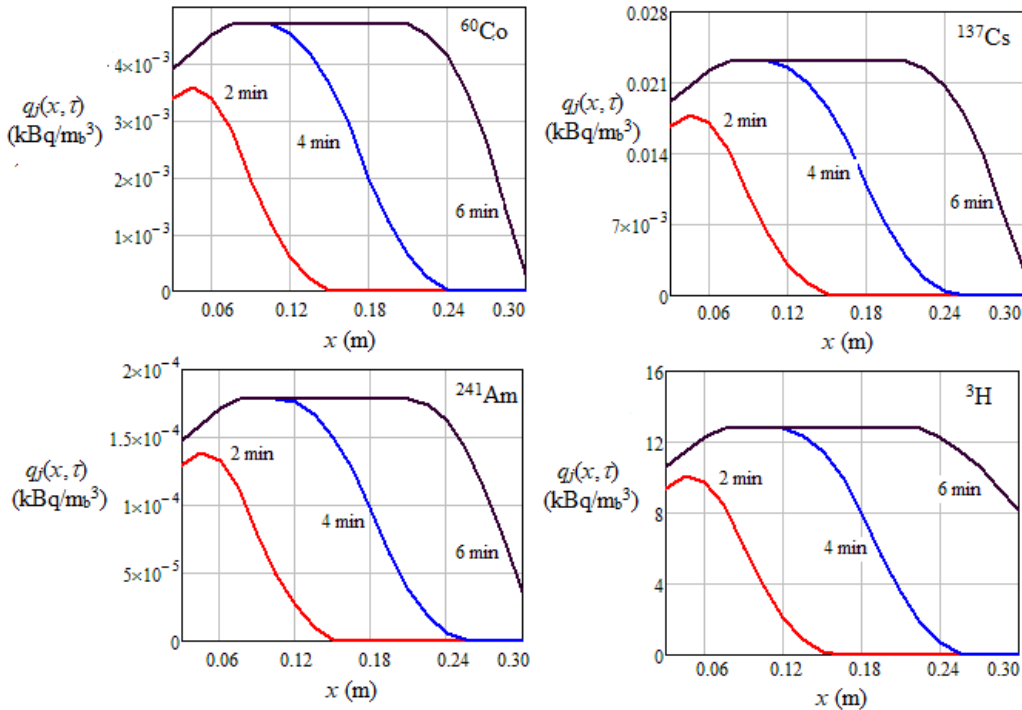


Figure 6.15. Predicted space and time variations of activity concentration of j radionuclide in the filtering bed for radionuclide sorption from liquid phase ((1) ^{60}Co , (2) ^{137}Cs , (3) ^{241}Am , (4) ^3H) ($c_{Co,0} = 1.49 \text{ kBq/m}^3$, $c_{Cs,0} = 18.50 \text{ kBq/m}^3$, $c_{Am,0} = 0.25 \text{ kBq/m}^3$, $c_{H,0} = 32000 \text{ kBq/m}^3$, $D = 0.5 \text{ mm}$, $H = 0.3 \text{ m}$, $c_{p0} = 0.223 \text{ kg}_p/\text{m}^3$, $w = 0.003 \text{ m/s}$, and $t = 25^\circ\text{C}$)

6.4. Conclusions

Numerous mathematical models have been developed to estimate removal efficiency of deep bed filters. Microscopic models were used to compute the initial removal efficiency. These models are able to predict the removal efficiency under favorable filtration conditions quantitatively, but they underestimate the removal efficiency under unfavorable conditions. Thereby, semi-empirical formulations were developed to assess initial removal efficiency under unfavorable conditions. Also, the introduction of some correction factors improved the results obtained for removal efficiency. Macroscopic models considering the removal of particles under favorable conditions and the accumulation of impurities on the filter grains during the transient stages were also developed.

The problem of ARW containing fine suspended solids by deep filtration is analyzed by modelling and experimental investigation. The experimental investigation was oriented so that it allows identification of the parameters of the models considered for characterization of fine solids retention and radionuclides sorption in a sand bed. Performances of aqueous

suspension treatment by rapid sand filtration were measured and predicted. Diluted suspensions of clay particles ($20 \mu\text{m}$) were processed by DBSF under different experimental conditions. A faster saturation of the bed was attained for higher levels of sand grain size ($D = 0.5, 0.8 \text{ mm}$), suspended solid concentration in the influent ($c_{p0} = 1, 2 \text{ kg}_p/\text{m}^3$), suspension superficial velocity ($w = 0.015, 0.020 \text{ m/s}$), and operating temperature ($t = 25, 45^\circ\text{C}$) as well as a lower value of bed depth ($H = 0.2, 0.4 \text{ m}$).

A semiempirical deterministic model and a stochastic one were used to describe the deposition of clay particles on the sand grains. Adjustable model parameters were fitted based on experimental data and correlated by multiple linear relationships with the process factors. These correlations were used to predict the pressure loss dynamics and the bed radioactivity dynamics due to the deposition of radioactive solid particles ($> 50 \text{ nm}$) from ARW. By processing an ARW volume of 10 m^3 by DBSF ($D = 0.5 \text{ mm}$, $H = 0.3 \text{ m}$, $c_{p0} = 0.223 \text{ kg}_p/\text{m}^3$, $w = 0.003 \text{ m/s}$, and $t = 25^\circ\text{C}$), a removal of 98.7% of suspended particles containing ^{60}Co , ^{137}Cs , and ^{241}Am was achieved.

A deterministic model based on mass balance, kinetic, and interface equilibrium equations was developed to describe the multicomponent sorption of ^{60}Co , ^{137}Cs , ^{241}Am , and ^3H radionuclides ($0.12 - 0.30 \text{ nm}$) from ARW on the sand grains covered by radioactive suspended particles. An algorithm was considered to determine the model parameters from experimental data. Simulated results highlighted that the bed was saturated with radionuclides after about 10 min. For a treated ARW volume of 10 m^3 , saturation bed radioactivity caused by the sorption of radionuclides (0.01 kBq/kg_b) was 50 - 180 times lower than the bed radioactivities determined by the deposition of radioactive particles.

ARW treated by DBSF can be further processed by ion exchange, fixed bed adsorption or membrane-based techniques (*e.g.*, ultrafiltration, reverse osmosis). The models developed to describe DBF process could be coupled with characteristic models of further ARW processing for predicting the performances of integrated separations/purifications.

REFERENCES

- [1] C. Tien, *Classification of Filtration Processes* in *Principles of filtration 1st edition*, Elsevier, 3-6, 2012
- [2] T. Sparks, G. Chase, *Other Separation Precesses and Equipment* in *Filters and Filtration Handbook 6th Edition*, Elsevier, 361-380, 2015
- [3] T. Iwasaki, *Some notes on sand filtration*, J. Am. Water Works Assoc., **29(5)**, 1591–1602, 1937
- [4] D.M. Mints, *Kinetics of filtration of low-concentration water suspensions in water purification filters*, Doklady Akademii Nauk SSSR **78(2)**, 315–318, 1951
- [5] A. Amirtharajah, *Some theoretical and conceptual views of filtration*, J. Am. Water Works Assoc. **80**, 36–46, 1988
- [6] G. Keir, V. Jegatheesan, S. Vigneswaran, *Deep Bed Filtration: Modelling Theory and Practice in Waste Water Treatment Technologies*, S. Vigneswaran (ed), EOLSS Publishers, Oxford, 263-307, 2009
- [7] J. P. Herzig, D. M. Leclerc ,P. Le Goff, *Flow of suspension through porous media-application to deep filtration*, J. Ind. Eng. Chem., **65(5)**, 8-35, 1970
- [8] A. Zamani, B. Maini, *Flow of dispersed particles through porous media — Deep bed filtration*, J. Pet. Sci. Eng., **69**, 71–88, 2009
- [9] K.J. Ives, *Rapid filtration*, Water Research, **4**, 201–223, 1970
- [10] V. Gitis, I. Rubinstein, M. Livshits, G. Ziskind, *Deep-bed filtration model with multistage deposition kinetics*, Chem. Eng. J., **163**, 78–85, 2010
- [11] Y.S. Polyakov, *Phenomenological theory of depth membrane filtration*, Chem. Eng. Sci., **62**, 1851-1860, 2007
- [12] M.M. Sharma, Y.C. Yortsos, *A network model for deep bed filtration processes*, AIChE J., **33(10)**, 1644-1653, 1987
- [13] M. Elimelech, X. Jia, J. Gregory, R. Williams, *Modelling of particle deposition onto ideal collectors* in *Particle Deposition and Aggregation:, Measurement, Modelling, and Simulation*, Butterworth-Heinemann, Oxford/Boston, 113-154, 1995
- [14] Y. S. Kim, A. Whittle, *Filtration in a Porous Granular Medium: 1. Simulation of Pore-Scale Particle Deposition and Clogging*, Transport in Porous Media, **1**, 53–87, 2006
- [15] K.C. Khilar, H.S Fogler, *Practical Consequences of Release and Migration of Fines in Porous Media* in *Migration of Fines in Porous Media*, Kluwer Academic Publishers, Dordrecht–Boston–London, 1-8, 1998
- [16] D.J Logan, *Filtration ModelsTransport in Modelling in Hydrogeochemical Systems*, Springer-Verlag New York, 113-134, 2001
- [17] O. F. Eker, F. Camci, and I. K. Jennions, *Physics-Based Degradation Modelling for Filter Clogging*, The 2nd European Conference of the Prognostics and Health Management Society, July 8-10, 2014, Nantes, France

- [18] S. Pang, M.M. Sharma., *A model for predicting injectivity decline in water injection wells*, 69th Annual Technical Conference and Exhibition, September 25–28, 1994; New Orleans, USA
- [19] K.E. Wennberg, M.M. Sharma, *Determination of the filtration coefficient and the transition time for water injection*, Proceedings of the SPE European Formation Damage Conference, June 2–3, 1997, The Hague, The Netherlands
- [20] T. Harter, S. Wagner, *Colloid transport and filtration of Cryptosporidium parvum in sandy soils and aquifer sediments*, Environ. Sci. Technol., **34(1)**, 62–70, 2000
- [21] P.G. Bedrikovetsky, D. Marchesin, F. Checaira, , A.L. Serra, E Resende, *Characterization of deep bed filtration system from laboratory pressure drop measurements*, J. Pet. Sci. Eng., **64(4)**, 167–177, 2001
- [22] M. Elimelech, C. R. O'Melia, *Effect of particle size on collision efficiency in the deposition of Brownian particles with electrostatic energy barriers*, Langmuir, **6(6)**, 1153–1163, 1990
- [23] H. Fallah, H. B. Fathi, H. Mohammadi, *The Mathematical Model for Particle Suspension Flow through Porous Medium*, Geomaterials, **2**, 57-62, 2012
- [24] N. Tufenkji, J.A. Redman, M. Elimelech, *Interpreting deposition patterns of microbial particles in laboratory-scale column experiments*, Environ Sci Technol., **37(3)**, 616-623, 2003
- [25] S.A. Bradford, N. Toride, *A Stochastic Model for Colloid Transport and Deposition*, J. Environ. Qual., **36**, 1346-1356, 2007
- [26] J.S. Chang, S. Vigneswaran, J.K. Kandasamy, L.J. Tsai, *Effect of Pore Size and Particle Size Distribution on Granular Bed Filtration and Microfiltration*, Sep. Sci. Technol., **43**, 1771-1784, 2008
- [27] B. Berkowitz, A. Cortis, M. Dentz, H. Scher, *Modelling non-Fickian transport in geological formations as a continuous time random walk*, Rev. Geophys., **44**, 1-49, 2006
- [28] G. Kosakowski, B. Berkowitz, H. Scher, *Analysis of field observations of tracer transport in a fractured till*, J. Contam. Hydrol., **47**, 29–51, 2001
- [29] N. Tufenkji, M. Elimelech, *Breakdown of Colloid Filtration Theory: Role of the Secondary Energy Minimum and Surface Charge Heterogeneities*, Langmuir **21(3)**, 841–852, 2005
- [30] A. Cortis, *Péclet-dependent memory kernels for transport in heterogeneous media*, Physical Review E **76**, RG2003, 2007
- [31] A. Cortis, Y. Chen, H. Scher, B. Berkowitz, *Quantitative characterization of pore-scale disorder effects on transport in “homogeneous” granular media*, Physical Review E **70**, 041108, 2004
- [32] R. Farajzadeh, *An Experimental Investigation into Internal Filtration and External Cake Build Up*, MSc. Thesis, Delft University of Technology, The Netherlands, 2004
- [33] J. Litwiniszyn, *The Model of a Random Walk of Particles Adapted to Researches on Problems of Mechanics of Loose Media*, Bulletin de L' Académie Polonaise des Sciences Techniques, **11**, 593-602, 1963

- [34] C. Tien, *Macroscopic Description of FixedBed Granular Filtration in Granular Filtration of Aerosols and Hydrosols: Butterworths Series in Chemical Engineering*, Howard Brenner (Ed.), Butterworth-Heinemann, 17-47, 2013
- [35] L. T. Fan, R. Nassar, S. H. Hwang, S. T. Chou, *Analysis of Deep Bed Filtration Data: Modelling as a Birth-Death Process*, AIChE J., **31(11)**, 1781-1790, 1985
- [36] T. Dobre., J.M. Sanchez., *Stochastic mathematical modelling in Chemical Engineering Modelling*, Simulation and Similitude, Wiley VCH, 180-308, 2007
- [37] O. Iordache, *Compound stochastic Processes Applied in Transport Phenomena*, Romanian Academy, Bucharest, 1981
- [38] R.S. Cushing, D.F Lawler, *Depth filtration: Fundamental investigation through three-dimensional trajectory analysis*, Environ. Sci. Tehnol., **32**, 3793–3801, 1988
- [39] B. Ding, C. Li, Y. Wang, J. Xu, *Effects of pore size distribution and coordination number on filtration coefficients for straining-dominant deep bed filtration from percolation theory with 3D networks*, Chem. Eng. Sci. **175**, 1–11, 2018
- [40] V. Gitis, I. Rubinstein, M. Livshits, G. Ziskind, *Deep-bed filtration model with multistage deposition kinetics*, Chem. Eng. J. **163**, 78–85, 2010
- [41] K.J. Ives, *Filtration of clay suspensions through sand*, Clay Miner. **22**, 49–61, 1987
- [42] V. Jegatheesan, S. Vigneswaran, *Deep bed filtration: Mathematical models and observations*, Crit. Rev. Environ. Sci. Technol. **35**, 515–569, 2005
- [43] S.D. Rege, H.S. Fogler, *A network model for deep bed filtration of solid particles and emulsion drops*, AIChE J. **34(11)**, 1761-1772, 1988
- [44] A. Rushton, A.S. Ward, R.G. Holdich, *Solid-Liquid Filtration and Separation Technology 2nd, completely revised edition*, Wiley VCH, Weinham, 2000
- [45] R. Šećerov Sokolović, S. Sokolović, D. Govendarica, *Performance of expanded polystyrene particles in deep bed filtration*, Sep. Purif. Technol. **68(2)**, 267-272, 2009
- [46] A. Vaz, P. Bedrikovetsky, P.D. Fernandes, A. Badalyan, T. Carageorgos, *Determining model parameters for non-linear deep-bed filtration using laboratory pressure measurements*, J. Pet. Sci. Eng. **151**, 421–433, 2017
- [47] J. Altmann, D. Rehfeld, K. Träder, A. Sperlich, M. Jekel, *Combination of granular activated carbon adsorption and deep-bed filtration as a single advanced wastewater treatment step for organic micropollutant and phosphorus removal*, Water Res. **92**, 375-383, 2016
- [48] C.P. Huang, T.Y. Lin, L.H. Chiao, H.B. Chen, *Characterization of radioactive contaminants and water treatment trials for the Taiwan Research Reactor's spent fuel pool*, J. Hazard. Mat. **233–234**, 140-147, 2012
- [49] J. Löwenberg, A. Zenker, T. Krahnstöver, M. Boehler, M. Baggenstos, G. Koch, T. Wintgens, *Upgrade of deep bed filtration with activated carbon dosage for compact micropollutant removal from wastewater in technical scale*, Water Res. **94**, 246-256, 2016

- [50] EPA (Environmental Protection Agency), *Water Treatment Manuals–Filtration*, Ardcavan, Wexford, Ireland, 1995.
- [51] R.O.A. Rahman, H.A. Ibrahium, Y.T. Hung, *Liquid radioactive wastes treatment: A review.*, Water **3**, 551-565, 2011
- [52] DOE HDBK-1169-2003, *Nuclear Air Cleaning Handbook*, U.S. Department of Energy, Washington DC 20585, USA, 2003
- [53] A.H. Ali, S.H. Othman, *A physico-chemical parametric study on the retention of radioactive ions in a fixed bed reactor*, Chem. Eng. J. **178**, 374-385, 2011
- [54] C.Tien, A.C. Payatakes, *Advances in deep bed filtration*, AIChE J. **25(5)**, 737-759, 1979
- [55] Z. You, P. Bedrikovetsky, L. Kuzmina, *Asymptotic model for deep bed filtration*, Chem. Eng. J. **258**, 374–385, 2014
- [56] O. Iordache, *Polystochastic Models in Chemical Engineering*. VNU Science Press, Utrecht, the Netherlands, 1987
- [57] G. Andrew, G.B Mathews, *A Treatise on Bessel Functions and Their Applications to Physics*. Forgotten Books, www.forgottenbooks.com., 2016
- [58] T. Dobre, O.C. Pârvulescu, L. Calotă, I. Jipa, *Modelling of fixed bed multicomponent ion exchange*, Rev. Chim. (Bucharest), **61(2)**, 213-217, 2010
- [59] A. Miura, *Determination of cesium adsorption breakthrough curves using carbonized rice hull and beech sawdust as adsorbents*, Environment and Ecology Research **5(6)**, 461-466, 2017
- [60] A. Negrea, L. Lupa, M. Ciopec, P. Negrea, *Experimental and modelling studies on As (III) removal from aqueous medium on fixed bed column*, Chem. Bull. POLITEHNICA Univ. (Timisoara) **56(70)**, 89-93, 2011
- [61] T.W. Weber, R.K. Chakravorti, *Pore and solid diffusion models for fixed-bed adsorbers*, AIChE J. **20(2)**, 228-238, 1974
- [62] S. Gupta, B.V. Babu, *Experimental investigations and theoretical modelling aspects in column studies for removal of Cr (VI) from aqueous solutions using activated tamarind seeds*, J. Water Resource Prot. **2**, 706-716, 2010
- [63] J.R.F. Guedes de Carvalho, J.M.P.Q. Delgado, M.A. Alves, *Mass transfer between flowing fluid and sphere buried in packed bed of inerts*, AIChE J. **50(1)**, 65-74, 2004
- [64] P. Stoodley, S. Yang, H. Lappin-Scott, Z. Lewandowski, *Relationship between mass transfer coefficient and liquid flow velocity in heterogenous biofilms using microelectrodes and confocal microscopy*, Biotechnol. Bioeng. **56(6)**, 681-688, 1997

CHAPTER 7. CONCLUSIONS AND DIRECTIONS FOR FUTURE RESEARCH

Liquid waste generated at nuclear facilities requires treatment for removal of radioactive contaminants. In liquid radioactive waste processing, as a rule, two major problems are to be solved:

(1) decontamination from radionuclides and harmful chemical substances to levels prescribed by regulations and

(2) reduction of the volume of secondary radioactive waste to a maximum possible extent. Judicious approach to these issues considerably reduces the cost of waste management. In these circumstances, an extensive research addressed to a broad scale of treatment techniques dedicated to both solid and liquid waste treatment should be in attention of each waste processor in order to achieve the best results. The types and quantities of radioactive waste varie from country to country. Their generation depends on the scale of applications and activities associated with nuclear and radioactive material use in that country.

The nuclear industry and institutional applications of radioisotopes produce a broad sweeping of low and intermediate level liquid radioactive waste. These liquid waste may vary considerably in volume, radioactivity and chemical composition, hence, a wide range of treatment methods has been used by the waste processors to treat these waste. Treatment methods applicable to ARW purification are the ones commonly used as conventional processes for industrial and municipal water treatment. These methods include chemical treatment, adsorption, filtration, ion exchange and evaporation. But they have some disadvantages, such as the inability to eliminate all contaminants or high operating costs, especially in the case of evaporation, that involves also large quantities of secondary solid waste. In trend are modular approach, meaning systems that consist of specially designed modules that can be assembled in particular configurations to address the special chemical and radioactive characteristics of the waste. Because of the large variations in the influent wastewater flow rate, concentration and composition, wastewater treatment processes are innately dynamic. In general, a better understanding of the dynamic behavior of the process, adequate mathematical models and identification of model parameters allow to solve operational problems and to reduce operational costs.

As described in this thesis following treatment methods: deep bed filtration, ultrafiltration, reverse osmosis and Cs^+ sorption on a selective inorganic sorbent, were investigated as candidate methods to be combined in an ARW treatment system. Mathematical models were constructed and experimental studies were conducted to find suitable models and corresponding identification algorithms for their parameters. A

commercial RO membrane was tested for ARW treatment and membrane performance was determined.

Significant contributions of this work are:

1. A semiempirical deterministic model and a stochastic one were used to describe the deposition of clay particles on the sand grains. Adjustable model parameters were fitted based on experimental data and correlated by multiple linear relationships with the process factors. These correlations were used to predict the pressure loss dynamics and the bed radioactivity dynamics due to the deposition of radioactive solid particles (> 50 nm) from ARW. By processing an ARW volume of 10 m^3 by DBSF ($D = 0.5 \text{ mm}$, $H = 0.3 \text{ m}$, $c_{p0} = 0.223 \text{ kg}_p/\text{m}^3$, $w = 0.003 \text{ m/s}$, and $t = 25 \text{ C}$), a removal of 98.7% of suspended particles containing ^{60}Co , ^{137}Cs , and ^{241}Am was achieved.

A deterministic model based on mass balance, kinetic, and interface equilibrium equations was developed to describe the multicomponent sorption of ^{60}Co , ^{137}Cs , ^{241}Am , and ^3H radionuclides (0.12 - 0.30 nm) from ARW on the sand grains covered by radioactive suspended particles. An algorithm was considered to determine the model parameters from experimental data. Simulated results highlighted that the bed was saturated with radionuclides after about 10 min. For a treated ARW volume of 10 m^3 , saturation bed radioactivity caused by the sorption of radionuclides (0.01 kBq/kg_b) was 50 - 180 times lower than the bed radioactivities determined by the deposition of radioactive particles.

So, ARW treated by DBSF need further treatment for complete removal of all contaminants.

2. The experimental investigation of an ultrafiltration process using a spiral-wound polysulphonamide membrane was performed. The influence of process factors on its performances was quantified using a 2^3 factorial plan. Regression equations shown below were obtained and applied to predict the values of permeate flux and TSS at levels of process factors in the ranges considered in the experimental study.

$$j_P = 118.25 + 4.50x_1 + 67.25x_2 - 8x_3 + 2.75x_1x_3 - 4.50x_2x_3$$

$$TSS_P = 10.662 - 3.287x_1 - 2.688x_2 + 9.438x_3 - 2.413x_1x_3 - 2.413x_2x_3$$

A simulated aqueous waste obtained by adding of fresh clay in actual waste was used to estimate the effect of solid concentration of processed ARW on membrane clogging. A generator function of random variable n (blocked pores number at membrane surface) was built to express the time evolution of the permeate flow rate. The clogging parameters, α and β , were identified by experimental measurements, minimizing mean quadratic deviation between the experimental and calculated permeate specific flow rate.

A mathematical model of ultrafiltration device composed by a system with 13 differential equations completed with algebraic equations was established to describe the concrete action of units of ultrafiltration device and a numerical simulation process was initiated in order to be used as a powerful tool to increase the understanding of this process.

3. A commercial membrane, Hydranautics SWC1-4040 RO membrane, was tested for ARW treatment. The membrane was found to be sensitive to various operating parameters such as feed ARW pressure, pH and temperature. Maximum flux and salt rejection were obtained at 4 MPa, but the permeate flux decreases rapidly at this pressure value. Because RO is a pressure-driven process and the main energy consumers in any membrane desalination plant are the high pressure pumps, an operating pressure of 2.5 MPa was selected in order to reduce the energy required and, consequently, the costs.

The results obtained have shown a severe decrease in time of the permeate flux in the case of feed waste with neutral or high pH. For a low pH (acidic conditions), the permeate flux remained almost constant and, fortunately, permeate conductivity and salt rejection also increased. An increased waste temperature leads to an increased permeate flux, but with an inappropriate quality due to salt rejection decrease..

So, RO membrane has shown to be effective in rejecting dissolved species while maintaining higher flux, but the feed ARW requires pretreatment like ultrafiltration and pH adjustment.

Based on membrane performance, during these experiments has been gathered the key technical information and have been determined the acceptable limits for parameters variability for which treatment process meets a good performance. A more rigorous approach requests the determination of the variation in membrane properties with time. Long-term experiments to study the fouling effects on the performance and economy of the process are both complex and interesting and may be more useful area for future research.

4. Potassium nickel ferrocyanide, precipitated on silica gel particles was tested as inorganic ion exchange material for the removal of cesium ions from ARW. Batch experiments were performed under kinetic and equilibrium condition. The kinetic was experimentally studied and the obtained rate data were analyzed using simple kinetic models. The value 0.999, obtained for the correlation coefficient, R^2 , and agreement of calculated and amount of ions adsorbed per unit mass of sorbent at equilibrium, q_e , with experimental data lead to the conclusion that pseudo second-order sorption mechanism is dominant and the overall rate constant of sorption process appeared to be controlled by a chemical sorption process.

Equilibrium isotherms have been determined and tested for different isotherm expressions and the sorption data were successfully modelled using Langmuir and Freundlich approaches. The Langmuir separation factor R_L value for Cs^+ was found to be 0.019, indicating a favorable

sorption process. The Freundlich intensity constant n was greater than unity indicating an increase in sorption tendency at increasing of Cs species concentration.

R^2 values determined, 0.9955 for Langmuir model and 0.9946 for Freundlich model do not allow the selection of a certain model but can be accepted that Langmuir isotherm honourable covers experimental data. In this situation it can be accepted that adsorption behavior of Cs species onto investigated sorbent appears to be homogeneous rather than heterogeneous.

The values of thermodynamic parameters were calculated and indicated the endothermic and spontaneous nature of this sorption process.

Fixed-bed column experiments were conducted and, on the basis of the experimental results the adsorption of PNF-SG was found to be dependent on the flow rate, the initial Cs concentration and bed height. All investigated experimental conditions show that the prediction of complete breakthrough curve was effective with Thomas and Yoon–Nelson models. Values of R^2 of the breakthrough curves obtained, in the ranges 0.9470 to 0.9996 for Thomas model and 0.9415 and 0.9996 for Yoon–Nelson model, shown that both models can be used to describe the behavior of Cs ion exchange on potassium nickel ferrocyanide, precipitated on silica gel, in a fixed-bed column.

So, the behavior of the potassium nickel ferrocyanide, precipitated on silica gel and the determined coefficients of the models for different operating conditions can be used to scale up the process.

The results obtained and presented here can form a tool that allows the investigation of the ARW treatment in a modular installation without performing – or at least reducing the number of – practical experiments that could involve time, extra-costs and, very important, works in radioactive environments. The mathematical models can be very helpful in order to develop a library of mathematical models able to reproduce the behavior of ARW treatments. In addition, this knowledge may be very useful in the upgrading of the existing treatment plants or in the design of the plants to be constructed in the future. For instance, the need for chemical treatment in different treatment stages involves the design of intermediate tanks, possibility of homogenization, prelevation points etc.

In this research, each separation method was treated in isolation from the rest of the process plant. In reality, a combination of treatment modules can be used so as the system can be easily customised to the specific ARW quality. The interaction with other modules and equipment will have a significant impact on the productivity of the separation system. Obviously, approaching the problem as a whole will provide a much better solution than if each module is considered independently. Information as equipment type and size, flow-sheet

layout, environment variables, nominal operating conditions have an important influence and have to be taken into account.

Recommendations for further research identified during this work and given in this report have the aim to suggest future research areas to be approached in order to obtain a better understanding of the effectiveness of the purification methods in order to find the optimal operation regime and flow-sheet layout.

AUTHOR RESEARCH CONTRIBUTIONS

1. Tanase DOBRE, **Laura Ruxandra ZICMAN**, Oana Cristina PARVULESCU, Elena NEACSU, Catalin CIOBANU, Felicia Nicoleta DRAGOLICI , *Species removal from aqueous radioactive waste by deep-bed filtration* Environmental Pollution, Volume **241**, October 2018, Pages 303–310 (**IF 4.358**)
2. **Laura Ruxandra ZICMAN**, Elena NEACSU, Felicia Nicoleta DRAGOLICI, Catalin CIOBANU, Gheorghe DOGARU, Oana Cristina Parvulescu, Tanase DOBRE, *Experimental and Modelling of Aqueous Radioactive Waste Treatment by Ultrafiltration*, REV.CHIM.(Bucharest), **69**, No. 5, 2018 (**IF = 1.412**)
3. **Laura Ruxandra ZICMAN**, Elena NEACSU, Laurentiu DONE, Liviu Cornel TUGULAN, Carmela ALEXANDRU, Felicia Nicoleta DRAGOLICI, Mihaela NICU, Laura Florina IONASCU, Bogdan Tudor OBREJA, Gheorghe DOGARU, Tanase DOBRE, *Investigation and modeling of fixed bed cesium sorption on nickel ferrocyanide precipitated on silica gel*, Romanian Journal of Physics **62**, 806 (2017) (**IF = 1.433**)
4. Mihaela NICU, Laura IONASCU, Felicia DRAGOLICI, Elena NEACSU, **Laura ZICMAN**, Bogdan OBREJA, *Comparison study of inorganic cements to the conditioning of the secondary radioactive waste*, Romanian Journal of Physics **62**, 805 (2017) (**IF = 1.433**)
5. **Laura Ruxandra ZICMAN**, Elena NEACSU, Laurentiu DONE, Felicia Nicoleta DRAGOLICI, Tanase DOBRE, *Effect of process factors on the performances of reverse osmosis process in an aqueous radioactive waste treatment plant*, U.P.B. Sci. Bull., Series B, Vol. **79**, Iss. 4, p 143-156, 2017 (**ISSN 1454-2331**)
6. Bogdan Tudor OBREJA, Elena NEACSU, Laurentiu DONE, Felicia DRAGOLICI, Liviu TUGULAN , **Laura ZICMAN** , Daniel SCRADAENAU, *Evaluation of environmental monitoring data at low and intermediate-level radioactive waste repository Baia, Bihor, Romania* , Romanian Journal of Physics , Vol. **61**, Nos. 3–4, p. 718–727, Bucharest, 2016 (**IF = 1.398**)
7. **Laura Ruxandra ZICMAN**, Elena NEACSU, Laurentiu DONE, Liviu Cornel TUGULAN, Felicia Nicoleta DRAGOLICI, Bogdan Tudor OBREJA, Tanase DOBRE, *Removal of ¹³⁷Cs ions from aqueous radioactive waste using nickel ferrocyanide, precipitated on silica gel*, Bulletin of Romanian Chemical Engineering Society, **2** (1), 84–99 (2015) (**ISSN:2360-4697**)



Species removal from aqueous radioactive waste by deep-bed filtration[☆]

Tănase Dobre ^a, Laura Ruxandra Zicman ^{a,b}, Oana Cristina Pârvulescu ^{a,*}, Elena Neacșu ^b, Cătălin Ciobanu ^b, Felicia Nicoleta Drăgolici ^b

^a University POLITEHNICA of Bucharest, Chemical and Biochemical Department, 1-6 Gheorghe Polizu, 011061, Bucharest, Romania

^b Horia Hulubei National Institute for R&D in Physics and Nuclear Engineering (IFIN-HH), P.O.Box MG-6, RO-077125 Bucharest-Magurele, Romania



ARTICLE INFO

Article history:

Received 23 February 2018

Received in revised form

18 May 2018

Accepted 18 May 2018

Keywords:

Aqueous radioactive waste

Deep-bed filtration

Modeling

Sorption

Wastewater treatment

ABSTRACT

Performances of aqueous suspension treatment by deep-bed sand filtration were experimentally studied and simulated. A semiempirical deterministic model and a stochastic model were used to predict the removal of clay particles ($20\text{ }\mu\text{m}$) from diluted suspensions. Model parameters, which were fitted based on experimental data, were linked by multiple linear correlations to the process factors, i.e., sand grain size (0.5 and 0.8 mm), bed depth (0.2 and 0.4 m), clay concentration in the feed suspension (1 and $2\text{ kg}_\text{p}/\text{m}^3$), suspension superficial velocity (0.015 and 0.020 m/s), and operating temperature (25 and 45°C). These relationships were used to predict the bed radioactivity determined by the deposition of radioactive suspended particles ($>50\text{ nm}$) from low and medium level aqueous radioactive waste. A deterministic model based on mass balance, kinetic, and interface equilibrium equations was developed to predict the multicomponent sorption of ^{60}Co , ^{137}Cs , ^{241}Am , and ^3H radionuclides (0.1–0.3 nm). A removal of 98.7% of radioactive particles was attained by filtering a radioactive wastewater volume of 10 m^3 (0.5 mm sand grain size, 0.3 m bed depth, $0.223\text{ kg}_\text{p}/\text{m}^3$ suspended solid concentration in the feed suspension, 0.003 m/s suspension superficial velocity, and 25°C operating temperature). Predicted results revealed that the bed radioactivity determined by the sorption of radionuclides ($0.01\text{ kBq/kg}_\text{b}$) was significantly lower than the bed radioactivities caused by the deposition of radioactive particles (0.5–1.8 kBq/kg_b).

© 2018 Elsevier Ltd. All rights reserved.

1. Introduction

Deep-bed filtration (DBF) is a method widely used for separation of inorganic and organic particles from suspensions with low levels of suspended solids. When a diluted suspension flows through a filtering granular bed, the particles to be removed approach the filter grains (collectors) by various transport mechanisms (direct interception, inertia, sedimentation, molecular diffusion, electrostatic forces, hydrodynamic action) and they can further adhere to the collector surface (by van der Waals forces, electric double layer interactions, hydrogen bonding, mutual adsorption of polymeric species) (Cushing and Lawler, 1988; Ding et al., 2018; Dobre and Sanchez Marcano, 2007; Gitis et al., 2010; Ives, 1987; Jegatheesan and Vigneswaran, 2005; Rege and Fogler, 1988; Rushton et al.,

2000; Šećerov Sokolović et al., 2009; Vaz et al., 2017; Zamani and Maini, 2009). DBF involves two stages, i.e., an initial (clean bed) one, wherein the deposition of particles occurs on the clean filter grains, followed by a transient stage, wherein the particles are deposited on the filter grains which are partially covered by other particles (Jegatheesan and Vigneswaran, 2005; Zamani and Maini, 2009). In the transient stage both attachment and detachment forces should be considered.

DBF performances, usually evaluated in terms of suspended solid concentration in the effluent (filtrate quality) and head loss across the bed, are affected by various process factors. Accordingly, they depend on physical and chemical characteristics of both filtration medium (material, shape, size distribution, density, and surface charge of filter grains, depth and void fraction of fixed bed) and suspension (type, shape, size distribution, surface charge, density and concentration of particles, age and viscosity of suspension) as well as on the operating conditions (suspension flow rate, operating temperature and pressure).

* This paper has been recommended for acceptance by Prof. Joerg Rinklebe.

[†] Corresponding author.

E-mail address: oana.pavulescu@yahoo.com (O.C. Pârvulescu).

Sand, anthracite coal, granular activated carbon, garnet, natural zeolites, synthetic inorganic sorbents, ion exchange resins, glass and expanded polystyrene beads, are common granular materials used to remove TSS from a diluted suspension by DBF (Altmann et al., 2016; Cushing and Lawler, 1988; Gitis et al., 2010; Huang et al., 2012; Ives, 1987; Löwenberg et al., 2016; Rushton et al., 2000; Šećerov Sokolović et al., 2009). Rapid sand filtration is widely applied to water treatment (EPA, 1995; Ives, 1987).

In aqueous radioactive waste (ARW) processing, the knowledge that exists on water purification can be applied. However, there are some additional problems referring to the specialized requirements of radioactive waste management. ARW treatment by deep-bed sand filtration (DBSF) could lead to an effluent with an acceptable level of residual radioactivity for discharge or further processing by other separation methods (e.g., ion exchange, fixed-bed adsorption, ultrafiltration, reverse osmosis) as well as a low amount of secondary radioactive waste (Abdel Rahman et al., 2011; Huang et al., 2012). Moreover, the rapid sand filters involve simple and relatively inexpensive operation and maintenance. The first application of DBSF in nuclear engineering dates from 1948, when this process was used to air purification (DOE HDBK, 2003).

The process control based on modeling could offer valuable information that may be applied to reduce the treatment costs and to protect the health of employees. A DBSF model for the removal of radioactive pollutants from medium and low level ARW could be very useful to design and optimize the process, because it determines a decrease in the number of experiments, which can be expensive, may require considerable time and, most important, increase the radiological dose of workers.

The quality of ARW treated by rapid sand filtration was measured and simulated in this paper. Mathematical models were adopted to predict the process performance and their adjustable parameters were fitted based on experimental data. The models developed to describe DBF process could be coupled with characteristic models of further ARW processing for predicting the performances of integrated separations/purifications.

2. Experimental

Two experimental studies of DBSF were conducted under various operating conditions using silica sand as a filtering medium. Diluted clay suspensions were processed in the first study, whereas ARW was treated in the second one.

2.1. DBSF of clay suspensions

DBSF experiments were performed using a pilot scale setup (Fig. 1) consisting of: (i) a metallic column (90 cm height and 5 cm inner diameter) equipped with manometers at its top and bottom, (ii) a pressurized vessel (400 L volume) for suspension storage, (iii) a compressed air supply for maintaining a constant pressure (1.5–2 bar) in the storage vessel, and (iv) flow rate control valves.

Gravel was placed on a sieve at the column bottom to support the granular bed and to distribute uniformly the suspension. Uniform sand grains, either 0.5 or 0.8 mm diameter (D), were packed in the column resulting in bed void fractions (ϵ_b) of 0.324 and $0.377 \text{ m}^3/\text{m}^3$, respectively. Clay suspensions were obtained by adding 200 and 400 g of clay particles (20 μm mean diameter (d_p) and $1400 \text{ kg}_p/\text{m}^3$ density (ρ_p)), respectively, in 200 L tap water. Pressure difference between the bed inlet and outlet ($\Delta p = p_{in} - p_{out}$) was continuously measured.

Effluent samples were collected at regular intervals and mass concentration of particles (c_p) was determined for each sample. A volume of sample was filtered on a Whatman® quantitative filter paper, ashless, Grade 40 (8 μm pore size). The filter paper with solid residue retained was dried into an oven at 105 °C for 2 h, placed into a desiccator to cool to room temperature, and then weighed. The effects of sand grain size ($D=0.5, 0.8 \text{ mm}$), bed depth ($H=0.2, 0.4 \text{ m}$), mass concentration of particles in the influent ($c_{p0}=1, 2 \text{ kg}_p/\text{m}^3$), suspension superficial velocity ($w=0.015, 0.020 \text{ m/s}$), and operating temperature ($t=25, 45^\circ\text{C}$) on c_p/c_{p0} were evaluated.

2.2. DBSF of ARW

Experiments of DBSF were conducted in a column (Fig. 2) of a filtration module for ARW treatment. It consisted of three metallic columns (114 cm height and 35 cm inner diameter), tanks for ARW and effluent storage, a submersible pump for feed, piping, measuring and control equipment.

Samples from collecting tank were taken at regular intervals and mass concentration of particles (c_p^c) as well as activity concentration of radionuclides (^{60}Co , ^{137}Cs , ^{241}Am , and ^3H) in suspended particles and liquid phase were measured for each sample. TSS (c_p^c) was determined by filtering on a 50 nm Whatman membrane using a Varian DS 102A vacuum pump (Agilent). The membrane was further dried into an oven at 105 °C for 2 h, cooled to room temperature in a desiccator, and then weighed. Activity concentrations of γ -emitting radionuclides (^{60}Co , ^{137}Cs , and ^{241}Am) in the particles

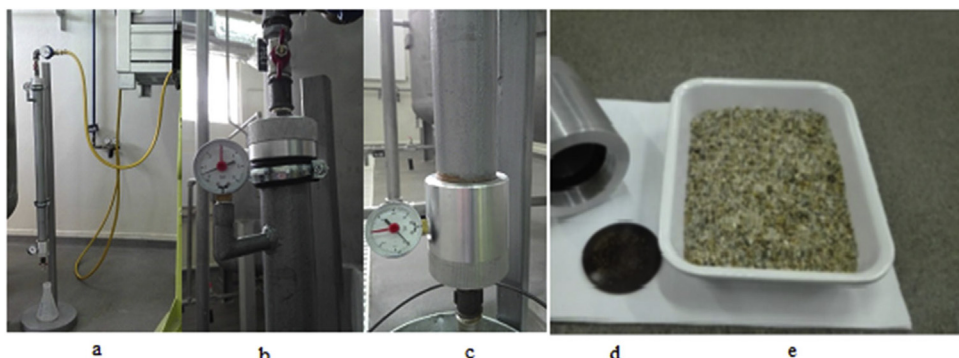


Fig. 1. Pilot scale setup for DBSF of clay suspensions:

(a) fixed bed column and filtrate collector vessel, (b) valve and manometer at the column top, (c) manometer at the column bottom, (d) sieve, and (e) gravel for supporting the fixed-bed sand.



Fig. 2. Metallic columns for ARW treatment by DBSF.

and liquid phase were evaluated based on a Laboratory SOurceless Calibration Software (LabSOCS) version 3.2 integrated in a Genie 2000 γ -ray spectrometry system (Canberra). Activity concentration of β -emitting radionuclide (^{3}H) in the liquid phase was determined using a Tri-Carb 2910 TR Liquid Scintillation Analyzer (PerkinElmer). The values of process factors for ARW treatment by DBSF were as follows: $D=0.5\text{ mm}$, $H=0.3\text{ m}$, $c_{p0}=0.223\text{ kg}_p/\text{m}^3$, $w=0.003\text{ m/s}$, and $t=25^\circ\text{C}$.

3. Modeling of DBF process

DBF process can be described by microscopic or macroscopic models, including trajectory analysis, deterministic or stochastic phenomenological ones (Ali and Othman, 2011; Cushing and Lawler, 1988; Ding et al., 2018; Dobre and Sanchez Marcano, 2007; Gitis et al., 2010; Herzig et al., 1970; Ives, 1987; Jegatheesan and Vigneswaran, 2005; Rege and Fogler, 1988; Rushton et al., 2000; Tien and Payatakes, 1979; Vaz et al., 2017; You et al., 2014; Zamani and Maini, 2009). Bench or pilot scale tests are usually conducted under different operating conditions to fit model adjustable parameters and to validate the models (Ali and Othman, 2011; Cushing and Lawler, 1988; Ding et al., 2018; Gitis et al., 2010; Ives, 1987; Rege and Fogler, 1988; Vaz et al., 2017; You et al., 2014; Zamani and Maini, 2009). A physical model associated to a trajectory analysis microscopic approach is presented in Fig. S1 (Dobre and Sanchez Marcano, 2007). The prediction of the trajectory of a particle around a filter grain is very difficult due to a large number of forces involved, e.g., interception, inertial, gravitational, diffusion, electrostatic, hydrodynamic, van der Waals, electric double layer.

In this paper macroscopic approaches were selected to predict the process performances. A filtration coefficient semiempirical deterministic model and a two-state stochastic model were used to simulate the separation of clay particles ($d_p=20\text{ }\mu\text{m}$) from suspensions as well as of radioactive suspended particles ($d_p>50\text{ nm}$) from ARW. Characteristic adjustable parameters of the models were estimated based on pilot scale measurements performed under various conditions.

3.1. Filtration coefficient (FC) semiempirical deterministic model

A filtration coefficient, $\lambda(\text{m}^{-1})$, is defined by Eq. (1), where $c_p(\text{kg}_p/\text{m}^3)$ is the mass concentration of particles (suspended solids) in the suspension and $x(\text{m})$ the space coordinate (Ives, 1987; Jegatheesan and Vigneswaran, 2005; Rege and Fogler, 1988; Zamani and Maini, 2009). For a diluted suspension flowing through the filtering bed, the mass balance of particles in a bed control volume

led to Eq. (2), where $A(\text{m}^2)$ is the cross-sectional area of granular bed, $G_V(\text{m}^3/\text{s})$ the volumetric flow rate of suspension, $q_p(\text{kg}_p/\text{m}^3)$ the mass concentration of particles retained in the bed (specific deposit), $w(\text{m/s})$ the superficial velocity of suspension, and $\tau(\text{s})$ the time.

$$\lambda = -\frac{1}{c_p} \frac{\partial c_p}{\partial x} \quad (1)$$

$$-\frac{\partial c_p}{\partial x} = \frac{A}{G_V} \frac{\partial q_p}{\partial \tau} = \frac{1}{w} \frac{\partial q_p}{\partial \tau} \quad (2)$$

Under clean bed (initial) conditions ($\tau=0$), Eq. (3) was obtained by substituting Eq. (1) into Eq. (2). In the transient stage ($\tau>0$), both attachment and detachment of particles are considered by Eq. (4), where $\alpha(\text{s}^{-1})$ is the detachment coefficient of particles and $\lambda_0(\text{m}^{-1})$ the initial filtration coefficient (Dobre and Sanchez Marcano, 2007).

$$\frac{\partial q_p}{\partial \tau} = w\lambda_0 c_p \tau = 0 \quad (3)$$

$$\frac{\partial q_p}{\partial \tau} = w\lambda_0 c_p - \alpha q_p \tau > 0 \quad (4)$$

Eq. (4) was substituted into Eq. (2) resulting in Eq. (5) and further in Eq. (6), which is the derivative of Eq. (5) with respect to time. By substituting Eq. (2) into Eq. (6), Eq. (7) was obtained (Mints, 1951). Taking into account the initial and boundary conditions expressed by Eqs. (8)–(10), the analytical solution of Eq. (7) is given by Eqs. (11)–(13).

$$-\frac{\partial c_p}{\partial x} = \lambda_0 c_p - \frac{\alpha}{w} q_p \quad (5)$$

$$-\frac{\partial^2 c_p}{\partial x \partial \tau} = \lambda_0 \frac{\partial c_p}{\partial \tau} - \frac{\alpha}{w} \frac{\partial q_p}{\partial \tau} \quad (6)$$

$$\frac{\partial^2 c_p}{\partial x \partial \tau} + \lambda_0 \frac{\partial c_p}{\partial \tau} + \alpha \frac{\partial c_p}{\partial x} = 0 \quad (7)$$

$$\tau = 0 \quad 0 \leq x \leq H \quad c_p = 0 \quad (8)$$

$$\tau > 0 \quad x = 0 \quad c_p = c_{p0} \quad (9)$$

$$\tau > 0 \quad x = H \quad \frac{\partial c_p}{\partial x} = 0 \quad (10)$$

$$\frac{c_p}{c_{p0}} = \sum_{i=1}^{\infty} \exp(-\lambda_0 x) \frac{(\lambda_0 x)^{i-1}}{(i-1)!} Q_i \exp(-\alpha \tau) \quad (11)$$

$$Q_i = Q_{i-1} - \frac{(\alpha \tau)^{i-2}}{(i-2)!} \quad i \geq 2 \quad (12)$$

$$Q_1 = \exp(\alpha \tau) \quad (13)$$

Based on experimental data of suspended solid concentration in the effluent ($x=H$) of DBF device, i.e., $c_{pk}(H, \tau_k)$, $1 \leq k \leq N$, α and λ_0 adjustable parameters can be determined by minimizing the root mean square error (RMSE) between the experimental and predicted data expressed by Eq. (14).

$$F(\lambda_0, \alpha) = \sqrt{\frac{1}{N} \sum_{k=1}^N \left[\frac{c_{pk}(H, \tau_k)}{c_{p0}} - \sum_{i=1}^{\infty} \exp(-\lambda_0 H) \frac{(\lambda_0 H)^{i-1}}{(i-1)!} Q_i \exp(-\alpha \tau_k) \right]^2} \quad (14)$$

3.2. Two-state (TS) stochastic model

Two elementary processes can be identified for particle evolution in the filtrating granular bed (Lordache, 1987), i.e., a first one (1) considering that the particle moves with the velocity $v_1 = v$ determined by the fluid flowing over the filter grains and a second one (2) taking into account the particle deposition ($v_2 = 0$). Accordingly, based on a Markov type connection between (1) and (2) states, the unsteady balance of probabilities to locate the particle at x and τ coordinates, $P_1(x, \tau)$ and $P_2(x, \tau)$, is given by Eqs. (15) and (16), where $\beta \Delta \tau$ is the probability of transition from (1) to (2) states and $\gamma \Delta \tau$ the probability of transition from (2) to (1) states (Dobre and Sanchez Marcano, 2007).

$$\frac{\partial P_1(x, \tau)}{\partial \tau} = -v \frac{\partial P_1(x, \tau)}{\partial x} - \beta P_1(x, \tau) + \gamma P_2(x, \tau) \quad (15)$$

$$G(\beta, \gamma) = \sqrt{\frac{1}{N} \sum_{k=1}^N \left\{ \frac{c_{pk}(H, \tau_k)}{c_{p0}} - 1 + \exp \left[- \left(\frac{(\beta + \gamma)H}{v} + \gamma \tau_k \right) \right] \sum_{i=1}^{\infty} \left(\frac{\gamma v \tau_k}{(\beta + \gamma)H} \right)^{\frac{i}{2}} I_i \left[\left(\frac{(\beta + \gamma) \gamma H \tau_k}{v} \right)^{\frac{1}{2}} \right] \right\}^2} \quad (23)$$

$$\frac{\partial P_2(x, \tau)}{\partial \tau} = \beta P_1(x, \tau) - \gamma P_2(x, \tau) \quad (16)$$

By substituting Eqs. (15) and (16) into Eq. (17), which represents the derivative of Eq. (15) with respect to time, Eq. (18) was obtained. By dividing its terms to v and neglecting $\frac{1}{v} \frac{\partial^2 P_1(x, \tau)}{\partial \tau^2}$ (Dobre and Sanchez Marcano, 2007), Eq. (18) became Eq. (19).

$$\frac{\partial^2 P_1(x, \tau)}{\partial \tau^2} = -v \frac{\partial^2 P_1(x, \tau)}{\partial x \partial \tau} - \beta \frac{\partial P_1(x, \tau)}{\partial \tau} + \gamma \frac{\partial P_2(x, \tau)}{\partial \tau} \quad (17)$$

$$\begin{aligned} \frac{\partial^2 P_1(x, \tau)}{\partial \tau^2} &= -v \frac{\partial^2 P_1(x, \tau)}{\partial x \partial \tau} - \beta \frac{\partial P_1(x, \tau)}{\partial \tau} - \gamma \left(\frac{\partial P_1(x, \tau)}{\partial \tau} \right. \\ &\quad \left. + v \frac{\partial P_1(x, \tau)}{\partial x} \right) \end{aligned} \quad (18)$$

$$\frac{\partial^2 P_1(x, \tau)}{\partial x \partial \tau} + \frac{\beta + \gamma}{v} \frac{\partial P_1(x, \tau)}{\partial \tau} + \gamma \frac{\partial P_1(x, \tau)}{\partial x} = 0 \quad (19)$$

Taking into account the boundary condition expressed by Eq. (20), the analytical solution of Eq. (19) is given by Eqs. (21) and (22), where I_i is the modified Bessel function of the first kind (Andrew and Mathews, 2016).

$$x = 0 \quad \tau > 0 \quad P_1(0, \tau) = 1, \quad P_2(0, \tau) = 0 \quad (20)$$

$$\begin{aligned} \frac{P_1(x, \tau)}{P_1(0, \tau)} &= 1 - \exp \left[- \left(\frac{(\beta + \gamma)x}{v} + \gamma \tau \right) \right] \\ &\times \sum_{i=1}^{\infty} \left(\frac{\gamma v \tau}{(\beta + \gamma)x} \right)^{\frac{i}{2}} I_i \left[\left(\frac{(\beta + \gamma) \gamma x \tau}{v} \right)^{\frac{1}{2}} \right] \end{aligned} \quad (21)$$

$$I_i(u) = \sum_{m=0}^{\infty} \frac{\left(\frac{u}{2} \right)^{i+2m}}{m!(m+i)!} \quad (22)$$

Based on the similarity between Eqs. (7) and (19), β and γ parameters can be adjusted using experimental data ($c_{pk}(H, \tau_k)$, $1 \leq k \leq N$) by minimizing RMSE expressed by Eq. (23), where the real velocity of particle (v) is defined by Eq. (24) depending on suspension superficial velocity (w) and bed void fraction (ϵ_b).

4. Results and discussion

4.1. DBSF of clay suspensions

Experimental dynamics of the ratio between the concentration of clay particles in the effluent and that in the influent (c_p/c_{p0}) under various operating conditions are presented in Figs. S2–S6, where the bullets represent experimental data and the lines are experimental data processed by *upsimooth(vx, vy)* function in Mathcad 15. Depicted results highlight that all process factors, i.e., D (0.5 and 0.8 mm), H (0.2 and 0.4 m), c_{p0} (1 and 2 kg_p/m³), w (0.015 and 0.020 m/s), and t (25 and 45 °C), influence the dynamics of c_p/c_{p0} . Higher levels of sand grain size (Fig. S2), suspended solid concentration in the influent (Fig. S4), suspension superficial velocity (Fig. S5), and operating temperature (Fig. S6) as well as a lower value of bed depth (Fig. S3) resulted in sharper breakthrough curves, indicating a faster saturation of the bed.

Based on experimental data shown in Figs. S2–S6, values of adjustable parameters of FC model (λ_0, α) and TS stochastic model (β, γ) were determined by minimizing the RMSE expressed by Eqs. (14) and (23), i.e., $F(\lambda_0, \alpha)$ and $G(\beta, \gamma)$. Table 1 contains values of model parameters under different experimental conditions ($F_{min}(\lambda_0, \alpha) = 0.15 \pm 0.06$ and $G_{min}(\beta, \gamma) = 0.11 \pm 0.02$). Data

Table 1

Effect of process factors on the parameters of FC deterministic model (λ_0 , α) and TS stochastic model (β , γ).

No.	D (mm)	H (m)	c_{p0} (kg _p /m ³)	w (m/s)	t (°C)	λ_0 (m ⁻¹)	$\alpha \times 10^3$ (s ⁻¹)	$\beta \times 10^3$ (min ⁻¹)	$\gamma \times 10^3$ (min ⁻¹)
1	0.5	0.4	2	0.020	25	9.19	2.33	2.34	1.97
2	0.8	0.4	2	0.020	25	7.51	3.92	4.56	3.42
3	0.8	0.2	2	0.020	25	13.3	6.54	7.87	3.17
4	0.8	0.4	2	0.020	25	7.84	3.21	3.69	3.18
5	0.8	0.4	1	0.020	25	9.24	2.30	4.11	3.07
6	0.8	0.4	2	0.020	25	7.81	3.21	3.69	3.28
7	0.8	0.4	1	0.015	25	10.4	1.99	4.31	3.52
8	0.8	0.4	1	0.020	25	7.80	3.20	3.69	2.99
9	0.8	0.4	2	0.020	45	7.39	3.96	4.62	3.88
10	0.8	0.4	2	0.020	25	7.79	3.20	3.71	3.01
Multiple determination coefficient (R^2)									
0.964									
Adjusted multiple determination coefficient (R_{adj}^2)									
0.919									
Standard deviation ($\sigma \times 10^3$)									
526 m ⁻¹									
$\sigma_\lambda = 0.526 \text{ m}^{-1}$									
$\sigma_\alpha = 0.443 \times 10^{-3} \text{ s}^{-1}$									
$\sigma_\beta = 0.402 \times 10^{-3} \text{ min}^{-1}$									
$\sigma_\gamma = 0.152 \times 10^{-3} \text{ min}^{-1}$									

summarized in Table 1 were processed by multiple linear regression analysis and Eqs. (25)–(28), expressing the model parameters (λ_0 (m⁻¹), α (s⁻¹), β (min⁻¹), and γ (min⁻¹)) depending on the process factors (D (mm), H (m), c_{p0} (kg_p/m³), w (m/s), and t (°C)), were obtained. The values of determination coefficient ($R^2 = 0.947\text{--}0.965$), adjusted determination coefficient ($R_{adj}^2 = 0.881\text{--}0.920$), and standard deviation ($\sigma_\lambda = 0.526 \text{ m}^{-1}$, $\sigma_\alpha = 0.443 \times 10^{-3} \text{ s}^{-1}$, $\sigma_\beta = 0.402 \times 10^{-3} \text{ min}^{-1}$, and $\sigma_\gamma = 0.152 \times 10^{-3} \text{ min}^{-1}$) of multiple linear regressions are also presented in Table 1.

$$\lambda_0 = 32.255 - 4.842D - 27.813H - 0.783c_{p0} - 376w - 0.017t \quad (25)$$

$$\alpha = (1.853 + 3.517D - 15.775H + 0.635c_{p0} + 152w + 0.029t) \times 10^{-3} \quad (26)$$

$$\beta = (8.365 + 5.242D - 19.788H + 0.013c_{p0} - 82w + 0.035t) \times 10^{-3} \quad (27)$$

$$\gamma = (-0.531 + 4.175D + 0.263H + 0.193c_{p0} - 98w + 0.033t) \times 10^{-3} \quad (28)$$

Tabulated values of model parameters were used to estimate the dynamics of pressure loss for DBSF with a constant filtrate flow rate. In this case the pressure must increase in order to compensate the increase in the pressure loss caused by the deposition of particles in the bed. Dimensionless pressure loss ($\Delta p/\Delta p_0$) was determined using Eq. (29) (Rushton et al., 2000), where f (m³/m³) is the pore filling degree, ϵ_b (m³/m³) the bed void fraction, ρ_p (kg_p/m³) the particle density, and $q_p(x, \tau, \lambda_0, \alpha)$ is given by Eq. (30) depending on $c_p(x, \tau, \lambda_0, \alpha)$ (according to Eq. (2)).

$$\frac{\Delta p}{\Delta p_0} = \left(1 + \frac{\frac{1}{H} \int_0^H q_p(x, \tau, \lambda_0, \alpha) dx}{f \epsilon_b \rho_p} \right) \quad (29)$$

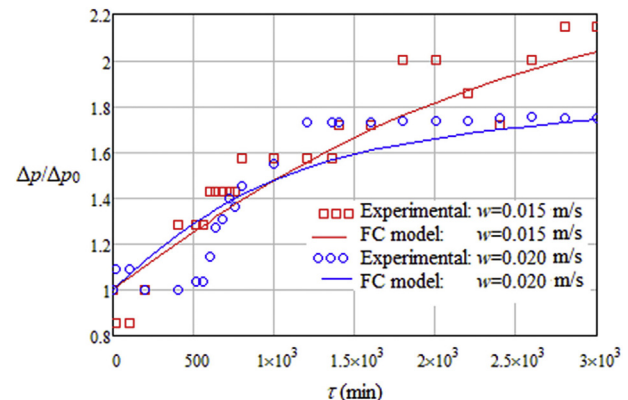


Fig. 3. Dynamics of pressure loss for DBSF with a constant flow rate ($D = 0.8 \text{ mm}$, $H = 0.4 \text{ m}$, $c_{p0} = 2 \text{ kg}_p/\text{m}^3$, $t = 25^\circ\text{C}$, $f = 0.7 \text{ m}^3/\text{m}^3$, $\epsilon_b = 0.377 \text{ m}^3/\text{m}^3$, $\rho_p = 1400 \text{ kg}_p/\text{m}^3$).

Experimental and predicted (FC model) dynamics of $\Delta p/\Delta p_0$ for 2 runs (nos. 7 and 8) in Table 1 are presented in Fig. 3. Suspension superficial velocity was the only process factor that varied in the experimental runs (nos. 7 and 8), i.e., $w_7 = 0.015 \text{ m/s}$ and $w_8 = 0.020 \text{ m/s}$. Measured values of initial pressure loss corresponding to w_7 and w_8 were $\Delta p_{0,7} = 0.28 \text{ bar}$ and $\Delta p_{0,8} = 0.27 \text{ bar}$, respectively. Data depicted in Fig. 3 reveal an acceptable agreement between experimental and predicted values of $\Delta p/\Delta p_0$ (RMSE of 0.11 and 0.12 for $w_7 = 0.015 \text{ m/s}$ and $w_8 = 0.020 \text{ m/s}$, respectively).

4.2. DBSF of ARW

Physical characteristics of feed and treated ARW, including pH, electrical conductivity, TDS, TSS, activity concentrations of radionuclides (^{60}Co , ^{137}Cs , ^{241}Am , and ^3H) in suspended particles and liquid phase, are summarized in Table 2.

Values of parameters presented in Table 2 highlight an advanced retention of 98.7% (from 0.223 to 0.003 kg_p/m³) of radioactive suspended particles containing γ -emitting radionuclides (^{60}Co , ^{137}Cs , and ^{241}Am) as well as a removal of ^{60}Co , ^{137}Cs , ^{241}Am , and ^3H from liquid phase of 24.8, 5.41, 16, and 0.31%, respectively. Bed radioactivities determined by the deposition of radioactive particles loaded with γ -emitting radionuclides and the sorption of radionuclides from the liquid phase were predicted.

Bed radioactivity caused by the deposition of radioactive

Table 2

Physical parameters of feed and treated ARW ($D=0.5$ mm, $H=0.3$ m, $w=0.003$ m/s, $t=25^\circ\text{C}$).

ARW	Feed	Treated
Volume of ARW treated by DBSF (m ³)	0	10
pH	7.10	8.35
Electrical conductivity (μS/cm)	1240	1140
TDS (kg/m ³)	0.720	0.710
TSS (kg _p /m ³)	0.223	0.003
Activity concentration of γ radionuclides in suspended particles (kBq/kg _p)	⁶⁰ Co ¹³⁷ Cs	²⁴¹ Am
in suspended particles (kBq/kg _p)	9.54	26.85
in liquid phase (kBq/m ³)	1.49	18.50
Activity concentration of β radionuclides in liquid phase (kBq/m ³)	³ H	0.25
	32000	1.12
		¹³⁷ Cs ²⁴¹ Am
		— —
		17.50 0.21
		31900

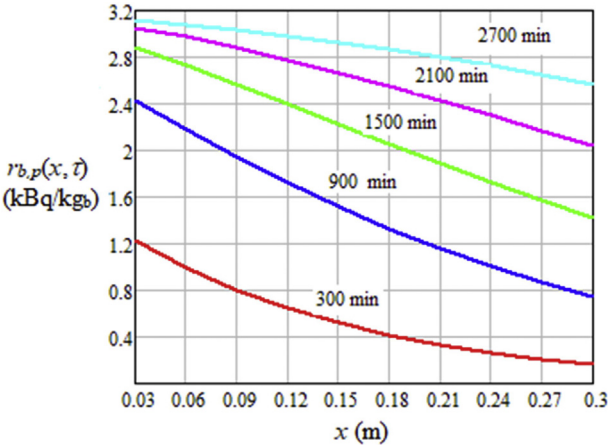


Fig. 4. Predicted space and time variations of bed radioactivity determined by the deposition of radioactive suspended particles ($d_p > 50$ nm) from ARW on the sand grains ($D=0.5$ mm, $H=0.3$ m, $c_{p0}=0.223$ kg_p/m³, $w=0.003$ m/s, and $t=25^\circ\text{C}$).

particles (loaded with γ -emitting radionuclides) on the filtering grains, $r_{b,p}$ (kBq/kg_b), can be expressed by Eq. (31), where q_p (kg_p/m³) is the mass concentration of particles deposited in the bed, $r_p = 210.01$ kBq/kg_p the particle radioactivity (total activity concentration of γ -emitting radionuclides in the particles), $\rho_b = 1300$ kg_b/m³ the bed density, λ_0 (m⁻¹) and α (h⁻¹) the adjustable parameters of FC model estimated by Eqs. (25) and (26). Space and time variations of bed radioactivity given by Eq. (31) are presented in Fig. 4. Depicted results highlight larger values of $r_{b,p}$ for higher levels of τ and lower levels of x . Moreover, the bed radioactivity is almost constant for $\tau > 2700$ min, indicating that the bed is close to saturation with particles.

$$r_{b,p}(x, \tau, \lambda_0, \alpha) = \frac{q_p(x, \tau, \lambda_0, \alpha)}{\rho_b} r_p \quad (31)$$

A deterministic model was developed to describe the sorption of radionuclides (0.1–0.3 nm) from ARW on the filtering grains covered by radioactive suspended particles. It consists of equations of mass balance in the filtering bed (Eq. (32)), overall sorption rate (Eq. (33)), interface equilibrium (Eq. (34)), mass balance in the tank of treated water (Eq. (35)), limit and boundary conditions (36)–(38), where c_j (kBq/m³) and q_j (kBq/m_b³) are the activity concentrations of j radionuclide in the liquid phase and the filtering bed, respectively, q_p (kg_p/m³) is the mass concentration of particles deposited on the grains, ε_b (m³/m³) the initial bed void fraction, ε_d (m³/m³) the deposit porosity, ρ_p (kg_p/m³) the particle density, and * superscript denotes the equilibrium state. Adjustable model parameters, i.e., transfer coefficient (k_{tj}) and distribution coefficient (k_{dj}) of j species, were fitted based on experimental dynamics of

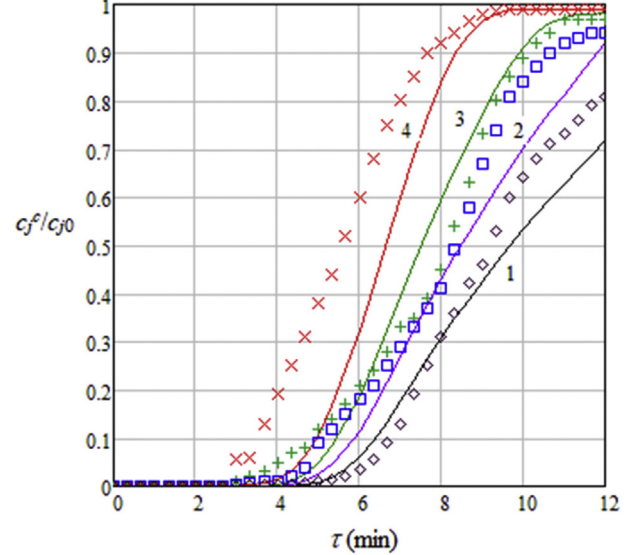


Fig. 5. Experimental (points) and predicted (line) dynamics of dimensionless concentration of radionuclides ((1) ⁶⁰Co, (2) ¹³⁷Cs, (3) ²⁴¹Am, (4) ³H) in the collecting tank ($c_{Co,0}=1.49$ kBq/m³, $c_{Cs,0}=18.50$ kBq/m³, $c_{Am,0}=0.25$ kBq/m³, $c_{H,0}=32000$ kBq/m³, $D=0.5$ mm, $H=0.3$ m, $c_{p0}=0.223$ kg_p/m³, $w=0.003$ m/s, and $t=25^\circ\text{C}$).

dimensionless concentration of j radionuclide (⁶⁰Co, ¹³⁷Cs, ²⁴¹Am, and ³H) in the collecting tank (c_j^e/c_{j0}), which are presented in Fig. 5.

$$\frac{\partial}{\partial \tau} \left(\varepsilon_b - \frac{q_p}{(1-\varepsilon_d)\rho_p} \right) c_j + w \frac{\partial c_j}{\partial x} = - \frac{\partial q_j}{\partial \tau} \quad (32)$$

$$\frac{\partial q_j}{\partial \tau} = \frac{6 \left(1 - \varepsilon_b + \frac{q_p}{(1-\varepsilon_d)\rho_p} \right)}{D} k_{tj} \left(\varepsilon_b - \frac{q_p}{(1-\varepsilon_d)\rho_p} \right) (c_j - c_j^*) \quad (33)$$

$$c_j^* = k_{dj} q_j \quad (34)$$

$$\frac{dc_j^e}{d\tau} = \frac{c_j(H, \tau)}{\tau} \quad (35)$$

$$\tau = 0 \quad 0 \leq x \leq H \quad c_j(0, x) = 0 \quad q_j(0, x) = 0 \quad (36)$$

$$\tau > 0 \quad x = 0 \quad c_j(0, \tau) = c_{j0} \quad q_j(0, \tau) = q_{j0}^* \quad (37)$$

$$\tau = 0 \quad c_j^e(0) = 0 \quad (38)$$

Table 3

Characteristic parameters of multicomponent sorption model for ARW processing by DBSF.

<i>j</i>	Radioactive species	k_{dj} (m^3/m^3)	$k_{tj} \times 10^5$ (m/s)	τ_{sj} (s)	ϕ_j (-)	χ_j (s^{-1})
1	^{60}Co	300	0.95	240	-8.928	0.069
2	^{137}Cs	800	0.98	230	-7.261	0.069
3	^{241}Am	1400	1.05	210	-6.982	0.062
4	^3H	2500	1.15	160	-8.564	0.058

A procedure similar to those reported for fixed bed sorption (Dobre et al., 2010; Gupta and Babu, 2010; Miura, 2017; Negrea et al., 2011, 2018; Weber and Chakravorti, 1974) was used to identify the model parameters. Algorithm steps were as follows: (i) a set of k_{dj} and k_{tj} values, where k_{tj} value was estimated by assuming $Sh_j = 2$ (Guedes de Carvalho et al., 2004; Stoodley et al., 1997), was selected; (ii) $c_j(H, \tau)$ dynamics were predicted depending on k_{dj} and k_{tj} values according to Eqs. (32)–(34); (iii) a logistic function (39) was used to express analytically the dependence between c_j and τ ; characteristic parameters of logistic function, i.e., ϕ_j , χ_j , and τ_{sj} , were fitted based on $c_j(H, \tau)$ predicted breakthrough curve; (iv) $c_j(\tau)$ dynamics were simulated by integrating Eq. (35); (v) it was established the correctness of values by comparing the experimental and simulated data; if they were in a good agreement, k_{dj} value was considered as acceptable; otherwise, another value of k_{dj} was selected and the algorithm was repeated.

$$c_j(H, \tau) = \frac{e^{\phi_j + \chi_j(\tau - \tau_{sj})}}{1 + e^{\phi_j + \chi_j(\tau - \tau_{sj})}} \quad (39)$$

Values of k_{dj} , k_{tj} , ϕ_j , χ_j , and τ_{sj} parameters corresponding to the experimental conditions ($c_{Co,0} = 1.49 \text{ kBq/m}^3$, $c_{Cs,0} = 18.50 \text{ kBq/m}^3$, $c_{Am,0} = 0.25 \text{ kBq/m}^3$, $c_{H,0} = 32000 \text{ kBq/m}^3$, $D = 0.5 \text{ mm}$, $H = 0.3 \text{ m}$, $c_{p0} = 0.223 \text{ kg}_p/\text{m}^3$, $w = 0.003 \text{ m/s}$, and $t = 25^\circ\text{C}$) are summarized

in Table 3. High values of k_{dj} ($300\text{--}2500 \text{ mb}^3/\text{m}^3$) indicate low equilibrium activity concentrations of radionuclides retained in the filtering bed. Experimental and predicted dynamics of dimensionless radionuclide concentration in the collecting tank (Fig. 5) highlight an acceptable agreement.

Simulations of activity concentration of j radionuclide in the filtering bed (q_j), which are presented in Fig. 6, highlight a rapid saturation (after about 10 min) of the bed with radionuclides transferred from the liquid phase. Saturation activity concentrations of radionuclides in the filtering bed, are as follows: $q_{Co,s} = 4.7 \times 10^{-3} \text{ kBq}/\text{m}^3$, $q_{Cs,s} = 23 \times 10^{-3} \text{ kBq}/\text{m}^3$, $q_{Am,s} = 0.18 \times 10^{-3} \text{ kBq}/\text{m}^3$, and $q_{H,s} = 13 \text{ kBq}/\text{m}^3$. Accordingly, saturation bed radioactivity caused by the sorption of radionuclides on the filtering grains, given by Eq. (40), is $r_{b,r} = 0.01 \text{ kBq}/\text{kg}_b$. After 600 min, corresponding to a treated ARW volume of 10 m^3 at $w = 0.003 \text{ m/s}$ ($G_V = 1 \text{ m}^3/\text{h}$), this value is significantly lower than those predicted for the bed radioactivity determined by the deposition of radioactive particles (Fig. 4), i.e., $r_{b,p} = 0.5\text{--}1.8 \text{ kBq}/\text{kg}_b$, and it can be considered as negligible.

$$r_{b,r} = \frac{\sum_{j=1}^4 q_{j,s}}{p_b} \quad (40)$$

5. Conclusions

Performances of medium and low level ARW treatment by rapid sand filtration were predicted by modeling based on both deposition of radioactive suspended particles ($>50 \text{ nm}$) on the sand grains and sorption of radionuclides ($0.1\text{--}0.3 \text{ nm}$) on the grains covered with radioactive particles. Model parameters were determined from experimental data. In order to estimate the model parameters depending on the process factors, diluted suspensions of clay

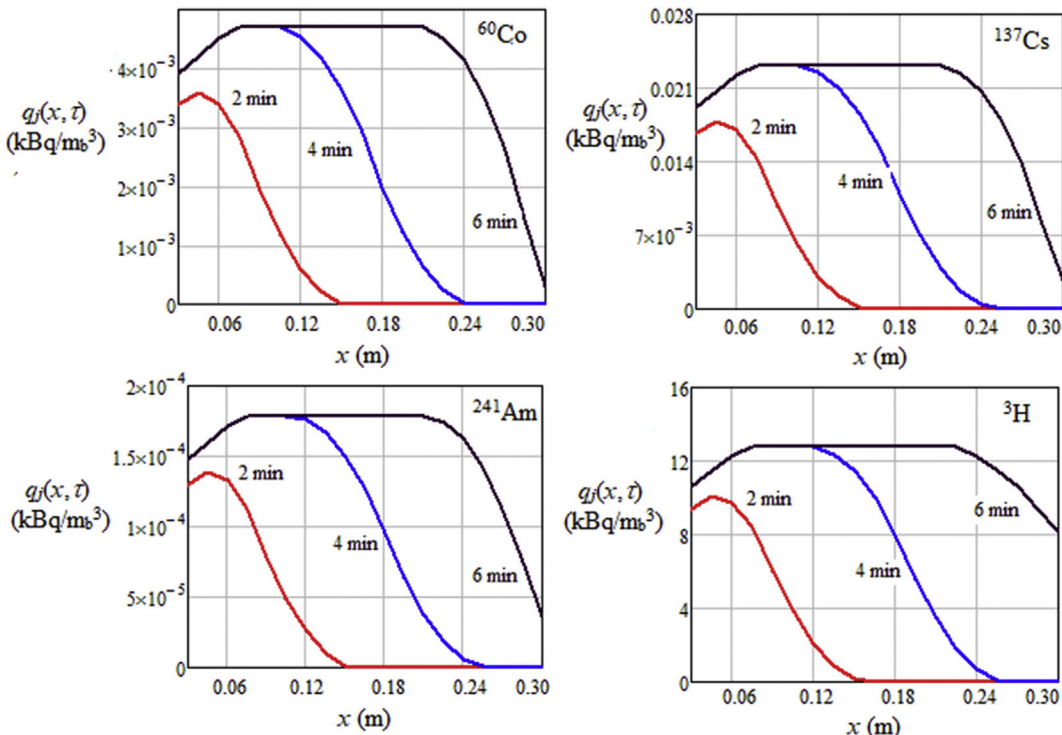


Fig. 6. Predicted space and time variations of activity concentration of j radionuclide in the filtering bed for radionuclide sorption from liquid phase ($c_{Co,0} = 1.49 \text{ kBq}/\text{m}^3$, $c_{Cs,0} = 18.50 \text{ kBq}/\text{m}^3$, $c_{Am,0} = 0.25 \text{ kBq}/\text{m}^3$, $c_{H,0} = 32000 \text{ kBq}/\text{m}^3$, $D = 0.5 \text{ mm}$, $H = 0.3 \text{ m}$, $c_{p0} = 0.223 \text{ kg}_p/\text{m}^3$, $w = 0.003 \text{ m/s}$, and $t = 25^\circ\text{C}$).

particles ($20\text{ }\mu\text{m}$) were processed by DBSF under different experimental conditions. The treatment of clay suspensions aimed at avoiding a large number of experiments involving ARW, which are time-consuming and increase the radiological dose of workers.

A faster saturation of the bed was attained for higher levels of sand grain size ($D=0.5$, 0.8 mm), clay concentration in the influent ($c_{p0}=1, 2\text{ kg}_p/\text{m}^3$), clay suspension superficial velocity ($w=0.015, 0.020\text{ m/s}$), and operating temperature ($t=25, 45\text{ }^\circ\text{C}$) as well as a lower value of bed depth ($H=0.2, 0.4\text{ m}$). A semiempirical deterministic model and a stochastic one were used to describe the deposition of clay particles on the sand grains. Adjustable model parameters were fitted based on experimental data and correlated by multiple linear relationships with the process factors. These correlations were used to predict the pressure loss dynamics and the bed radioactivity dynamics due to the deposition of radioactive solid particles from ARW. A removal of 98.7% of radioactive suspended particles containing ^{60}Co , ^{137}Cs , and ^{241}Am radionuclides was achieved by processing an ARW volume of 10 m^3 by DBSF ($D=0.5\text{ mm}$, $H=0.3\text{ m}$, $c_{p0}=0.223\text{ kg}_p/\text{m}^3$, $w=0.003\text{ m/s}$, and $t=25\text{ }^\circ\text{C}$).

A deterministic model based on mass balance, kinetic, and interface equilibrium equations was developed to describe the sorption of ^{60}Co , ^{137}Cs , ^{241}Am , and ^{3}H radionuclides from ARW on the sand grains covered by radioactive suspended particles. An algorithm was considered to determine the model parameters from experimental data. Simulated results highlighted that the bed was saturated with radionuclides after about 10 min. For a treated ARW volume of 10 m^3 , saturation bed radioactivity caused by the sorption of radionuclides (0.01 kBq/kg_b) was 50–180 times lower than the bed radioactivities determined by the deposition of radioactive particles.

Acknowledgements

The authors thank Cristian RADUCANU for his support, kindness, time, and patience.

Appendix A. Supplementary data

Supplementary data related to this article can be found at <https://doi.org/10.1016/j.envpol.2018.05.065>.

References

- Abdel Rahman, R.O., Ibrahium, H.A., Hung, Y.T., 2011. Liquid radioactive wastes treatment: a review. *Water* 3, 551–565.
- Ali, A.H., Othman, S.H., 2011. A physico-chemical parametric study on the retention of radioactive ions in a fixed bed reactor. *Chem. Eng. J.* 178, 374–385.
- Altmann, J., Rehfeld, D., Träder, K., Sperlich, A., Jekel, M., 2016. Combination of granular activated carbon adsorption and deep-bed filtration as a single advanced wastewater treatment step for organic micropollutant and phosphorus removal. *Water Res.* 92, 375–383.
- Andrew, G., Mathews, G.B., 2016. A Treatise on Bessel Functions and Their Applications to Physics. Forgotten Books. www.forgottenbooks.com.
- Cushing, R.S., Lawler, D.F., 1988. Depth filtration: fundamental investigation through three-dimensional trajectory analysis. *Environ. Sci. Technol.* 32, 3793–3801.
- Ding, B., Li, C., Wang, Y., Xu, J., 2018. Effects of pore size distribution and coordination number on filtration coefficients for straining-dominant deep bed filtration from percolation theory with 3D networks. *Chem. Eng. Sci.* 175, 1–11.
- Dobre, T., Părvulescu, O.C., Calotă, L., Jipa, I., 2010. Modelling of fixed bed multicomponent ion exchange. *Rev. Chim. (Bucharest)* 61, 213–217.
- Dobre, T., Sanchez Marcano, J., 2007. Chemical Engineering—modelling, Simulation, and Similitude. Wiley VCH, Weinheim, Germany.
- DOE HDBK-1169-2003, 2003. Nuclear Air Cleaning Handbook. U.S. Department of Energy, Washington, DC 20585.
- EPA (Environmental Protection Agency), 1995. Water Treatment Manuals—filtration. Ardcavan, Wexford, Ireland, 1995.
- Gitis, V., Rubinstein, I., Livshits, M., Ziskind, G., 2010. Deep-bed filtration model with multistage deposition kinetics. *Chem. Eng. J.* 163, 78–85.
- Guedes de Carvalho, J.R.F., Delgado, J.M.P.Q., Alves, M.A., 2004. Mass transfer between flowing fluid and sphere buried in packed bed of inerts. *AIChE J* 50, 65–74.
- Gupta, S., Babu, B.V., 2010. Experimental investigations and theoretical modeling aspects in column studies for removal of Cr (VI) from aqueous solutions using activated tamarind seeds. *J. Water Resour. Protect.* 2, 706–716.
- Herzig, J.P., Leclerc, D.M., Le Goff, P., 1970. Flow of suspensions through porous media—Application to deep bed filtration. *Ind. Eng. Chem.* 62, 8–35.
- Huang, C.P., Lin, T.Y., Chiao, L.H., Chen, H.B., 2012. Characterization of radioactive contaminants and water treatment trials for the Taiwan Research Reactor's spent fuel pool. *J. Hazard Mater.* 233–234, 140–147.
- Iordache, O., 1987. Polystochastic Models in Chemical Engineering. VNU Science Press, Utrecht, the Netherlands.
- Ives, K.J., 1987. Filtration of clay suspensions through sand. *Clay Miner.* 22, 49–61.
- Jegatheesan, V., Vigneswaran, S., 2005. Deep bed filtration: mathematical models and observations. *Crit. Rev. Environ. Sci. Technol.* 35, 515–569.
- Löwenberg, J., Zenker, A., Krahnstöver, T., Boehler, M., Baggenstos, M., Koch, G., Wintgens, T., 2016. Upgrade of deep bed filtration with activated carbon dosage for compact micropollutant removal from wastewater in technical scale. *Water Res.* 94, 246–256.
- Mints, D.M., 1951. Kinetics of filtration of low-concentration water suspensions in water purification filters. *Dokl. Akad. Nauk SSSR* 78, 315–318.
- Miura, A., 2017. Determination of cesium adsorption breakthrough curves using carbonized rice hull and beech sawdust as adsorbents. *Environment and Ecology Research* 5, 461–466.
- Negrea, A., Lupa, L., Ciopec, M., Negrea, P., 2011. Experimental and modelling studies on as (III) removal from aqueous medium on fixed bed column. *Chem. Bull. POLITEHNICA Univ. (Timisoara)* 56 (2), 89–93.
- Negrea, A., Gabor, A., Davidescu, C.M., Ciopec, M., Negrea, P., Duteanu, N., Barbulescu, A., 2018. Rare earth elements removal from water using natural polymers. *Sci. Rep.* 8 <https://doi.org/10.1038/s41598-017-18623-0>.
- Rege, S.D., Fogler, H.S., 1988. A network model for deep bed filtration of solid particles and emulsion drops. *AIChE J.* 34, 1761–1772.
- Rushton, A., Ward, A.S., Holdich, R.G., 2000. Solid-liquid Filtration and Separation Technology (2nd, Completely Revised Edition). Wiley VCH, Weinheim, Germany.
- Šećerov Sokolović, R., Sokolović, S., Govendarica, D., 2009. Performance of expanded polystyrene particles in deep bed filtration. *Separ. Purif. Technol.* 68, 267–272.
- Stoodley, P., Yang, S., Lappin-Scott, H., Lewandowski, Z., 1997. Relationship between mass transfer coefficient and liquid flow velocity in heterogenous biofilms using microelectrodes and confocal microscopy. *Biotechnol. Bioeng.* 56, 681–688.
- Tien, C., Payatakes, A.C., 1979. Advances in deep bed filtration. *AIChE J.* 25, 737–759.
- Vaz, A., Bedrikovetsky, P., Fernandes, P.D., Badalyan, A., Carageorgos, T., 2017. Determining model parameters for non-linear deep-bed filtration using laboratory pressure measurements. *J. Petrol. Sci. Eng.* 151, 421–433.
- Weber, T.W., Chakravorti, R.K., 1974. Pore and solid diffusion models for fixed-bed adsorbers. *AIChE J.* 20, 228–238.
- You, Z., Osipov, Y., Bedrikovetsky, P., Kuzmina, L., 2014. Asymptotic model for deep bed filtration. *Chem. Eng. J.* 258, 374–385.
- Zamani, A., Maini, B., 2009. Flow of dispersed particles through porous media—Deep bed filtration. *J. Petrol. Sci. Eng.* 69, 71–88.

Experimental and Modelling of Aqueous Radioactive Waste Treatment by Ultrafiltration

LAURA RUXANDRA ZICMAN^{1,3}, ELENA NEACSU¹, FELICIA NICOLETA DRAGOLIC¹, CATALIN CIOBANU^{1,2}, GHEORGHE DOGARU¹, OANA CRISTINA PARVULESCU^{3*}, TANASE DOBRE³

¹Horia Hulubei National Institute for R&D in Physics and Nuclear Engineering (IFIN-HH), 30 Reactorului Str., 077125, Bucharest - Magurele, Romania

²Techical University of Civil Engineering of Bucharest, 124 Lacul Tei Blvd., 020396, Bucharest, Romania

³University Politehnica of Bucharest, Faculty of Applied Chemistry and Materials Science, 1-7 Gheorghe Polizu Str., 011061, Bucharest, Romania

Ultrafiltration of untreated and pretreated aqueous radioactive wastes was conducted using a spiral-wound polysulphonamide membrane. The influence of process factors on its performances was experimental studied and predicted. Permeate volumetric flux and permeate total suspended solids (TSS) were measured at different values of feed flow rate (7 and 10 m³/h), operating pressure (0.1-0.4 MPa), and feed TSS (15 and 60 mg/L). Permeate flux (42-200 L/(m²·h)) increased with feed flow rate and operating pressure as well as it decreased with an increase in feed TSS, whereas permeate TSS (0.1-33.2 mg/L) exhibited an opposite trend. A 2³ factorial plan was used to establish correlations between dependent and independent variables of ultrafiltration process.

Keywords: aqueous radioactive waste, factorial experiment, spiral-wound membrane, total suspended solids, ultrafiltration

Low and intermediate level radioactive wastes are mainly generated within the nuclear fuel cycle as well as during the production and application of radioisotopes [1,2]. Radioactive wastes are harmful to living organisms, natural resources, and environment [3].

Treatment is an essential phase in the management of aqueous radioactive wastes (ARW). It mainly depends on the type, radioactivity level, and chemical composition of the waste. After the treatment phase, ARW are separated into two parts, i.e., a small amount of secondary waste containing the bulk of radionuclides and a large volume of aqueous solution with low radioactivity that can be discharged into the environment after achieving the regulatory requirements [1].

Treatment methods for ARW generally include chemical treatment, adsorption, filtration, ion exchange, and evaporation. However, these techniques are unable to remove all contaminants, involve high operating costs, and produce large amounts of secondary waste.

Membrane separation processes used for decontamination of radioactive water have been extensively studied in recent years [1-9]. Ultrafiltration and reverse osmosis have gained considerable attention due to their relatively low capital and operating costs. A wide range of contaminants present in untreated water, municipal and industrial wastewater discharges, e.g., suspended and dissolved solids, organic matter, heavy metals, bacteria, viruses, can be removed by these processes. Membrane separation processes are often applied in the nuclear industry for removing radioisotopes and obtaining small amounts of secondary waste [9].

This paper has aimed at studying the ultrafiltration of untreated and pretreated ARW through a spiral-wound polysulphonamide membrane. The effects of process factors on membrane productivity and separation efficiency were measured and predicted.

Experimental part

ARW ultrafiltration was conducted in AQUA-EXPRESS installation (SIA "Radon", Moscow, Russia) shown in figure

1. Ultrafiltration module of this installation contains an ERU-100-1016 membrane element (JSC STC Vladipor, Russia) (fig. 2). Main characteristics of membrane are summarized in table 1.

Membrane productivity expressed by permeate volumetric flux, j_p (L/(m²·h)), and separation efficiency evaluated as permeate total suspended solids, TSS_p (mg/L), were measured at different values of process factors, i.e., feed flow rate ($G_f=7, 10$ m³/h), operating pressure ($p=0.1-0.4$ MPa), and feed TSS ($TSS_f=15, 60$ mg/L). The high value of TSS_p corresponds to untreated ARW, whereas its low level characterizes the waste pretreated by sand filtration. TSS was determined based on vacuum filtration using a 50 nm nylon membrane.



Fig. 1. AQUA-EXPRESS installation:
(1) sand filtration module, (2) ultrafiltration module, (3) reverse osmosis module



Fig. 2. ERU-100-1016 ultrafiltration membrane element

* Email: oana.parvulescu@yahoo.com

Table 1
MEMBRANE CHARACTERISTICS

Configuration	Spiral-wound
Polymer	Polysulphonamide
Nominal area	5 m ²
Length	1016 mm
Outer diameter	100 mm
Molecular weight cut-off	100 kDa

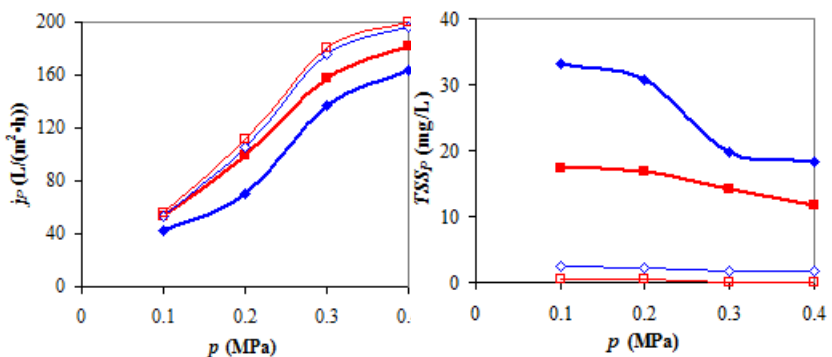


Fig. 3. Permeate flux and permeate TSS vs. operating pressure for different feed flow rates of untreated ($TSS_F=60 \text{ mg/L}$) and pretreated ($TSS_F=15 \text{ mg/L}$) ARW (untreated: $\blacklozenge G_v=7 \text{ m}^3/\text{h}$, $\blacksquare G_v=10 \text{ m}^3/\text{h}$; pretreated: $\diamond G_v=7 \text{ m}^3/\text{h}$, $\square G_v=10 \text{ m}^3/\text{h}$)

Table 2
EXPERIMENTAL MATRIX OF 2³ FACTORIAL EXPERIMENT

Exp.	G_V (m ³ /h)	p (MPa)	TSS_F (mg/L)	x_1	x_2	x_3	j_p (L/(m ² ·h))	TSS_P (mg/L)
1	7	0.1	15	-1	-1	-1	53	2.4
2	7	0.1	60	-1	-1	1	42	33.2
3	7	0.4	15	-1	1	-1	196	1.8
4	7	0.4	60	-1	1	1	164	18.4
5	10	0.1	15	1	-1	-1	56	0.6
6	10	0.1	60	1	-1	1	53	17.2
7	10	0.4	15	1	1	-1	200	0.1
8	10	0.4	60	1	1	1	182	11.6

Results and discussions

Experimental data

The effects of process factors on permeate performances in terms of its volumetric flux ($j_p=42-200 \text{ L}/(\text{m}^2\cdot\text{h})$) and TSS ($TSS_p=0.1-33.2 \text{ mg/L}$) are highlighted by the experimental results represented in figure 3. Depicted data emphasize the following issues: (i) j_p increases with *operation pressure* ($p=0.1-0.4 \text{ MPa}$) up to about 4 times, whereas TSS_p decreases with an increase in p (up to 1.8 times for untreated and up to 6 times for pretreated ARW); (ii) j_p increases with *feed flow rate* ($G_v=7, 10 \text{ m}^3/\text{h}$), i.e., 1.1-1.4 times for untreated and up to 1.1 times for pretreated ARW, whereas TSS_p decreases with an increase in G_v (1.4-1.9 times for untreated and 4-18 times for pretreated ARW); (iii) j_p is 1.1-1.5 higher and TSS_p is 11-141 lower (up to 15 times for $G_v=7 \text{ m}^3/\text{h}$ and over 28 times for $G_v=10 \text{ m}^3/\text{h}$) for *pretreated* ($TSS_F=15 \text{ mg/L}$) than for *untreated* ($TSS_F=60 \text{ mg/L}$) ARW. Accordingly, j_p increases with p and G_v as well as it decreases with an increase in TSS_F , whereas TSS_p exhibits an opposite trend.

Statistical model

Permeate flux, j_p (L/(m²·h)), and permeate TSS, TSS_p (mg/L), were selected as process dependent variables (responses). Their final values, as well as dimensionless values of process factors determined by eqs. (1)-(3), are given in table 2. Tabulated data were processed using the procedure recommended for a 2³ factorial plan resulting in eqs. (4) and (5).

$$x_1 = \frac{G_V - 8.5}{1.5} \quad (1)$$

$$x_2 = \frac{p - 0.25}{0.15} \quad (2)$$

$$x_3 = \frac{TSS_F - 37.5}{22.5} \quad (3)$$

$$j_p = 118.25 + 4.50x_1 + 67.25x_2 - 8x_3 + x_1x_2 +$$

$$+ 2.75x_1x_3 - 4.50x_2x_3 + 0.75x_1x_2x_3 \quad (4)$$

$$TSS_p = 10.662 - 3.287x_1 - 2.688x_2 + 9.438x_3 + 1.163x_1x_2 - \\ - 2.413x_1x_3 - 2.413x_2x_3 + 1.138x_1x_2x_3 \quad (5)$$

Statistical models described by eqs. (6) and (7) were obtained after eliminating insignificant regression coefficients in eqs. (4) and (5) [10-13].

$$j_p = 118.25 + 4.50x_1 + 67.25x_2 - 8x_3 + 2.75x_1x_3 - 4.50x_2x_3 \quad (6)$$

$$TSS_p = 10.662 - 3.287x_1 - 2.688x_2 + 9.438x_3 - \\ - 2.413x_1x_3 - 2.413x_2x_3 \quad (7)$$

Regression equations (6) and (7) reveal the following issues: (i) permeate flux (j_p) increases with feed flow rate (x_1), operation pressure (x_2), and x_1x_3 interaction, decreases with an increase in feed TSS (x_3) and x_2x_3 interaction, as well as it is heavily affected by x_2 factor; (ii) permeate TSS (TSS_p) decreases with an increase in x_1 , x_2 , and x_1x_3 interaction, whereas it increases with x_3 and x_2x_3 interaction; moreover, x_3 factor has a more significant effect on TSS_p .

Statistical models expressed by Eqs. (6) and (7) may be applied to predict the values of permeate flux and permeate TSS at levels of process factors in the ranges considered in the study, i.e., $G_v=7-10 \text{ m}^3/\text{h}$, $p=0.1-0.4 \text{ MPa}$, and $TSS_F=15-60 \text{ mg/L}$.

Conclusions

ARW ultrafiltration was performed using an installation containing spiral-wound polysulphonamide membrane modules. Permeate volumetric flux (j_p) and permeate TSS (TSS_p) were measured at different values of feed flow rate ($G_v=7, 10 \text{ m}^3/\text{h}$), operating pressure ($p=0.1-0.4 \text{ MPa}$), and feed TSS ($TSS_F=15, 60 \text{ mg/L}$). Permeate flux (42-200 L/(m²·h)) increased with G_v (up to 1.4 times) and p (up to about 4 times), as well as decreased with an increase in

TSS_F (1.1-1.5 times). Permeate TSS (0.1-33.2 mg/L) exhibited an opposite trend, i.e., it increased with TSS_F (11-141 times) and decreased with an increase in G_V (1.4-18 times) and p (up to about 6 times). The influence of process factors on its performances was quantified using a 2^3 factorial plan. Regression equations which were obtained could be applied to predict the values of permeate flux and TSS at levels of process factors in the ranges considered in the experimental study.

References

1. ABDEL RAHMAN, R.O., IBRAHIM, H.A., HUNG, Y.T., Water, **3**, 2011, p. 551.
2. ZAKRZEWSKA-TRZNADEL, G., Nukleonika, **51** (S1), 2006, p. 101.
3. RANA, D., MATSUURA, T., KASSIM, M.A., ISMAIL, A.F., Desalination, **321**, 2013, p. 77.
4. MISRA, B.M., RAMACHANDRAN, V., Treatment of radioactive effluents: Introduction, fundamentals, and scope of different membrane processes, Handbook of Membrane Separations: Chemical, Pharmaceutical, and Biotechnological Applications (Chapter 29), 2008, p. 827, CRC Press, Boca Raton, FL.
5. CHMIELEWSKI, A.G., HARASIMOWICZ, M., ZAKRZEWSKA-TRZNADEL, G., Czech. J. Phys., **49** (S1), 1999, p. 979.
6. ZAKRZEWSKA-TRZNADEL, G., Radioactive waste processing: Advancement in pressure-driven processes and current world scenario, Handbook of Membrane Separations: Chemical, Pharmaceutical, and Biotechnological Applications (Chapter 30), 2008, p. 843, CRC Press, Boca Raton, FL.
7. PABBY, A.K., Membr. Technol., **11**, 2008, p. 9.
8. AMBASHTA, R.D., SILLANPAA, M.E.T., J. Environ. Radioact., **105**, 2012, p. 76.
9. SANCHO, M., ARNAL, J.M., VERDU, G., LORA, J., VILLAESCUSA, J.I., Desalination, **201**, 2006, p. 207.
10. ARUS, A.V., NISTOR, I.D., PLATON, N., ROSU, A.M., MUNTIANU, G., JINESCU, C., Rev. Chim. (Bucharest), **66**, no. 1, 2015, p. 88.
11. CIOROIU, D.R., PARVULESCU, O.C., KONCSAG, C.I., DOBRE, T., Rev. Chim. (Bucharest), **68**, no. 10, 2017, p. 2311.
12. DOBRE, T., STOICA, A., PARVULESCU, O.C., STROESCU, M., IAVORSCHI, G., Rev. Chim. (Bucharest), **59**, no. 5, 2008, p. 590.
13. ION, V.A., PARVULESCU, O.C., DOBRE, T., Appl. Surf. Sci., **335**, 2015, p. 137.
14. ORBECI, C., PARVULESCU, O.C., ACCELEANU, E., DOBRE, T., Rev. Chim. (Bucharest), **68**, no. 10, 2017, p. 2325.

Manuscript received: 9.08.2017

INVESTIGATION AND MODELING OF FIXED BED CESIUM SORPTION ON NICKEL FERROCYANIDE, PRECIPITATED ON SILICA GEL

L.R. ZICMAN^{1,2}, E. NEACSU¹, L. DONE¹, L.C. TUGULAN¹, C. ALEXANDRU¹,
F.N. DRAGOLICI¹, M. NICU¹, L.F. IONASCU¹, B.T. OBREJA^{1,3}, G. DOGARU¹, T. DOBRE⁴

¹*Horia Hulubei National Institute for R&D in Physics and Nuclear Engineering (IFIN-HH),
P.O.Box MG-6, RO-077125 Bucharest-Magurele, Romania, E-mails: laura.zicman@nipne.ro;
egneacsu@nipne.ro; donelaur@nipne.ro; liviu.tugulan@nipne.ro; carmela.alexandru@nipne.ro;*

mniciu@nipne.ro; laura_ionascu@nipne.ro; bogdan.obreja@nipne.ro; dogaru@nipne.ro

²*Politehnica University of Bucharest, Doctoral School Applied Chemistry and Materials Science,
1–7 Gheorghe Polizu Street, sector 1, 011061, Bucharest, Romania*

³*University of Bucharest, Doctoral School of Geology, 36–46 Mihail Kogalniceanu Avenue,
P.O. Box 050107, Bucharest, Romania*

⁴*Politehnica University of Bucharest, Faculty of Applied Chemistry and Materials Science,
1–7 Gheorghe Polizu Street, sector 1, 011061, Bucharest, Romania, E-mail: tghdobre@gmail.ro*

Received October 10, 2016

Abstract. Cesium sorption on nickel ferrocyanide, precipitated on silica gel (PNF-SG) from low and intermediate level liquid radioactive waste was investigated in a fixed-bed column. The breakthrough characteristics of the ion-exchange system were studied at different Cs concentrations (50–150 mg/L), bed heights (20–60 mm) and feed flow rates (1–6 mL/min).

Mathematical models of Thomas and Yoon–Nelson were applied to the experimental data to investigate the column performance. The results fitted well the Thomas and Yoon–Nelson models with correlation coefficient values of $R^2 \geq 0.91$.

Key words: cesium, nickel ferrocyanide, breakthrough, modelling.

1. INTRODUCTION

In spent fuel storage pools, as coolant and, at the same time, as a protection against radiation, deionized water is used. Fuel cladding could be damaged and the fuel's volatile fission products, including 30-year halflife ^{137}Cs , would be released. ^{137}Cs is an important radio-contaminant and represents a serious radiological hazard because cesium and potassium belong to the same group in the periodic table and, consequently, potassium can be easily replaced by cesium in living cells which are able to take up cesium using the potassium transporters [1]. Chemical precipitation, adsorption, and ion exchange were applied for radioactive wastes treatment [2–5].

Ion exchange technique in which various types of ion exchangers have been widely used is an attractive method because of its simplicity, selectivity and efficiency [6–11]. The transition metal ferrocyanides were immobilized on different support materials and were used to remove cesium ions. The transition metal ferrocyanides immobilized on an anion exchange resin are simple and easy to prepare and obtainable in any given conditions: they are non hygroscopic and granular, thus they can be in a dry state. Several applications of these resins to remove radioactive cesium ions have been reported [12–13]. Composite sorbents based on potassium nickel ferrocyanide embedded in silica gel matrix were prepared and characterised by powdered X-ray diffraction analysis, IR spectra, Mössbauer spectra and electron microscopy [14].

Adsorption of Cs ions onto nickel ferrocyanide, precipitated on silica gel (PNF-SG) has been previously studied using batch-adsorption techniques. The equilibrium adsorption isotherms were used to predict how much solute can be adsorbed by PNF-SG. Batch equilibrium isotherm data were tested with Langmuir and Freundlich adsorption models and both models were found to fit the sorption isotherm data well; also cesium exchange on PNF-SG followed pseudo second-order kinetics. The results obtained in this study were presented elsewhere [15].

The objective of the present work was to study the removal of cesium ions from aqueous effluents by sorption using PNF-SG, investigated in a fixed-bed column. Fixed-bed column performance is described by the concept of the breakthrough curve. Breakthrough is said to take place when the effluent concentration crosses a set value (typically 5% of influent concentration) and exhaustion of the bed takes place when the effluent concentration is equal to another set value (typically 95% of the influent concentration) [16]. Complete exhaustion occurs when the effluent concentration is equal to the influent concentration [16–18], which might take a long time. Breakthrough capacity and percentage utilization of the column depend strongly on the operating parameters of the column, in addition to the ion exchanger properties.

Column performance of Cs ion-exchange on PNF-SG was studied at different Cs concentrations (50–150 mg/L), bed heights (20–60 mm) and flow rates (1–6 mL/min). Samples were collected at regular intervals and the breakthrough characteristics of the ion-exchange system were determined.

2. MATERIALS AND METHODS

Fixed-bed column experiments were conducted at room temperature using a glass column with an internal diameter of 20 mm and a height of 25 cm. The column was packed with PNF-SG on supporting layers of glass-wool to prevent the loss of the sorbent. The required Cs concentrations were obtained using inactive CsCl, ^{137}Cs being used as tracer. Water from Interim Spent Fuel Storage Pools with 3300 Bq/L ^{137}Cs concentration was used. Cesium was as cesium

chloride from Sigma–Aldrich Company. Work solutions were prepared by dissolving CsCl in radioactive water from spent nuclear fuel pool.

The initial pH was adjusted at 3 (determined in batch investigation) using dilute solution of hydrochloric acid.

Cesium concentration was determined by gamma spectrometry using a high resolution gamma-ray spectrometer, Canberra type, GENIE 2000 version 3.2 software and Laboratory SOurceless Calibration Software (LabSOCS), with 47.5% relative efficiency.

Breakthrough and exhaustion were considered as $C/C_0 = 0.05$ and 0.95, respectively.

3. RESULTS AND DISCUSSION

3.1. EFFECT OF INFLUENT CONCENTRATION

The breakthrough curves were obtained for different influent Cs concentrations ($C_0 = 50, 100$ and 150 mg/L) and following parameters:

- column – $\emptyset = 20 \text{ mm}$, $H = 20 \text{ mm}$
- PNF-SG weight – 5 g
- flow rate (Q) – 3 mL/min
- initial radioactive concentration of ^{137}Cs – 3300 Bq/L
- pH = 3.

The effect of influent Cs concentration on breakthrough is shown in Figure 1a.

The exhaust occurred after 315 min for 50 mg/L initial cesium concentration, while the breakthrough occurred at 180 and 150 min for 100 and 150 mg/L. For the same flow rate and bed height, when the influent concentration of Cs was increased, sharper breakthrough curves were obtained and a steep breakthrough curve was obtained at 150 mg/L. This is due to the increase in concentration gradient, which affects the ion exchange rate.

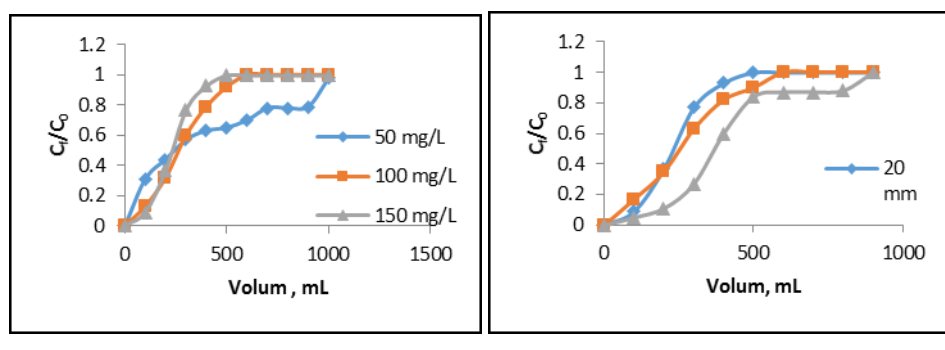
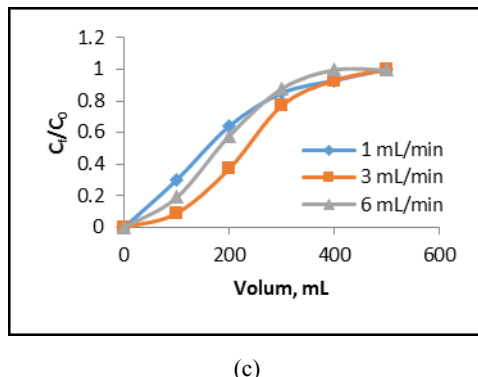


Fig. 1



(c)

Fig. 1 (continued) – Breakthrough curves: (a) the effect of influent concentrations ($Q = 3 \text{ mL/min}$; $H = 20 \text{ mm}$); b) the effect of bed heights ($C_0 = 150 \text{ mg/L}$; $Q = 3 \text{ mL/min}$); c) the effect of flow rates of feed ($C_0 = 150 \text{ mg/L}$; $H = 20 \text{ mm}$).

3.2. EFFECT OF BED HEIGHT

Effect of bed height on breakthrough curve was studied by operating the column at three different bed heights ($H = 20, 40$ and 60 mm) by charging 5, 10 and 15 g of PNF-SG, respectively. Work conditions were:

- flow rate (Q) – 3 mL/min
- influent Cs concentration – 150 mg/L
- initial radioactive concentration of ^{137}Cs – 3300 Bq/L
- pH = 3.

As can be seen from Fig. 1b, the volume of solution treated increased with the increase in bed height, due to higher availability of exchange sites. The exhaust time grew from 150 to 190 min and 295 min, when the bed height was increased from 20 mm to 40 mm and 60 mm, respectively. An increase in column length (the other parameters being kept constant) improves both the breakthrough and the overall capacity. There is a greater quantity of PNF-SG in the column and consequently, availability of ion exchange sites increases linearly with the height of the column.

3.3. EFFECT OF FEED FLOW RATE

To study the effect of flow rate, columns were charged at flow rates of 1, 3 and 6 mL/min with initial Cs concentration maintained at 150 mg/L and:

- column – $\emptyset = 20 \text{ mm}$, $H = 20 \text{ mm}$
- PNF-SG weight – 5 g
- initial radioactive concentration of ^{137}Cs – 3300 Bq/L
- pH = 3.

Since the flow rate is varying, breakthrough curves are shown in Figure 1c.

The experimental exhaust times were observed to be 157, 150 and 123 min when flow rate is increased from 1 to 3 mL/min and 6 mL/min. Earlier breakthrough and exhaustion were observed with increase in flow rate. This reduction is due to insufficient contact time in the bed. At higher flow rates, slope of the curve decreased showing high volume of unsaturated zone as a result of insufficient contact.

3.4. APPLICATION OF DYNAMIC MODELS

For the design of column exchange process, breakthrough curves for different operating conditions are required. In the absence of experimental data, these curves can be generated if a suitable model is available and the model constants are known. Solving the differential equation based models of proposed rate mechanisms is a difficult process and also they cannot be solved for all the operating conditions. Simple models which would predict the breakthrough behavior of an adsorption process are suitable for analyzing the column studies. The analysis of the breakthrough curve was done using two of these models, the Thomas model and the Yoon–Nelson one.

Thomas model

Thomas model is based on the assumption that the process follows Langmuir kinetics with no axial dispersion; the rate driving force follows second order reversible reaction kinetics. The expression of the Thomas model for a column operation is [19]:

$$\frac{C}{C_0} = \frac{1}{1 + \exp[K_{Th}q_0m/Q - K_{Th}C_0t]} \quad (1)$$

and its linearized form is:

$$\ln\left(\frac{C_0}{C} - 1\right) = \frac{K_{Th}q_0m}{Q} - K_{Th}C_0t, \quad (2)$$

where K_{Th} is the Thomas rate constant (L/min mg); q_0 is the maximum solid-phase concentration of Cs (mg/g); m is the amount of the PNF-SG in the column (g); Q is the flow rate (L/min.); C is the cesium concentration in effluent (mg/L) and C_0 is cesium concentration in influent (mg/L).

Thomas model was applied to the data at C/C_0 values between 0.05 and 0.95 for different operating conditions. The values of K_{Th} and q_0 were obtained from the plot of $\ln(C_0/C - 1)$ versus time and given in Table 1. It can be seen that R^2 values ranged from 0.9470 to 0.9996, indicating the suitability of Thomas model.

Table 1

Thomas model parameters for Cs uptake of PNF-SG for different experimental conditions

Flow rate Q , (mL/min)	Initial conc. C_0 , (mg/L)	Bed height H , (cm)	Thomas constant K_{Th} , (L/min mg) $\times 10^{-4}$	q_0 (model) (mg/g)	R^2
1	150	2	1.14	5.51	0.9996
3	150	2	3.31	7.02	0.9983
6	150	2	4.60	4.91	0.9833
3	50	2	2.68	2.89	0.9470
3	100	2	3.2	5.44	0.9994
3	150	2	3.31	7.02	0.9983
3	150	2	3.31	7.02	0.9983
3	150	4	1.92	3.87	0.9922
3	150	6	1.73	4.16	0.9654

Thomas rate constant (K_{Th}) increased from 2.68×10^{-4} to 3.31×10^{-4} with increasing the influent concentration from 50 to 150 mg/L. The rate constant was observed to grow with increasing the flow rate and to decrease with increasing the bed height. The model or theoretical breakthrough curves for Cs ion exchange on PNF-SG were obtained using the parameters K_{Th} and q_0 determined from the available experimental data for different operating conditions. The experimental and model breakthrough curves are shown in Figure 2. The breakthrough curves confirm the applicability of this model in describing the experimental data.

Yoon–Nelson model

This model was based on the assumption that the rate of decrease in the probability of adsorption for each adsorbate molecule was proportional to the probability of adsorbate adsorption and the probability of adsorbate breakthrough on the adsorbent. The Yoon–Nelson model is not only less complicated than other models, but also requires no detailed data concerning the characteristics of sorbate, the type of adsorbent, and the physical properties of sorption bed.

The Yoon–Nelson equation regarding a single component system was expressed as equation [19]:

$$\frac{C_t}{C_0 - C_t} = \exp(K_{YN}t - \tau K_{YN}), \quad (3)$$

where K_{YN} is the rate constant (h^{-1}), τ the time required for 50% sorbate breakthrough and t is the time (h).

For a symmetric breakthrough curve the quantity of solute sorbed at time τ equals half of the removal capacity, and it is calculated relative to the initial concentration and flow rate. The uptake capacity q can be calculated as equation:

$$q = \frac{C_0 Q \tau}{m}, \quad (4)$$

where m is the mass of the sorbent (g), Q the flow rate (mL/min).

From a linear plot of $\ln[C/(C_0 - C)]$ against sampling time (t), values of K_{YN} and τ were determined from the intercept and slope of the plot.

The values of K_{YN} and τ determined for different operating conditions are listed in Table 2. It was observed that the rate constant K_{YN} increased from 1.72×10^{-2} to 6.98×10^{-2} with increasing Cs inlet concentration from 50 to 150 mg/L. When the bed height increased from 2 to 6 cm, the values of K_{YN} decreased. As the flow rate increased, also K_{YN} increased.

Table 2

Yoon Nelson model parameters for Cs uptake of PNF-SG for different experimental conditions

Flow rate Q , (mL/min)	Initial conc. C_0 , (mg/L)	Bed height H , (cm)	Yoon–Nelson rate constant K_{YN} , (L/min mg) $\times 10^{-4}$	q_0 (model) (mg/g)	τ (min)	R^2
1	150	2	0.75	2.97	50	0.9415
3	150	2	3.21	5.42	69	0.9994
6	150	2	4.98	7.01	57	0.9983
3	50	2	1.72	5.52	70	0.9996
3	100	2	4.98	7.01	71	0.9983
3	150	2	6.98	4.92	69	0.9831
3	150	2	4.98	7.01	69	0.9983
3	150	4	2.88	3.87	72	0.9924
3	150	6	2.59	4.16	130	0.9654

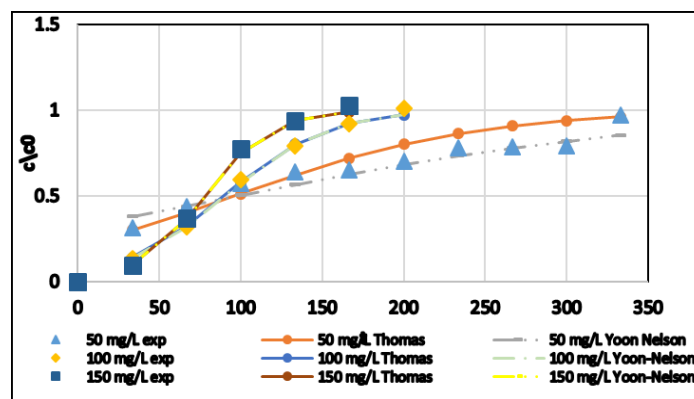


Fig. 2

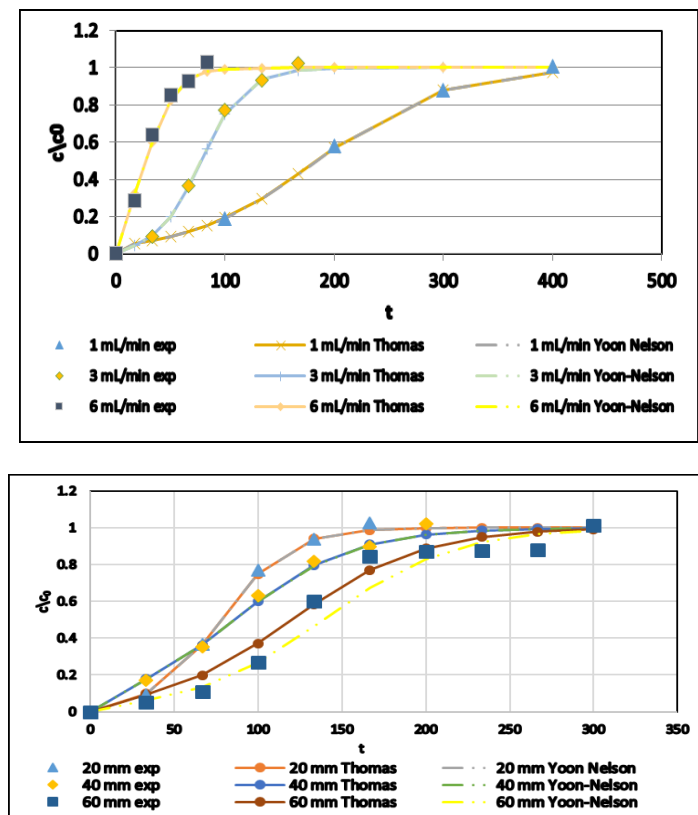


Fig. 2 (continued) – Comparison of experimental and model breakthrough curves for different feed concentrations (a), feed flow rates (b) and bed heights (c).

Table 2 indicates that the model and experimental uptake capacities were comparable and the regression coefficient (R^2) varies between 0.9415 and 0.9996. The model curves were compared with the experimental curves as shown in Figure 2. This model provided a good fit of the experimental data for all the effects studied with good correlation coefficients.

4. CONCLUSIONS

On the basis of the experimental results of this investigation, the following conclusion can be drawn: the adsorption of PNF-SG was dependent on the flow rate, the initial Cs concentration and bed depth. All experimental conditions studied show that the prediction of whole breakthrough curve is effective with the Thomas and Yoon–Nelson models. Comparing the values of R^2 of the breakthrough curves, both models can be used to describe the behavior of Cs ion exchange on PNF-SG

in a fixed-bed column. The behavior of the PNF-SG and the determined coefficients of the models for different operating conditions can be used to scale up the process.

Acknowledgments. Authors acknowledge support from the project PN II-PT-PCCA-2011-3.2-0334-SARAWAD-BB (Contract No. 156/2012).

REFERENCES

1. M. Okuda, T. Hashiguchi, M. Joyo, K. Tsukamoto, M. Endo, K. Matsumaru, N. Goto-Yamamoto, H. Yamaoka, K. Suzuki, H. Shimoji, *The transfer of radioactive cesium and potassium from rice to sake*, J. Biosci. Bioeng., **116** (3), 340–362 (2013).
2. K. Shakir, M. Sohsah, M. Soliman, *Removal of cesium from aqueous solutions and radioactive waste simulants by coprecipitate flotation*, Sep. Purif. Technol., **54**, 373–381 (2007).
3. E. Bascetin, G. Atun, *Adsorptive removal of strontium by binary mineral mixtures of montmorillonite and zeolite*, J. Chem. Eng. Data, **55**, 783–788 (2010).
4. C. Zhang, P. Gu, J. Zhao, D. Zhang, Y. Deng, *Research on the treatment of liquid waste containing cesium by an adsorption–microfiltration process with potassium zinc hexacyanoferrate*, J. Hazard. Mater., **167**, 1057–1062 (2009).
5. G. Lujaniene, S. Meleshevych, V. Kanibolotskyy, J. Sapalait, V. Strelko, V. Remeikis, O. Oleksienko, K. Ribokaite, T. Sciglo, *Application of inorganic sorbents for removal of Cs, Sr, Pu and Am from contaminated solutions*, J. Radioanal. Nucl. Chem., **282**, 787–791 (2009).
6. G.M. Walker, J.-A. Hanna, S.J. Allen, *Treatment of hazardous shipyard wastewater using dolomitic sorbents*, Water Res., **39**, 2422–2428 (2005).
7. A.M. Puziy, *Cesium and strontium exchange by the framework potassium titanium silicate $K_3Ti_4O_4(SiO_4)_3 \cdot 4H_2O$* , J. Radioanal. Nucl. Chem., **237**, 73–80 (1998).
8. T.A. Todd, K.N. Brewer, D.J. Wood, P.A. Tullock, N.R. Mann, L.G. Olson, *Evaluation and testing of inorganic ion exchange sorbents for the removal of cesium-137 from Idaho chemical processing plant acidic tank waste*, Sep. Sci. Technol., **36**, 999–1016 (2001).
9. A.M. El-Kamash, *Evaluation of zeolite A for the sorptive removal of Cs⁺ and Sr²⁺ ions from aqueous solutions using batch and fixed bed column operations*, J. Hazard. Mater., **151**, 432–445 (2008).
10. P.A. Hass, *A Review of Information on Ferrocyanide Solids for Removal of Cesium from Solutions*, Separ. Sci. Technol., **28** (17–18), 2479–2506 (1993).
11. Y. Lin, G.E. Fryxell, H. Wu, M. Engelhard, *Selective sorption of cesium using selfassembled monolayers on mesoporous supports*, Environ. Sci. Technol., **35** (19), 3962–3968 (2001).
12. H.-J. Won, J.-K. Moon, C.-H. Jung, W.-Y. Chung, *Evaluation of ferrocyanide anion exchange resins regarding the uptake of Cs⁺ ions and their regeneration*, Nuclear Engineering and Technology, **40** (6), 489–496 (2008).
13. K. Watari, K. Imai, Y. Ohmomo, Y. Muramatsu, Y. Nishimura, M. Izawa, L.R. Baciles, *Simultaneous adsorption of Cs-137 and I-131 from water and milk on metal ferrocyanide-anion exchange resin*, J. Nucl. Sci. Techn., **25** (5), 495–499 (1988).
14. J. Orechovská, P. Rajec, *Sorption of cesium on composite sorbents based on nickel ferrocyanide*, J. Radioanal. Nucl. Chem., **242** (2), 387–390 (1999).
15. L.R. Zicman, E. Neacsu, L. Done, L.C. Tugulan, F.N. Dragolici, B.T. Obreja, T. Dobre, *Removal of ¹³⁷Cs ions from aqueous radioactive waste using nickel ferrocyanide, precipitated on silica gel*, Bulletin of Romanian Chemical Engineering Society, **2** (1), 84–99 (2015).

16. K. Naddafi, R. Nabizadeh, R. Saeedi, A.H. Mahvi, F. Vaezi, K. Yaghmaeian, A. Ghasri, S. Nazmara, *Biosorption of lead (II) and cadmium (II) by protonated Sargassum glaucescens biomass in a continuous packed bed column*, J. Hazard. Mater., **147** (3), 785–791 (2007).
17. O. Hamdaoui, *Dynamic sorption of methylene blue by cedar sawdust and crushed brick infixed bed columns*, J. Hazard. Mater. **138** (2), 293–303 (2006).
18. O. Hamdaoui, *Removal of copper (II) from aqueous phase by purolite C100-MB cation exchange resin in fixed bed columns: modeling*, J. Hazard. Mater., **161** (2–3), pp. 737–746 (2009).
19. C. Mahendra, P.M. Sathya Sai, C. Anand Babu, K. Revathy, K.K. Rajan, *Analysis and modeling of fixed bed sorption of cesium by AMP-PAN*, J. Environ. Chem. Eng., **3** (3), 1546–1554 (2015).

COMPARISON STUDY OF INORGANIC CEMENTS TO THE CONDITIONING OF THE SECONDARY RADIOACTIVE WASTE

M. NICU¹, L. IONASCU¹, F. DRAGOLICI¹, E. NEACSU¹, L. ZICMAN^{1,2}, B. OBREJA^{1,3}

¹*Horia Hulubei* National Institute of Physics and Nuclear Engineering, P.O. Box MG-6, RO-077125 Magurele, Romania

²*Politehnica* University of Bucharest, Doctoral School Applied Chemistry and Materials Science, 1–7 Gheorghe Polizu street, sector 1, 011061, Bucharest, Romania

³University of Bucharest, Doctoral School of Geology, 36–46 Mihail Kogalniceanu Avenue, P.O. Box: 050107, Bucharest, Romania,
E-mails: mniciu@nipne.ro; laura_ionascu@nipne.ro; fdrag@nipne.ro; egneacsu@nipne.ro;
laura.zicman@nipne.ro; bogdan.obreja@nipne.ro

Received September 14, 2016

Abstract. Portland cement is currently the most widely used as a matrix for shielding and immobilization of low level radioactive waste. Performance in the long term of cement based matrix depends on the cement formulation as well as the interactions between cement and radioactive waste components. Also a comparison of Portland cement with other composite cements was made. This paper presents the results regarding the influence of cement and the concentrate content on properties of waste form cement, such as: fluidity, setting time, and compressive strength (in fresh and hardened state). A simulated concentrate and different types of cement were used in this study. The engineering properties of the resulting paste or mortar are correlated with XRD characterization data in order to obtain an optimized formula of cement based matrix.

Key words: Cement, radioactive waste, XRD, mechanical tests.

1. INTRODUCTION

During the treatment of aqueous radioactive waste by membrane separation processes, two effluents streams result. These are the clarified permeate and a quantity of concentrate containing the particulate and colloidal material rejected by the membrane [1–4]. Membrane process used for liquid radioactive waste treatment offer a series of advantages with high decontamination factors, large volume reduction and low energy consumption [5–6]. The use of cement to immobilize concentrates from liquid radioactive treatment has been an attractive process because of the strength and durability of properly set compositions. The chemical and physical properties of cement are well known and experience in using it for construction extends over many decades.

Cement technology has been developed to meet the demands for improved quality of the solidified waste forms. Conventional cementitious materials such as Portland cement and Portland composite cements made with supplementary cementitious materials in the form of fly ash, iron blast furnace slag, silica fume, natural pozzolans, can be used to create reliable immobilizing elements for safe storage and disposal of wastes [7].

The concentrate must be immobilized into a structural stable waste form with acceptable mechanical, chemical and physical properties that provide integrity during handling, storage, transportation, disposal and the long term stability of the waste form in disposal environment. The immobilization implies the mixing of the concentrate with various cement types (OPC and composite cements) to convert this radioactive waste in a matrix environmentally acceptable from the radioactive safety point of view for interim storage and/or final disposal [8–13]. The presence of this concentrate can change the properties of the cement waste form and an upper limit for its loading may be imposed. The chemistry of the waste and the matrix must be compatible in order to satisfy the processing requirements [14]. The matrix material must be adapted to the radioactive components in the waste, the chemical and physical properties of the waste type; and the behavior of the package with regard to disposal conditions. Primary barriers for limiting the release of radionuclides are formed during the immobilization process. The accumulated knowledge data established that there are two mechanism involved for the radioactive waste conditioning in cement-based matrices: physical immobilization and chemical interaction. Experiments are carried out to characterize in terms of their setting behaviour, solid phases by XRD and mechanical strength development.

This paper presents the results obtained from analyzing of the potential cement form matrix realized with two types of cement and different ratio of concentrate.

2. EXPERIMENTAL PART

2.1. RAW MATERIALS

To determine the effect of composite cement on the mechanical properties and microstructural characterization, blends of different cement and sand with a range of possible concentrate were prepared.

The raw materials used for this work were two types of cement and sand. A commercially available composite cements CEM III/A 42.5 N-LH and CEM V/A (S-V) 42.5 N from Lafarge Romania were used as the binder material in this study. Also, sand was added in samples which act as filler in the mix design.

The main constituents of these composite cements are reported in Table 1.

Table 1

Composite cement composition

Cement	Composition (SR EN 197-1)				
	Clinker Portland (%)	Filler-Blast furnace slag (%)	Filler-Ash (%)	Calcium sulfate (%)	Ferrous sulfate (%)
CEM III/A	35 ÷ 64	36 ÷ 65	–	0 ÷ 5	< 1%
CEM V/A	40 ÷ 64	18 ÷ 30	18 ÷ 30	0 ÷ 5	< 1%

The chemical composition of blends components was characterized by X-ray fluorescence spectrometry (Xenemetrix EX-6600 SDD model) and the results are listed in Table 2. The spectral analyses were performed with nEXt software, version 2.0.q.6.

Table 2

Chemical composition (weight %) of blends components

Chemical composition	Blends components	
	CEM III/A	CEM V/A
CaO	61.21	54.65
SiO ₂	25.18	27.12
Al ₂ O ₃	5.68	9.45
MgO	3.82	2.81
Fe ₂ O ₃	2.37	4.14
K ₂ O	0.74	0.96
Na ₂ O	0.4	–
TiO ₂	0.32	0.56
MnO	0.23	0.22
SrO	0.05	0.05
ZnO	–	0.02
ZrO ₂	–	0.01

2.2. PREPARATION OF THE SAMPLES

In order to obtain an optimized formula of cement matrix form was simulated the composition of radioactive concentrate. In a previous paper were prepared samples based on Portland cement with concentrate with different pH values and they were mechanically tested for compression in order to obtain optimal value of pH that does not influence negatively mechanical properties of the cement matrix [15]. For assess if the content of concentrate and cement have harmful effects on the concrete stability, a simulated concentrate with pH 8 was prepared and the composition is listed in Table 3.

Table 3
The chemical composition of simulated concentrate

Chemical composition	Units	Concentrate
CaCl ₂	g/l	46.9
FeSO ₄	g/l	44.3
K ₂ SO ₄	g/l	50
Co(NO ₃) ₂	g/l	1.65
Sodium citrate	g/l	20
Na ₃ PO ₄	g/l	5.3
Na ₂ CO ₃	ml	125 solution (20%)

Once different composite cement and contents of concentrate were formulated, the selection was refined by tests on mortar. In this paper samples based on composite cement with different concentrations of concentrate (20%, 30% and 45% by weight) were prepared.

For convenience, the cement formulations investigated are noted CMV-%C/CMIII-%C.

The mix ingredients and proportions are provided in Table 4.

Table 4
Mortar mixture designs

Sample symbol	CEM III-A/Sand ratio	CEM V-A/Sand ratio	Concentrate (%)	Water/cement ratio
CMIII-ref	1:1	—	—	0.45
CMV-ref	—	1:1	—	0.45
CMIII-20	1:1	—	20	0.25
CMIII-30	1:1	—	30	0.15
CMIII-45	1:1	—	45	—
CMV-20	—	1:1	20	0.25
CMV-30	—	1:1	30	0.15
CMV-45	—	1:1	45	—

Mixes of composite cement-concentrate mortars were prepared with different cement and filler in order to obtain a better understanding of the raw material characteristics and material reactions.

The concentrate weight loading was calculated from the weight value of cement.

The pastes of cement formulations were obtained by mixing cement powder, sand and concentrate. For samples with a proportion lower than 45% was added water. The water that is necessary for the mixing of components may rapidly become chemically bound in the system. For all these samples no water bleeding observed.

On these samples were performed tests of compressive strength and microstructural characterization in order to obtain results regarding the influence of cement type on the conditioning matrix. Prisms specimens with dimensions of $40 \times 40 \times 160$ mm were used to determine the compressive strength of the corresponding curing age. The compression tests, performed on samples, were done in a construction material laboratory using a digital press machine type MATEST, with loading rates of 1.2 MPa/s.

The hydration products were studied using a Bruker X-ray diffractometer using Cu K α radiation ($\lambda = 1.5418$ Å), diffraction angle 2 theta ranged between 5° and 70° , a step size of 0.02° and an acquisition time of 4 sec/step. Powder X-ray diffraction (XRD) was performed at 5 days cure time. A criterion for the analysis precision is the sample preparation. In order to obtain a reproducible result, the samples were grounded to a specific particle size (< 100 μm) for analysis by X-ray diffraction.

3. RESULTS

Characterizations performed on the cement based matrix used in this work were compressive strength and X-ray diffraction.

Compressive strength

Prisms specimens with dimensions of $40 \times 40 \times 160$ mm were mechanically tested after 7, 14 and 28 days from preparation. For the presented composite cement systems were obtained compressive strength values according to Fig. 1 and Fig. 2 which were compared with the reference cement-water system.

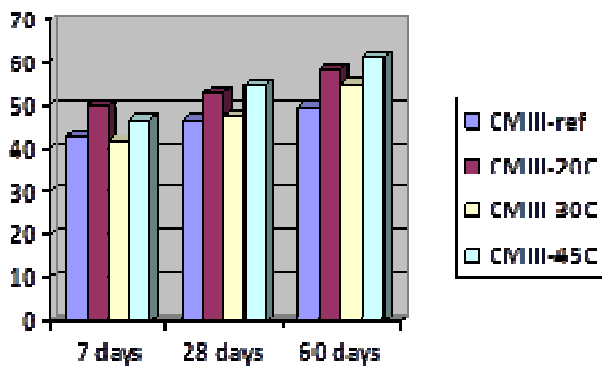


Fig. 1 – The compressive strength evolution in time for cement III – concentrate system.

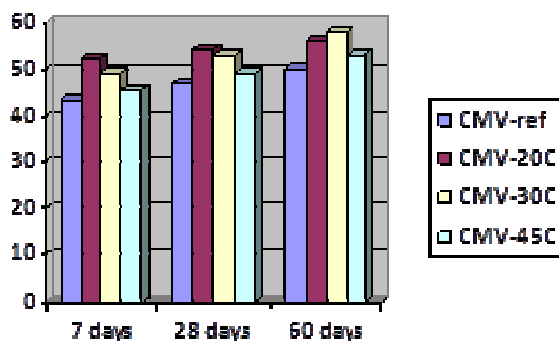


Fig. 2 – The compressive strength evolution in time for cement V – concentrate system.

4. DISCUSSION OF RESULTS

The quality of the waste form can be determined and controlled by the physic-chemical properties of the conditioned waste. The mechanical strength is an important property of cemented waste forms. The mechanical strength increases with decreasing w/c ratios. Increasing amounts of concentrate in cemented waste forms lead to a small decrease in the mechanical strength.

The samples of cement systems have developed a good mechanical structure and the compressive strength values are included in the accepted limits for the matrix durability, much higher than the minimum strength of 5 MPa needed for waste form.

Phase analysis

To assess the composition of the samples, powder X-ray diffraction (XRD) was used.

X-ray diffraction was conducted on set and cured mixtures (5 days) to ensure the hydration products are formed. The results obtained as reference sample through XRD on the hydrated cement (hydrated CEM III-A and hydrated CEM V-A) were subject of a previous paper [16] and are presented in Figures 3 and 4.

The XRD spectrum of the hydrated CEM III/A (Fig. 3) emphasizes the appearance of the crystalline hydrated compounds such as: tricalciumhydrosulfataluminate similar to the natural ettringite, calcium hydroxide well crystallized from the intergranular solution, the hexagonal calcium hydroaluminate and the compound $\text{Ca}_2(\text{AlO}_2)_3(\text{OH})(\text{H}_2\text{O})$. There were also identified compounds which remain unreacted: tricalcium silicate (C_3S), dicalcium silicate (C_2S), dicalcium aluminoferrite (C_2AF) and quartz (SiO_2).

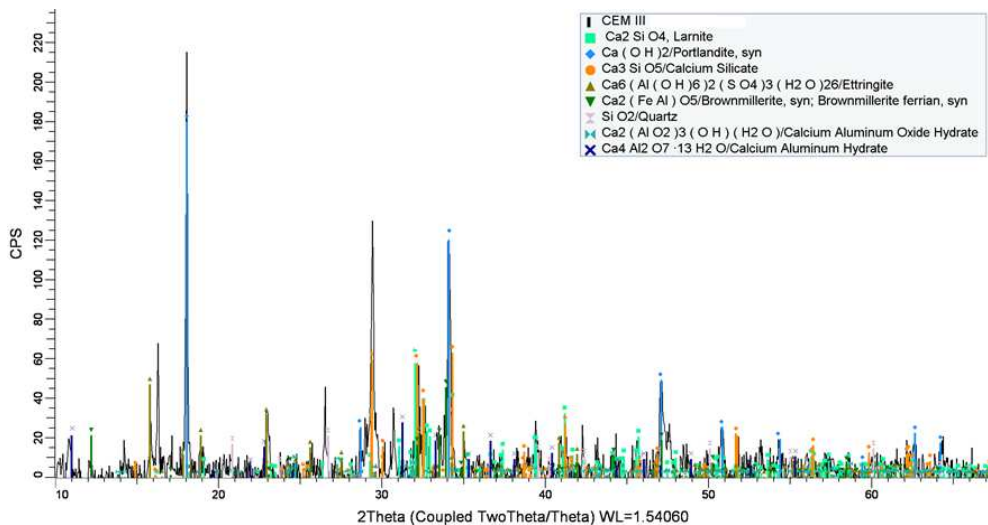


Fig. 3 – Diffraction spectrum for hydrated CEMIII-A.

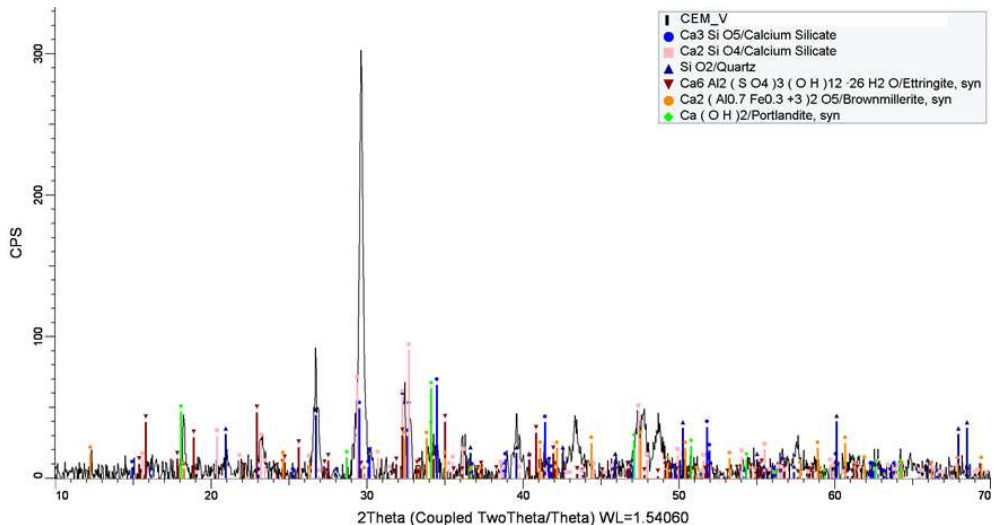


Fig. 4 – Diffraction spectrum for hydrated CEMV-A.

In the diffractogram obtained on the hydrated sample CEM V/A (Fig. 4) is observed, as in the case of sample hydrated CEM III/A, the appearance of the hydration formations tricalciumhydrosulfataluminite and the calcium hydroxide. Its characteristic lines are smaller than those obtained in hydrated CEM III/A. The mineralogical compounds tricalcium silicate (C_3S), dicalcium silicate (C_2S), dicalcium aluminoferrite and quartz, remained unreacted and are emphasized

through their specific peaks and are in higher quantities than in case of the hydrated sample CEM III/A.

The powder XRD patterns for cement formulations (CMIII-20, CMIII-30, CMIII-45 and CMV-20, CMV-30, CMV-45) are given in Figures 5 and 6.

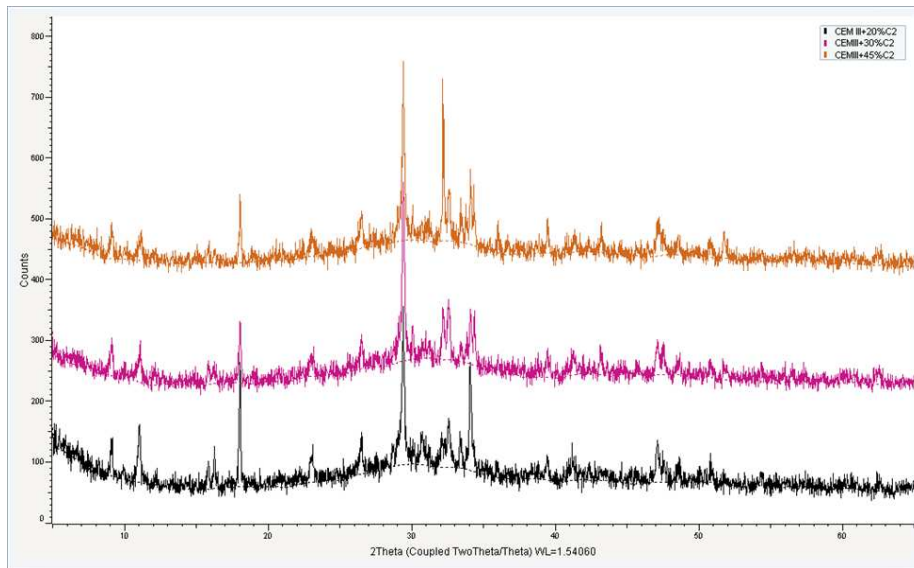


Fig. 5 – Diffraction spectra for cement systems based on CEM III-A with concentrate.

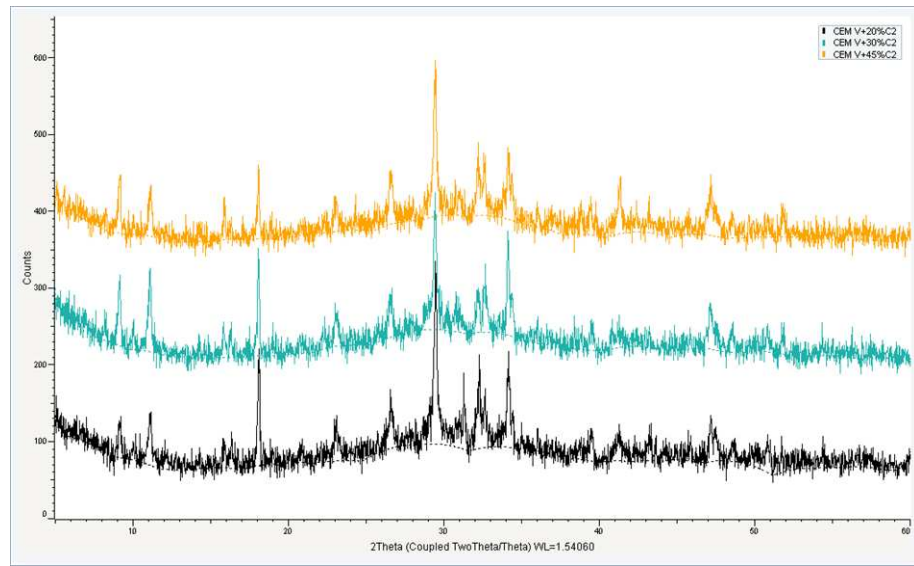


Fig. 6 – Diffraction spectra for cement systems based on CEM V-A with concentrate.

From the presented diffraction spectra (Figs. 5 and 6), both in the case of CEM III and also in the case of CEM V, we can notice that the specific peaks intensities of the anhydride cement components (tricalcium silicate C_3S and dicalcium silicate C_2S) are not decreasing and also the hydrosilicates of calcium which are formed through the cement hydration are lower and have a low degree of crystallinity than in the sample of the cement without the addition of concentrate.

It was noticed that, when embedding concentrate in cement, the characteristic peaks of $Ca(OH)_2$ become low in intensity but the chemical interactions occur without affecting the cement hydration products and also the chemical stability.

5. CONCLUSIONS

In this research, two types of the reference composite cements (CEM III-A and CEM V-A) were used to provide comparative characteristics to cement based matrix.

The main conclusions of the paper are as follows:

- Both cement systems with CEM-III and CEM-V have almost similar compressive strength values that are included in the accepted limits for the matrix durability (above 5MPa) and these values revealed a dense matrix.
- The structural investigation by X-ray diffraction of the samples prepared with different type of composite cement and concentrate at different concentration offer structural information regarding the interaction between the concentrate with the major hydration products of the matrix.
- Embedding of concentrate in different type of cement do not lead to important changes in the cement hardening structure so it has no negative influences on the cement hydration products.
- The final matrix obtained by embedding in cement of the concentrate is a quite complex physical-chemical system, as structure and composition, far from the chemical equilibration of the subsystems components.

Acknowledgements. Funding for this research was provided from the project IFIN-JINR no. 44/04-4-1121-2015/2017.

REFERENCES

1. *Advances in Technologies for the Treatment of Low and Intermediate Level Radioactive Liquid Wastes*, IAEA, Technical Report Series TRS-370 (1994).
2. International Atomic Energy Agency, *Application of membrane technologies for liquid radioactive waste processing*, Technical Report Series No. 431, IAEA, Vienna, 2004.
3. S.K. Sen Gupta, L.P. Buckley, S. Rimpelainen, A.Y. Tremblay, *Liquid Radwaste Processing with Spiral Wound Reverse Osmosis*, WM'96 Conference, Tucson, Arizona (1996).

4. Dulama M., Deneanu N., Pavelescu M., Pasare L., *Combined radioactive liquid waste treatment processes involving inorganic sorbents and micro/ultrafiltration*. Rom. J. Phys., **54**, 851–859 (2009).
5. Grazyna Zakrzewska-Trznadel, *Advances in membrane technologies for the treatment of liquid radioactive waste*, Desalination 321 (2013), pp 119–130.
6. Anil Kumar Pabby, *Membrane techniques for treatment in nuclear waste processing: global experience*, Membr. Tecnol., 11, (2008), 9–13.
7. International Atomic Energy Agency, *The Behaviours of Cementitious Materials in Long Term Storage and Disposal of Radioactive Waste*, IAEA-TECDOC-1701 (2013).
8. International Atomic Energy Agency, *Improved Cement Solidification of Low and Intermediate Level Radioactive Waste*, IAEA, Technical Report Series TRS-350 (1992).
9. C.H. Mattus, T.M. Gillian, *A Literature review of mixed waste components: sensitivities and effects upon solidification/stabilization in cement – based matrices*, ORNL/TM-12656 (1994).
10. *Handling and Processing of Radioactive Waste from Nuclear Applications*, IAEA, Technical Report Series TRS-402 (2001).
11. C. Shi and R. Spence, *Designing of Cement – Based Formula for Solidification/Stabilization of Hazardous, Radioactive and Mixed Wastes*, Critical Reviews in Environmental Science and Technology 34, 391–417 (2004), Taylor and Frances Inc.
12. R. Molviga and R. Chandhany, *Factors affecting hazardous waste solidification/stabilization: A review*, J. Hazardous Waste B 137, 267–276 (2006).
13. N.D.M. Evans, *Binding mechanisms of radionuclides to cement*, Cement and Concrete Research, 38, 543–553 (2008).
14. International Atomic Energy Agency, *Treatment and conditioning of spent ion exchange resins from research reactors, precipitation sludges and other radioactive concentrates*, IAEA-TECDOC-689 (1993).
15. M. Nicu, L. Ionascu, F. Dragolici and E. Neacsu, *The influence of chemical composition of the secondary radioactive waste on cement matrix conditioning*, Energy and Clean Technologies, Vol. 1, SGEM2016 Conference Proceedings, ISBN 978-619-7105-63-6/ISSN 1314-2704, Book4, 2016, 49–55.
16. L. Ionascu, M. Nicu, C. Turcanu, F. Dragolici, Gh. Rotarescu, *Study of the conditioning matrices for aluminitium radioactive wastes*, Rom. J. Phys., **59**, 360–368 (2014).

EFFECT OF PROCESS FACTORS ON THE PERFORMANCES OF REVERSE OSMOSIS PROCESS IN AN AQUEOUS RADIOACTIVE WASTE TREATMENT PLANT

Laura Ruxandra ZICMAN¹, Elena NEACSU², Laurentiu DONE³,
Felicia Nicoleta DRAGOLICI⁴, Tanase DOBRE⁵

This paper has aimed at studying the effect of process factors on the performances of the reverse osmosis (RO) process in an aqueous low and intermediate level radioactive waste treatment plant. The experiments were performed using actual aqueous radioactive waste (ARW) containing various radionuclides and nonradioactive chemical species. Feed ARW pressure (2-4 MPa), pH (4.8-8.2) and temperature (25-45°C) were considered as process factors. Performances of polyamide Hydranautics SWC1-4040 membrane were evaluated in terms of its productivity and efficiency. Membrane productivity was expressed as permeate flux (20-140 L/(m²·h)) and its efficiency as permeate conductivity (150-270 µS/cm) and salt rejection (79-87%), as well as permeate cobalt concentration (0.1-0.9 mg/L) and cobalt rejection (43-95%).

Keywords: reverse osmosis, aqueous radioactive waste, permeate flux, salt rejection

1. Introduction

Due to a high efficiency, easy operation, compact equipment, simplicity in the process control, low capital and operating expenses, membrane technology is being used extensively for various separation and purification processes [1-10]. Reverse osmosis (RO) as a feasible separation process is a relatively young technology. Osmosis is a natural phenomenon in which a solvent (usually water) passes through a semipermeable barrier from the side with lower solute concentration to the one with higher solute concentration (Fig. 1a). Water

¹Ph.D. Student, Faculty of Applied Chemistry and Materials Science, University POLITEHNICA of Bucharest, Romania / Engineer, Horia Hulubei National Institute for R&D in Physics and Nuclear Engineering (IFIN-HH), Romania, e-mail: laura.zicman@nipne.ro

²Senior Engineer for Technological Development, Horia Hulubei National Institute for R&D in Physics and Nuclear Engineering (IFIN-HH), Romania, e-mail: egneacsu@nipne.ro

³Physicist, Horia Hulubei National Institute for R&D in Physics and Nuclear Engineering (IFIN-HH), Romania, e-mail: donelaur@nipne.ro

⁴Senior Researcher, Horia Hulubei National Institute for R&D in Physics and Nuclear Engineering (IFIN-HH), Romania, e-mail: fdrag@nipne.ro

⁵Prof., Dept. of Chemical and Biochemical Engineering, University POLITEHNICA of Bucharest, Romania, e-mail: tghdobre@gmail.com

continues to flow until the chemical potential equilibrium of the solvent is established (Fig. 1b). Osmotic pressure is the pressure required to stop water flow and reach the equilibrium.

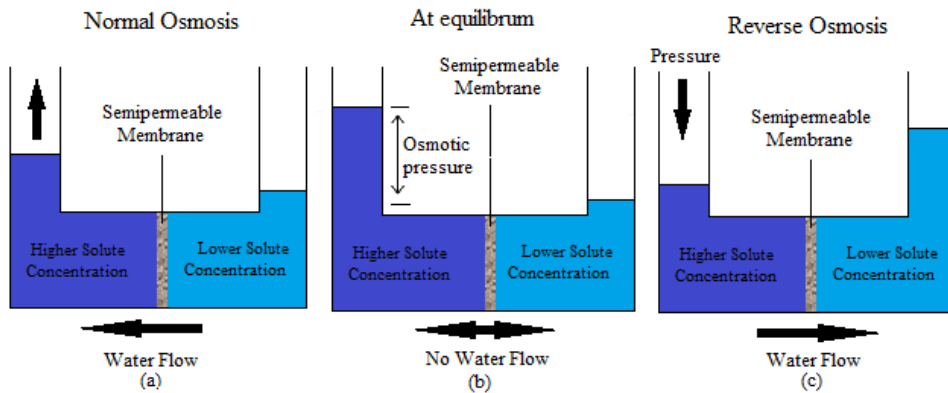


Fig. 1. Schematic of normal osmosis (a), equilibrium (b) and reverse osmosis (c) phenomena

If a pressure difference greater than the osmotic pressure difference is applied, the flow of water (solvent) is reversed, as it can be seen in Fig. 1c; as a result, separation of water from the solution occurs as pure water flowing from the high concentration side to the low concentration side. This phenomenon is termed reverse osmosis.

A RO membrane acts as a semipermeable barrier allowing a selective passage of a particular species (solvent) while partially or completely retaining other species (solutes). Chemical potential gradients across the membrane provide the driving forces for solute and solvent transport across the membrane. The solute chemical potential gradient is usually expressed in terms of concentration, whereas the water (solvent) chemical potential gradient is generally expressed as pressure difference across the membrane [11].

Three streams (and associated variables) of the RO membrane process are involved: *the feed water* enters the RO membrane under pressure (enough pressure to overcome osmotic pressure), the water molecules pass through the semi-permeable membrane resulting in the *permeate* (or *product*) *stream* while the salts and other contaminants are not allowed to pass and are discharged through the *concentrate* (or *reject*) *stream*, which goes to drain or can be fed back into the feed water supply to be recycled through the RO system. A few important parameters of RO process are further highlighted.

The water flux through the membrane, J_w , is defined by Eq. (1), where G_w is the volumetric or mass flow rate of water and A_m the membrane surface area.

$$J_w = \frac{G_w}{A_m} \quad (1)$$

The solute mass flux, J_{ms} , is given by Eq. (2), where G_{ms} is the mass flow rate of solute.

$$J_{ms} = \frac{G_{ms}}{A_m} \quad (2)$$

The solute rejection, R , is expressed by Eq. (3), where C_P is the permeate solute concentration and C_F the feed solute concentration.

$$R = 1 - \frac{C_P}{C_F} \quad (3)$$

The quantity of water that passes through the membrane (the permeate) is evaluated in terms of water recovery, r , defined by Eqs. (4) and (5) for a batch and a continuous RO system, respectively, where V_F is the feed volume, V_P the permeate volume, F_F the feed flow rate, F_P the permeate flow rate and Δt the operating time.

$$r = \frac{\sum J_w A_m \Delta t}{V_F} = \frac{V_P}{V_F} \quad (4)$$

$$r = \frac{J_w A_m}{F_F} = \frac{F_P}{F_F} \quad (5)$$

The concentration factor, CF , is defined by Eq. (6) as the ratio between the solute concentration in the concentrate stream (C_C) and its concentration in the feed stream (C_F).

$$CF = \frac{C_C}{C_F} \quad (6)$$

RO is used industrially for the production of drinking water from saline or brackish waters and is increasingly being used for the treatment of wastewaters. RO membranes have been recently applied to process the liquid radioactive waste from commercial nuclear power plants [12-14]. Because nearly all contaminants from a solution (dissolved gases and tritium being two exceptions) are rejected by RO, the high purity product water is usually of such low activity (sometimes after ion exchange polishing) that it is suitable for discharge into the environment. A RO system in the nuclear industry is usually a part of an integrated liquid waste treatment system and is used to replace or improve the existing evaporation and/or ion exchange technology.

Experiments were conducted at Horia Hulubei National Institute for R&D in Physics and Nuclear Engineering (IFIN-HH) in a low and intermediate level

radioactive waste (LILRW) treatment plant. Aqueous radioactive waste (ARW) was treated in order to determine the influence of different parameters, *i.e.*, feed pressure, pH and temperature, on membrane productivity and efficiency. Membrane productivity was evaluated by permeate volumetric flux and its efficiency was assessed by measuring permeate conductivity and Co (radioactive species) concentration in permeate (representing a measure of rejection of all salts and Co, respectively).

2. Materials and method

RO membrane element (Hydranautics SWC1-4040, Italy) used in this experiment is presented in Fig. 2 and its main characteristics are summarized in Table 1. The membrane consists of a compact base of 30–60 nm polyamide (PA), whose microstructure is shown in Fig. 3. Initial pH of ARW was adjusted using concentrated nitric acid and 30% sodium hydroxide solution.

Table 1

Membrane characteristics

Membrane type	Spiral wound
Membrane material	Composite polyamide
Membrane surface area	6.5 m ²
Permeate flowrate	4.5 m ³ /day
Salt rejection capacity	Min. 99.5%
Working pressure	Max. 6.9 MPa
Permeate chlorine concentration	Max. 0.1 ppm
Operating temperature	Max. 45 °C
pH range	3-10
Feed water turbidity	1.0 NTU
Concentrate:permeate flow rate ratio	Min. 5:1



(a)

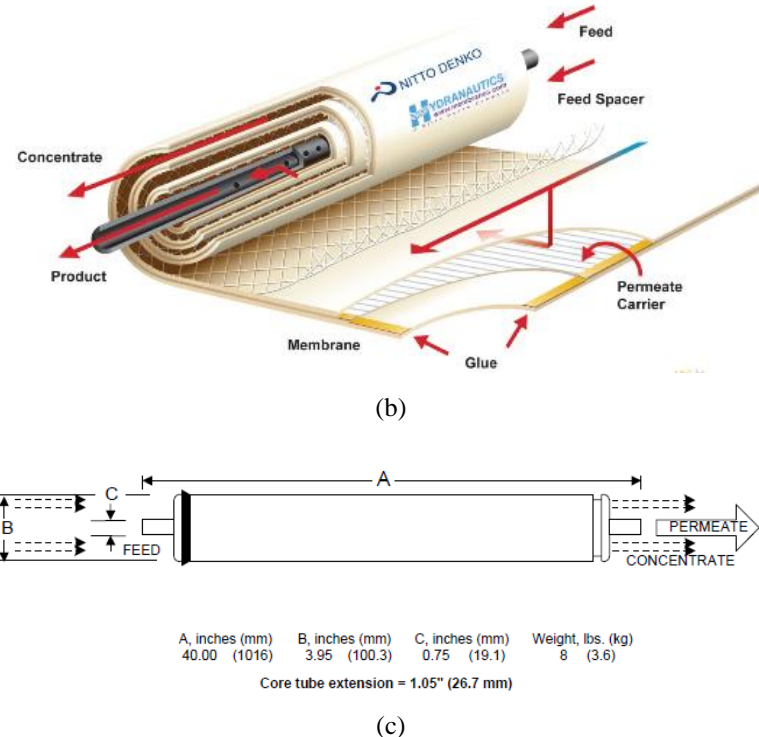


Fig. 2. Hydranautics SWC1-4040 RO membrane element (a), membrane structure (b) and geometric dimensions (c) [15].

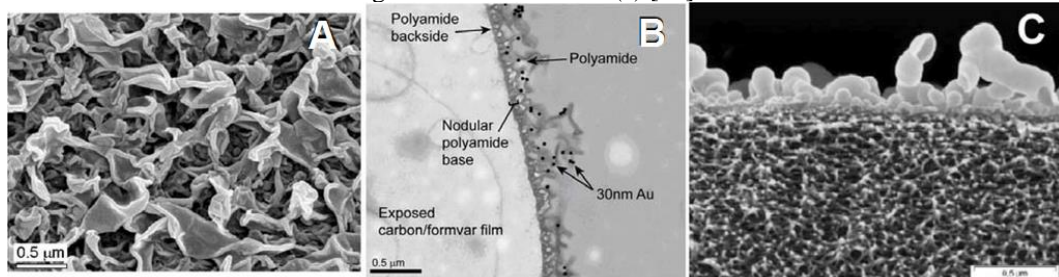


Fig. 3. Electron micrographs of the polyamide (PA) layer:
 (A) structure of the PA surface [16]; (B) TEM cross section of an isolated PA layer [17];
 (C) SEM cross section of a PA layer [18].

Feed, permeate and concentrate flow rates were measured with flowmeters. Conductivity was measured with Schott Lab 960 conductivity meter equipped with two conductivity cells, LF413T and LF313T, for high and low values, respectively. Co concentration was measured using Co^{60} as tracer. Co^{60} activity was determined by gamma spectrometry using a high resolution gamma-ray spectrometer, Canberra type, GENIE 2000 version 3.2 software and

Laboratory SOurceless Calibration Software (LabSOCS). RO process studied in this paper is included in the technological scheme shown in Fig. 4.

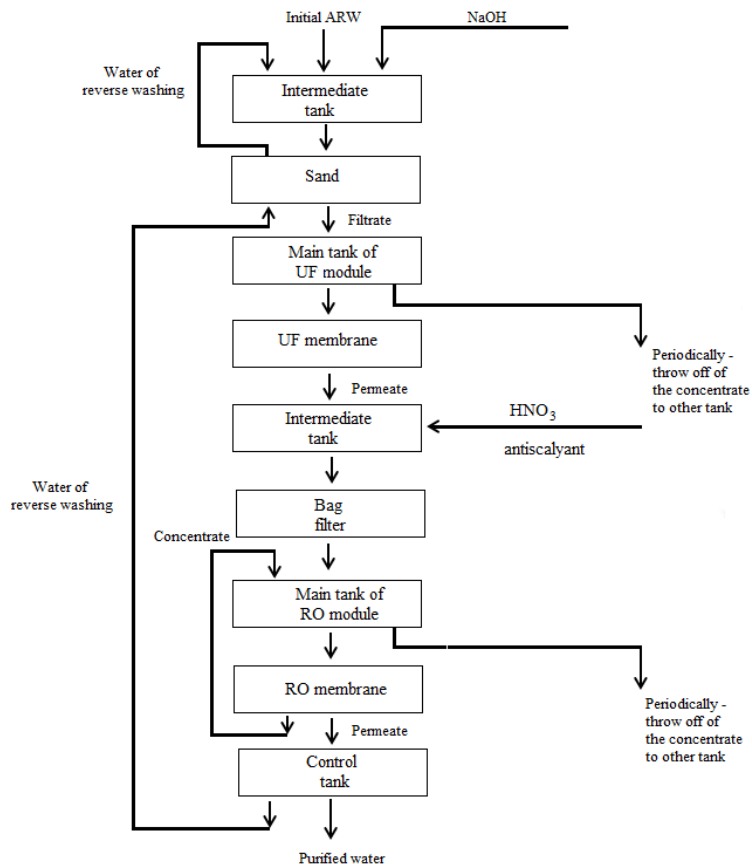


Fig. 4. Technological scheme for treating the ARW.

The permeate obtained after ultrafiltration module represented the RO module feed. It was characterized and its parameters are shown in Tables 2 and 3.

**Table 2
Radioactivity concentration of RO module feed**

Radionuclide	Activity, Bq/L
Co-60	10.68
Cs-137	1.62
Am-241	1.90

Table 2

Table 3

Physico-chemical parameters of RO module feed

No.	Parameter	Value	No.	Parameter	Value
1	pH	7.1	17	Al ³⁺	<0.01 mg/ dm ³
2	Conductivity	1240 µS/cm	18	S ²⁻	<0.1 mg/ dm ³
3	TDS	720 mg/dm ³	19	SO ₃ ²⁻	<1 mg/ dm ³
4	NH ₄ ⁺	<0.01 mg/ dm ³	20	As ⁺	<0.01 mg/ dm ³
5	NO ₃ ⁻	3.56 mg/ dm ³	21	Pb ²⁺	<0.01 mg/ dm ³
6	NO ₂ ⁻	<0.01 mg/ dm ³	22	Cd ²⁺	0.09 mg/ dm ³
7	SO ₄ ²⁻	137.1 mg/ dm ³	23	Cr ³⁺ + Cr ⁶⁺	0.02 mg/ dm ³
8	Cl ⁻	100 mg/ dm ³	24	Fe ²⁺ + Fe ³⁺	0.48 mg/ dm ³
9	Br ⁻	<0.01 mg/ dm ³	25	Cu ²⁺	0.46 mg/ dm ³
10	F ⁻	0.39 mg/ dm ³	26	Ni ²⁺	0.34 mg/ dm ³
11	PO ₄ ³⁻	3.43 mg/ dm ³	27	Zn ²⁺	0.16 mg/ dm ³
12	Ca ²⁺	76.13 mg/ dm ³	28	Hg ²⁺	<0.01 mg/ dm ³
13	Mg ²⁺	35.61 mg/ dm ³	29	Ag ⁺	<0.01 mg/ dm ³
14	Na ⁺	238.86 mg/ dm ³	30	Mo ²⁺	<0.01 mg/ dm ³
15	K ⁺	14.64 mg/ dm ³	31	Mn	0.21 mg/ dm ³
16	Li ⁺	0.03 mg/ dm ³	32	Co ²⁺	1.59 mg/ dm ³

The working pressure in the RO module ranged from 2 to 4 MPa, the temperature from 25 to 45°C and the pH values from 4 to 9. The permeate was collected in a tank and its flux was continuously monitored.

After each purification experiment, permeate samples have been taken and the conductivity and radioactivity of Co⁶⁰ were measured.

3. Results and discussion

Effect of feed waste pressure

The most important operational parameter in a RO system is the feed pressure. The effect of pressure on the membrane performance was studied keeping all other parameters constant (pH=6.2, t=25 °C). Plots of permeate flux depending on operating time and pressure are illustrated in Fig. 5. The influence of feed pressure on conductivity and Co concentration of permeate, as well as on salt and Co rejection is shown in Figs. 6 and 7, respectively.

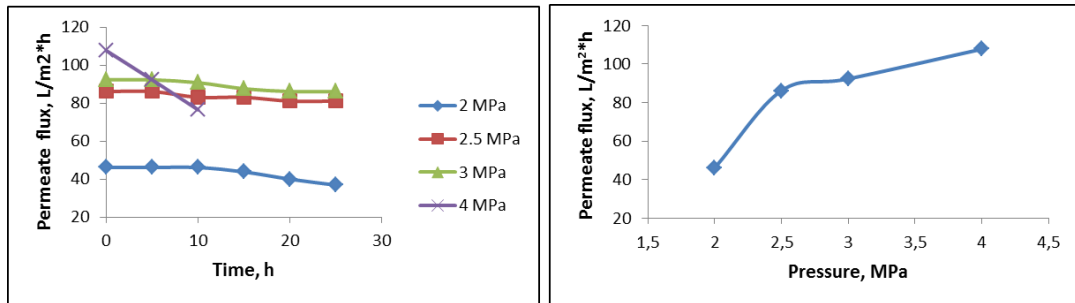


Fig. 5. Permeate flux depending on operating time and feed pressure.

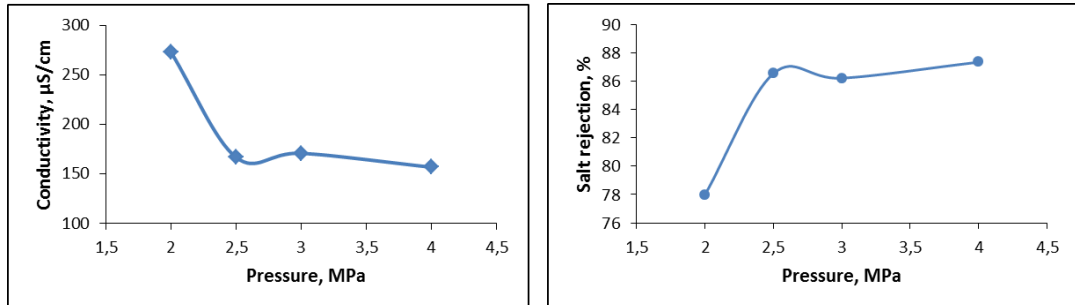


Fig. 6. Effect of feed waste pressure on permeate conductivity/salt rejection.

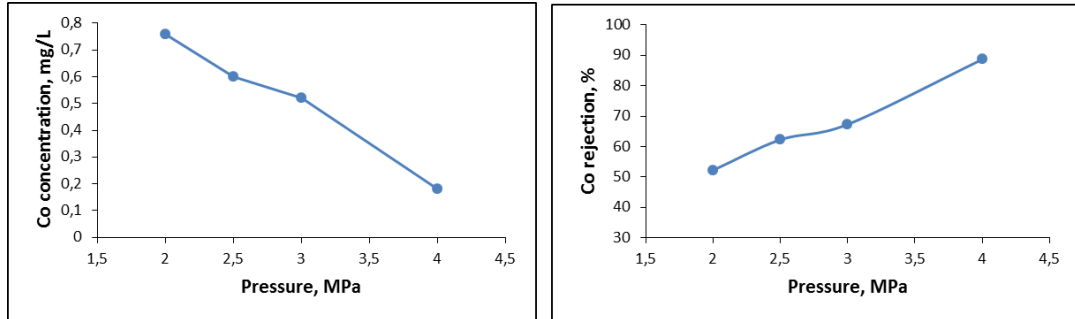


Fig. 7. Effect of feed waste pressure on Co concentration in permeate/Co rejection.

As depicted in these Figures, the permeate flux increases as the work pressure increases, but at higher pressure a more rapid decline in the flux occurs because the higher permeate rates at higher pressures led to enhanced transport of foulants to the membrane, greater compaction of the fouling layer and increased hydrodynamic resistance. Regarding the conductivity and Co concentration of permeate as a measure of salt rejection, their values decreased with an increase in the pressure. Pressure increases the driving force for the solvent and decreases osmotic pressure hence more amount of water can pass through the membrane resulting in an increase in salt rejection [19].

From these graphs it can be seen that maximum flux and salt rejection were obtained at 4 MPa, but the permeate flux decreases rapidly at this pressure value. No considerable effect can be observed if pressure varied in 2.5-3 MPa range. RO is a pressure-driven process and the main energy consumers in any membrane desalination plant are the high pressure pumps. An operating pressure of 2.5 MPa was selected in order to reduce the energy required for processing the feed waste.

Effect of feed waste pH

Experiments were conducted at $p=2.5$ MPa and $t=25$ °C under different pH levels of feed waste. The pH was adjusted with concentrated nitric acid and 30% sodium hydroxide solution and the feed waste was recirculated 2 h for homogenization. The variations of permeate flux depending on time and initial pH are shown in Fig. 8.

The effect of pH on conductivity and Co concentration of permeate, as well as on salt and Co rejection is shown in Figs. 9 and 10, respectively.

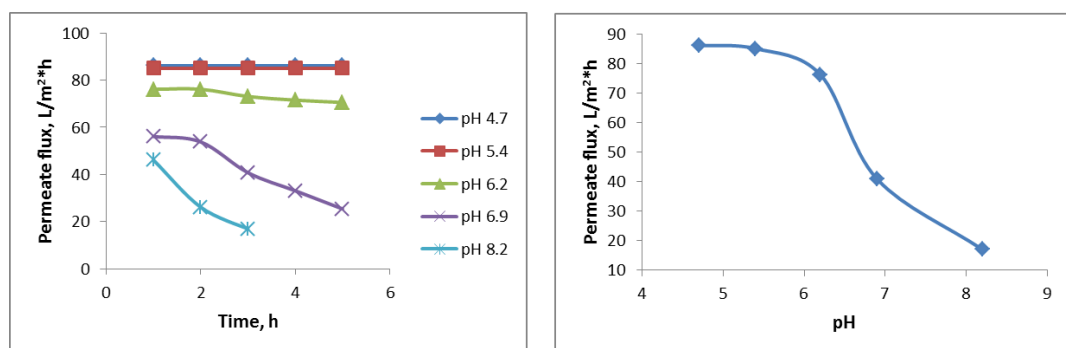


Fig. 8. Permeate flux depending on time and pH.

The results obtained have shown a decrease in time of the RO module treatment capacity in the case of feed waste with neutral or high pH. For a low pH (acidic conditions), the permeate flux remained almost constant. This finding could be explained by the fact that the low pH conditions prevent the precipitation of Ca^{2+} , SO_4^{2-} and CO_3^{2-} ions.

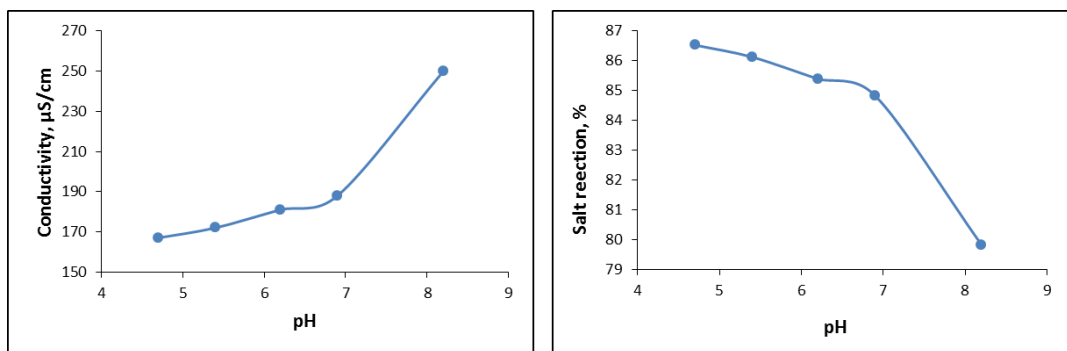


Fig. 9. Effect of feed waste pH on permeate conductivity/salt rejection

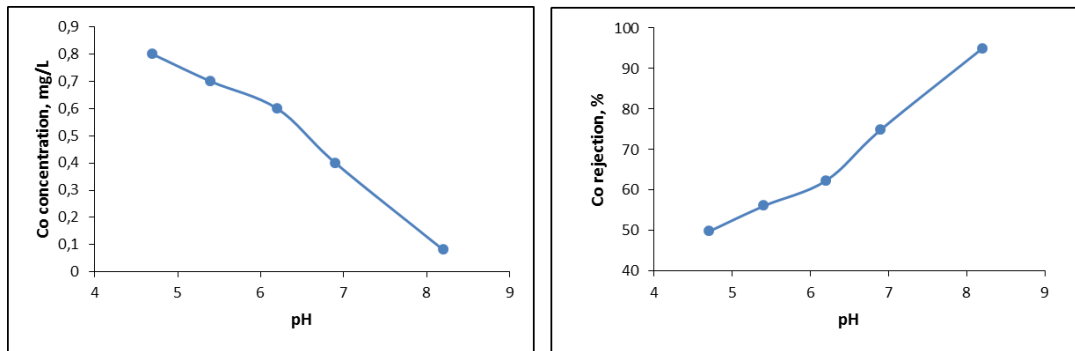


Fig. 10. Effect of feed waste pH on Co concentration in permeate/Co rejection.

It was observed that as feed pH increased, permeate conductivity and Co rejection also increased, while permeate Co concentration decreased.

The pH affects the separation performance by influencing the hydration and absorption capacity of solution on membrane. When a charged membrane is placed in a salt solution, a dynamic equilibrium is established [20-22]. The counter-ion of the solution, opposite in charge to the fixed membrane charge, is present in the membrane at a higher concentration than that of the co-ion (same charge as the fixed membrane charge) because of electrostatic attraction and repulsion effects. This creates a Donnan potential which prevents the diffusive exchange of the counter-ion and co-ion between the solution and membrane phase. When a pressure driving force is applied to force water through the charged membrane, the effect of the Donnan potential is to repel the co-ion from the membrane; since electroneutrality must be maintained in the solution phase, the counter-ion is also rejected and salt rejection occurs. As the fixed charge in polyamide membranes has the isoelectric point of the charged groups at a range of pH 3-4 [23], the membranes are negatively charged at pH>4 and the rejections of positive charged ions (see Table 2) decrease.

The rejection of Co ions at pH=4 significantly falls compared with pH>8. Co is present in feed waste as dissolved cobalt (Co^{2+}) and gives Co(OH)_2 at pH

>8. Co(OH)_2 stays in colloidal phase and is easily rejected by membrane. Therefore Co rejection increases at higher pH.

Effect of feed waste temperature

The effect of varying temperature on performance of RO membrane while keeping other parameters constant ($p=2.5 \text{ MPa}$, $\text{pH}=6.2$) is shown in graphs from Figs. 11-13.

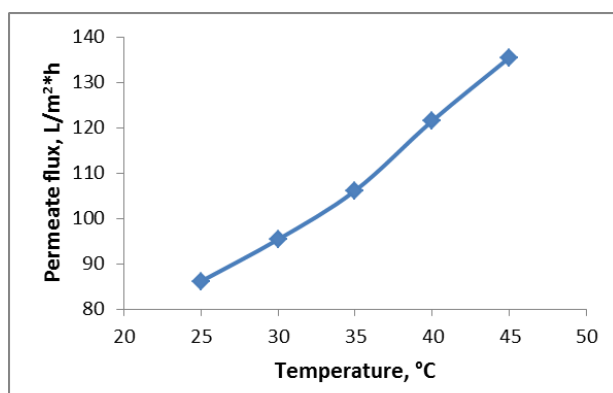


Fig. 11. Effect of feed waste temperature on permeate flux.

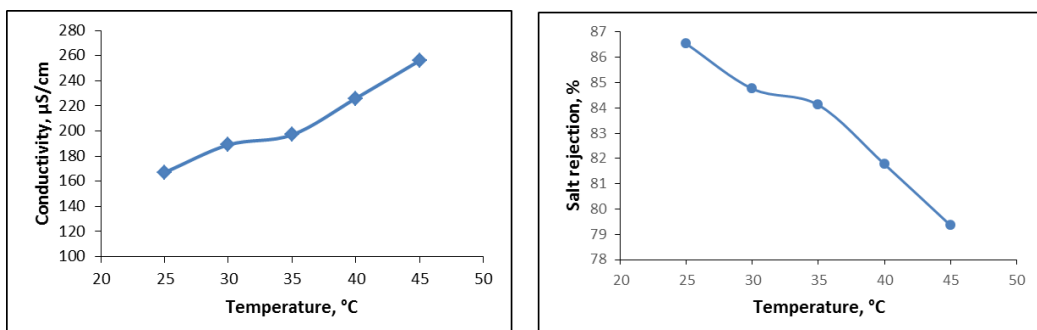


Fig. 12. Effect of feed waste temperature on permeate conductivity/salt rejection.

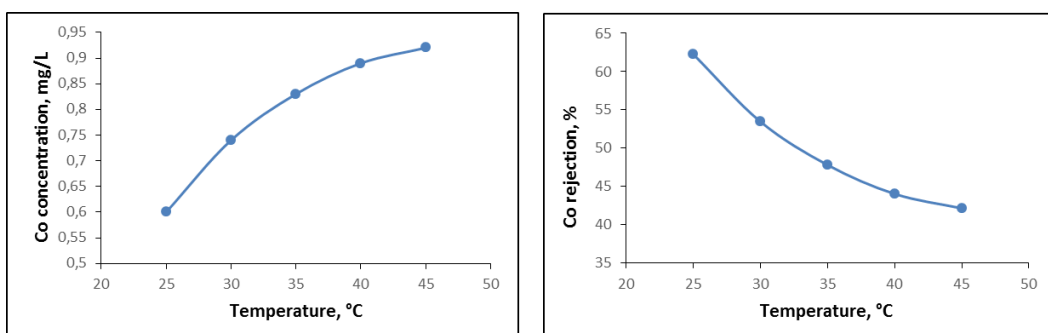


Fig. 13. Effect of feed waste temperature on Co concentration in permeate/Co rejection

It can be observed from Figs. 11-13 that as feed waste temperature increased, the flux, conductivity and Co concentration in permeate increased (salt rejection decreased). As temperature increases, viscosity decreases and water permeation rate through the membrane increases, but, also, the solubility of solute increases and higher diffusion rate of solute through the membrane is possible.

4. Conclusions

Practical experience in the development and operation of pilot and full-scale facilities utilizing RO process for treatment of liquid radioactive waste is considered to be of particular importance and interest. This research, but also the development and application of different new materials for treatment of liquid radioactive waste, aimed at improving the treatment efficiency.

Hydranautics SWC1-4040 RO membrane was tested for ARW treatment. The membrane was found to be sensitive to various operating parameters such as feed ARW pressure, pH and temperature. RO membranes have shown to be effective in rejecting dissolved species while maintaining higher flux, but the feed ARW requires pretreatment like ultrafiltration and pH adjustment.

Based on membrane performance, during these experiments has been gathered the key technical information and have been determined the acceptable limits for parameters variability for which treatment process meets a good performance. Long-term experiments should be conducted to study the fouling effects on the performance and economy of the process.

R E F E R E N C E S

- [1]. A.A.A. Al Janabi, O.C. Pârvulescu, T. Dobre, V.A. Ion, Pervaporation of aqueous ethanol solutions through pure and composite cellulose membranes, in Rev. Chim. (Bucharest), **vol. 67**, no. 1, 2016, pp. 150-156.
- [2]. A.A.A. Al Janabi, O.C. Pârvulescu, B. Trică, T. Dobre, Effect of process factors on pervaporation dehydration of isopropanol, in Rev. Chim. (Bucharest), **vol. 68**, no. 6, 2017, pp. 1302-1305.
- [3]. R.D. Ambashta, M.E.T. Sillanpää, Membrane purification in radioactive waste management: a short review, in J. Environ. Radioact., **vol. 105**, 2012, pp. 76-84.
- [4]. T. Dobre, O.C. Pârvulescu, J. Sanchez-Marcano, A. Stoica, M. Stroescu, G. Iavorschi, Characterization of gas permeation through stretched polyisoprene membranes, in Sep. Purif. Technol., **vol. 82**, 2011, pp. 202-209.
- [5]. Z. Dong, G. Liu, S. Liu, Z. Liu, W. Jin, High performance ceramic hollow fiber supported PDMS composite pervaporation membrane for bio-butanol recovery, in Membr. Sci., **vol. 450**, 2014, pp. 38-47.

- [6]. *R.O.A. Rahman, H.A. Ibrahim, Y.-T. Hung*, Liquid radioactive wastes treatment: A review, in Water, **vol. 3**, no. 2, 2011, pp. 551-565.
- [7]. *P. Salehian, W.F. Yong, T.-S. Chung*, Development of high performance carboxylated PIM-1/P84 blend membranes for pervaporation dehydration of isopropanol and CO₂/CH₄ separation, in J. Membrane Sci., **vol. 518**, 2016, pp. 110-119.
- [8]. *N. Uzal, A. Jaworska, A. Miśkiewicz, G. Zakrzewska-Trznadel, C. Cojocaru*, Optimization of Co²⁺ ions removal from water solutions via polymer enhanced ultrafiltration with application of PVA and sulfonated PVA as complexing agents, in J. Colloid Interface Sci., **vol. 362**, 2011, pp. 615-624.
- [9]. *Y.M. Xu, N.L. Le, J. Zuo, T.-S. Chung*, Aromatic polyimide and crosslinked thermally rearranged poly (benzoxazole-co-imide) membranes for isopropanol dehydration via pervaporation, in J. Membrane Sci., **vol. 499**, 2016, pp. 317-325.
- [10]. *G. Zakrzewska-Trznadel*, Advances in membrane technologies for the treatment of liquid radioactive waste, in Desalination, **vol. 321**, 2013, pp. 119-130.
- [11]. *D. Bhattacharyya, M. Williams*, Introduction and Definitions - Reverse Osmosis, in Membrane Handbook (Eds.: W. Ho and K. Sirkar), Van Nostrand Reinhold, New York, 1992, pp. 265-268.
- [12]. *J. Torbitt*, Nine mile point - unit 1 experience with membrane processing of radwaste, EPRI International LLRW Conference, TR-111657, Providence, July 1997.
- [13]. *J. Freeman*, Wolf Creek's liquid waste processing success where we were and where we are, in EPRI International LLRW Conference, TR-113702, East Brunswick, July 1999.
- [14]. *S.K. Sen Gupta, J.A. Slue, W.S. Tulk*, Liquid Radwaste Processing with Cross-flow Microfiltration and Spiral Wound Reverse Osmosis, in AECL-1170, AECL, Chalk River (ON), 1995.
- [15]. <http://www.membranes.com/pdf/HYDRABrochure.pdf>
- [16]. *F.A. Pacheco, I. Pinna, M. Reinhard, J.O. Leckie*, Characterization of isolated polyamide thin films of RO and UF membranes using novel TEM techniques, in J. Membrane Sci., **vol. 358**, 2010, pp. 51-59.
- [17]. *A.K. Ghosh, B.-H. Jeong, X. Huang, E.M.V. Hoek*, Impacts of reaction and curing conditions on polyamide composite reverse osmosis membrane properties, in J. Membrane Sci., **vol. 311**, 2008, pp. 34-45.
- [18]. *K. Gerstandt, K.V. Peinemann, S.E. Skilhagen, T. Thorsen, T. Holt*, Membrane processes in energy supply for an osmotic power plant, in Desalination, **vol. 224**, 2008, pp. 64-70.
- [19]. *M. Arora, R.C. Maheshwari, S.K. Jain, A. Gupta*, Use of membrane technology for potablewater production, in Desalination, **vol. 170**, 2004, pp. 105-112.
- [20]. *D. Berge, H. Gad, I. Khaled, M.A. Rayan*, An experimental and analytical study of RO desalination plant, in Mansoura Engineering Journal, **vol. 34**, 2009, pp. 71-92.
- [21]. *D. Bhattacharyya, C. Cheng*, Separation of Metal Chelates by Charged Composite Membranes, in Recent Developments in Separation Science (Ed.: N.N. Li), CRC Press, Boca Raton, FL, **vol. 9**, 1986, p. 707.

- [22]. *D. Bhattacharyya, M. Williams*, Theory - Reverse Osmosis, in Membrane Handbook (Eds.: W. Ho and K. Sirkar), Van Nostrand Reinhold, New York, 1992, pp. 269-280.
- [23]. *N. Hilal, A.F. Ismail, T. Matsuura; D. Oatley-Radcliffe*, Membrane Characterization, Elsevier, 2017, p. 405.

EVALUATION OF ENVIRONMENTAL MONITORING DATA AT LOW AND INTERMEDIATE-LEVEL RADIOACTIVE WASTE REPOSITORY BAITA, BIHOR, ROMANIA

B. T. OBREJA^{1,2}, E. NEACSU¹, L. DONE^{1,3}, F. DRAGOLICI¹, L. TUGULAN¹,
L. ZICMAN¹, D. SCRADAENAU⁴

¹ “Horia Hulubei” National Institute for Nuclear Physics and Engineering, P.O.Box MG-6,
RO-077125 Bucharest – Magurele, Romania, E-mails: bogdan.obreja@nipne.ro; egneacsu@nipne.ro;
donelaaur@nipne.ro; fdrag@nipne.ro; liviu.tugulan@nipne.ro; laura.zicman@nipne.ro

² University of Bucharest, Doctoral School of Geology, 36–46 Mihail Kogalniceanu Avenue,
P.O. Box: 050107, Bucharest, Romania

³ University of Bucharest, Doctoral School on Physics, POB MG-11, Magurele – Bucharest,
077125, Romania

⁴ University of Bucharest, 36–46 Mihail Kogalniceanu Avenue,
P.O. Box: 050107, Bucharest, Romania, E-mail: daniel.scradeanu@gg.unibuc.ro

Received June 16, 2015

In this paper we aim to present a study based on the results obtained in the frame of Environmental Monitoring Programme (EPM) for the Romanian National Repository for Low and Intermediate Radioactive Waste (DNDR) – Baita Bihor from 1998 to 2014. EPM involves the determination of artificial radionuclides activity per unit of mass or volume of samples from soil, vegetation, surface water and sediment, as well as the ambient dose equivalent rate, $H^*(10)$ at surface and at 1 m above the ground level. The obtained data were investigated in order to determine the impact of repository activity on population and environment. Our results demonstrate that the facility is operating safely, without any radiological impact to the surrounding environment.

Key words: Radioactive waste repository, environmental monitoring programme, ^{137}Cs .

1. INTRODUCTION

Baita Bihor repository is located in Apuseni Mountains, at an elevation of 840 m, in two disused exploration galleries of the Baita uranium mine, (Gallery 50 and Gallery 53 – the latter is currently being used for ventilation purposes) between two large ore pipes. The repository galleries are situated in the unsaturated zone, several hundred meters above the hydrostatic level. The distribution of infiltrations into the galleries is controlled by the location and nature of the faults and fracture zones that intersect them. Although the most infiltrating water is thought to be lost in the geosphere through repository floor cracks and through the drainage system, a small amount is likely to be discharged *via* an active drain to a collection tank. The collected water radioactivity is measured and, if the level is below the regulatory limits, it will be discharged down the hillside.

In 1986, when the repository was given into operation, it was implemented a monitoring programme, EPM, as an important element in order to ensure that the disposal facility provides the required level of containment, isolation and protection during the operational phase. The philosophical and technical bases for requirements on radioactive waste management are established in the IAEA Safety Fundamentals publication *The Principles of Radioactive Waste Management* [1].

EPM consists in doses measurement and radiological analysis of soil, water, sediment and vegetation samples.

2. ENVIRONMENTAL MONITORING PROGRAMME

Environmental radiation monitoring around the Baita Bihor repository is conducted for estimating the environmental doses and the long-term accumulation of radionuclides in the environment. Measuring and sampling locations are representative points located mainly around the disposal area and waste packages transport route. The samples are taken from soil, vegetation, sediment and water. In recent years, the monitoring programme has been completed with concentration measurement of radon in the repository galleries [2] and physico-chemical monitoring of water to detect potential leaching from the repository.

2.1. DOSE AND DOSE RATE MEASUREMENTS

The radiation dose rate measurement area is a circle with the repository entrance in center and a radius of 50 m. The measurements points are orientated to the cardinal points, from 10 to 10 m. Also, along the transportation route there have been established 18 measurement points (Figs. 1 and 2).

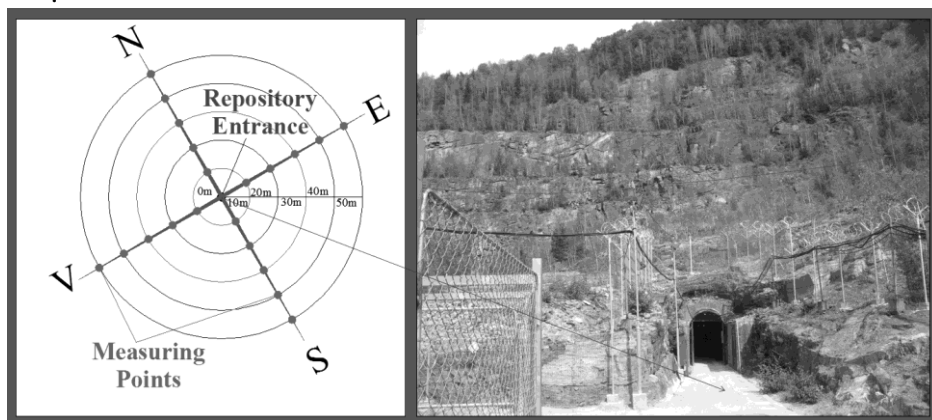


Fig. 1 – Dose rate measurements points around Baita Bihor repository entrance.



Fig. 2 – Environmental monitoring map along the transportation route (Google Earth).

The results from radiation surveys are values of the ambient dose equivalent rate, H^* (10) [$\mu\text{Sv h}^{-1}$] at surface [3] and at 1 m above ground level.

2.2. DETECTION OF RADIONUCLIDES IN ENVIRONMENTAL MATRICES

Terrestrial sampling points were selected in order to cover entire influence area of the repository. The monitoring zone spreads 20 km along Crisul Baita River valley, from repository entrance platform to Crisul Baita – Crisul Negru confluence.

Environmental monitoring programme started with commissioning of repository (1985) and it is still in progress, being optimised several times during the last years in order to obtain more specific data on the potential impact area.

Noncultivated soil sampling is performed after previous removal of leaves, roots and other debris. From each sampling point are collected about 2 kg of soil at 1–5 cm deep inside an area of 30×30 cm. In the winter, sampling is conditioned by snow thickness.

The sediment samples that are collected from the alluvial deposits weight approximately 3 kg. As possible, the sampling points are kept in the same location inside the riverbed.

The vegetation samples are constituted mostly of leaves, flowers and grass and they are collected from a surface of 1–2 m^2 and they weight about 1 kg humid mass. During the winter period, vegetation samples are not collected.

Water samples are collected from surface sources, from a depth of about 20 cm, in 1L clean and dry poliethylene containers. The samples are acidified with nitric acid to pH < 2 to prevent precipitation.

All matrices are subjected to gamma spectrometry and liquid scintillators counting.

3. MATERIALS AND METHODS

3.1. SAMPLES PREPARATION

The soil and sediment samples are prepared as follows: the samples are dried at 105 °C until constant mass is achieved, and then crushed, grinded and sieved up to 2 mm fraction. Resulted material is separated in sub-samples of 75 ± 1 g or 181 ± 1 g, depending on instrument calibration and sealed in SARPAGAN beakers.

The vegetation samples are dried at 40 °C until constant mass is achieved, and then crushed, grinded and sieved up to 2 mm fraction. Resulted material is separated in sub-samples of 25 ± 1 g and sealed in SARPAGAN beakers.

The water samples are filtered using cellulose acetate membrane of 0.45 µm porosity. 900 mL from each sample is sealed in Marinelli beakers.

All sub-samples are kept 30 days to achieve radioactive equilibrium between ^{222}Rn and its daughter products.

3.2. INSTRUMENTATION

The monitoring activities started with a poor relative efficiency HPGe detector based gamma spectrometer and a single detector β counting system and progressively moved ahead with the use of more sensitive systems.

Currently, the gamma spectrometric measurements are performed using a high resolution gamma-ray spectrometer, Canberra type, GENIE 2000 version 3.2 software and Laboratory SOurceless Calibration Software (LabSOCS), personalized for the detector. The laboratory used a Reverse-Electrode Germanium (REGe) semiconductor detector type, GR4020 model, 47.5% relative efficiency.

Tritium concentration from the water samples is determined using a liquid scintillation analyzer, Tri-Carb 2910 TR type. The sub-samples used for counting are prepared in glass vials with a volume of 20 mL, and the sample: liquid scintillation ratio is 1:3. The liquid scintillation used for the sample preparation is Ultima Gold type. For the samples chemical quenching parameters determination,

the device uses a Ba-133 external standard source. The acquisition and processing software is QuantaSmart.

In order to measure the dose equivalent rate is used an ARGUS 3PC dose rate meter.

4. RESULTS AND DISCUSSION

Previously, it was reported a study that investigated the EPM results obtained in the period 1984–1998 [4]. The radiometric, radiochemical and spectrometric analysis indicated no modification of the radiological state of the area as a result of the radioactive waste disposal activity.

4.1. AMBIENT DOSE

The measurement results of ambient dose equivalent rate at surface, along the transportation route, are shown in Figs. 3 and 4. As depicted in Fig. 3, the average ambient dose equivalent rate for the first 15 points along the transportation route appeared to be rather constant. Moreover, this parameter record a slight increase starting with the measuring point marking the former Bihor mining exploitation. Further, Fig. 4 shows the variation of average ambient dose equivalent rate for the last 4 points which record an increase as the distance to the uranium quarry is decreasing.

The graphs presenting the results of measurement dose corresponding to 1 m above the ground level were similar (data not shown).

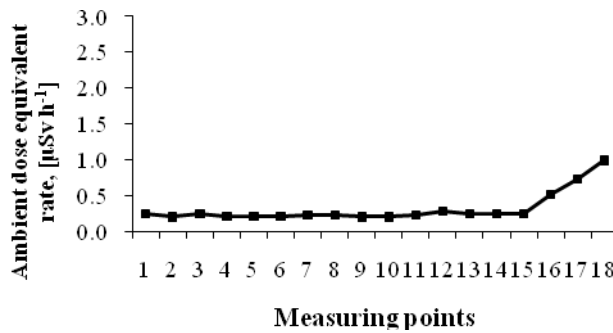


Fig. 3 – Average ambient dose equivalent rate, $H^*(10)$ in the 2000–2014 period, along the transportation route, at surface, $[\mu\text{Sv h}^{-1}]$.

Around the repository entrance are revealed large variations in ambient dose equivalent rate at surface (Fig. 5) as a normal consequence of uranium mining and of the uranium tailings presence.

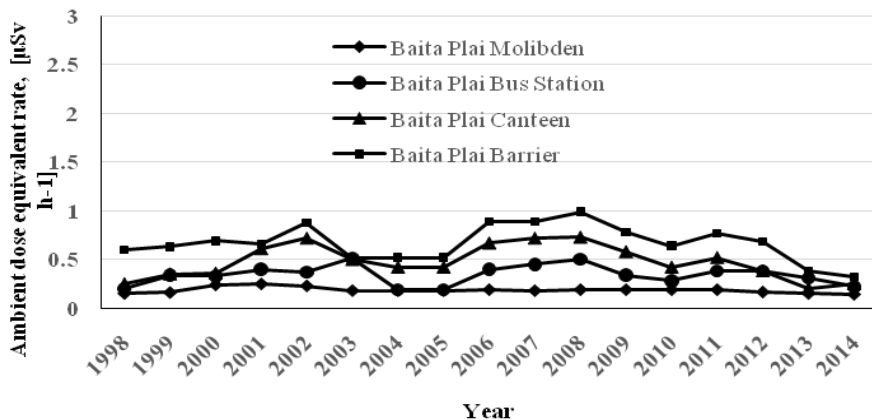


Fig. 4 – Average annual ambient dose equivalent rate, $H^*(10)$ in the last 4 point (15–18) along the transportation route, at surface, [$\mu\text{Sv h}^{-1}$].

Due to the fact that, in the past, the repository area has been exploited as an uranium surface quarry, the presence of uranium ore tailings over the large areas influences directly the environmental radioactivity of the repository surroundings, characterised by the presence of natural radionuclides in high concentrations. In addition, the widespread radioactive fallout from Chernobyl makes small contributions to overall doses. The environmental impact of uranium exploitation and milling activities is due to the presence of waste rocks from mining and tailings from ore processing. The natural γ -emitting radionuclides, ^{226}Ra , ^{214}Bi , ^{232}Th , $^{234\text{m}}\text{Pa}$, ^{235}U and ^{40}K were identified in soil samples and the annual natural dose rates values in the Baita Bihor area are estimated to be between 1610 and 5160 $\mu\text{Sv/year}$ for any source, except ^{222}Rn , ^{220}Rn and short-lived descendants [5, 6].

These results clearly indicate no preferential direction, distance or ascendent trend for ambient dose equivalent rate at surface and 1 m ground level, as well.

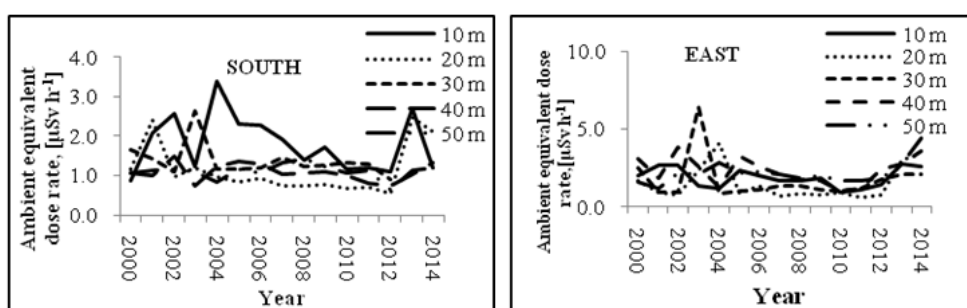


Fig. 5

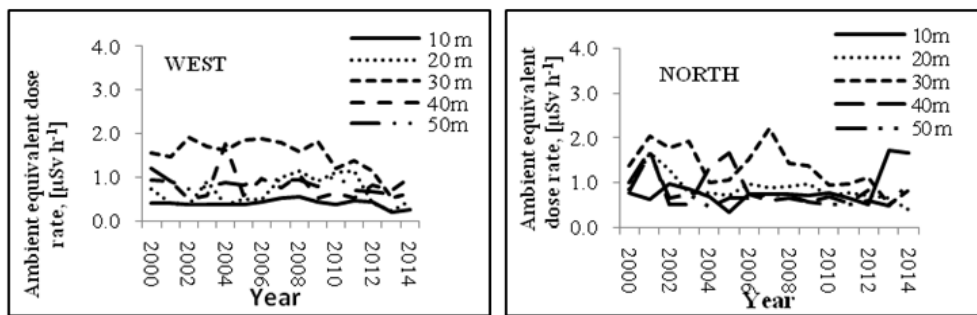


Fig. 5 (continued) – Average annual values of ambient dose equivalent rate, $H^*(10)$ around repository entrance, at surface, $[\mu\text{Sv h}^{-1}]$.

4.2. RADIONUCLIDES PRESENCE IN SURFACE WATERS, SOIL, VEGETATION, SEDIMENT

Anthropogenic radionuclide identified in environmental matrices is ^{137}Cs . Average annual concentration of ^{137}Cs in soil, vegetation and sediments samples are presented in Table 1.

As it is shown in Table 1 and Fig. 6, the ^{137}Cs activity concentrations in soil reach the highest level in point 1 (above repository entrance level) as compared with point 2 (under repository entrance level), indicating that ^{137}Cs presence is not due to dissemination from DNDR.

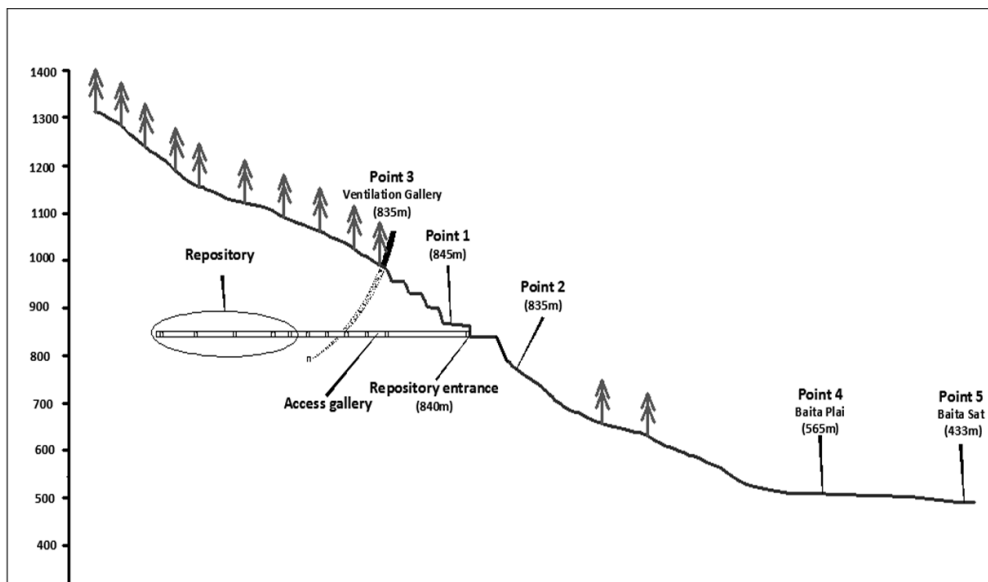


Fig. 6 – Soil, vegetation and sediment sampling points.

Table 1

Average annual concentration of ^{137}Cs in soil, vegetation and sediments samples, [Bq/kg]

Year	Soil (Bq/kg)					Vegetation (Bq/kg)			Sediments (Bq/kg)	
	Point 1	Point 2	Point 3	Point 4	Point 5	Point 1	Point 3	Point 4	Point 4	Point 5
2000	253	290	165	142	135	<4	261	<4	*	*
2001	214	337	323	50	47	84	165	82	*	*
2002	85	114	84	68	4	141	47	29	*	*
2003	25	27	65	54	29	82	32	29	*	*
2004	156	104	44	21	<2	80	8	12	*	*
2005	203	69	159	18	60	90	7	4	*	*
2006	152	101	37	41	9	7	12	15	*	*
2007	201	123	30	57	8	14	12	15	*	*
2008	165	94	20	58	3	7	4	4	<1	1
2009	129	92	21	61	20	41	2	2	2	2
2010	204	62	26	37	19	100	8	2	11	3
2011	229	38	24	41	6	9	<4	<2	3	1
2012	274	150	90	30	66	<4	<4	<2	2	3
2013	324	120	130	56	12	6	9	5	7	6
2014	124	80	140	47	8	9	7	3	5	5

In addition, for the vegetation samples, the highest ^{137}Cs concentrations are recorded also, in point 1. This observation could be explained by the fact that point 1 is located onto a flat area where a considerable accumulation of fine fraction and humus after old uranium quarry draining might occur. The high concentration could be correlated with atmospheric ^{137}Cs originated from Chernobyl fallout which affected the regions around Ukraine, including Transilvania, where Baita Bihor Repository is located [7, 8, 9].

Since 2008, sediment samples are also collected from points 4 and 5 area. The ^{137}Cs sediment concentration is smaller than soil samples concentration, indicating that the radionuclide has not been transported from upstream.

For all sample types (soil, vegetation and sediments) it can be concluded that ^{137}Cs presence is of atmospheric origin from Chernobyl fallout and not from DNDR presence.

In water samples (drainage system of the Access Gallery, Baita Plai, Baita Sat and Crisul Baita before of confluence with Crisul Negru) in the environmental monitoring interval, there were no γ -emitting radionuclides identified above the limit of detection (AMD), as presented in Table 2.

Table 2

AMD for radionuclides in water samples

Radionuclide	^{60}Co	^{137}Cs	^{235}U	^{241}Am	$^{234\text{m}}\text{Pa}$	^{214}Bi	^{214}Pb
AMD [Bq/kg]	0.1	0.1	0.9	0.9	11	0.2	0.2

In water samples there is also determined tritium concentration. In the points Baita Plai, Baita Sat and Crisul Baita before of confluence with Crisul Negru, tritium average annual concentrations are between 2–22 Bq/L and they are lower than 100 Bq/L, that is the maximum allowable limit for potable water. For drainage system of the Access Gallery sampling point tritium concentrations are between 26.85–825 Bq/L, the average annual concentrations being presented in Figure 7. It can be seen that maximum values are recorded in the period 2001–2003 and further, the values decreased over time until they approached the concentration values determined in the rest of the points.

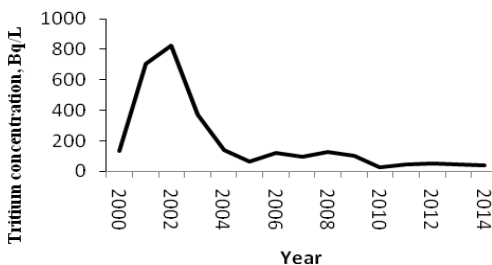


Fig. 7 – Average annual concentration of ^{3}H in the drainage system of the Acces Gallery water sample, [Bq/l].

This occurrence could be attributed to:

- natural tritium rainfall, as a result of direct infiltration or percolation, accumulated in the stationed upper layers of the deposit and infiltrated in the Access Gallery;
- tritium waste disposed, as a result of isotopic exchange reaction with water accumulated behind this infiltration;
- minimization of the volume of human activities within the repository, that reduced the period of operation of the ventilation system.

With the implementation of upgrading works at the repository, that involved replacing the electric, ventilation and drainage systems and, also, waterproofing of the disposal and transport galleries, the presence of tritium in water significantly decreased.

5. CONCLUSIONS

The results obtained in the frame of EPM, during the period 2000–2014, have shown that the repository activity exhibits no radiological impact for population or for surrounding environment.

Dose measurements show that in the DNDR area is recorded a decrease in the concentration of natural radioactivity with increasing distance from the old uranium mine. Moreover, the variations of dose values around the repository entrance are due to natural conditions specific for uranium mine areas.

There are no anthropogenic radionuclides identified, except ^{137}Cs , which are resulted from the Chernobyl fallout.

This paper, together with the conclusions presented by Dragolici *et al.* (2000), demonstrate that the Romanian National Repository for Low and Intermediate Radioactive Waste (DNDR) – Baita Bihor provided the required level of containment, isolation and protection during the almost 30 years of operation.

Acknowledgments. Authors acknowledge support from the projects PN II-PT-PCCA-2011-3.2-0334-SARAWAD-BB (Contract No. 156/2012) and POSDRU/159/1.5/S/133391 cofinanced by the European Social Fund within the Sectorial Operational Program Human Resources Development 2007–2013.

REFERENCES

1. INTERNATIONAL ATOMIC ENERGY AGENCY, The Principles of Radioactive Waste Management, Safety Series No. 111-F, IAEA, Vienna (1995).
2. A. PETRESCU, L. DONE, F. DRAGOLICI, I. PRISECARU, G. PAVEL, H. POPA ,*Thorough investigation of radon concentration variations in Baita Bihor (Romanian National Radioactive Waste Repository – DNDR)*, Rom. Journ. Phys., **59** (9–10), 1025–1034, 2014.
3. M. ANDOH, Y. NAKAHARA, S. TSUDA, T. YOSHIDA, N. MATSUDA, F. TAKAHASHI, S. MIKAMI, N. KINOUCHI, T. SATO, M. TANIGAKI, K. TAKAMIYA, N. SATO, R. OKUMURA, Y. UCHIHORI, AND K. SAITO, *Measurement of air dose rates over a wide area around the Fukushima Dai-ichi Nuclear Power Plant through a series of car-borne surveys*, Journal of Environmental Radioactivity, **139**, 266–289, 2014.
4. F. DRAGOLICI, G. ROTARESCU, A. LUCA, T. PEIC, C. POSTELNICU, A.C. DRAGOLICI, *Radioactivity studies in the Romanian National Repository for Radioactive Waste – Baita, Bihor Region, during 14 years of resource development*, International Conference on the Safety of Radioactive Waste Management, Cordoba, Spain, 13–17 March, (IAEA/CN/78/42), 170–174, 2000.
5. LITTLE R., DRAGOLICI, F., BOND, A., MATYASI, L., MATYASI, S., NAUM, M., NICULAE, O., THORNE, M., WATSON, S., (2007) “Preliminary Safety Analysis of the Baita Bihor Radioactive Waste Repository, Romania” Proc., 11th International Conference on Environmental Remediation and Radioactive Waste Management, ICEM, Bruges, Belgium, 1197–1200.
6. R.-CS. BEGY, H. SIMON, C. COSMA, *Radiological Assessment of Stream Sediments Between Băița-Plai and Beiș*, Rom. Journ. Phys., Vol. 58, Supplement, P. S22–S28, Bucharest, 2013.
7. DAN C. NIȚĂ, CONSTANTIN COSMA, AND ROBERT C. BEGY, *New data for Cesium from soil in Cluj-Napoca town after Chernobyl accident*, AES Bioflux, **3** (2), 229–235, 2011.
8. GRZEGORZ PORĘBA, ANDRZEJ BLUSZCZ, ZBIGNIEW SNIESZKO, *Concentration and vertical distribution of ^{137}Cs in agricultural and undisturbed soils from Chechlo and Czarnocin areas*, Geochronometria, **22**, 67–72, 2003.
9. M. TOMA, L. DINESCU, I. PAUNICA, C. OLTEANU, *Study of the radioactivity level around the National Radioactive Waste Repository – Baita, Bihor*, Journal of Environmental Protection and Ecology, **8** (4), 919–925, 2007.

REMOVAL OF ^{137}Cs IONS FROM AQUEOUS RADIOACTIVE WASTE USING NICKEL FERROCYANIDE, PRECIPITATED ON SILICA GEL

Laura Ruxandra ZICMAN^{1*}, Elena NEACSU¹, Laurentiu DONE^{1,3}, Liviu TUGULAN¹, Felicia DRAGOLICI¹, Bogdan Tudor OBREJA¹, Tanase DOBRE²

¹Horia Hulubei National Institute for Nuclear Physics and Engineering, P.O.Box MG-6, RO-077125 Bucharest-Magurele, Romania

²University Politehnica of Bucharest, Department of Chemical and Biochemical Engineering, 1-7 Polizu street , Bucharest, Romania

³University of Bucharest, Doctoral School on Physics, POB MG-11, Magurele-Bucharest, 077125, Romania

Abstract

The waste waters from nuclear engineering containing corrosion and fission products fall in the category of medium or low level radioactive wastes. These waste waters must be treated in order to decontaminate prior to be released in rivers or lakes. Additionally these waste waters can contain some organic products, like surfactants from laundry. The ion exchange is the most efficient treatment technology for radionuclides removal from a variety of waste water streams with low and intermediate pollution level. Unfortunately this technology is not selective because all ions from polluted waters are fixed. In the last time the selective separation of radioactive ions from this water type is an important research subject. Sorption with or without chemical interaction in solid phase of radioactive species is a promising procedure.

A study regarding removal of ^{137}Cs from radioactive waters from spent nuclear fuel pools using a synthetic inorganic sorbent was performed. Nickel ferrocyanide, precipitated on silica gel, with size of granules 0.5 - 0.8 mm, was used as sorbent. The aqueous radioactive waste initial characteristics were ^{137}Cs concentration 3000 Bq/L, pH 6.50, conductivity 6.44 $\mu\text{S}/\text{cm}$, chloride content < 0.01 ppm, and solid residue 3.90 mg/L. No fission or activation gamma emitter was identified. Batch experiments as a function of pH, contact time, sorbent/waste mass ratio were carried out. Isolated and synergic effects of process parameters were determined in order to establish acceptable limits for variability in performance.

Simple kinetic and thermodynamic models have been applied to the rate and isotherm sorption data and the relevant kinetic and thermodynamic parameters were obtained. The sorbent capacity was established using the Freundlich and Langmuir adsorption isotherm models. The decontamination factors in terms of separation yield were determined. The checked sorbent has a high separation capacity of Cs^+ from aqueous radioactive waste. Computation examples on the practical use of this sorbents are already presented.

Keywords: radioactive waste, cesium, ferrocyanide, kinetic, thermodynamic, sorption isotherm

* Corresponding author; Email: laura.zicman@nipne.ro (Laura Zicman)

1. Introduction

The increasing pressure to reduce the release of radioactive and other toxic substances into the environment requires constant improvement/upgrading of processes and technologies for treatment and conditioning of liquid radioactive waste. Treatment of liquid radioactive waste involves the application of different methods to meet the requirements both for the release of decontaminated effluents into the environment and the conditioning of waste concentrates for disposal.

At many of the nuclear power plant reactors, spent fuel from their operations is stored, pending decisions on its final disposition. Currently, most spent nuclear fuel is safely stored in specially designed pools at individual reactor sites around the world, but some problems associated with this spent fuel storage have emerged and caught the attention in the international nuclear community. Concerns principally focus on the ageing fuel storage facilities, their life extension, and the ultimate disposal of spent fuel assemblies [1]. Spent nuclear fuel pools (SNFP) were established only for temporal spent fuel storage for at most 20 years. It has been assumed that it is sufficient period to which final disposal of spent nuclear fuel would be determined. However, nowadays it is more convenient in many nuclear power plants to enhance pool capacity and to store spent fuel during the whole nuclear power plant lifetime, which is about 40 years.

As coolant and, at the same time, as a protection against radiation, deionized water is used in storage pools. In spent fuel storage pools fuel cladding could be damaged and the fuel's volatile fission products, including 30-year half-life ^{137}Cs , would be released. ^{137}Cs is an important radio-contaminant and represents a serious radiological hazard because as an alkaline element, it is easily assimilable by living organisms [2]. Different methods such as chemical precipitation, adsorption, and ion exchange are applied for radioactive wastes treatment [3–9]. Ion exchange technique in which various type of ion exchangers have been widely used is an attractive method because of its simplicity, selectivity, and efficiency [10–17].

The transition metal ferrocyanides were immobilized on different support materials and were used to remove cesium ions. The transition metal ferrocyanides immobilized on an anion exchange resin are simple and easy to prepare, and obtainable in any given conditions: they are non hygroscopic and granular, thus they can be in a dry state. Several applications of these resins to remove radioactive caesium ions have been reported [18 - 21]. Composite sorbents based on potassium nickel ferrocyanide embedded in silica gel matrix were prepared and characterised by powdered X-ray diffraction analysis, IR spectra, Mössbauer spectra and electron microscopy [22].

Spent nuclear fuel generated in VVR-S Research Reactor at Magurele, Romania was stored in the Interim Spent Fuel Storage Facility, away from the reactor building. Two failed fuel elements allowed ^{137}Cs to be released in storage water from one pool. ^{137}Cs concentration is 3000Bq/L, pH 6.50, conductivity 6.44 $\mu\text{S}/\text{cm}$, chloride content < 0.01 ppm, and solid residue 3.90 mg/L. No fission or activation gamma emitter was identified.

Considering the above mentioned facts, the principal purpose of this study was to evaluate the removal of ^{137}Cs from radioactive waters from spent nuclear fuel pools using potassium nickel ferrocyanide, precipitated on silica gel (PNF-SG). Taking in consideration that one gram of ^{137}Cs has an activity of 3.215 terabecquerel [23], the Cs concentrations required were obtained using inactive CsCl, ^{137}Cs being used as tracer. The effect of different parameters such as pH, contact time, sorbent/waste mass ratio, temperature and initial concentration on the adsorption process was investigated. The adsorption process is evaluated from kinetic, isotherm, and thermodynamic point of view. Also, the decontamination factors in terms of separation yield were determined.

2. Experimental

2.1. Chemicals and reagents

All the reagents used in this work were of AR grade chemicals and were used without further purification. Cesium as cesium chloride was purchased from Sigma–Aldrich Co. Working solutions were prepared by dissolving CsCl in radioactive water from spent nuclear fuel pool.

PNF-SG, was supplied as granules, 0.5 - 0.8 mm size, from SIA “Radon” Moscow, Russia.

2.2. Instrumentation

Cesium concentration was determined by gamma spectrometry using a high resolution gamma-ray spectrometer, Canberra type, GENIE 2000 version 3.2 software and Laboratory Sourceless Calibration Software (LabSOCS), with 47.5% relative efficiency.

2.3. Batch sorption studies

Batch experiments were performed under kinetic and equilibrium conditions. To determine the pH range at which the maximum uptake of Cs^+ ions would take place on PNF-SG, a series of 250mL polypropylene Erlenmeyer flasks, each containing 1g, 3 g and 5 g of PNF-SG was filled with 250 mL of 1000 mg/L Cs^+ solution. The initial pH was adjusted to values ranging from 3.0 to 10.0 using dilute solution of hydrochloric acid or sodium hydroxide. The flasks were shaken for 2h to attain equilibrium. Preliminary investigations showed that the sorption process of each studied ion was completed after 2h. The suspension obtained was filtered to separate the solid from the liquid phase. The radioactivity

of clear liquid phases obtained was measured in order to obtain quantitative data of Cs^+ adsorption.

2.3.1. Kinetic experiments

Kinetic studies were performed at four different temperatures (298, 308, 318 and 328 K) using an initial ion concentration of 1000 mg/L. Also, to study the kinetic of the reaction, the adsorption capacity of the PNF-SG was measured at different time intervals (30–120 min). For these investigations, adsorbent/waste mass ratio of 0.02 was used and the solution was kept under stirring in a thermostat shaker adjusted at the desired temperature. The amount of ion adsorbed at a time t , q_t (mg/g), and the distribution coefficient, k_d (mL/g) were calculated as follows:

$$q_t = (C_0 - C_t) \frac{V}{m} \quad (1)$$

$$k_d = \frac{(C_0 - C_t)}{C_t} \times \frac{V}{m} \quad (2)$$

where C_0 and C_t are the initial and equilibrium concentrations (mg/L) of Cs^+ in solution, V the solution volume (L) and m is the weight (g) of the PNF-SG.

2.3.2. Sorption equilibrium experiments

In the experiments of sorption isotherm measurements, 250 mL of the metal ion solution of different concentrations (100–1000 mg/L) were agitated with 5 g of PNF-SG at different temperatures (298, 308, 318 and 328 K) and at initial pH of 3.0. After the established contact time (2 h) was reached, the suspension obtained was filtered and the amount of the metal ion retained in the PNF-SG phase (mg/g) was estimated.

All batch experiments were carried out in duplicate and the mean values are presented.

3. Results and discussion

3.1. Effect of experimental condition on adsorption process

3.1.1. Dosage effect

The removal percentage of Cs^+ increases with increasing of solid to liquid ratio from 0.004 to 0.02 g/mL and the maximum uptake was achieved at 0.02 g/mL (Fig. 1). Therefore, the optimized solid to liquid ratio of 0.02 g/mL was selected for further experiments.

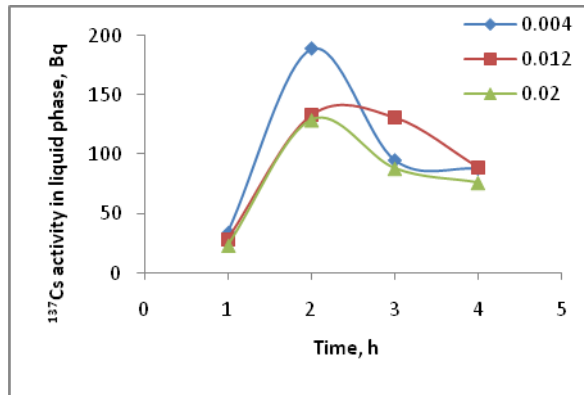


Fig. 1. Effect of solid/liquid ratio

3.2.2. Effect of contact time

The amount of adsorbed ions onto PNF-SG at different contact time is shown in Fig. 2. The uptake of ions increased with time and reached equilibrium after 90 min. The sorption process was initially very fast and between 80% and 90% of the maximal capacity was obtained within 30 min. This quite rapid removal was due to the porous structure of the composite, which allows the facile diffusion of the ions to the exchange sites. The adsorption of ions gradually decreased with time until saturation was attained. The two stage sorption mechanisms with the first rapid and quantitatively predominant and the second slower and quantitatively insignificant, has already been reported [24].

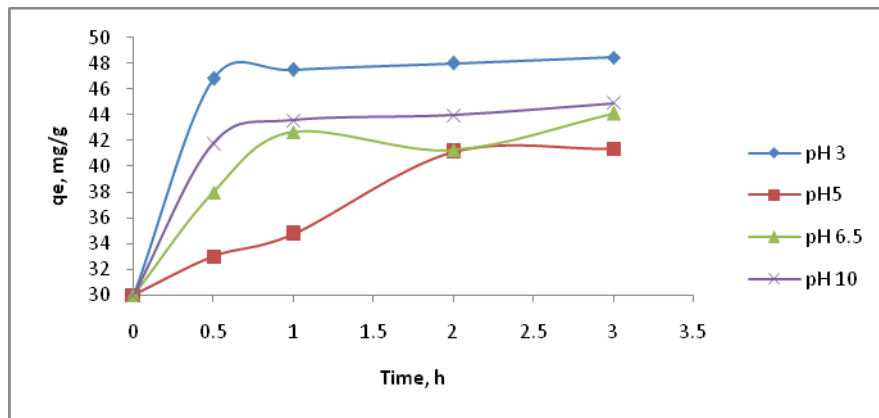


Fig. 2. Effect of contact time on Cs^+ adsorption

3.2.3. Effect of pH

Metal sorption from aqueous solutions can be greatly affected by the pH of the solution, which affect not only the binding sites (e.g. degree of protonation) but also the metal chemistry (e.g. speciation and precipitation).

The amount of Cs^+ uptake as a function of initial pH is shown in Fig. 3. It was concluded that acidic and alkaline media are favourable for uptake process. This could be attributed to:

- in acidic media Cs is present completely as soluble Cs^+ ;
- in alkaline solutions formation of mixed precipitates of transition metal ferrocyanides and hydroxides occurs [25].

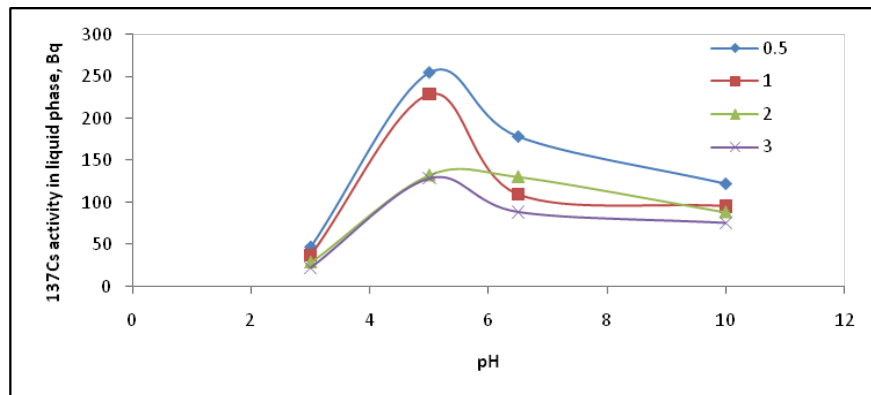


Fig. 3. Effect of initial pH on Cs^+ adsorption

The highest uptake was observed at pH 3 and pH 10. Since it has been reported dissolution of transition metal ferrocyanides at $\text{pH} > 10$ [25], all future sorption experiments in this work were carried out at initial pH value of 3.

3.2.4. Effect of temperature

The adsorption removal of Cs^+ onto PNF-SG at four different temperatures 298, 308, 318, 328 K was examined (Fig. 4). The adsorption capacity increases with increasing the temperature, confirming that the adsorption process was endothermic. The data were used to estimate the thermodynamic parameters.

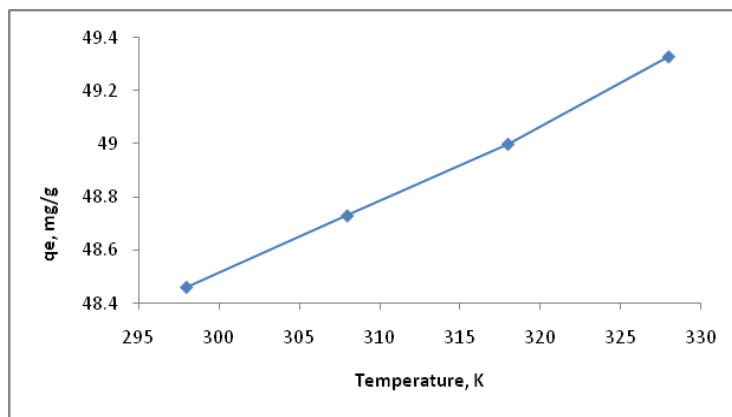


Fig. 4. Effect of temperature

3.3. Kinetic sorption modeling

Two kinetic models including pseudo-first-order and the pseudo-second-order were used to estimate the kinetic parameters. The integrated pseudo-first-order model expressed as follows [26]:

$$\ln(q_e - q_t) = \ln q_e - k_1 t \quad (3)$$

where q_e and q_t are respectively the amount of ions adsorbed per unit mass of PNF – SG at equilibrium and at any time t (mg/g); k_1 is the rate constant of pseudo-first-order sorption model (min^{-1}).

The slope and intercept of the plot of $\ln(q_e - q_t)$ against t is shown in Fig. 5 and they were used to calculate k_1 and q_e (Table 1).

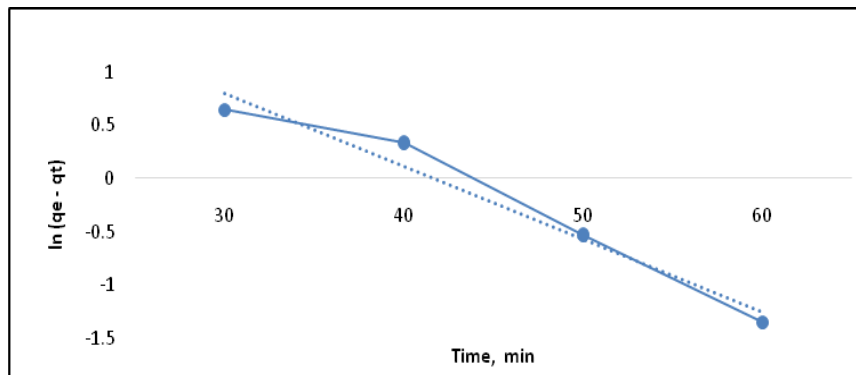


Fig. 5. Pseudo first-order kinetic plots for the sorption of Cs^+ onto PNF – SG at 298 K

The pseudo-second-order model and initial sorption rate (h) are written as [25]:

$$\frac{t}{q_t} = \frac{1}{k_2 q_e^2} + \frac{1}{q_e} t \quad (4)$$

$$h = k_2 q_e^2 \quad (5)$$

where k_2 is the rate constant of pseudo second-order equation (g/mg min) and $h = k_2 q_e^2$ is the initial sorption rate (mg/g min).

The values of t/q_t were linearly correlated with t as it can be seen in Fig. 6.

The important parameters including pseudo-second-order rate constant, k_2 (g/mg min), the equilibrium sorption capacity, q_e and the initial sorption rate, h (mg/g min) were determined from the slope and the intercept of the plot (Table 1).

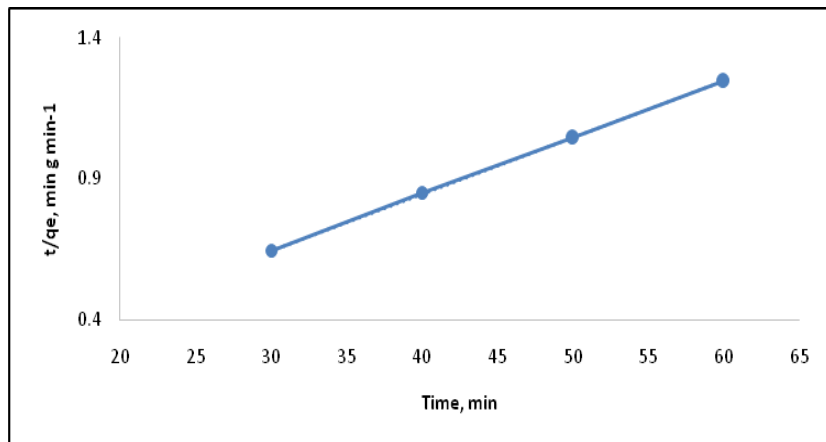


Fig. 6. Pseudo second-order kinetic plots for the sorption of Cs^+ onto PNF – SG at 298 K

Table 1.
The calculated parameters of the pseudo first-order and pseudo second-order kinetic models for Cs^+ ions sorbed onto PNF – SG at 298 K

First-order kinetic parameters			Second-order kinetic parameters				$q_e, \text{exp}, (\text{mg/g})$
k_1 (min^{-1})	$q_e, \text{calc},$ mg/g	R^2	k_2 (g/mg min)	$q_e, \text{calc},$ mg/g	h (mg/g min)	R^2	
0.683	4.406	0.965	0.0087	50	21.74	0.999	48.46

The value of the correlation coefficients (R^2) and agreement of calculated q_e with experimental data revealed that sorption process can be described well by pseudo-second-order equation. The rate of ion exchange process is governed by film diffusion, particle diffusion, or chemical exchange (chemisorptions). It is reported that the rate of ion exchange is controlled by chemical exchange if experimental data are fitted to pseudo-second-order equation [27].

From Table 1, one could see that the values of the initial sorption rate (h) and rate constant (k_2) were increased with the increase in temperature. The correlation coefficient R^2 has an extremely high value (>0.99), and its calculated equilibrium sorption capacity (q_e) is consistent with the experimental data. Therefore, the overall rate constant of both sorption process appear to be controlled by the chemical sorption process.

To estimate the activation energy of the adsorption (E_a) the Arrhenius equation was used:

$$\ln k_2 = \ln A - \frac{E_a}{RT} \quad (6)$$

where k_2 and A ($\text{g}/\text{mmol min}$) are respectively the rate constant and temperature independent factor, E_a is the activation energy of the adsorption (J/mol), R is the

gas constant (8.314 J/molK), and T is absolute temperature (K). The plot of $\ln k_2$ against $1/T$ is shown in Fig. 7.

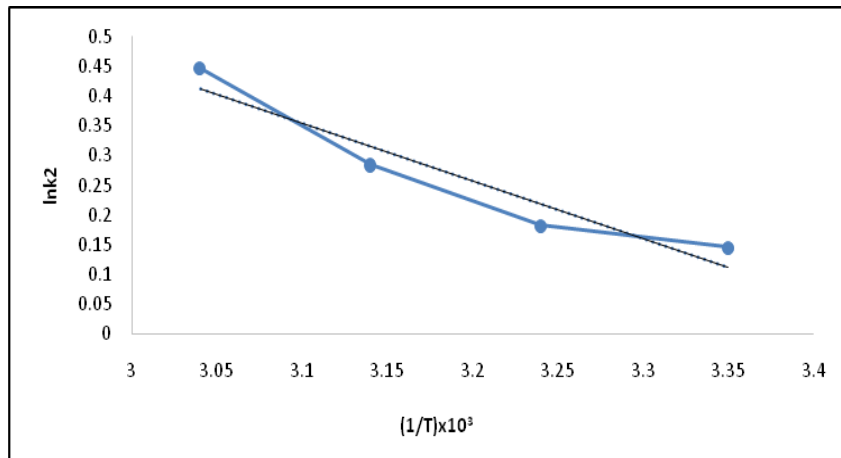


Fig. 7. Linear least square plots for obtaining E_a

Adsorption of Cs^+ was followed with low potential energy as show in Table 2 (E_a was less than 42.0 J/mol)[28].

3.4. Evaluation of thermodynamic parameters

The values of enthalpy change (ΔH°) and entropy change (ΔS°) were determined using linear plot of Van't Hoff equation:

$$\ln k_d = -(\Delta H^\circ / RT) + (\Delta S^\circ / R) \quad (7)$$

where k_d is the distribution coefficient, R is the gas constant, and T is the absolute temperature. A plot of $\ln k_d$ versus $1/T$ is shown in Fig. 8.

The value of free energy change (ΔG°) was calculated from:

$$\Delta G^\circ = \Delta H^\circ - T \Delta S^\circ \quad (8)$$

The calculated thermodynamic parameters are listed in Table 2.

Table 2.
Thermodynamic parameters of Cs^+ adsorption

E_a (kJ/mol)	ΔH° (kJ/mol)	ΔS° (kJ/mol J)	ΔG° (kJ/mol)			
			298 K	308 K	318 K	328 K
8.06	22.92	0.137	-17.91	-19.28	-20.65	-22.02

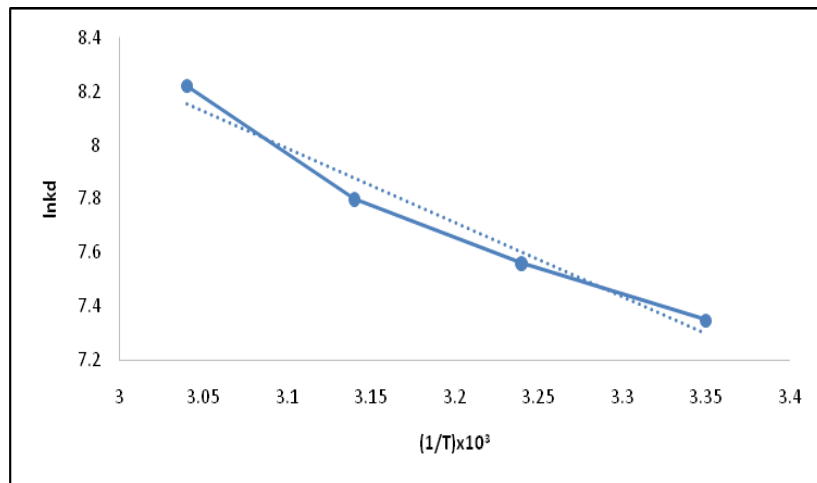


Fig. 8. Van't Hoff plot of Cs^+ adsorption

The positive values of ΔH° revealed the endothermic nature of the adsorption process. The positive values of ΔS° indicated that randomness of the system increased during the sorption process. The ΔH° values were negative and decreased with increasing temperature, indicating adsorption of Cs^+ occurred spontaneously.

3.5. Sorption isotherms

The relationship between the amount of ions adsorbed by unit mass of the PNF – SG and the concentration of remaining ions in solution represented sorption isotherm [29] (Fig. 9).

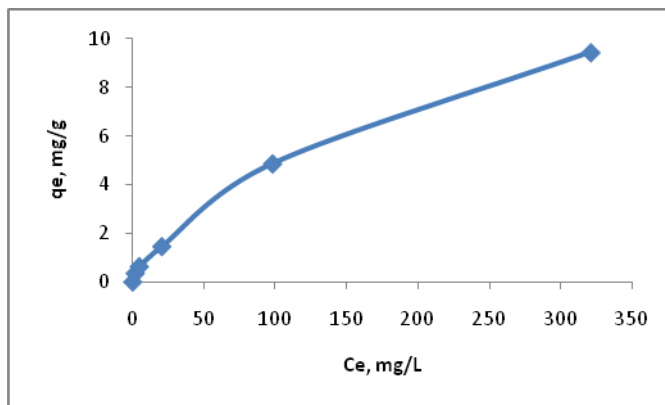


Fig. 9. Sorption isotherm of Cs^+ at 298 K

The isotherm is regular, positive, and concave to the concentration axis.

Two isotherm models including Langmuir and Freundlich were used to describe the equilibrium experimental data.

The linearized form of the Langmuir equation is [28]:

$$\frac{C_e}{q_e} = \frac{1}{Q_0 b} + \frac{C_e}{Q_0} \quad (9)$$

where Q_0 (mg/g), the saturation adsorption capacity and b the constant related to the free energy of adsorption were calculated from the slope and the intercept of plot of (C_e/q_e) against C_e (Fig. 10).

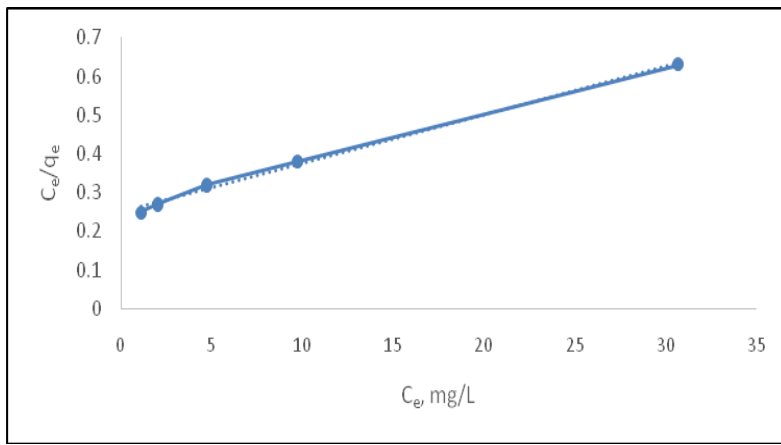


Fig. 10. Langmuir plots of Cs⁺ adsorption

The most important parameter of Langmuir isotherm model, separation factor (R_L) can be defined as:

$$R_L = \frac{1}{1 + bC_0} \quad (10)$$

where C_0 (mg/L) is the highest initial ions concentration. The value of R_L indicated the type of Langmuir isotherm. The sorption process may be irreversible ($R_L = 0$), favourable ($0 < R_L < 1$), linear ($R_L = 1$), and unfavourable ($R_L > 1$) [31].

The calculated values of Q_0 , b and R_L are listed in Table 3.

The linearized form of Freundlich model is written as follows [32]:

$$\log q_e = \log K_f + \frac{1}{n} \log C_e \quad (11)$$

where K_f is the Freundlich constant related to the adsorbent capacity and n is the constant indicative to the intensity of the adsorption process. The plot of $\log q_e$ versus $\log C_e$ is shown in Fig. 11. The values of the constant n and K_f were calculated from the slope and the intercepts of the plot and listed in Table 3.

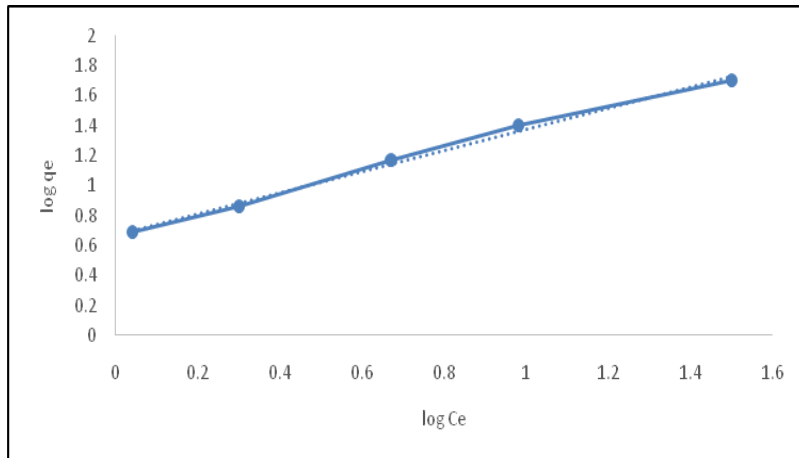


Fig. 11. Freundlich plots of Cs^+ adsorption

Table 3.

Adsorption isotherm parameters for Cs^+

Isotherm	Model parameter			
Langmuir	Q_0 (mg/g)	b (L/mg)	R_L	R^2
	80	0.05	0.019	0.9955
Freundlich	n	K_f (mg/g)	-	R^2
	1.4	4.7	-	0.9946

The adsorption data obey both Langmuir and Freundlich isotherms. The R_L values for Cs^+ is 0.019, indicating that the sorption process was favourable. The Freundlich intensity constant n is greater than unity indicating an increase tendency for sorption with the concentration increase.

Comparison with R^2 values determines which model best represents the adsorption behaviour of the adsorbent. In this case, Langmuir represents the best model, so the adsorption behaviour is homogeneous rather than heterogeneous.

3.6. Decontamination factor

Decontamination factor (DF) was calculated in terms of separation yield as the ratio of initial Cs^+ concentration to final concentration resulting from a separation process. In order to establish acceptable limits for variability in separation process performance, isolated and synergic effects of parameters were determined by calculating DFs (Figs. 12-14).

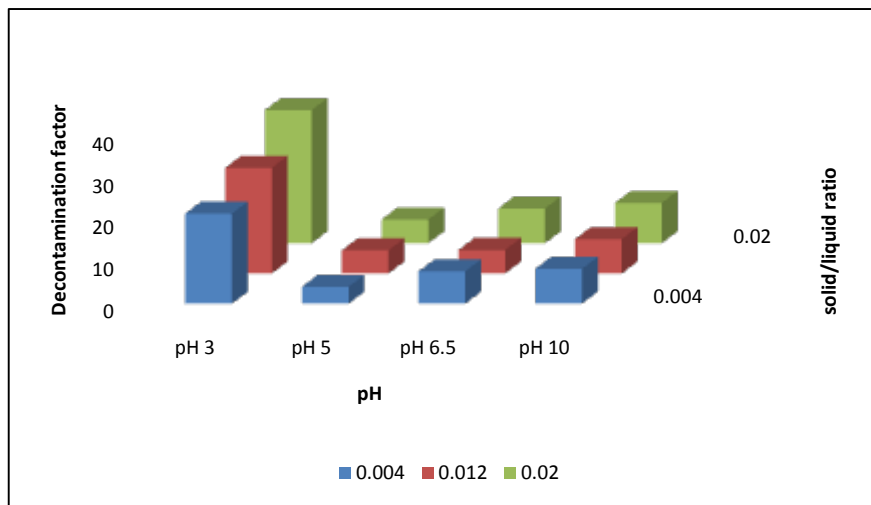


Fig. 12. Graph of calculated DF versus pH and solid/liquid ratio, contact time 2 h, temperature=25 °C, initial Cs⁺ concentration=1000 mg/L

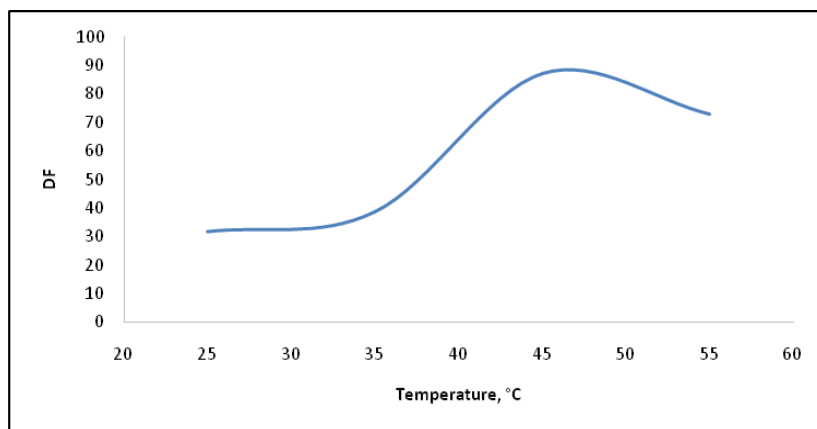


Fig. 13. Graph of calculated DF versus temperature, contact time 2 h, solid/liquid ratio=0.02, pH=3, initial Cs⁺ concentration=1000 mg/L

As it can be seen from these figures, DF is strongly affected by all process parameters. The parameter that has the most influence is temperature. By increasing the process temperature up to 50°C, DFs could reach 100. Moreover, acidic medium promotes the achievement of values up to 40, and DFs increase with increasing initial Cs⁺ concentration up to 800 mg/L. A further increase in initial Cs⁺ concentration had a negligible effect on the DFs. That could be caused by the decrease of the ratio of number of vacant sites/number of Cs⁺ ions on the sorbent surface. According to initial radioactive waste characteristics, the best combination of influencing parameter scan can be chosen and acceptable limits for variability in separation process can be established.

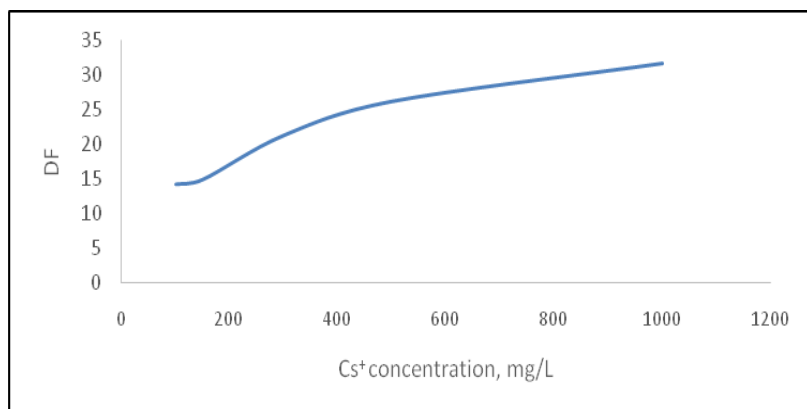


Fig. 14. Graph of calculated DF versus initial Cs^+ concentration, contact time of 2 h, solid/liquid ratio=0.02, pH=3, temperature=25 °C

4. Conclusion

Potassium nickel ferrocyanide, precipitated on silica gel beds, was tested as inorganic ion exchange material for the removal of cesium ions from aqueous solutions. The kinetic was experimentally studied and the obtained rate data were analyzed using simple kinetic models. Results reveal that the pseudo second-order sorption mechanism is predominant and the overall rate constant of sorption process appears to be controlled by chemical sorption process. Equilibrium isotherms have been determined and tested for different isotherm expressions and the sorption data were successfully modelled using Langmuir and Freundlich approaches. The values of thermodynamic parameters indicated endothermic and spontaneous nature of the adsorption process. Analysis of the kinetic data showed that the pseudo-second-order model fitted well with the experimental data confirming that the chemical sorption was the determining step.

Decontamination factors were calculated in order to identify all influencing parameters and acceptable limits for variability in the separation process.

REFERENCES

- [1] Ritchie I.G., Growing dimensions. Spent fuel management at research reactors, *IAEA Bull.*, 40, (1998), 29–31.
- [2] Coughtrey P. J., Thorne M. C., Radionuclide Distribution and Transport in Terrestrial and Aquatic Ecosystems, A. A. Balkema, Rotterdam, 1983.
- [3] Shakir K., Sohsah M., Soliman M., Removal of cesium from aqueous solutions and radioactive waste simulants by coprecipitate flotation, *Sep. Purif. Technol.*, 54, (2007), 373–381.
- [4] Bascetin E., Atun G., Adsorptive removal of strontium by binary mineral mixtures of montmorillonite and zeolite, *J. Chem. Eng. Data*, 55, (2010), 783–788.

- [5] Balarama Krishna M.V., Rao S.V., Arunachalam J., Murali M.S., Kumar S., Manchanda V.K., Removal of ^{137}Cs and ^{90}Sr from actual low level radioactive waste solutions using moss as a phyto-sorbent, *Sep. Purif. Technol.*, 38, (2004), 149–161.
- [6] Cheng Z., Gao Z., Ma W., Sun Q., Wang B., Wang X., Preparation of magnetic Fe_3O_4 particles modified sawdust as adsorbent to remove strontium ions, *Chem. Eng., J.* 209, (2012), 451–457.
- [7] Zhang C., Gu P., Zhao J., Zhang D., Deng Y., Research on the treatment of liquid waste containing cesium by an adsorption–microfiltration process with potassium zinc hexacyanoferrate, *J. Hazard. Mater.*, 167, (2009), 1057–1062.
- [8] Lujaniene G., Meleshevych S., Kanibolotskyy V., Sapolait J., Strelko V., Remeikis V., Oleksienko O., Ribokaite K., Sciglo T., Application of inorganic sorbents for removal of Cs, Sr, Pu and Am from contaminated solutions, *J. Radioanal. Nucl. Chem.*, 282, (2009), 787–791.
- [9] Duff M.C., Hunter D.B., Hobbs D.T., Fink S.D., Dai Z., Bradley J.P., Mechanisms of strontium and uranium removal from high-level radioactive waste simulant solutions by the sorbent monosodium titanate, *Environ. Sci. Technol.*, 38, (2004), 5201–5207.
- [10] Walker G.M., Hanna J.-A., Allen S.J., Treatment of hazardous shipyard wastewater using dolomitic sorbents, *Water Res.*, 39, (2005), 2422–2428.
- [11] Puziy A.M., Cesium and strontium exchange by the framework potassium titanium silicate $\text{K}_3\text{Ti}_4\text{O}_4(\text{SiO}_4)3\cdot4\text{H}_2\text{O}$, *J. Radioanal. Nucl. Chem.*, 237, (1998), 73–80.
- [12] Shabana E.I., El-Dessouky M.I., Sorption of cesium and strontium ions on hydrous titanium dioxide from chloride medium, *J. Radioanal. Nucl. Chem.*, 253, (2002), 281–284.
- [13] Todd T.A., Brewer K.N., Wood D.J., Tullock P.A., Mann N.R., Olson L.G., Evaluation and testing of inorganic ion exchange sorbents for the removal of cesium-137 from Idaho chemical processing plant acidic tank waste, *Sep. Sci. Technol.*, 36, (2001), 999–1016.
- [14] El-Kamash A.M., Evaluation of zeolite A for the sorptive removal of Cs^+ and Sr^{2+} ions from aqueous solutions using batch and fixed bed column operations, *J. Hazard. Mater.*, 151, (2008), 432–445.
- [15] Ghaemi A., Torab-Mostaedi M., Ghannadi-Maragheh M., Characterizations of strontium(II) and barium(II) adsorption from aqueous solutions using dolomite powder, *J. Hazard. Mater.*, 190, (2011), 916–921.
- [16] Hass P. A., A Review of Information on Ferrocyanide Solids for Removal of Cesium from Solutions, *Separ. Sci. Technol.*, 28(17-18), (1993), 2479–2506.
- [17] Lin Y., Fryxell G. E., Wu H., Engelhard M., Selective sorption of cesium using self-assembled monolayers on mesoporous supports, *Environ. Sci. Technol.*, 35(19), (2001), 3962–3968.
- [18] Won H.-J., Moon J.-K., Y.Chung C.-H., Evaluation of ferrocyanide anion exchange resins regarding the uptake of Cs^+ ions and their regeneration, *Nuclear Engineering and Technology*, 40(6), (2008), 489–496.
- [19] Watari K., Imai K., Ohmomo Y., Muramatsu Y., Nishimura Y., Izawa M., Baciles L. R., Simultaneous adsorption of Cs-137 and I-131 from water and milk on metal ferrocyanide-anion exchange resin, *J. Nucl. Sci. Techn.*, 25(5), (1988), 495–499.
- [20] Folsom T. R., Hansen N., Tatum T. J., Hodge V. F., Recent developments in method for concentrating and analyzing radiocesium in sea water, *J. Radiation. Res.*, 16, (1975), 19–27.
- [21] Mann D. R., Casso S. A., In situ chemisorption of radiocesium from sea water, *Marine Chem.*, 14(4), (1984), 307–328.
- [22] Orechovská J., Rajec P., Sorption of cesium on composite sorbents based on nickel ferrocyanide, *J. Radioanal. Nucl. Chem.*, 242(2), (1999), 387–390.
- [23] "NIST Nuclide Half-Life Measurements". NIST. Retrieved 13 March, 2011.
- [24] Abd El-Latif M.M., Elkady M.F., Kinetics study and thermodynamic behaviour for removing cesium, cobalt and nickel ions from aqueous solution using nano-zirconium vanadate ion exchange, *Desalination*, 271, (2011), 41–54.

- [25] Milyutin V.V., Mikheev S.V., Gelis V.M., Kononenko O.A., Coprecipitation of microamounts of cesium with precipitates of transition metal ferrocyanides in alkaline solutions, *Radiokhimiya*, 51(3), (2009), 258–260.
- [26] Lagergren S., About the theory of so-called adsorption of soluble substances, *K. Sven. Vetenskapsakad. Handl.* 24, (1898), 1–39.
- [27] Ho Y.S., McKay G., Pseudo second-order model for sorption processes, *Process. Biochem.* 34, (1999), 451–465.
- [28] Scheckel K. G., Sparks D. L., Temperature effects on nickel sorption kinetics at mineral water interface, *Soil. Sci. Soc. Am. J.*, 65, (2001), 719–728.
- [29] Peric J., Trgo M., Medvidovic N.V., Removal of zinc, copper and lead by natural zeolite-a comparison of adsorption isotherms, *Water Res.*, 38, (2004), 1839–1899.
- [30] Langmuir I., The adsorption of gases on plane surfaces of glass, mica and platinum, *J. Am. Chem. Soc.*, 40, (1918), 1361–1403.
- [31] Mohan D., Chander S., Single, binary and multicomponent sorption of iron and manganese on lignite, *J. Colloid Interface Sci.*, 299, (2006), 57–76.
- [32] Freundlich H., Adsorption in solution, *Phys. Chem.*, 57, (1906), 384–401.